Aus dem
Charité Centrum für Grundlagenmedizin (CC2)
Institut für Vegetative Anatomie
Direktor: Prof. Dr. Sebastian Bachmann

Habilitationsschrift

Rolle des antidiuretischen Hormons in der Regulation der renalen Na-(K)-Cl Transporter

zur Erlangung der Lehrbefähigung
für das Fach Anatomie

vorgelegt dem Fakultätsrat der Medizinische Fakultät
Charité – Universitätsmedizin Berlin

von

Dr. Kerim Mutig
geboren in Semipalatinsk

Eingereicht: Februar 2014

Dekanin: Professor Dr. med. A. Grüters-Kieslich

1. Gutachter/in: Prof. Dr. A. Kurtz

2. Gutachter/in: Prof. Dr. H. Ehmke

Inhaltsverzeichnis

List of abbreviations (Abkürzungsverzeichnis)

AVP	Arginine Vasopressin
AngII	Angiotensin II
AQP2	Aquaporin 2
CCC	Cation-Chloride Cotransporter
CD	Collecting Duct
CNT	Connecting Tubule
DCT	Distal Convoluted Tubule
FL	Full Length
KS	Kidney Specific
NKCC2	Na^+-K^+-Cl^- -cotransporter type 2
NCC	Na^+-Cl^- -cotransporter
OSR1	Oxidative Stress Responsive kinase 1
PKA	Protein Kinase A
RAAS	Renin-Angiotensin-Aldosterone System
SPAK	SPS-related Proline/Alanine-rich Kinase
TAL	Thick Ascending Limb
THP	Tamm-Horsfall Protein (uromoduline)
V1a	Vasopressin V1a receptor
V1b	Vasopressin V1b receptor
V2R	Vasopressin V2 receptor
WNK	With No lysine [K] kinase

1 Introduction (Einleitung)

General aspects of AVP action in the kidney

The kidney provides essential functions for the maintenance of water and electrolyte homeostasis of the body. Changes in blood volume or osmolality activate central and peripheral mechanisms leading to adaptive adjustments of the renal reabsorptive function. Physiologically, renal salt and water handling is tightly regulated by the neurohypophyseal hormone vasopressin (AVP, antidiuretic hormone), components of the renin-angiotensin-aldosterone system (RAAS), and several other hormones [1–3]. AVP is secreted in response to increased plasma osmolality or decreased plasma volume to induce a number of cellular responses mediated by distinct AVP receptors [4]. Many effects of AVP can be understood as part of its principal function to conserve water. In addition, AVP is involved in blood pressure control via modulation of the RAAS activity and by its vascular effects [5–7]. Three types of AVP receptors have been identified so far, the V1a receptor (V1aR), V1b receptor (V1bR), and V2 receptor (V2R) [8–10]. The V1aR is expressed in blood vessels and some epithelia, the V1bR predominantly in the brain, and the V2R chiefly in kidney epithelia of the distal nephron and collecting duct [11]. V2R-mediated effects of AVP are vital for the urinary concentrating mechanism [4]. The lack of circulating AVP or inability of the kidney to respond to the hormone due to congenital V2R defects cause central or nephrogenic diabetes insipidus, respectively, with polyuria and polydipsia related to the severe failure of urinary concentration [4,12]. Renal V2R distribution has been addressed in a number of previous studies [11,13,14]. While all studies convincingly documented the expression of the receptor in principal cells of the connecting tubule (CNT) and collecting duct (CD), presence of V2R in the distal nephron, comprising the thick ascending limb (TAL) and the distal convoluted tubule (DCT), has been a matter of debate [4,11,13,14]. The cellular mechanisms of AVP action have been best characterized in the principal cells of the CD. Here, activation of V2R has been shown to facilitate the apical trafficking and membrane insertion of the aquaporin 2 water channel via a cAMP/protein kinase A (PKA)-dependent mechanism, thus enabling efficient transcellular water reabsorption and urinary concentration [15]. The hypertonicity of the renal medullary interstitium along with the hypotonicity of the urine in CD are the prerequisites for the passive movement of water via aquaporin water channels from the tubular lumen into the interstitium. Generation of the medullary osmotic gradient essentially depends on the active reabsorption of NaCl in the water-impermeable TAL [16]. Earlier micropuncture- and microperfusion studies have demonstrated that TAL responds to AVP with increased NaCl transport [17,18]. The cellular effects of AVP in TAL are related with the V2R-mediated increase in cAMP and activation of PKA which eventually stimulates apical trafficking of the $Na^+,K^+,2Cl^-$ -cotransporter (NKCC2) [1,19]. The resulting increase in NKCC2 surface expression and function promotes the generation of the longitudinal osmotic gradient along the TAL [4,16]. Moreover, AVP-induced, V2R-mediated signaling in TAL increases the apical abundance of rat outer medullary potassium (K) channel

(ROMK, Kir1.1), which supports the function of NKCC2 [20].

Apart from its role in the urinary concentrating mechanism, AVP has been further implicated in volume regulation and blood pressure control [4,21–23]. On the one hand, AVP substantially modulates the RAAS activity; these effects are mediated by the extravascular V1aR expressed in the suprarenal gland and the macula densa cells, as well as by the pituitary V1bR [24,25]. On the other hand, activation of V2R in the CD has been shown to stimulate salt reabsorption in CD via the epithelial sodium channel (ENaC) [23,26,27]. Thus, several lines of evidence have so far suggested that effects of AVP are not solely restricted to water conservation but are also important for the renal salt handling [23,28]. In this context, effects of AVP on the salt transporters along the distal nephron have received surprisingly little attention in the past.

Role of the distal nephron

The distal nephron has been increasingly recognized as a key element in the regulation of renal salt handling and blood pressure [29,30]. Salt reabsorption in the distal nephron is accomplished by the kidney-specific members of the family of electroneutral cation-chloride cotransporters (CCC). The bumetanide-sensitive type 2 Na^+,K^+,Cl^--cotransporter (the reabsorptive isoform, NKCC2) is exclusively expressed in TAL and Macula densa and plays an essential role an essential role in urinary concentration as well as in the tubular-glomerular feedback mechanism. The thiazide-sensitive Na^+,Cl^-- cotransporter (NCC) resides in the DCT and is instrumental for fine tuning of the renal salt excretion and potassium handling [29]. Inactivating mutations of either NKCC2 or NCC cause monogenic disorders known as Bartter's or Gitelman's syndrome, respectively [31]. Both syndromes are characterized by pronounced salt loss, low blood pressure, and hypokalemic alkalosis, with a more severe disease course in Bartter's syndrome [31]. In contrast, excessive activity of the distal transporters can lead to salt retention, increased circulating volume, and high blood pressure [32]. Pharmacologic inhibition of NKCC2 or NCC with respective diuretic drugs found broad clinical application in patients with hypertension or edema. Thus, physiologic and clinical data emphasize the important role of NKCC2 and NCC in the maintenance of such vital body functions as electrolyte balance, extracellular volume, and arterial pressure [29]. Molecular mechanisms involved in the regulation of the transporters in health and disease have been intensively studied during the last two decades [29]. Recently, their phosphorylation has been recognized as an important posttranslational step which contributes to modulate their activity [19,33]. Several activating phosphoacceptors have been identified within the N-terminus of NKCC2 [19,34]. These sites are highly conserved between the members of the CCC family including NKCC1 (the ubiquitous isoform), NKCC2, and NCC [33,34]. The search for kinases involved in their phosphorylation has identified two homologous Ste20-related serine/threonine kinases SPAK (SPS-related *proline/alanine-rich kinase*) and OSR1 (oxidative stress responsive kinase 1) which were capable of direct interaction with and phosphorylation of NKCC1, NKCC2, or NCC *in vitro*. The two kinases themselves are regulated by phosphorylation

within their catalytic and regulatory domains by upstream WNK (with no lysine [K]) kinases [35]. In particular, WNK1 and WNK4 appear to play crucial role in the renal salt handling and volume regulation as reflected by hypertensive phenotype of patients with the Familial Hyperkalemic Hypertension (FHHt; Gordon syndrome) caused by their gain-of-function mutations [30,32]. In addition, a truncated WNK1 splice variant lacking the catalytic domain has been shown to play an important regulatory role in the DCT via inhibiting the catalytic active WNK forms in a dominant negative fashion (Figure 1) [36]. There is now increasing evidence that WNK, SPAK, and OSR1 kinases represent important molecular switches mediating the effects of functional stimuli on the CCC transporters in the kidney [2,37].

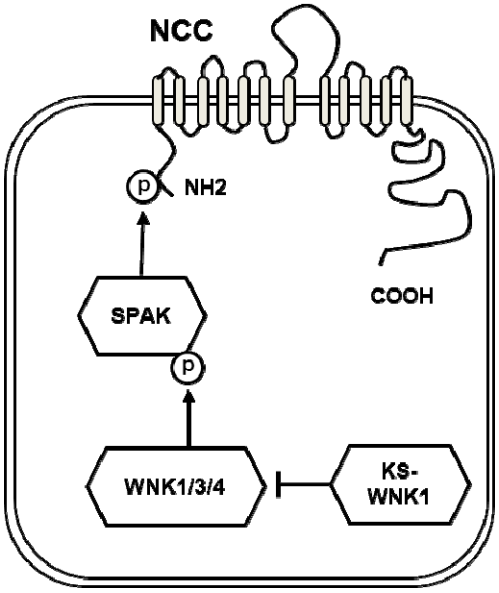

Figure 1. Simplified model of the kinase pathways involved in the activating phosphorylation of renal CCC, as exemplified by NCC phosphorylation in the DCT. WNK1, WNK3, and WNK4 kinases phosphorylate and thereby activate SPAK, which in turn phosphorylates and activates NCC. A catalytically inactive, truncated WNK1 variant, termed KS-WNK1 for its kidney-specific (KS) expression, counteracts the catalytic action of the full-length WNK isoforms in a dominant-negative manner [36].

Endocrine regulation of NKCC2 and NCC

The distal nephron responds to a variety of hormones. AVP and effectors of the RAAS are widely recognized, potent endocrine stimuli which also affect distal nephron function. Their impact on NKCC2 and NCC functions has been established [2,19,28,29].

AVP, acting via V2R, is essential for maintaining of NKCC2 activity, as evident from the decreased NKCC2 abundance and function in AVP-deficient Brattleboro rats [1,28,38]. Acute administration of AVP or dDAVP has been shown to facilitate luminal trafficking of NKCC2 and NaCl reabsorption in the TAL [18,19]. The mechanisms of AVP action in TAL have been linked with the G-protein-dependent stimulation of the adenylyl cyclase VI and increase in intracellular cAMP formation [18,39]. Increased intracellular cAMP levels induce NKCC2 expression via a cAMP-responsive element in the NKCC2 promoter and stimulate the apical trafficking of the transporter via PKA activation [1,29,40]. In addition, AVP has been shown to promote N-terminal NKCC2 phosphorylation, although the kinases involved herein remain to be identified [19]. Compared to NKCC2, effects of AVP on NCC received less attention. Chronic administration of dDAVP increased NCC abundance in Brattleboro rats, although it was unclear whether this

result was caused by direct effects of V2R activation in DCT, or whether it reflected systemic adaptations of RAAS [5,7,28]. Several attempts to clarify the effects of AVP in the DCT have been undertaken in the past, but the data remained inconclusive [41–43]. Earlier studies have demonstrated effects of AVP on chloride transport, magnesium conductance, and cAMP generation in the DCT [42–44]. Another study, however, failed to detect any significant responses to AVP in this nephron segment [41]. It remained unclear, whether AVP directly affects NCC function, and the mechanisms of AVP signaling in DCT have all in all been poorly characterized in previous work.

In contrast, major focus of prior and recent research has been placed on the regulation of NCC by the RAAS effector hormones, especially angiotensin II (AngII) and aldosterone [2,29]. AngII increased the abundance, surface expression, and phosphorylation of NCC in acute and chronic experimental settings and is now considered as one of the most potent activators of the transporter [2,45,46]. The late portion of DCT is part of the aldosterone-sensitive distal nephron and responds to this hormone with increased abundance, phosphorylation, and function of NCC [47–50]. These effects of RAAS on NCC are, at least in part, mediated by the WNK-SPAK/OSR1 kinase pathway [2,33,49].

Recent progress in genetic research has identified multiple links between mutations or polymorphisms of genes involved in the WNK-SPAK/OSR1-NKCC2/NCC signalling pathway and several hereditary and acquired forms of hypertension [30,32,50]. At the same time, AVP has been increasingly recognized as an essential component of the blood pressure control [4,22,23]. The publications presented in this habilitation thesis address functional and molecular aspects of the AVP/V2R signaling axis along the distal nephron. Since several selective V2R antagonists have become available for clinical use, results of these studies have translational aspects.

2 Aims of the work (Zielsetzung)

AVP has been recognized as the most potent endocrine stimulus of the urinary concentrating mechanism. Previous work has established the role of AVP in the regulation of water reabsorption in principal cells of collecting duct, whereas its action in the distal nephron was less characterized. In particular, no conclusive information was available on the expression of the vasopressin V2 receptor (V2R) and V2R-mediated effects along the distal convoluted tubule. The distal salt transporters, NKCC2 and NCC, play an important role in renal salt handling and volume regulation. The present habilitation thesis aimed at elucidating the action of AVP along the distal nephron. Therefore, effects of AVP on NKCC2 and NCC were studied, and the molecular pathways involved in AVP signaling were characterized. The publications presented in this thesis address critical issues in this field, namely the characterization of the cellular distribution of V2R along the nephron and the elucidation of the AVP-related kinase pathways mediating the regulation of NKCC2 and NCC.

3 Publications (Eigene Arbeiten)

3.1 Vasopressin V2 receptor expression along rat, mouse, and human renal epithelia with focus on TAL.

Mutig K, Paliege A, Kahl T, Jöns T, Müller-Esterl W, Bachmann S.

***Am J Physiol Renal Physiol.* 2007 Oct;293(4):F1166-77.**

This study presents a comprehensive analysis of renal V2R distribution in rat, mouse, and human kidneys. Evaluation of V2R expression by in situ hybridization revealed similar immunoreactive patterns across the species showing substantial expression of the receptor throughout the distal nephron and principal cells of CNT and CD. These results were corroborated by immunohistochemical data using an anti-V2R antibody. While confirming the substantial V2R expression in CNT and CD, the present study provided conclusive information on the distribution of the receptor along TAL and DCT. In view of the previous controversy regarding the presence and functional relevance of the V2R-mediated signaling in TAL, we have additionally evaluated effects of acute V2R stimulation on NKCC2 activity in terms of its phosphorylation in AVP-deficient Brattleboro rats and cultured rat TAL cells. Overall, results of this study have robustly demonstrated the expression of V 2R along the entire distal nephron thus providing the necessary morphologic basis for our later functional and mechanistic studies of the AVP signaling here.

Am J Physiol Renal Physiol 293: F1166–F1177, 2007.
First published July 11, 2007; doi:10.1152/ajprenal.00196.2007.

Vasopressin V_2 receptor expression along rat, mouse, and human renal epithelia with focus on TAL

K. Mutig,[1] A. Paliege,[1] T. Kahl,[1] T. Jöns,[1] W. Müller-Esterl,[2] and S. Bachmann[1]

[1]*Department of Anatomy, Charité Universitätsmedizin, Berlin; and* [2]*Institute of Biochemistry II, University of Frankfurt Medical School, Frankfurt, Germany*

Submitted 24 April 2007; accepted in final form 27 June 2007

Mutig K, Paliege A, Kahl T, Jöns T, Müller-Esterl W, Bachmann S. Vasopressin V_2 receptor expression along rat, mouse, and human renal epithelia with focus on TAL. *Am J Physiol Renal Physiol* 293: F1166–F1177, 2007. First published July 11, 2007; doi:10.1152/ajprenal.00196.2007.—In renal epithelia, vasopressin influences salt and water transport, chiefly via vasopressin V_2 receptors (V_2Rs) linked to adenylyl cyclase. A combination of vasopressin-induced effects along several distinct portions of the nephron and collecting duct system may help balance the net effects of antidiuresis in cortex and medulla. Previous studies of the intrarenal distribution of V_2Rs have been inconclusive with respect to segment- and cell-type-related V_2R expression. Our study therefore aimed to present a high-resolution analysis of V_2R mRNA expression in rat, mouse, and human kidney epithelia, supplemented with immunohistochemical data. Cell types of the renal tubule were identified histochemically using specific markers. Pronounced V_2R signal in thick ascending limb (TAL) was corroborated functionally; phosphorylation of Na^+-K^+-$2Cl^-$ cotransporter type 2 (NKCC2) was established in cultured TAL cells from rabbit and in rats with diabetes insipidus that were treated with the V_2R agonist desmopressin. We found solid expression of V_2R mRNA in medullary TAL (MTAL), macula densa, connecting tubule, and cortical and medullary collecting duct and weaker expression in cortical TAL and distal convoluted tubule in all three species. Additional V_2R immunostaining of kidneys and rabbit TAL cells confirmed our findings. In agreement with strong V_2R expression in MTAL, kidneys from rats with diabetes insipidus and cultured TAL cells revealed sharp, selective increases in NKCC2 phosphorylation upon desmopressin treatment. Macula densa cells constitutively showed strong NKCC2 phosphorylation. Results suggest comparably significant effects of vasopressin-induced V_2R signaling in MTAL and in connecting tubule/collecting duct principal cells across the three species. Strong V_2R expression in macula densa may be related to tubulovascular signal transfer.

antidiuretic hormone; thick ascending limb; kidney; sodium-potassium-chloride cotransporter type 2; bumetanide-sensitive cotransporter type 1

ANTIDIURETIC HORMONE [arginine vasopressin (AVP)] serves to regulate body fluid osmolality, blood volume, blood pressure, and vascular tone. In the kidney, two major receptor subtypes [V_{1a} and V_2 receptors (V_{1a}R and V_2R)] have been characterized (22, 24). V_{1a}Rs are principally localized in the renal vasculature and glomeruli and mediate the vasopressor effect of AVP (2, 32). The tubular antidiuretic effect of AVP is mediated by the V_2R and adenylyl cyclase-dependent cAMP signaling (13, 22). Since the early work of Morel (25), sites of V_2R-mediated AVP action along the nephron have been defined at different levels, such as transport (13, 15, 17), ligand binding (2, 35, 44), receptor mRNA expression (9, 32, 47), and immunohistochemical localization (30, 39). The collecting duct (CD) is generally considered the principal target for the antidiuretic action of AVP, but available data suggest a role for AVP also in the distal tubule (4, 38, 39). At both sites, AVP serves to control the renal concentrating mechanism. In the thick ascending limb (TAL), AVP stimulates transepithelial NaCl transport via increased abundance and phosphorylation of Na^+-K^+-$2Cl^-$ cotransporter type 2 (NKCC2) (10, 11, 14, 15). In the CD, the main action of AVP is promotion of water reabsorption via the aquaporin type 2 (AQP-2) water channel (13, 17, 28). Clinically, defective V_2R function is associated with nephrogenic diabetes insipidus (DI) (22). Vasopressin agonists and antagonists have been characterized in animal models and studied for use in clinical medicine (10, 11, 43).

Regarding the prominent functional role of V_2R-mediated effects of AVP in the kidney, an exact mapping to the renal nephron segments and cell types is of major importance. Previous work has presented information on V_2R distribution across several mammalian species, but results have in part been inconclusive, and information on cell-type-specific localization of V_2R biosynthesis is scarce (9, 30, 32, 39, 47). These studies showed solid V_2R expression in the CD, with some reference to regional differences in intensity believed to reflect AVP-induced effects on the stimulation/insertion of AQP-2 and urea transporter(s) (4, 28, 36). Localization of V_2R was further reported in rat kidney TAL (10, 39) and macula densa (32); binding of oxytocin, which is structurally related to AVP, and expression of oxytocin receptor in macula densa as well (33, 45) support a role for AVP and, possibly, oxytocin in the regulation of glomerular filtration rate (37). A recent study analyzing V_2R distribution in mouse and human kidney confirmed V_2R expression in CD, but not in TAL (9).

Interest in genetically engineered mice, as well as recent data on the functional significance of AVP-related signaling in the distal tubule, has stimulated us to study in more detail the distribution of the V_2R in mouse nephron segments with use of nonradioactive in situ hybridization and antibody staining combined with immunostaining by segment- and cell-type-specific markers, and we have analyzed the rat kidney in parallel. Since there is further awareness of the potency to clinically manipulate AVP-related effects in volume disorders and edema, we have extended our approach to the study of the human kidney.

Our results have clearly shown dominant expression of the V_2R in medullary TAL (MTAL), macula densa, and medullary CD (MCD), intermediate expression in connecting tubule (CNT) and cortical CD (CCD), and low expression in cortical

Address for reprint requests and other correspondence: S. Bachmann, Institut für Vegetative Anatomie, Charité-Universitätsmedizin Berlin, Campus Charité-Mitte, Philippstr. 12, D-10115 Berlin, Germany (e-mail: sbachm@charite.de).

The costs of publication of this article were defrayed in part by the payment of page charges. The article must therefore be hereby marked "*advertisement*" in accordance with 18 U.S.C. Section 1734 solely to indicate this fact.

TAL (CTAL) and distal convoluted tubule (DCT) in all three species. To illustrate the functional significance of V_2R signaling in TAL, we have studied short-term effects of the V_2R agonist desmopressin (dDAVP) in cultured TAL cells and in Brattleboro rats with central DI by evaluating the intensity and distribution of NKCC2 phosphorylation in the response.

MATERIALS AND METHODS

Animals, tissues, and cells. Adult male Wistar rats ($n = 3$), Brattleboro rats with DI (Harlan; $n = 20$), and C57/Bl6 mice ($n = 3$) were bred in the local animal facility (Charité Berlin) and kept on standard diet and tap water. Animals were anesthetized by an injection of pentobarbital sodium (0.06 mg/g body wt ip). The abdominal cavity was opened, and kidneys were perfused retrogradely through the abdominal aorta using 3% paraformaldehyde (41). Human kidney samples ($n = 3$) were derived from tumor nephrectomy; tissues from the healthy parts of the kidneys were immersion fixed in paraformaldehyde. The local council on animal care approved the protocols (permission number G006-2/05 Land Berlin); the standards correspond to the requirements of the American Physiological Society. The human kidneys were from tumor nephrectomy material obtained after written consent of the respective patients from Charité hospital. Tissues were prepared for standard cryostat and paraffin sectioning. Series of 5-μm-thick consecutive sections were cut from rat, mouse, and human kidney samples for in situ hybridization and immunohistochemistry. For study of V_2R-mediated changes in expression and phosphorylation status of NKCC2, DI rats were randomly divided into three groups: *1*) control, vehicle (intraperitoneal saline)-treated animals ($n = 8$), *2*) animals treated with desmopressin [1-desamino-8-D-Arg vasopressin (dDAVP); 1 ng/g body wt ip] for 30 min ($n = 8$), and *3*) animals treated with vehicle and then subjected to 4 h (from 4 to 8 PM) of water deprivation ($n = 4$). At the end of the experiments, four DI rats, each from *groups 1, 2*, and *3*, were perfusion fixed for morphological analysis. The remaining DI rats of *groups 1* and *2* were killed by an overdose of pentobarbital sodium (Nembutal), the kidneys were removed, and pieces of outer medulla and cortex were dissected. Simian virus 40-transformed rabbit TAL (rbTAL) cells obtained from rabbit kidney medulla were cultured as described elsewhere (48). Cells were incubated with vehicle or dDAVP (1×10^{-7} mol/l; Sigma) in FCS-free culture medium for 30 min. Cells were then harvested and homogenized in sucrose buffer.

In situ hybridization. In situ hybridization was performed as described elsewhere (42). Briefly, a 584-bp PCR product was amplified from rat kidney cDNA using specific primers for V_2R: 5′ CAg CAg CCA ggA ggA ACT AC 3′ (forward) and 5′ gTg CCA CAA ACA CCA TCA Ag 3′ (reverse). The amplified fragment was cloned into the pCR4-TOPO vector (Invitrogen) and verified by DNA sequencing. The digoxigenin (DIG)-11-UTP-labeled antisense riboprobe was synthesized by in vitro transcription (DIG RNA labeling kit Sp6/T7, Roche). Since sequence homology was high across species (97% for mouse and 85% for human V_2R), the same probe was used for all species. For in situ hybridization, dewaxed paraffin sections were treated with proteinase K, hybridized for 18 h at 40°C with hybridization mix (2.5 ng mRNA/μl), washed, and incubated with sheep anti-DIG alkaline phosphatase-conjugated antibody (DAKO). Signal was generated using 4-nitro blue tetrazolium chloride. For control, a 592-bp nonsense probe was applied in parallel with the antisense probe. Sections were rinsed with PBS, coverslips were applied using PBS-glycerol, and sections were viewed by bright-field microscopy.

Immunohistochemistry. For identification of V_2 mRNA-expressing tubular segments, rabbit polyclonal antibody against V_2R was applied (39). For further cell-type-specific identification of the in situ signal, segment-specific antibodies were applied using double labeling or separate labeling of consecutive sections (3, 6, 7). The following polyclonal antibodies were used: guinea pig antibody against the NH_2-terminal 85 amino acids of NKCC2 (2.1 antibody) (41) and sheep anti-Tamm-Horsfall protein (THP) antibody (BioTrend) for TAL; rabbit anti-Na^+-Cl^- cotransporter (NCC) antibody (provided by D. H. Ellison, Portland, OR) for DCT; sheep anti-11β-hydroxysteroid dehydrogenase (11β-HSD2) antibody (Chemicon) for late distal convoluted tubule (DCT2), CNT, and CCD (7); goat anti-AQP-2 antibody (Santa Cruz Biotechnology) for CNT, CCD, and MCD principal cells; and rabbit anti-vacuolar H^+-ATPase antibody (Santa Cruz Biotechnology) or rabbit anti-anion exchanger 1 (AE1) (16) antibody for intercalated cells. For separate immunohistochemical labeling, sections were dewaxed and boiled in citrate buffer (pH 6.0) for 5 min. Sections were blocked with 5% milk powder in PBS for 1 h and incubated with primary antibody diluted in 5% milk powder for 1 h at room temperature and then incubated overnight at 4°C. For multiple staining, antibodies were sequentially applied, with a wash step between applications. Next, appropriate secondary fluorescent Cy3- or Cy2-conjugated antibodies (DIANOVA) were applied over a 2-h period. For bright-field V_2R detection, an LSAB-2 System-AP enhancer kit (DakoCytomation) was used. Sections were washed, coverslips were applied with PBS-glycerol, and sections were viewed in a Leica DMRB microscope equipped with a SPOT 32 camera and MetaView 3.6a software (Diagnostic Instruments, Universal Imaging).

Evaluation of phosphorylated NKCC2. For analysis of NKCC2 phosphorylation, rabbit antiserum against phosphorylated NKCC2 (2 NH_2-terminal threonines; see Ref. 11 for peptide sequence) was produced and affinity purified using selection with phosphorylated and nonphosphorylated peptides (Pineda, Berlin, Germany). The affinity-purified antibody against phosphorylated NKCC2 was termed pT2 antibody. Preabsorption tests were performed immunohistochemically using the phosphorylated, as well as the nonphosphorylated, peptides (10-fold excess). The size of phosphorylated NKCC2 as recognized by pT2 antibody was confirmed by Western blot on rat kidney extracts. Specificity was further confirmed by colocalization with 2.1 antibody. Paraffin sections of human kidney were incubated with pT2 antibody and then horseradish peroxidase (HRP) for detection. For double staining, incubation of frozen sections with pT2 antibody was followed by application of 2.1 antibody. HRP- and fluorescent Cy3-coupled secondary antibodies were used for detection.

Western blot. Nuclei were removed by homogenization of excised rat kidney zones and rbTAL cells in sucrose-triethanolamine buffer and centrifugation at 1,000 *g* for 15 min at 4°C. The supernatants were separated by PAGE [50 μg protein/lane, as determined by a bicinchoninic acid protein assay reagent kit (Pierce); 8–10% gel]. After electrophoretic transfer to PVDF membrane, equity in protein loading and blotting was verified by membrane staining using 0.1% Ponceau red staining. After they were blocked in 5% milk, PVDF membranes were incubated with mouse monoclonal antibody against the COOH-terminal 310 amino acids of NKCC2 (T4 antibody; Developmental Studies Hybridoma Bank, University of Iowa) or pT2 or 2.1 primary antibodies for 1 h at room temperature, incubated overnight at 4°C, and then exposed to HRP-conjugated secondary antibodies for 2 h at room temperature. Immunoreactive bands were detected by chemiluminescence and exposed to X-ray films, and the signals were scanned and densitometrically evaluated. Monoclonal mouse anti-β-actin antibody (Sigma) was used to normalize all data for expression of the housekeeping gene β-actin.

Real-time PCR. Samples of the outer medulla and cortex from DI rats were homogenized, and total RNA was prepared using the RNeasy total RNA kit (Qiagen). Genomic DNA was digested by DNase, and cDNA was synthesized by reverse transcription of 5 μg of total RNA (cDNA synthesis kit, Invitrogen). Specific TaqMan gene expression assays for NKCC2 and GAPDH were generated by Applied Biosystems. Amplification was performed using the real-time PCR TaqMan Fast 7500 (Applied Biosystems). Samples were incubated at 94°C for 10 min, and then 45 cycles of 95°C (3 s) and 60°C (30 s) were run. Threshold cycle (C_t) values were set in the linear phase of exponential amplification. The difference between values obtained for NKCC2 and the housekeeping gene GAPDH (ΔC_t) was calculated and compared between treatments and kidney zones.

Analysis of data. Western blot and real-time PCR results were evaluated using routine parametric descriptive statistics. Groups were compared with two-way ANOVA and *t*-tests; Bonferroni's correction was used as appropriate. $P < 0.05$ was accepted as significant. Values are means ± SD.

RESULTS

We have localized V_2R mRNA using DIG-labeled antisense probes hybridized to rat, mouse, and human kidney. For additional information, we have used specific antibody to V_2R. Double-staining techniques or serial sectioning was applied for cell type and segment identification. Results were largely similar among species. Overviews of coronal kidney sections present a clear predominance of V_2R mRNA expression intensity within the inner stripe of the outer medulla, intermediate strength in the inner medulla, and weaker signals in the outer stripe and the cortical segments. The dominant outer medullary signal was due to the parallel, strong V_2R expression in MTAL and MCD (Fig. 1). V_2R immunoreactive signal essentially paralleled these patterns but revealed less axial heterogeneity in the distal tubule segments.

Cortical vasculature, interstitium, glomeruli, and proximal nephron. Generally, no significant V_2R mRNA expression was encountered in cortical and medullary vasculature, interstitium, glomeruli, proximal tubules, or thin limbs of the loop of Henle of rat and mouse kidneys. In human kidney, the findings were similar, except for positive signals occasionally found in glomerular parietal epithelium and in the glomerular tuft; the latter, however, was irregular and could not be clearly assigned to a cell type.

Hypothalamic V_2R mRNA signal. In situ hybridization of rat brain sections was performed for additional confirmation of the specificity of the applied V_2R riboprobe. Hybridization with the antisense riboprobe produced a specific signal in hypothalamic paraventricular nucleus, as previously characterized functionally (50), whereas application of the nonsense probe did not produce a signal (Fig. 2, *g* and *h*).

TAL. The TAL, identified by concomitant staining with antibody against NKCC2 or THP, displayed significant V_2R mRNA expression in the medullary part. The intensity of the inner stripe MTAL signal was strongest (Fig. 1, *g–i*; Fig. 2, *a* and *b*; Fig. 3, *a* and *b*; and Fig. 4, *a* and *b*), whereas the intensity of the outer stripe MTAL signal was intermediate. In the cortical part, expression was weak, except for the macula densa cells, which showed strong V_2R mRNA expression; cells were identified by the absence of THP (Fig. 2, *e* and *f*; and Fig. 4, *e* and *f*) or by their specific topography (Fig. 3, *e* and *f*).

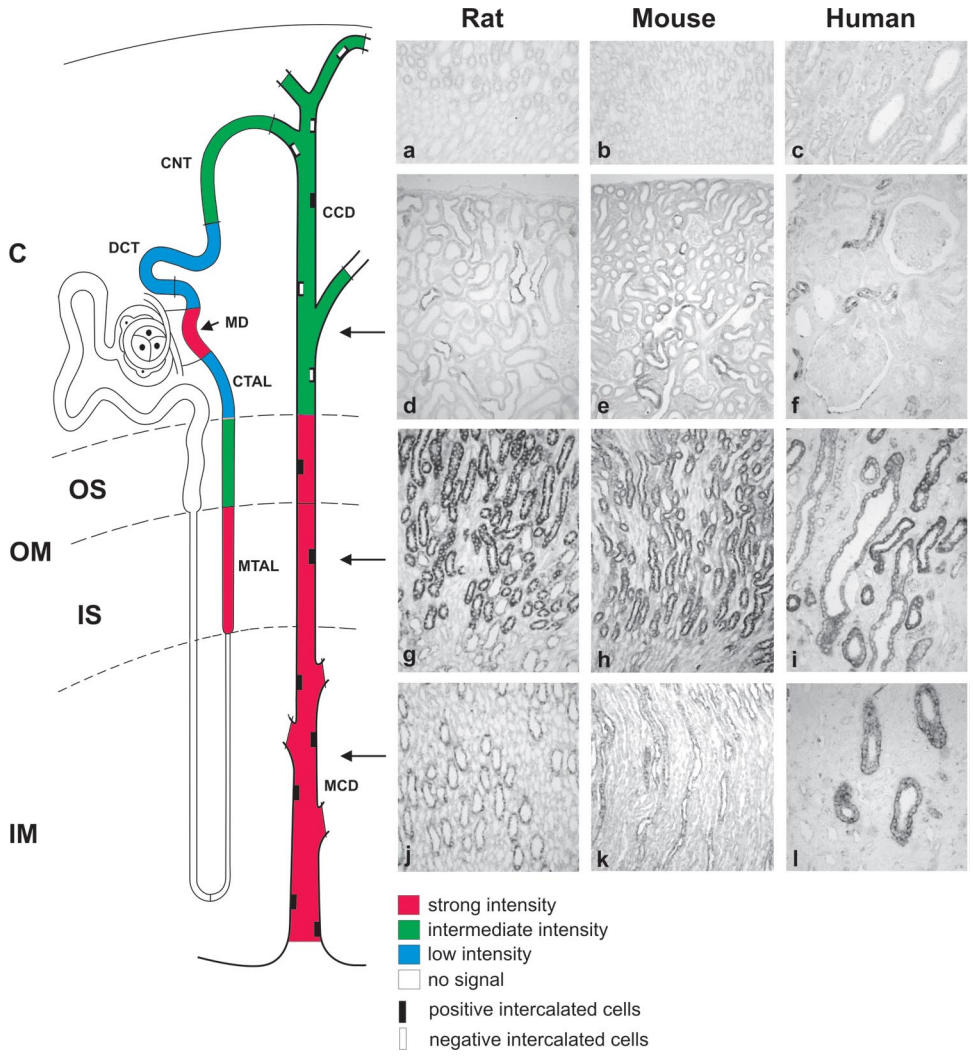

Fig. 1. Zonal and segmental distribution of baseline vasopressin V_2 receptor (V_2R) mRNA expression in rat, mouse, and human renal epithelia. *Left*: schematic representation of V_2R mRNA distribution (see Figs. 2–7). *Right*: overview scale in situ hybridization images across species. Approximate intensity levels of V_2R mRNA expression are represented by different colors. Kidney zones are as follows: cortex (C), outer medulla (OM) with outer stripe (OS) and inner stripe (IS), and inner medulla (IM). Tubule segments are as follows: medullary and cortical thick ascending limb (MTAL and CTAL), macula densa (MD), distal convoluted tubule (DCT), connecting tubule (CNT), and cortical and medullary collecting duct (CCD and MCD). *a–c*: Nonsense probe hybridization control images at outer-to-inner medullary transition. *d–l*: Representative images of V_2R mRNA expression in renal cortex (*d–f*), at outer-to-inner medullary transition (*g–i*; note strong labeling of MTALs), and in inner medulla (*j–l*). Arrows point to corresponding kidney zones. Original magnification ×200.

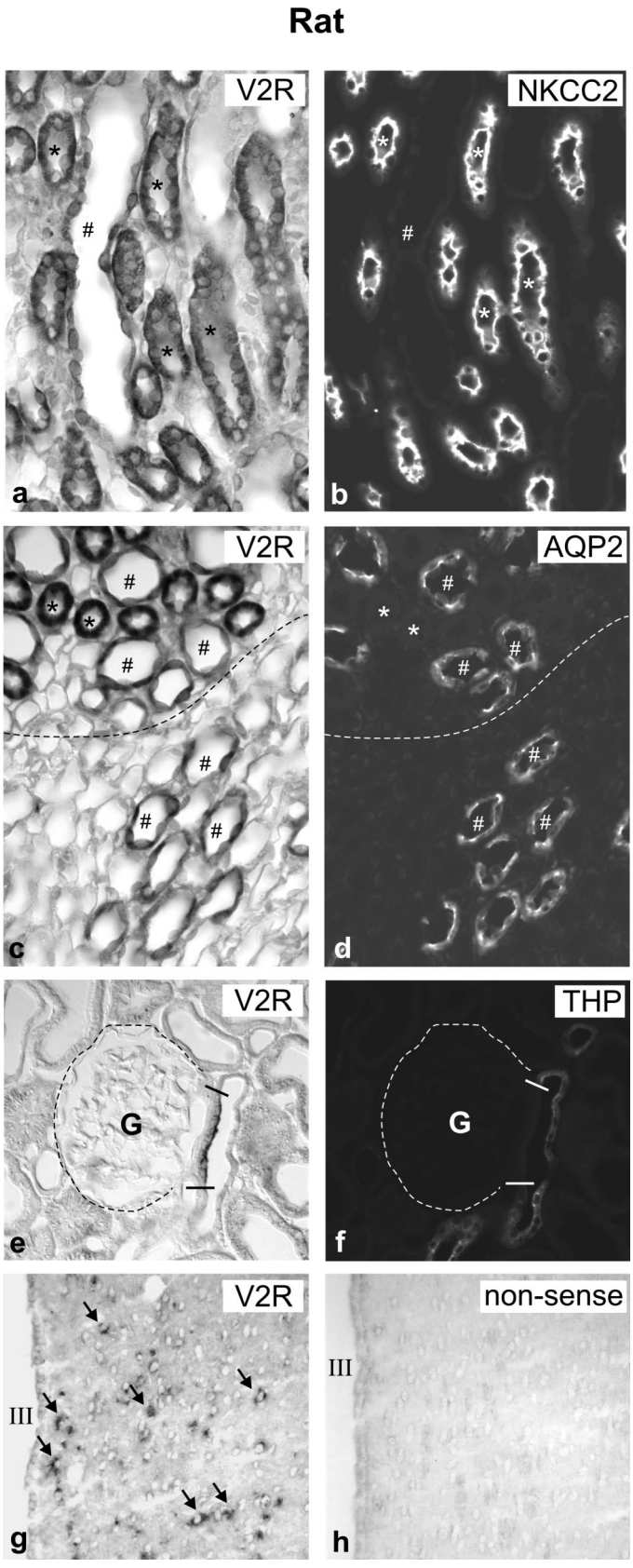

Specific antibody to V_2R showed significant staining of MTAL and CTAL segments across species as well (Figs. 3, *g* and *h*; and Fig. 4, *g* and *h*). Staining was stronger at the luminal than at the basolateral cell aspect and, particularly, in mice showed somewhat less pronounced axial heterogeneity than the mRNA signal.

DCT, CNT, and CCD. In DCT, identified by concomitant NCC immunostaining, there was significant V_2R mRNA expression that was moderately stronger than in the preceding CTAL (Fig. 5, *a–i*; and Fig. 6, *a* and *b*). In the CNT and CCD immunostained by AQP-2, V_2R mRNA signals were of intermediate intensity (Fig. 1). CNT segments were identified by their initial transition from DCT2 immunostained for NCC and 11β-HSD2 or for complementary expression of NCC and AQP-2 (Fig. 5, *a–i*; and Fig. 6, *c* and *d*). The majority of cortical intercalated cells of CNT and CCD, as identified by parallel H^+-ATPase immunostaining, were V_2R mRNA negative; those with cytosolic/basolateral H^+-ATPase staining, likely to correspond to the B phenotype, were generally unstained, whereas those with luminal staining, corresponding to the A phenotype, in part expressed the receptor (Fig. 7, *a–d*).

Medullary vasculature, interstitium, thin limbs, and MCD. Medullary vasculature, interstitium, and thin limbs were devoid of V_2R signal. In the MCD, identified by AQP-2 immunostaining, V_2R mRNA was markedly expressed in all three species, with the strongest label in human kidney (Fig. 2, *c* and *d*; Fig. 3, *c* and *d*; and Fig. 4, *c* and *d*). Medullary type A intercalated cells, identified by basolateral AE1 and apical H^+-ATPase immunoreactivity and lack of AQP-2 signal, strongly expressed V_2R mRNA throughout (Fig. 4, *c* and *d*; and Fig. 7, *e–l*). V_2R expression in MCD and CCD was further confirmed by immunohistochemistry, which revealed a strong signal in MCD and a weaker signal in CCD (Fig. 3*g*; and Fig. 4, *g* and *h*). The strength of the TAL and CD signals was similar. Medullary intercalated cells, as identified by their morphology, demonstrated strong immunoreactive V_2R signal throughout (Fig. 4*g*).

Effects of AVP on TAL transporter. To verify the significant V_2R expression in TAL, we studied AVP-dependent activation of the major TAL ion transporter NKCC2 in AVP-deficient DI rats that had been supplemented with dDAVP for 30 min or had been subjected to 4 h of water deprivation. Distribution and abundance of NKCC2, as well as phosphorylated NKCC2, were evaluated using 2.1 and pT2 antibodies, respectively.

In vehicle-treated DI rats, pT2 signal was not detectable in the medulla, whereas scattered pT2-positive TAL segments were observed in the cortex (Fig. 8, *a, d*, and *g*; Fig. 9, *b* and *f*). Macula densa cells showed selectively stronger expression

Fig. 2. V_2R mRNA distribution in rat kidney. *a* and *b*: Colocalization of V_2R mRNA in MTAL (∗) identified by Na^+-K^+-$2Cl^-$ type 2 cotransporter (NKCC2) immunostaining [antibody against NH_2-terminal 85 amino acids of NKCC2 (2.1)]. V_2R mRNA-positive MCD (#) are negative for NKCC2. *c* and *d*: V_2R mRNA expressing MCD are labeled by aquaporin type 2 (AQP-2) immunostaining, whereas MTAL are negative for AQP-2. Dashed lines, outer-to-inner medullary transitions. *e* and *f*: Juxtaglomerular thick ascending limb (TAL) expressing V_2R mRNA in macula densa (between flanking lines); parallel staining for Tamm-Horsfall protein (THP) in TAL spares macula densa. Glomeruli (G) are shown by dashed lines. *g* and *h*: Labeling of rat brain sections detects V_2R expression in neurons of hypothalamic paraventricular nucleus (arrows in *g*), whereas the nonsense probe does not produce a signal (*h*). III, 3rd ventricle. Original magnification ×400.

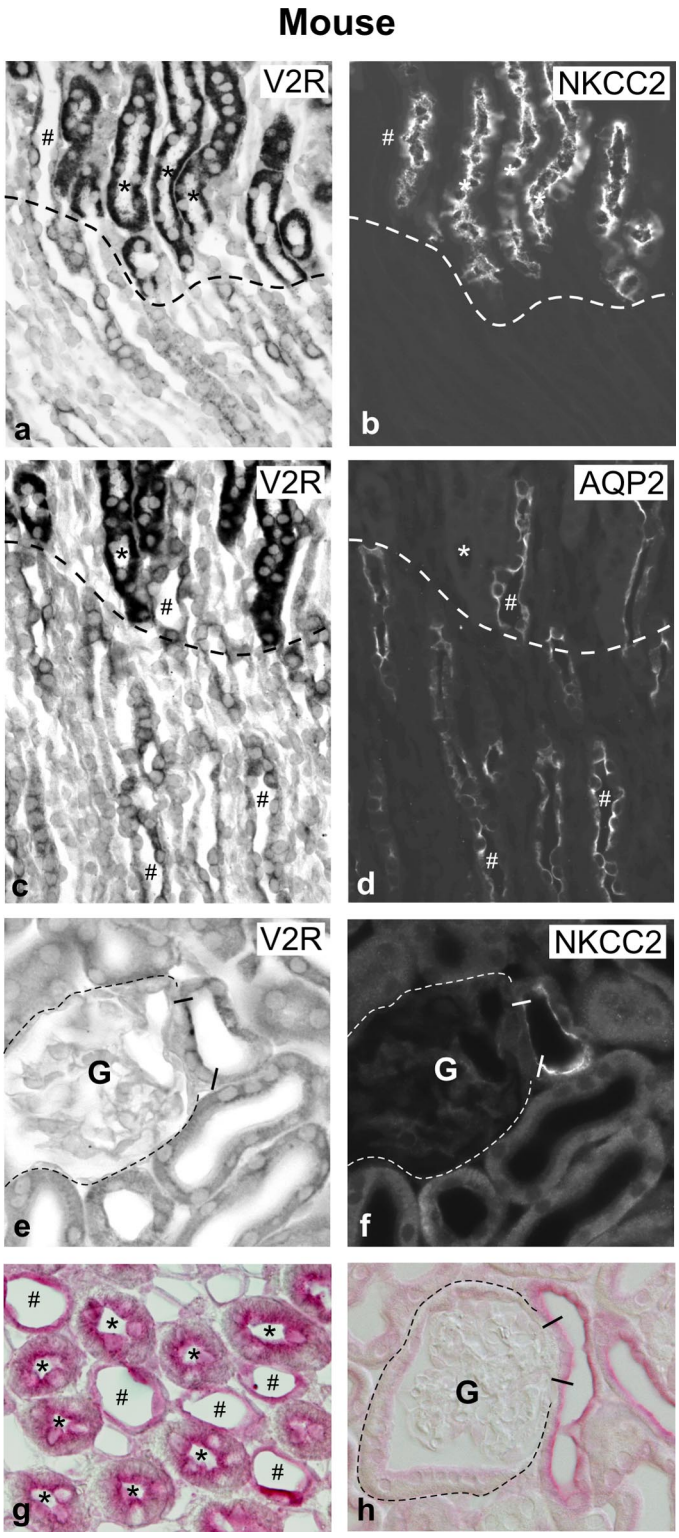

Fig. 3. V_2R distribution in mouse kidney. *a* and *b*: Colocalization of V_2R mRNA in MTAL (*) identified by NKCC2 immunostaining (2.1 antibody). V_2R mRNA-positive MCD (#) are negative for NKCC2. *c* and *d*: V_2R mRNA expressing MCD are labeled by AQP-2 immunostaining, whereas MTAL are negative for AQP-2. Dashed lines, outer-to-inner medullary transitions. *e* and *f*: juxtaglomerular TAL expressing V_2R mRNA in macula densa (between flanking lines) concomitantly immunolabeled for NKCC2; glomeruli (G) are shown by dashed lines. *g* and *h*: Immunohistochemical localization of V_2R in medulla (*g*) and cortex (*h*) showing TAL (*) and collecting duct (CD) profiles (#). Original magnification ×400.

of phosphorylated NKCC2 than adjacent TAL cells (Fig. 9, *i* and *j*). In low-power magnification, stimulation of DI rats with dDAVP resulted in drastic increases of pT2 signal intensities in CTAL and MTAL compared with vehicle treatment (Fig. 8, *a, b, d, e, g*, and *h*), whereas water deprivation for 4 h did not significantly affect NKCC2 phosphorylation (Fig. 8, *c, f*, and *i*). Detailed double-staining analysis revealed moderate increases in 2.1 signals, as opposed to more marked increases in pT2 signals, in single CTAL and MTAL profiles, respectively, upon dDAVP treatment (Fig. 9, *a–h*). pT2 signals on dDAVP-stimulated DI rat kidneys were completely abolished by preincubation with phosphorylated peptide used for immunization during the preabsorption test, whereas application of the nonphosphorylated peptide did not affect the reaction (Fig. 9, *k* and *l*); pT2 band specificity was also demonstrated by Western blot (Fig. 9*m*). These changes were confirmed by Western blot. Cortical and outer medullary kidney samples of vehicle- or dDAVP-treated DI rats were analyzed. dDAVP treatment resulted in augmented 2.1 signals (+79 ± 11% in cortex and +85 ± 11% in outer medulla, $P < 0.05$; Fig. 10, *a, b, g*, and *h*), as well as increased pT2 signals (+86 ± 5% in cortex and +198 ± 18% in outer medulla, $P < 0.005$; Fig. 10, *c, d, g*, and *h*). Data have been normalized for β-actin expression. Quantification of the NKCC2 mRNA in cortical and outer medullary samples did not reveal significant differences between treatments (Fig. 10, *i* and *j*). These results were extended to the study of cultured, immortalized rbTAL cells superfused with vehicle or dDAVP. rbTAL cells express V_2R (unpublished RT-PCR data and Western blot; Fig. 11*a*). Exposure to dDAVP for 30 min resulted in augmented T4 signals (+154 ± 32%, $P < 0.05$), as well as increased pT2 signals (+151 ± 37%, $P < 0.05$; Fig. 11*b*). Data have been normalized for β-actin expression.

Application of pT2 antibody to human kidney resulted in substantial CTAL (Fig. 12*a*) but weak MTAL staining (data not shown). This finding may be related to the functional and endocrine status of the patient's kidney during surgery, possibly preventing medullary activation of NKCC2. By contrast, similar to rodents, human macula densa cells showed a prominent, selective expression of phosphorylated NKCC2 exceeding the level in adjacent CTAL cells (Fig. 12*b*).

DISCUSSION

The present study shows the distribution of V_2R mRNA expression along the nephron in rat, mouse, and human kidneys, complemented with an immunohistochemical approach for detection of the immunoreactive protein. With respect to local AVP signaling in the loop of Henle, V_2R-dependent phosphorylation of NKCC2, reflecting surface expression of the transporter, was studied in TAL. Expression of V_2R was established along the major distal epithelia. Medullary and cortical TAL, macula densa and post-macula segment, distal convolutions, CCD and MCD epithelia, and a subset of type A intercalated cells of the three species expressed V_2R mRNA to distinct degrees of intensity, but with no major interspecies differences. Localization of V_2R mRNA to these epithelia likely reflected sites of receptor biosynthesis, since parallel immunohistochemistry from this and previous work has provided comparable results, and functional studies have, in part, indicated regional heterogeneity in the renal response to AVP

(10, 30, 39, 40). The topographical results have corroborated and extended earlier results obtained in rats by means of labeled ligand binding (20, 35), immunohistochemistry (30, 39), or in situ hybridization (32). We have extended the information on overall V_2R mRNA distribution and its cell-type assignment by analyzing mouse and human kidneys.

The major finding of the present study is the localization of significant V_2R mRNA synthesis to the TAL in the three species, revealing axial heterogeneity with solid expression in the medullary TAL and weak signal along the cortical TAL. This result has previously been obtained in rats at the mRNA (22, 32) and immunoreactive protein (30, 39) levels, although without clear assignment to the particular portions. A heterogeneity in V_2R mRNA signal intensity between long- and short-looped medullary TAL profiles, as reported earlier in rats (30), was not evident from our results; rather, staining was equally strong in all profiles in the three species. Extending molecular localization of V_2R to the mouse and human kidney, we have corroborated the significance of a marked medullary presence of the receptor in TAL across representative mammalian species. Concentration of the V_2R immunoreactive signal at the luminal aspect of TAL across species reflects earlier data from the rat (39) but is at variance with previous demonstration of V_2R signal located predominantly at the basolateral, and less so at the luminal, aspects (30). This difference may be antibody based; however, since, in TAL basolateral membrane, folding is extensive whereas the luminal plasma membrane has little surface amplification, the number of receptors per cell side, reflected by the distinct immunoreactivities, may still be comparable. If we consider the apparent presence of V_2R on both sides of TAL, strong luminal vs. weak basolateral staining may therefore reflect similar receptor densities on each cell pole. Whether this is associated with antagonistic AVP effects of the two locations, as described earlier for the MCD (30), is not clear from the present data.

Our results of a strong V_2R signal in TAL is at variance with another study reporting no V_2R mRNA in the TAL of mice and humans (9). The reason for this discrepancy may be technical, since less-resolving radio-labeled in situ hybridization was used in that study, and it was stated that a diffuse but intensive V_2R mRNA labeling was prevailing in medulla. Distal epithelia may therefore have escaped identification. In terms of specificity and resolution, our findings of rat hypothalamic paraventricular neurons showing distinct V_2R staining have demonstrated the viability of our tools.

Functionally, there is solid evidence of a role for V_2R signaling via cAMP accumulation in medullary ion transport by the TAL, promoting the "single effect" of the countercurrent multiplication as part of the urinary concentrating mechanism (38). In cortical TAL, AVP may further activate Mg^{2+} and Ca^{2+} transport, yet, probably via V_1R (29, 49). The zonal distribution of $V_1R/V_{1a}R$, however, remains obscure (12, 46),

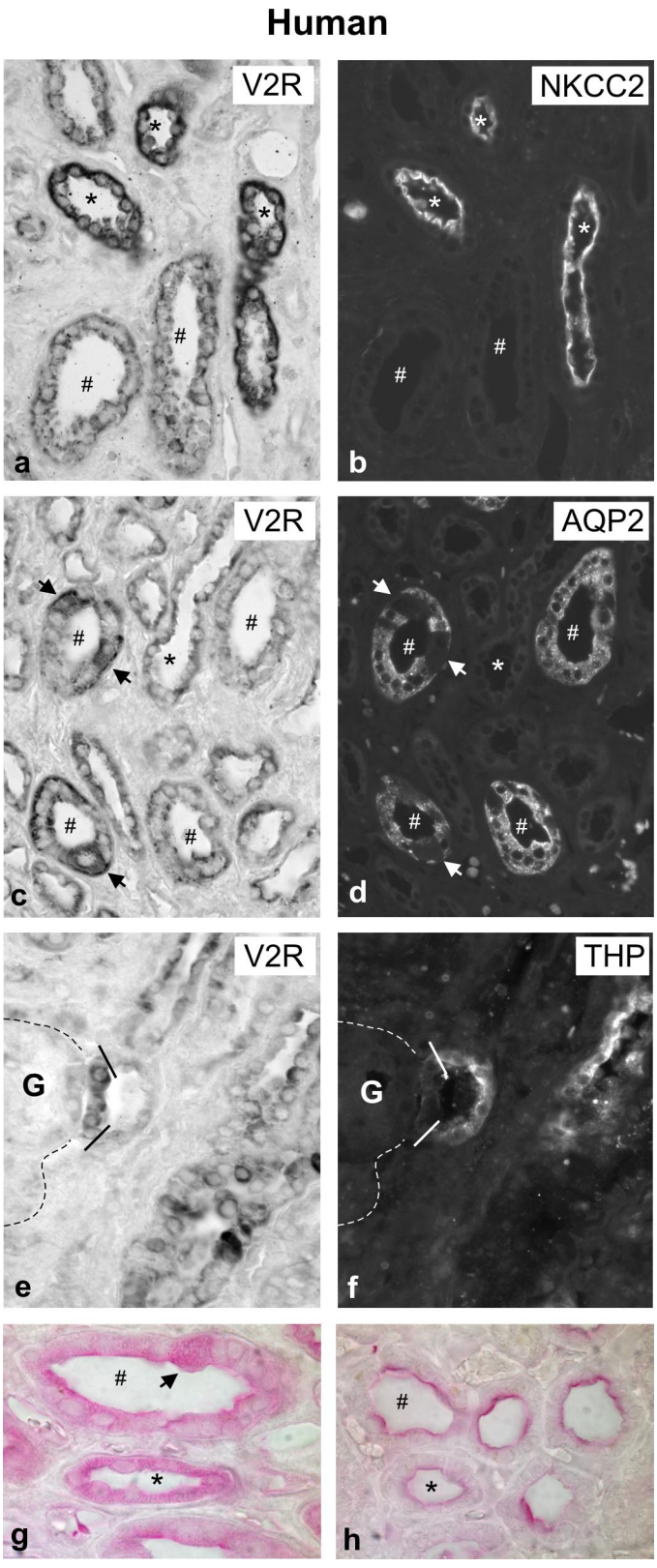

Fig. 4. V_2R distribution in human kidney. *a* and *b*: Colocalization of V_2R mRNA in MTAL (*) identified by NKCC2 immunostaining (2.1 antibody). V_2R mRNA-positive MCD (#) are negative for NKCC2. *c* and *d*: MCD are labeled by AQP-2 immunostaining, whereas MTAL are negative for AQP-2. Arrows point to intercalated cells, which show strong V_2R but no AQP-2 signals. *e* and *f*: Juxtaglomerular TAL with V_2R mRNA expressed in macula densa (between flanking lines) concomitantly immunolabeled for Tamm-Horsfall protein (THP) in CTAL, but not in macula densa; glomerulus (G) is shown by dashed lines. *g* and *h*: Immunohistochemical localization of V_2R in medulla (*g*) and cortex (*h*) showing TAL (*) and CD profiles (#). Arrow points to an intercalated cell (*g*). Original magnification ×400.

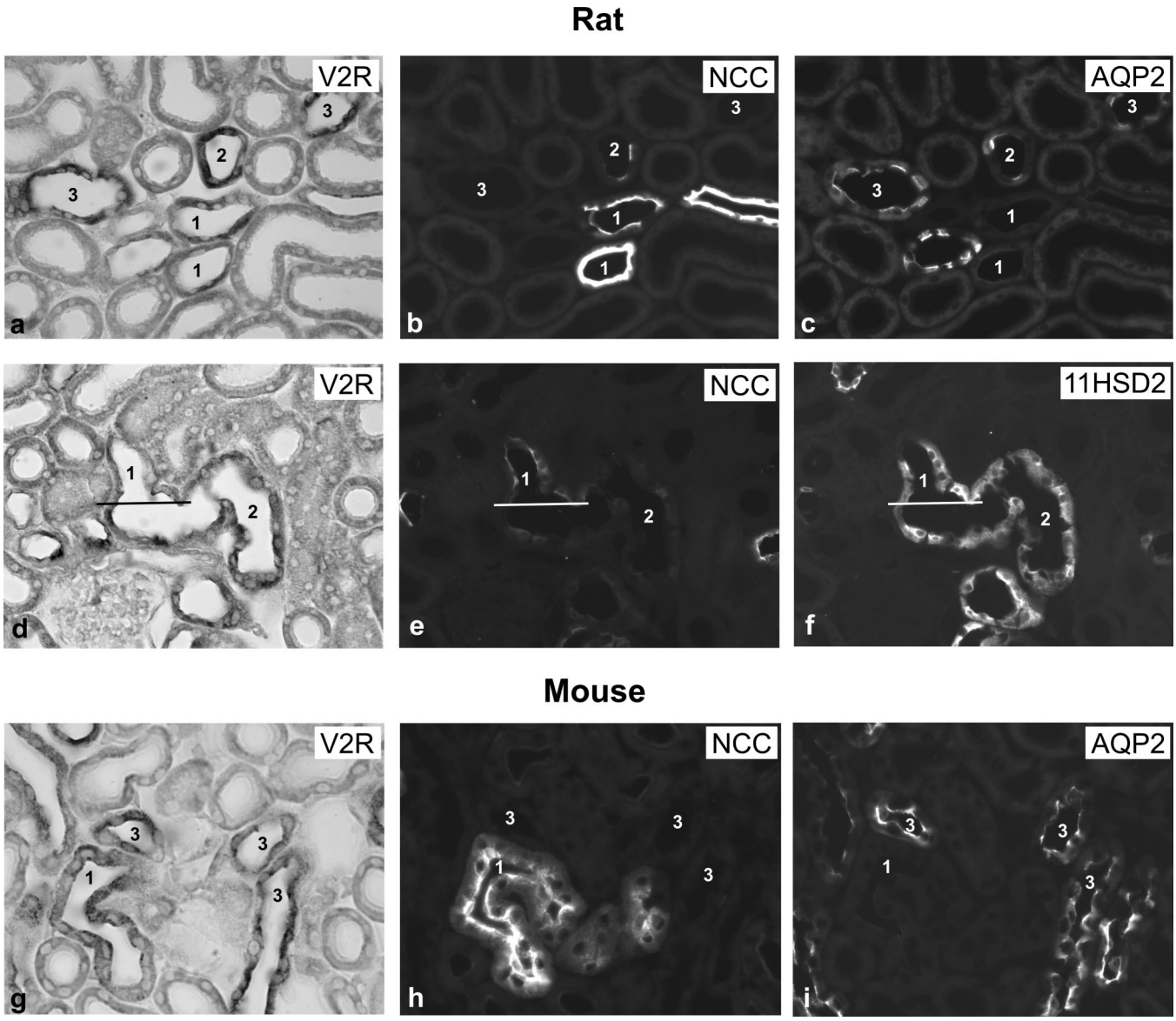

Fig. 5. V_2R mRNA distribution in distal convolutions and collecting ducts of rat (*a–f*) and mouse cortices (*g–i*). Multiple labeling in consecutive serial sections demonstrates low- to medium-intensity V_2R mRNA levels in DCTs (*1*) identified by Na^+-Cl^- cotransporter (NCC), 11β-hydroxysteroid dehydrogenase (11HSD2), and lack of AQP-2. CNT (*2*), the onset of which is defined by mutually exclusive NCC vs. AQP-2 signals or by partial overlap of NCC and 11HSD2, representing DCT-to-CNT transitions (horizontal bars), and NCC-negative AQP-2-positive CCD portions (*3*) showed stronger signals. Original magnification ×400.

and others explicitly found no $V_{1a}R$ transcripts in cortical TAL (9).

Effects of AVP and selective V_2R agonists and antagonists on TAL have been studied with respect to the gene products involved in transepithelial NaCl transport. Significant changes in the expression or phosphorylation state of key Na^+ transporters have been reported (10, 11, 18). In Brattleboro DI rats lacking circulating vasopressin, a decreased steady-state expression of the key ion transporters in TAL was shown to be restored after long-term application of the V_2R agonist dDAVP (10). Also, in the short term, dDAVP exerts significant effects in TAL, driving phosphorylation and apical trafficking of the major TAL transporter NKCC2 in mouse kidney (11, 31). Although this function has earlier been estimated to be relevant only in rodents with their specifically high concentrating ability by some (for review see Ref. 4), the high V_2R expression in the human kidney suggests an analogous, relevant function of AVP in medullary TAL as well. In addition, a parallel, AVP-independent mechanism was postulated on the basis of NKCC2 stimulation in DI rats after short-term water deprivation (23).

To functionally corroborate our data on V_2R expression in TAL, we have studied the short-term induction of NKCC2 by AVP in DI rats regionally, determining the abundance of NKCC2 mRNA, whole protein, and NH_2-terminal threonine phosphorylation. Data were supplemented by the study of our cultured rbTAL cell line, which expresses V_2R and NKCC2. Western blot V_2R signal in rbTAL cells showed an expected, dominant band at ~50 kDa (39); the NKCC2 band generated with the T4 antibody also corresponded to the expected size of 160 kDa (18). In DI rats, there were clear increases in phosphorylated NKCC2 signal along the entire length of the TAL, with a sharper rise in its medullary portion in DI rats. Corre-

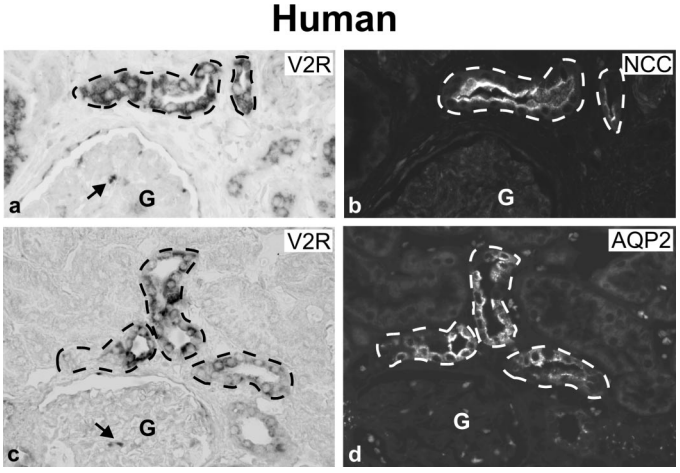

Fig. 6. V_2R mRNA distribution in distal convolutions and collecting ducts of human cortex. *a* and *b*: V_2R mRNA signal in NCC-positive DCTs. *c* and *d*: V_2R mRNA signal in AQP-2-positive CNT/CCD. Dashed lines, positive nephron segments. G, glomeruli. Arrows in *a* and *c* show occasional V_2R mRNA signal in glomerular cells. Original magnification ×400.

sponding changes were found in the rbTAL cells. In part, our observations thus mirror earlier data on NKCC2 trafficking in mice (11). However, at variance with the mouse data, simultaneous increases in the absolute amounts of NKCC2, but not NKCC2 mRNA, were found, possibly reflecting AVP-dependent changes in NKCC2 protein stability or posttranscriptional activation. By contrast, our study failed to reveal an increase of phosphorylated NKCC2 upon water deprivation in the DI rat, which underlines the unique relevance of AVP in TAL transepithelial transport stimulation.

We furthermore found consistent, selectively strong V_2R expression in macula densa cells in all three species. Previously, radiolabeled in situ signal was reported in rat kidney macula densa (32), and possible roles of vasopressin V_1 and oxytocin/oxytocin receptor signaling in macula densa function were highlighted (2, 33). In parallel with V_2R expression, we found high-level baseline signals of phosphorylated NKCC2 in macula densa across species, suggesting that AVP may influence tubuloglomerular signaling via modulation of NKCC2-dependent transpepithelial transport. This observation may be related to AVP-dependent acute changes in glomerular filtration rate in rat kidney (4, 37). However, the detection of selectively high phosphorylated NKCC2 immunoreactivity in DI rat macula densa underscores AVP-independent, constitutive activation of the cotransporter at this site.

Our results of V_2R expression in DCT, CNT, and CCD confirm previous findings in rat (30, 39) and extend the information on the cell-type-specific detail in the three species.

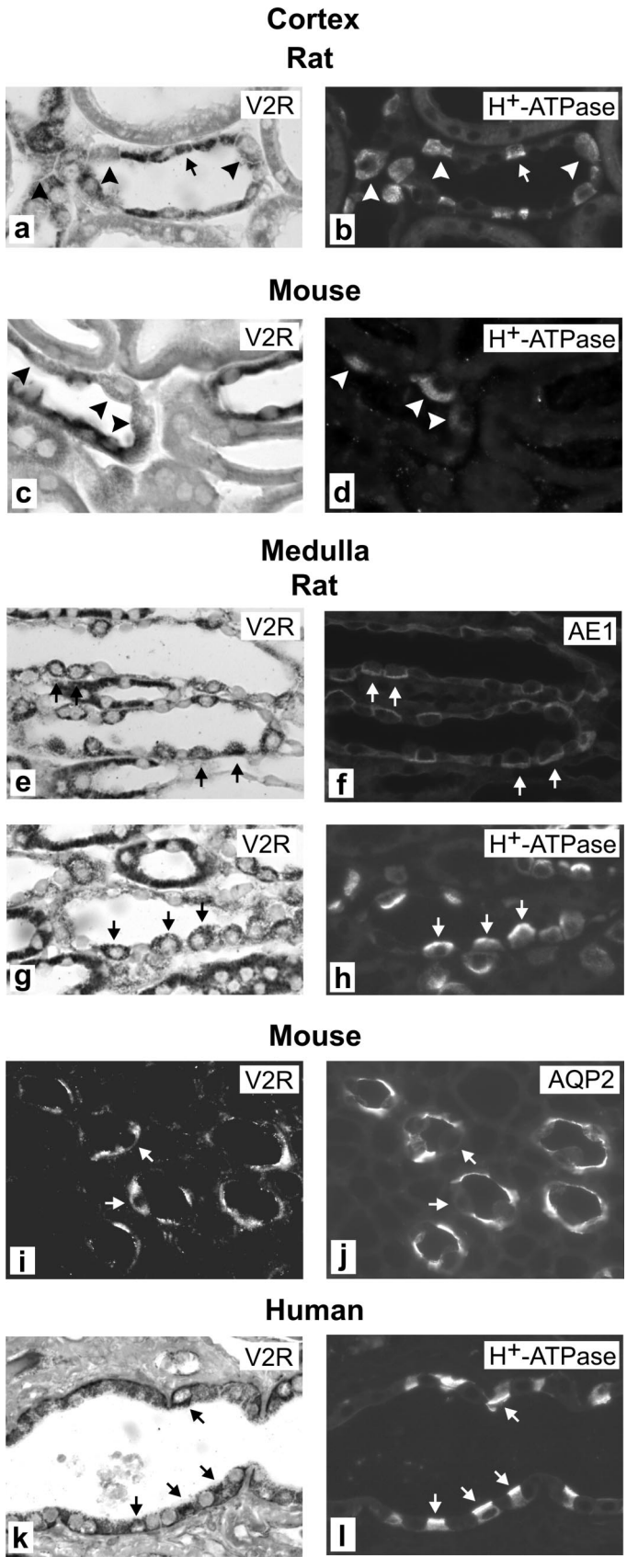

Fig. 7. V_2R expression in medullary and cortical intercalated cells across species. Intercalated cells are identified on consecutive or double-labeled sections immunostained for H^+-ATPase, anion exchanger type 1 (AE1), or AQP-2. Cortical and medullary type A intercalated cells (arrows) are labeled by apical H^+-ATPase or basolateral AE1 antibodies, whereas type B cells (arrowheads) show cytosolic/basolateral expression of H^+-ATPase. Some cortical type A cells express V_2R mRNA; cortical type B cells lack V_2R mRNA (*a*–*d*). Medullary intercalated cells express V_2R mRNA throughout in rat (*e*–*h*), show parallel V_2R-immunoreactive, AQP-2-negative signal in mouse (*i* and *j*), and express V_2R mRNA in human kidney (*k* and *l*). Original magnification ×400.

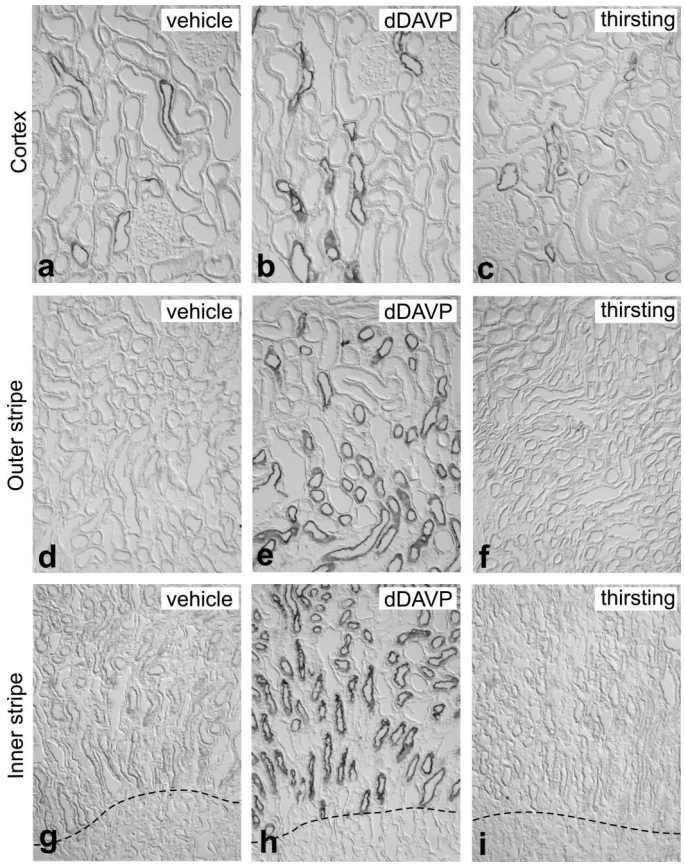

Fig. 8. Comparative overviews of experimentally altered NKCC2 phosphorylation in kidneys of Brattleboro rats with diabetes insipidus (DI) using affinity-purified antibody against phosphorylated NKCC2 (pT2 antibody). Zonal differences between groups are shown in vehicle-treated rats (*a, d*, and *g*), rats treated for 30 min with 1-desamino-8-D-Arg-vasopressin (dDAVP; *b, e*, and *h*), and rats deprived of water for 4 h (*c, f*, and *i*). Dashed lines, outer-to-inner medullary transitions. Original magnification ×200.

Functionally, the presence of V_2R in DCT, at least in its terminal portion (i.e., DCT2) (3), agrees with published data on increased NCC biosynthesis rate upon long-term dDAVP application in rats (10). The presence of mineralocorticoid receptors in DCT, CNT, and CCD and the presence of 11β-HSD2 in DCT2, CNT, and CCD, along with functional data, have underlined local steroid sensitivity of NaCl transport (for review see Refs. 3 and 21). The parallel expression of V_2R and the epithelial Na^+ channel (ENaC), the major distal Na^+ transporter, further emphasizes the manifold hormonal influences on the distal convolutions and collecting system. Functionally, Na^+ transport and ENaC abundance have been shown to increase under cAMP-dependent vasopressin/V_2R stimula-

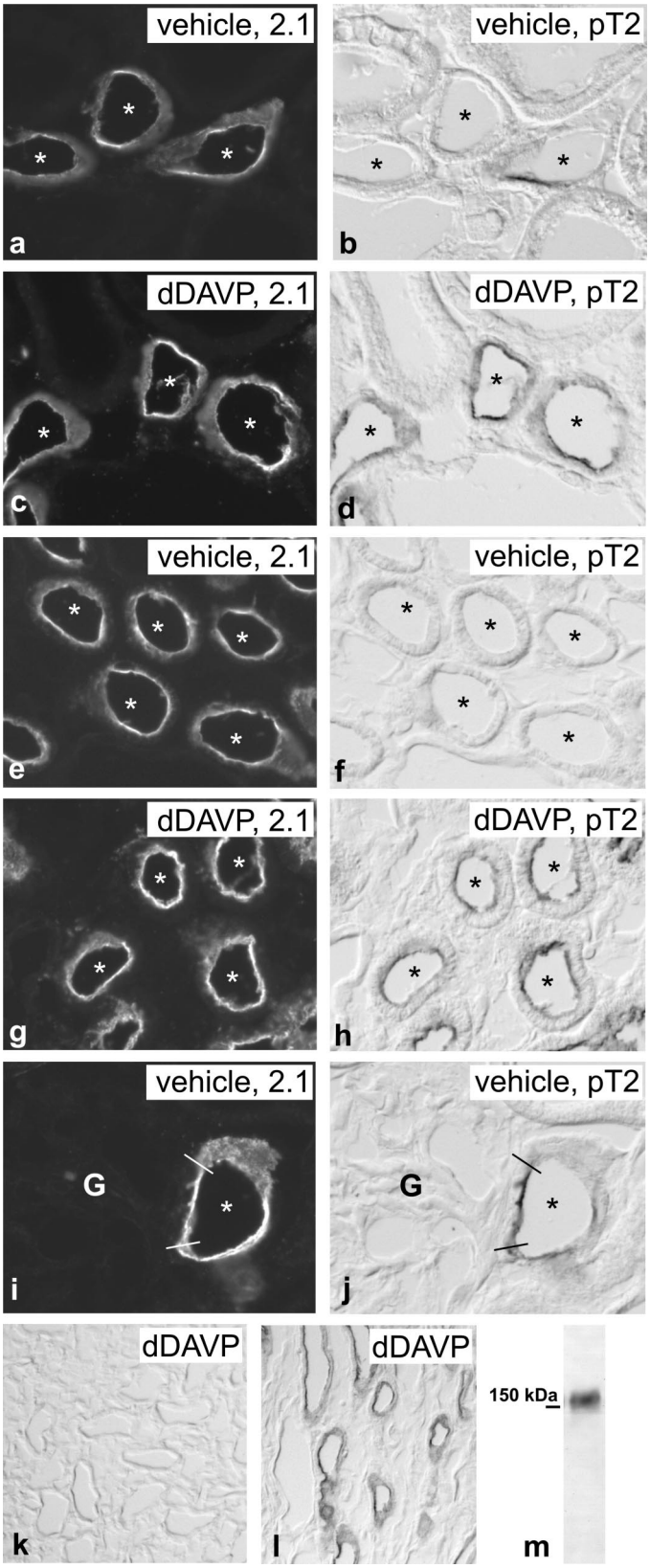

Fig. 9. Representative TAL profiles from vehicle- and dDAVP-treated DI rat kidneys. *a–j*: Image pairs after 2.1 (NKCC2) and pT2 (phosphorylated NKCC2) immunostaining. ∗, Double-stained profiles. *a–d*, Renal cortex; *e–h*, medulla; *i* and *j*, macula densa. Note mild increases in 2.1 signals as opposed to more pronounced increases in pT2 signals after dDAVP stimulation, indicating enhanced NKCC2 phosphorylation. Macula densa at steady state shows selectively high phosphorylated NKCC2 signal; glomerulus (G). Preabsorption of pT2 antibody with use of 10-fold excess of phosphorylated peptide abolished signal (*k*). Nonphosphorylated peptide had no influence on pT2 staining on TAL profiles (*l*). *m*: Single pT2 band on whole lane, Western blot, with size marker indicated. Original magnifications ×400 (*a–j*) and ×200 (*k* and *l*).

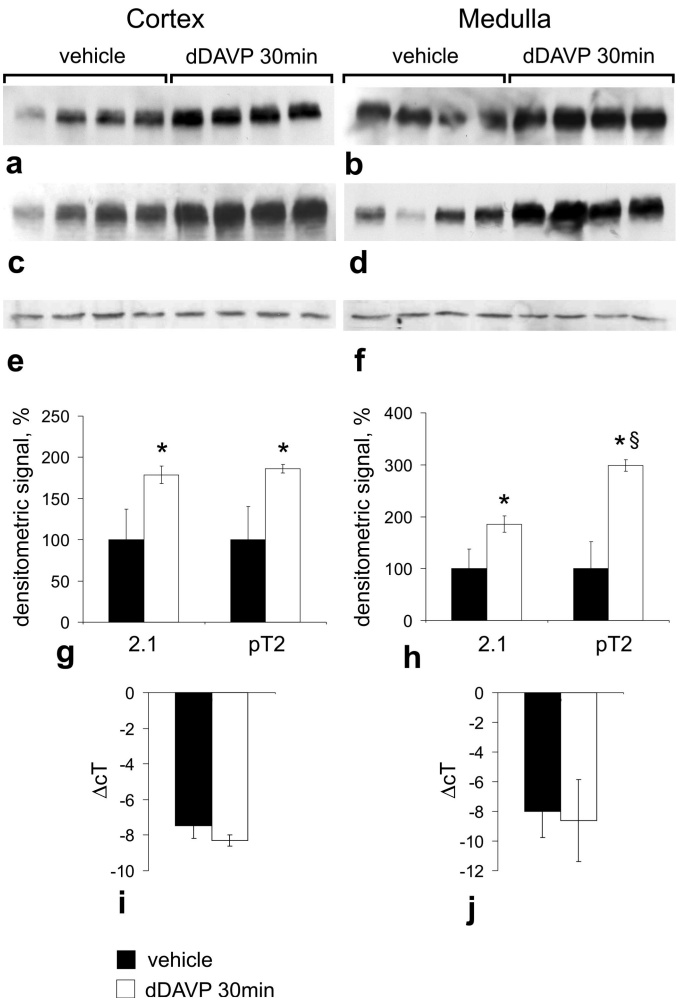

Fig. 10. Western blot and real-time PCR analyses of cortical (*left*) and outer medullary (*right*) tissues from vehicle- and dDAVP-treated DI rats. *a–d*: Representative blots revealing bands for 2.1 (*a* and *b*) and pT2 (*c* and *d*) antibody staining at 160 kDa. *e* and *f*: Loading controls (β-actin-immunoreactive bands). *g* and *h*: respective densitometric evaluations, with vehicle groups set at 100%. Note disproportionately enhanced signal for phosphorylated NKCC2 in medulla of the dDAVP group (*h*). *i* and *j*: Real-time PCR showing cycle threshold difference (ΔC_t) between values obtained for NKCC2 and housekeeping gene GAPDH. $^*P < 0.01$ vs. vehicle. §$P < 0.01$, pT2 vs. 2.1 in dDAVP group.

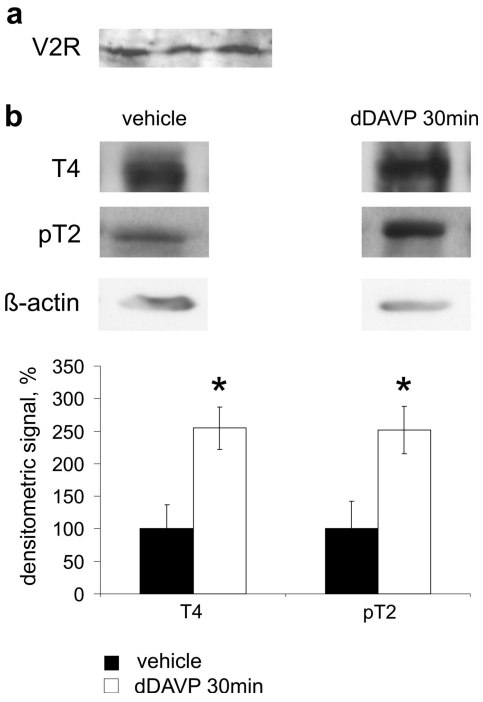

Fig. 11. Western blot analysis showing baseline immunoreactive V_2R levels (*a*) and vehicle vs. dDAVP treatment in TAL cells from rabbit (rbTAL, *b*). *a*: 3 representative bands from independent rbTAL lysates show V_2R at ~50 kDa. *b*: representative blots revealing bands for antibody against COOH-terminal 310 amino acids of NKCC2 (T4) and pT2 antibody staining at 160 kDa, as well as loading controls (β-actin) at 42 kDa (*top*) and respective densitometric evaluations of T4 and pT2 immunoreactivity, with the vehicle groups set at 100% (*bottom*). $^*P < 0.05$ vs. vehicle.

tion (8, 10, 26). A link to the colocalized V_1R expression (39, 46) and its potentially antagonistic role may be relevant with respect to the cellular control of luminal vs. basolateral transport (for review see Ref. 4).

The major function of vasopressin relates to the CD, with the hormone acting at physiological concentrations of 10^{-12} M to exert its antidiuretic actions; the V_2R-dependent effect is coupled to adenylyl cyclase, inducing PKA-mediated phosphorylation of AQP-2 and its translocation to the apical membrane of CD principal cells (for review see Ref. 27). Our findings of moderate cortical and stronger medullary V_2R mRNA expression levels across species agree with earlier histochemical (9, 30, 35, 39) and functional (4, 27) data. Less is known about intercalated cells with respect to AVP-induced signaling. This study has clearly defined that a subset of cortical type A intercalated cells and all medullary type A intercalated cells were expressing V_2R mRNA. Type A intercalated cells may modulate net acid excretion and bicarbonate reabsorption. Acute and chronic effects of vasopressin on acid-base transport have been partially characterized (1, 5, 34). Type A intercalated cells are dominant in the renal medulla (19). At this site, they have been shown to express a newly identified basolateral Cl^-/HCO_3^- exchanger upon dDAVP treatment in DI rats (34), suggesting a possible functional link to V_2R signaling. Type B intercalated cells, which constitute a significant fraction in the CNT and CCD in rat and mouse kidney, were devoid of V_2R mRNA. However, long-term dDAVP application in DI rats had

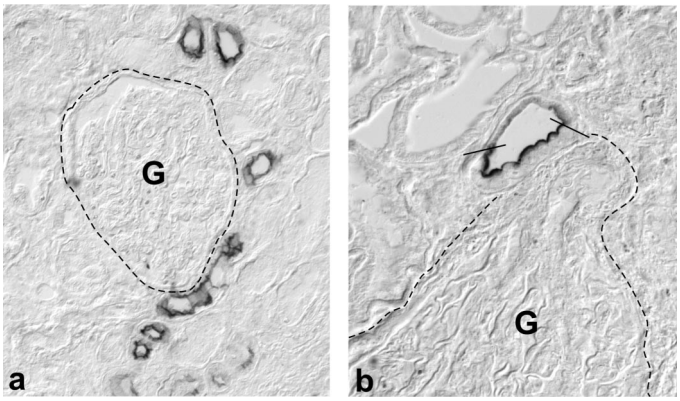

Fig. 12. Localization of phosphorylated NKCC2 in human kidney showing pT2-immunoreactive cortical TAL profiles (*a*) and selectively enhanced labeling of macula densa cells (between flanking lines; *b*). Glomeruli (G) are shown by dashed lines. Original magnification ×400.

marked effects on acid-base transporters also in the type B intercalated cells, possibly owing to the regulatory requirements induced by local solute concentrations (1).

In summary, a comparative, cell-type-oriented analysis of V_2R distribution in rat, mouse, and human kidney has been presented at high resolution. Similar expression patterns have been found across these species. Dominant V_2R expression was observed in medullary TAL and MCD, consistent with the prominent medullary effects of AVP on its major target products, AQP-2 and NKCC2. Functional analysis of AVP-dependent phosphorylation of NKCC2 in the different portions of TAL and cultured rbTAL cells has confirmed the role of V_2R expression in this segment. Our study provides new insights into the organization of renal volume handling.

ACKNOWLEDGMENTS

We thank F. Grams for expert technical assistance.

GRANTS

This project was supported by Deutsche Forschungsgemeinschaft Grant FOR 667.

REFERENCES

1. **Amlal H, Sheriff S, Faroqui S, Ma L, Barone S, Petrovic S, Soleimani M.** Regulation of acid-base transporters by vasopressin in the kidney collecting duct of Brattleboro rat. *Am J Nephrol* 26: 194–205, 2006.
2. **Arpin-Bott MP, Kaissling B, Waltisperger E, Rabhi M, Saussine P, Freund-Mercier MJ, Stoeckel ME.** Historadioautographic localization of oxytocin and V_{1a} vasopressin binding sites in the kidney of developing and adult rabbit, mouse and merione and of adult human. *Exp Nephrol* 10: 196–208, 2002.
3. **Bachmann S, Bostanjoglo M, Schmitt R, Ellison DH.** Sodium transport-related proteins in the mammalian distal nephron—distribution, ontogeny and functional aspects. *Anat Embryol (Berl)* 200: 447–468, 1999.
4. **Bankir L.** Antidiuretic action of vasopressin: quantitative aspects and interaction between V_{1a} and V_2 receptor-mediated effects. *Cardiovasc Res* 51: 372–390, 2001.
5. **Bichara M, Mercier O, Houillier P, Paillard M, Leviel F.** Effects of antidiuretic hormone on urinary acidification and on tubular handling of bicarbonate in the rat. *J Clin Invest* 80: 621–630, 1987.
6. **Biner HL, Arpin-Bott MP, Loffing J, Wang X, Knepper M, Hebert SC, Kaissling B.** Human cortical distal nephron: distribution of electrolyte and water transport pathways. *J Am Soc Nephrol* 13: 836–847, 2002.
7. **Bostanjoglo M, Reeves WB, Reilly RF, Velazquez H, Robertson N, Litwack G, Morsing P, Dørup J, Bachmann S, Ellison DH.** 11β-Hydroxysteroid dehydrogenase, mineralocorticoid receptor, and thiazide-sensitive Na-Cl cotransporter expression by distal tubules. *J Am Soc Nephrol* 9: 347–358, 1998.
8. **Butterworth MB, Edinger RS, Johnson JP, Frizzell RA.** Acute ENaC stimulation by cAMP in a kidney cell line is mediated by exocytic insertion from a recycling channel pool. *J Gen Physiol* 125: 81–101, 2005.
9. **Carmosino M, Brooks HL, Cai Q, Davis LS, Opalenik S, Hao C, Breyer MD.** Axial heterogeneity of vasopressin receptor subtypes along the human and mouse collecting duct. *Am J Physiol Renal Physiol* 292: F351–F360, 2007.
10. **Ecelbarger CA, Kim GH, Wade JB, Knepper MA.** Regulation of the abundance of renal sodium transporters and channels by vasopressin. *Exp Neurol* 171: 227–234, 2001.
11. **Gimenez I, Forbush B.** Short-term stimulation of the renal Na-K-Cl cotransporter (NKCC2) by vasopressin involves phosphorylation and membrane translocation of the protein. *J Biol Chem* 278: 26946–26951, 2003.
12. **Gonzalez CB, Figueroa CD, Reyes CE, Caorsi CE, Troncoso S, Menzel D.** Immunolocalization of V_1 vasopressin receptors in the rat kidney using anti-receptor antibodies. *Kidney Int* 52: 1206–1215, 1997.
13. **Grantham JJ, Burg MB.** Effect of vasopressin and cAMP on permeability of isolated collecting tubules. *Am J Physiol* 211: 255–259, 1966.
14. **Hebert SC, Culpepper RM, Andreoli TE.** NaCl transport in mouse medullary thick ascending limbs. I. Functional nephron heterogeneity and ADH-stimulated NaCl cotransport. *Am J Physiol Renal Fluid Electrolyte Physiol* 241: F412–F431, 1981.
15. **Hebert SC, Andreoli TE.** Effects of antidiuretic hormone on cellular conductive pathways in mouse medullary thick ascending limbs of Henle. II. Determinants of the ADH-mediated increases in transepithelial voltage and in net Cl^- absorption. *J Membr Biol* 80: 221–233, 1984.
16. **Huber S, Asan E, Jöns T, Kerscher C, Püschel B, Drenckhahn D.** Expression of rat kidney anion exchanger 1 in type A intercalated cells in metabolic acidosis and alkalosis. *Am J Physiol Renal Physiol* 277: F841–F849, 1999.
17. **Inoue T, Nonoguchi H, Tomita K.** Physiological effects of vasopressin and atrial natriuretic peptide in the collecting duct. *Cardiovasc Res* 51: 470–480, 2001.
18. **Kim GH, Ecelbarger CA, Mitchell C, Packer RK, Wade JB, Knepper MA.** Vasopressin increases Na-K-2Cl cotransporter expression in thick ascending limb of Henle's loop. *Am J Physiol Renal Physiol* 276: F96–F103, 1999.
19. **Kim J, Kim YH, Cha JH, Tisher CC, Madsen KM.** Intercalated cell subtypes in connecting tubule and cortical collecting duct of rat and mouse. *J Am Soc Nephrol* 10: 1–12, 1999.
20. **Kirk KL, Buku A, Eggena P.** Cell specificity of vasopressin binding in renal collecting duct: computer-enhanced imaging of a fluorescent hormone analog. *Proc Natl Acad Sci USA* 84: 6000–6004, 1987.
21. **Loffing J, Kaissling B.** Sodium and calcium transport pathways along the mammalian distal nephron: from rabbit to human. *Am J Physiol Renal Physiol* 284: F628–F643, 2003.
22. **Lolait SJ, O'Carroll AM, McBride OW, Konig M, Morel A, Brownstein MJ.** Cloning and characterization of a vasopressin V_2 receptor and possible link to nephrogenic diabetes insipidus. *Nature* 357: 336–339, 1992.
23. **Michimata M, Mizukami K, Suzuki M, Kazama I, Nakamura Y, Suzuki K, Yanagisawa T, Imai Y, Sasaki S, Matsubara M.** Vasopressin-independent renal urinary concentration: increased rBSC1 and enhanced countercurrent multiplication. *Kidney Int* 64: 933–938, 2003.
24. **Morel A, O'Carroll AM, Brownstein MJ, Lolait SJ.** Molecular cloning and expression of a rat V_{1a} arginine vasopressin receptor. *Nature* 356: 523–526, 1992.
25. **Morel F.** Sites of hormone action in the mammalian nephron. *Am J Physiol Renal Fluid Electrolyte Physiol* 240: F159–F164, 1981.
26. **Nicco C, Wittner M, DiStefano A, Jounier S, Bankir L, Bouby N.** Chronic exposure to vasopressin upregulates ENaC and sodium transport in the rat renal collecting duct and lung. *Hypertension* 38: 1143–1149, 2001.
27. **Nielsen S, Kwon TH, Christensen BM, Promeneur D, Frokiær J, Marples D.** Physiology and pathophysiology of renal aquaporins. *J Am Soc Nephrol* 10: 647–663, 1999.
28. **Nishimoto G, Zelenina M, Li D, Yasui M, Aperia A, Nielsen S, Nairn AC.** Arginine vasopressin stimulates phosphorylation of aquaporin-2 in rat renal tissue. *Am J Physiol Renal Physiol* 276: F254–F259, 1999.
29. **Nitschke R, Frobe U, Greger R.** Antidiuretic hormone acts via V_1 receptors on intracellular calcium in the isolated perfused rabbit cortical thick ascending limb. *Pflügers Arch* 417: 622–632, 1991.
30. **Nonoguchi H, Owada A, Kobayashi N, Takayama M, Terada Y, Koike J, Ujiie K, Marumo F, Sakai T, Tomita K.** Immunohistochemical localization of V_2 vasopressin receptor along the nephron and functional role of luminal V_2 receptor in terminal inner medullary collecting ducts. *J Clin Invest* 96: 1768–1778, 1995.
31. **Ortiz PA.** cAMP increases surface expression of NKCC2 in rat thick ascending limbs: role of VAMP. *Am J Physiol Renal Physiol* 290: F608–F616, 2006.
32. **Ostrowski NL, Young WS 3rd, Knepper MA, Lolait SJ.** Expression of vasopressin V_{1a} and V_2 receptor messenger ribonucleic acid in the liver and kidney of embryonic, developing, and adult rats. *Endocrinology* 133: 1849–1859, 1993.
33. **Ostrowski NL, Lolait SJ.** Oxytocin receptor gene expression in female rat kidney. The effect of estrogen. *Adv Exp Med Biol* 395: 329–340, 1995.
34. **Petrovic S, Amlal H, Sun X, Karet F, Barone S, Soleimani M.** Vasopressin induces expression of the Cl^-/HCO_3^- exchanger SLC26A7 in kidney medullary collecting ducts of Brattleboro rats. *Am J Physiol Renal Physiol* 290: F1194–F1201, 2006.
35. **Phillips PA, Abrahams JM, Kelly JM, Mooser V, Trinder D, Johnston CI.** Localization of vasopressin binding sites in rat tissues using specific V_1 and V_2 selective ligands. *Endocrinology* 126: 1478–1484, 1990.
36. **Promeneur D, Kwon TH, Frokiær J, Knepper MA, Nielsen S.** Vasopressin V_2-receptor-dependent regulation of AQP2 expression in Brattleboro rats. *Am J Physiol Renal Physiol* 279: F370–F382, 2000.

37. **Roald AB, Tenstad O, Aukland K.** The effect of AVP-V_2 receptor stimulation on local GFR in the rat kidney. *Acta Physiol Scand* 168: 351–359, 2000.
38. **Sands JM, Kokko JP.** Current concepts of the countercurrent multiplication system. *Kidney Int Suppl* 57: S93–S99, 1996.
39. **Sarmiento JM, Ehrenfeld P, Anazco CC, Reyes CE, Troncoso S, Figueroa CD, Müller-Esterl W, Gonzalez CB.** Differential distribution of the vasopressin V_2 receptor along the rat nephron during renal ontogeny and maturation. *Kidney Int* 68: 487–496, 2005.
40. **Sauter D, Fernandes S, Goncalves-Mendes N, Boulkroun S, Bankir L, Loffing J, Bouby N.** Long-term effects of vasopressin on the subcellular localization of ENaC in the renal collecting system. *Kidney Int* 69: 1024–1032, 2006.
41. **Schmitt R, Ellison DH, Klussmann E, Bachmann S.** Renal expression of sodium transporters and aquaporin-2 in hypothyroid rats. *Am J Physiol Renal Physiol* 284: F1097–F1104, 2003.
42. **Schmitt R, Kahl T, Mutig K, Bachmann S.** Selectively reduced expression of thick ascending limb Tamm-Horsfall protein in hypothyroid kidneys. *Histochem Cell Biol* 121: 319–327, 2004.
43. **Serradeil-Le Gal C, Wagnon J, Valette G, Garcia G, Pascal M, Maffrand JP, Le Fur G.** Nonpeptide vasopressin receptor antagonists: development of selective and orally active V_{1a}, V_2 and V_{1b} receptor ligands. *Prog Brain Res* 139: 197–210, 2002.
44. **Stoeckel ME, Freund-Mercier MJ, Palacios JM, Richard P, Porte A.** Autoradiographic localization of binding sites for oxytocin and vasopressin in the rat kidney. *J Endocrinol* 113: 179–182, 1987.
45. **Stoeckel ME, Freund-Mercier MJ.** Autoradiographic demonstration of oxytocin-binding sites in the macula densa. *Am J Physiol Renal Fluid Electrolyte Physiol* 257: F310–F314, 1989.
46. **Tashima Y, Kohda Y, Nonoguchi H, Ikebe M, Machida K, Star RA, Tomita K.** Intranephron localization and regulation of the V_{1a} vasopressin receptor during chronic metabolic acidosis and dehydration in rats. *Pflügers Arch* 442: 652–661, 2001.
47. **Terada Y, Tomita K, Nonoguchi H, Yang T, Marumo F.** Different localization and regulation of two types of vasopressin receptor messenger RNA in microdissected rat nephron segments using reverse transcription polymerase chain reaction. *J Clin Invest* 92: 2339–2345, 1993.
48. **Welker P, Geist B, Frühauf JH, Salanova M, Groneberg DA, Krause E, Bachmann S.** Role of lipid rafts in membrane delivery of renal epithelial Na^+,K^+-ATPase, thick ascending limb. *Am J Physiol Regul Integr Comp Physiol* 293: R1328–R1337, 2007.
49. **Wittner M, di Stefano A, Wangemann P, Nitschke R, Greger R, Bailly C, Amiel C, Roinel N, de Rouffignac C.** Differential effects of ADH on sodium, chloride, potassium, calcium and magnesium transport in cortical and medullary thick ascending limbs of mouse nephron. *Pflügers Arch* 412: 516–523, 1988.
50. **Yang J, Chen JM, Song CY, Liu WY, Wang G, Wang CH, Lin BC.** Through the central V_2, not V_1 receptors influencing the endogenous opiate peptide system, arginine vasopressin, not oxytocin in the hypothalamic paraventricular nucleus involves in the antinociception in the rat. *Brain Res* 1069: 127–138, 2006.

3.2 Short-term stimulation of the thiazide-sensitive Na+-Cl- cotransporter by vasopressin involves phosphorylation and membrane translocation.

Mutig K, Saritas T, Uchida S, Kahl T, Borowski T, Paliege A, Böhlick A, Bleich M, Shan Q, Bachmann S.

***Am J Physiol Renal Physiol.* 2010 Mar;298(3):F502-9.**

Substantial V2R expression along the entire distal nephron has been established in our previous work (see 3. 1). These findings were the prerequisite for the present study which addresses the effects of AVP in DCT. The V2 receptor agonist dDAVP was administered in Brattleboro rats deficient for AVP, as well as in isolated DCT tubules. As the major readout of this treatment, surface expression and activating phosphorylation of NCC were evaluated. Due to complete absence of circulating AVP at baseline, Brattleboro rats exhibit a rapid and prominent response to the extrinsic stimulation of the AVP/V2R axis which renders them a valuable model for evaluation of the effects of the hormone. The use of isolated DCT segments permitted us to evaluate the direct effects of V2R activation in the absence of potential systemic adaptations. Short term application of dDAVP produced rapid and substantial increases of NCC phosphorylation in both settings, suggesting that AVP-induced activation of NCC is, at least in part, directly mediated by V2R activation in DCT. In addition, dDAVP induced a moderate, albeit significant increase of NCC surface expression *in vivo*. Since transport activity of NCC ultimately depends on its surface expression and phosphorylation, we concluded that AVP stimulates NaCl reabsorption in DCT. Results of the present study provide new insights into the role of AVP in renal salt handling and therefore contribute to the understanding of volume regulation and blood pressure control by the kidney [23].

Am J Physiol Renal Physiol 298: F502–F509, 2010.
First published December 9, 2009; doi:10.1152/ajprenal.00476.2009.

Short-term stimulation of the thiazide-sensitive Na^+-Cl^- cotransporter by vasopressin involves phosphorylation and membrane translocation

K. Mutig,[1] T. Saritas,[1] S. Uchida,[2] T. Kahl,[1] T. Borowski,[1] A. Paliege,[1] A. Böhlick,[1] M. Bleich,[3] Q. Shan,[3] and S. Bachmann[1]

[1]*Department of Anatomy, Charité Universitätsmedizin, Berlin;* [3]*Department of Physiology, Christian-Albrechts-Universität, Kiel, Germany; and* [2]*Department of Nephrology, Tokyo Medical and Dental University, Tokyo, Japan*

Submitted 17 August 2009; accepted in final form 2 December 2009

Mutig K, Saritas T, Uchida S, Kahl T, Borowski T, Paliege A, Böhlick A, Bleich M, Shan Q, Bachmann S. Short-term stimulation of the thiazide-sensitive Na^+-Cl^- cotransporter by vasopressin involves phosphorylation and membrane translocation. *Am J Physiol Renal Physiol* 298: F502–F509, 2010. First published December 9, 2009; doi:10.1152/ajprenal.00476.2009.—Vasopressin influences salt and water transport in renal epithelia. This is coordinated by the combined action of V_2 receptor-mediated effects along distinct nephron segments. Modulation of NaCl reabsorption by vasopressin has been established in the loop of Henle, but its role in the distal convoluted tubule (DCT), an effective site for fine regulation of urinary electrolyte composition and the target for thiazide diuretics, is largely unknown. The Na^+-Cl^- cotransporter (NCC) of DCT is activated by luminal trafficking and phosphorylation at conserved NH_2-terminal residues. Here, we demonstrate the effects of short-term vasopressin administration (30 min) on NCC activation in Brattleboro rats with central diabetes insipidus (DI) using the V_2 receptor agonist desmopressin (dDAVP). The fraction of NCC abundance in the luminal plasma membrane was significantly increased upon dDAVP as shown by confocal microscopy, immunogold cytochemistry, and Western blot, suggesting increased apical trafficking of the transporter. Changes were paralleled by augmented phosphorylation of NCC as detected by antibodies against phospho-threonine and phospho-serine residues (2.5-fold increase at Thr53 and 1.4-fold increase at Ser71). dDAVP-induced phosphorylation of NCC, studied in tubular suspensions in the absence of systemic effects, was enhanced as well (1.7-fold increase at Ser71), which points to the direct mode of action of vasopressin in DCT. Changes were more pronounced in early (DCT1) than in late DCT as distinguished by the distribution of 11β-hydroxysteroid dehydrogenase 2 in DCT2. These results suggest that the vasopressin-V_2 receptor-NCC signaling cascade is a novel effector system to adjust transepithelial NaCl reabsorption in DCT.

antidiuretic hormone; distal convoluted tubule; phosphorylation; sodium-chloride cotransporter trafficking

ANTIDIURETIC HORMONE [arginine vasopressin (AVP)] serves to control extracellular fluid homeostasis. The principal effect of AVP is found in the collecting duct where AVP increases water reabsorption. The prerequisite to ensure this function is the creation of a hypertonic interstitium via action of the thick ascending limb (TAL), which is also promoted by AVP. These epithelial effects of AVP are mediated by type 2 AVP receptors (V_2R) (2, 29), whereas type 1a receptor signaling rather serves to limit the antidiuretic effects of AVP (31). Mapping receptor-specific probes to the tubular segments has revealed subtype-selective distribution along TAL, macula densa, distal convolutions, and collecting ducts (3, 28). In TAL, strong V_2R expression has been observed, which agreed with increased abundance and phosphorylation of the furosemide-sensitive Na^+-K^+-$2Cl^-$ cotransporter (NKCC2) and enhanced NaCl reabsorption in TAL in response to AVP (8, 13, 28). V_2R signaling also activates epithelial Na^+ channel (ENaC)-dependent Na^+ reabsorption in collecting ducts (16); AVP-induced antinatriuresis in this segment has therefore been considered as a causal element in the context of salt-sensitive hypertension (23).

Significant V_2R expression has also been mapped to the distal convoluted tubule (DCT) (28), the site of the thiazide-sensitive Na^+-Cl^- cotransporter (NCC). The functional relevance of V_2R expression in this nephron segment is not clear. Like in TAL, AVP signaling likely occurs via $G\alpha_s$-coupled V_2R and cAMP release (25), but DCT cell culture experiments on the role of cAMP were inconclusive (14). Chronic AVP substitution in vasopressin-deficient Brattleboro rats with central diabetes insipidus (DI) using V_2R agonist markedly augmented the abundance of NCC (8), suggesting AVP sensitivity within DCT. However, the action of aldosterone may be involved as well under this condition (8), leading to an activation of NCC and ENaC along the terminal, preferentially mineralocorticoid-sensitive portion of DCT (DCT2) (1, 24, 26). Aldosterone-induced activation of NCC via specific phosphokinases has been demonstrated (5).

NKCC2 and NCC are the principal renal members of the electroneutral cation-Cl^- cotransporter family (CCC) (11). The two proteins share significant structural homology, and extensive work has established that they can be activated by common mechanisms that include their surface expression and phosphorylation of conserved NH_2-terminal threonines (13, 30, 33, 34, 36, 39). For NCC, an additional activating phosphorylation site (Ser71) has been identified (5). Phosphorylation of NKCC2 and NCC also utilizes the same pathways involving the serine/threonine kinases, with no lysine K (WNK) and STE20/SPS1-related Pro/Ala-rich kinase (SPAK) (5, 6, 24, 34).

The substantial contribution of AVP to activate NKCC2 led us to hypothesize the existence of a similar, V_2R-mediated pathway regulating the activity of the related NCC. To clarify this issue, short-term effects of the V_2R agonist desmopressin (dDAVP) on NCC trafficking and phosphorylation steps were studied in rats. Our results demonstrate significant increases of NCC surface expression and phosphorylation in response to V_2R stimulation. Vasopressin-dependent activation of salt reabsorption in the DCT may therefore be regarded as a novel, potentially powerful component in renal volume conservation.

Address for reprint requests and other correspondence: S. Bachmann, Institut für Vegetative Anatomie, Charité-Universitätsmedizin Berlin, Campus Charité-Mitte, Philippstr. 12, D-10115 Berlin, Germany (e-mail: sbachm@charite.de).

MATERIALS AND METHODS

Animals, tissues, treatments. Adult (10–12 wk) male Brattleboro rats with central DI (Harlane; $n = 25$) and Wistar rats ($n = 4$) were obtained from the local animal facility (Charité Berlin) and kept on standard diet and tap water. DI rats received dDAVP by intraperitoneal injection [1 ng/g body wt or 0.3 pg/g body wt or vehicle (saline)]. After 30 min, rats were separated for morphological or biochemical analysis. For morphology, rats were anesthetized by an intraperitoneal injection of pentobarbital sodium (0.06 mg/g body wt). The kidneys were perfused retrogradely through the abdominal aorta using PBS/sucrose adjusted to 330 mosmol/kgH_2O, pH 7.4, for 20 s, followed by 3% paraformaldehyde in PBS for 5 min. Kidneys were removed, dissected, and shock-frozen in liquid nitrogen-cooled isopentane. For biochemical analysis, rats were killed, the kidneys were removed, and cortex and outer medulla were dissected. To prepare suspensions of renal tubules, pieces of cortex from Wistar rats were digested with a mix of type II collagenase (306 U/ml; Pan Biotech) and type XIV protease (9.4 U/ml; Sigma) for 15 min at 37°C. The resulting tubular suspensions were washed and then incubated with dDAVP (10^{-6} M) in renal epithelial growth medium (REGM; Lonza) or REGM alone. Suspensions were kept at 37°C for 30 min under agitation and then fixed in 3% paraformaldehyde and placed on microscopic slides coated with poly-L-lysine for immunohistochemical analysis. All experiments were approved by the Berlin Senate (GO 062/05).

Immunohistochemistry. Rabbit antisera directed against NH_2-terminal phosphorylation sites of rat NCC (anti-phospho-Thr53 [pT53-NCC] and anti-phospho-Ser71 [pS71-NCC]; both 1:1,500 dilution) (5, 40), guinea pig anti-NKCC2 antibody directed against NH_2-terminal 85 amino acids (1:1,000 dilution; gift from D. H. Ellison, Portland, Oregon) (28), rabbit anti-NCC antibody (1:1,000 dilution; gift from D. H. Ellison) (28), and sheep anti-11β-hydroxysteroid dehydrogenase 2 (11HSD2) antibody (1:500 dilution; Chemicon) were the primary antibodies used. Sets of cryostat sections from each experiment were processed exactly in the same fashion with samples from the compared groups placed on the same slide. Sections or tubular suspensions were incubated with blocking medium (30 min), followed by primary antibody diluted in blocking medium (1 h). For multiple staining, antibodies were sequentially applied, separated by a washing step. Fluorescent Cy2- or Cy3-conjugated antibodies (DIANOVA) were applied for detection. Sections were evaluated in a Leica DMRB microscope or a Zeiss confocal microscope (LSM 710) and ZEN-software (Zeiss). Evaluation of luminal pS71-NCC immunoreactive signal intensity was performed in a standardized approach within a nonsaturated range of signal intensity, using constant optical field dimensions for all measurements.

Ultrastructural analysis. For immunogold evaluation of NCC, perfusion-fixed kidneys were embedded in LR White resin. Ultrathin sections were incubated with anti-NCC antibody. Signal was detected with 5 nm nanogold-coupled secondary antibody (Amersham). With the use of transmission electron microscopy, immunogold signal in DCT (DCT1 and DCT2) was quantified by counting gold particles over the luminal plasma membrane or cytoplasmic vesicular compartment. Evaluation was performed in a blinded fashion. Quantification of NCC signals was performed on micrographs recorded at ×16,700 and printed at ×50,000 magnification according to an established protocol (38, 39). At least 10 DCT profiles containing an average of 5 cells/profile were evaluated per individual. Gold particles were attributed to the apical cell membrane when located near (within 20 nm of distance) or within the bilayer; particles found below 20 nm of distance to the membrane up to a depth of 2 μm or until the nuclear envelope were assigned to cytoplasmic localization.

Western blot. Procedures were as described previously (37). Briefly, kidney cortices were excised and homogenized in buffer containing 250 mM sucrose, 10 mM triethanolamine, protease inhibitors (Complete; Roche Diagnostics), and phosphatase inhibitors (Phosphatase Inhibitor Cocktail 1; Sigma) (pH 7.5). The homogenates

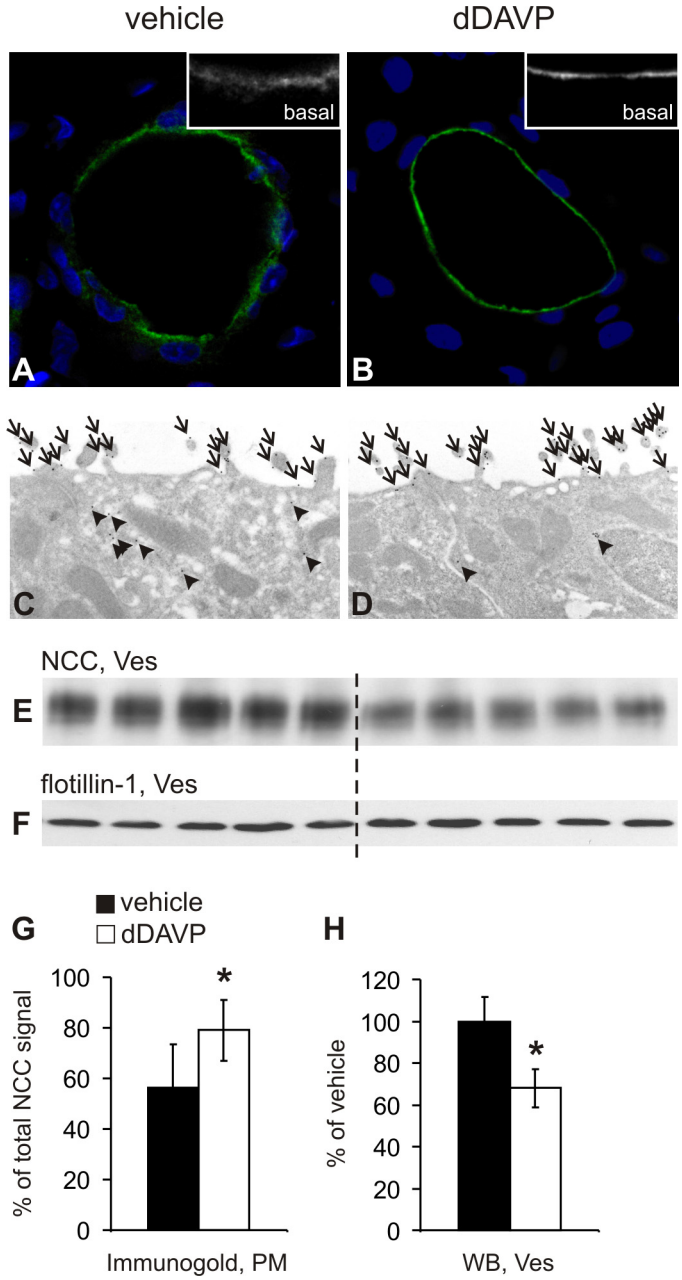

Fig. 1. Effects of desmopressin (dDAVP) on intracellular distribution of Na^+-Cl^- cotransporter (NCC). *A* and *B*: representative confocal images of early distal convoluted tubule [DCT1; as identified by the absence of 11β-hydroxysteroid dehydrogenase 2 (11HSD2)] from Brattleboro rats with central diabetes insipidus (DI) showing signal for NCC (green) and counterstained nuclei (blue); note the shift of staining from diffuse, cytoplasmic to strictly luminal upon type 2 vasopressin receptor (V_2R) agonist dDAVP. *Insets*: high resolution of the apical cell aspect. *C* and *D:* NCC signal (5 nm gold particles) at apical membrane (arrows) and subapical vesicles (arrowheads) of DCT; note enhanced luminal signal upon dDAVP. *E* and *F:* Western blots (WB) showing NCC immunoreactivity (~160 kDa) in vesicle-enriched fractions from kidney cortex (Ves; *E*) with corresponding loading controls (*F*; flotillin-1, ~48 kDa). *G*: numerical evaluation of NCC immunogold signal at the plasma membrane (PM). *H*: densitometry of Western blot signals. Data are means ± SD from $n = 5$ rats/group; $^*P < 0.05$; original magnification ×630 (*A* and *B*) and ×16,700 (*C* and *D*).

were subjected to sequential centrifugation steps to obtain postnuclear fractions by removing nuclei (1,000 *g*, 15 min) and vesicle-enriched fractions (removal of the large plasma membrane fragments at 17,000 *g* for 1 h and subsequent spinning at 200,000 *g* for 1 h). Pellets containing the vesicle-enriched fractions were separated in 8% polyacrylamide minigels, electrophoretically transferred to polyvinylidene fluoride membranes, and analyzed using primary antibodies against NCC (diluted 1:500), pS71-NCC (1:300), pT53-NCC (1:300), flotillin-1 (1:10,000; BD Biosciences), or β-actin (1:20,000; Sigma), horseradish peroxidase-conjugated secondary antibodies (1:3,000; Dako Cytomation), induction of chemiluminescence, exposure of X-ray films, and densitometric evaluation. Signals from the vesicle-enriched fractions were normalized for flotillin-1 as a membrane resident protein; signals from the postnuclear fractions were normalized for β-actin. The linear range of the detection was controlled by reducing the load of the postnuclear homogenates to 50%, which produced corresponding decreases of target protein (NCC: $-58.5 \pm 26\%$; $P < 0.05$) and loading control (β-actin: $-57 \pm 9\%$; $P < 0.05$) [Supplemental Fig. 1 (Supplemental data for this article can be found on the *American Journal of Physiology: Renal Physiology* website.]).

Bands obtained with pT53-NCC and pS71-NCC antibodies at 160 kDa corresponded to NCC monomers, those above 250 kDa to multimers (data not shown) (40). Both revealed similar changes in treated and control samples. However, because reducing conditions were used, only the monomer bands were used for safer densitometric evaluation.

Analysis of data. Results were evaluated using routine parametric descriptive statistics. Groups were compared with two-way ANOVA and *t*-tests, Bonferroni corrected as appropriate. A probability level of $P < 0.05$ was accepted as significant. Values are given as means ± SD.

RESULTS

Effects of dDAVP on NCC trafficking. In TAL, short-term administration of vasopressin induces significant trafficking of NKCC2 to the luminal membrane in mouse (13) and rat kidney (28, 44), which agrees with the significant expression of V_2R at this site. Assuming that similar changes occur in DCT, the

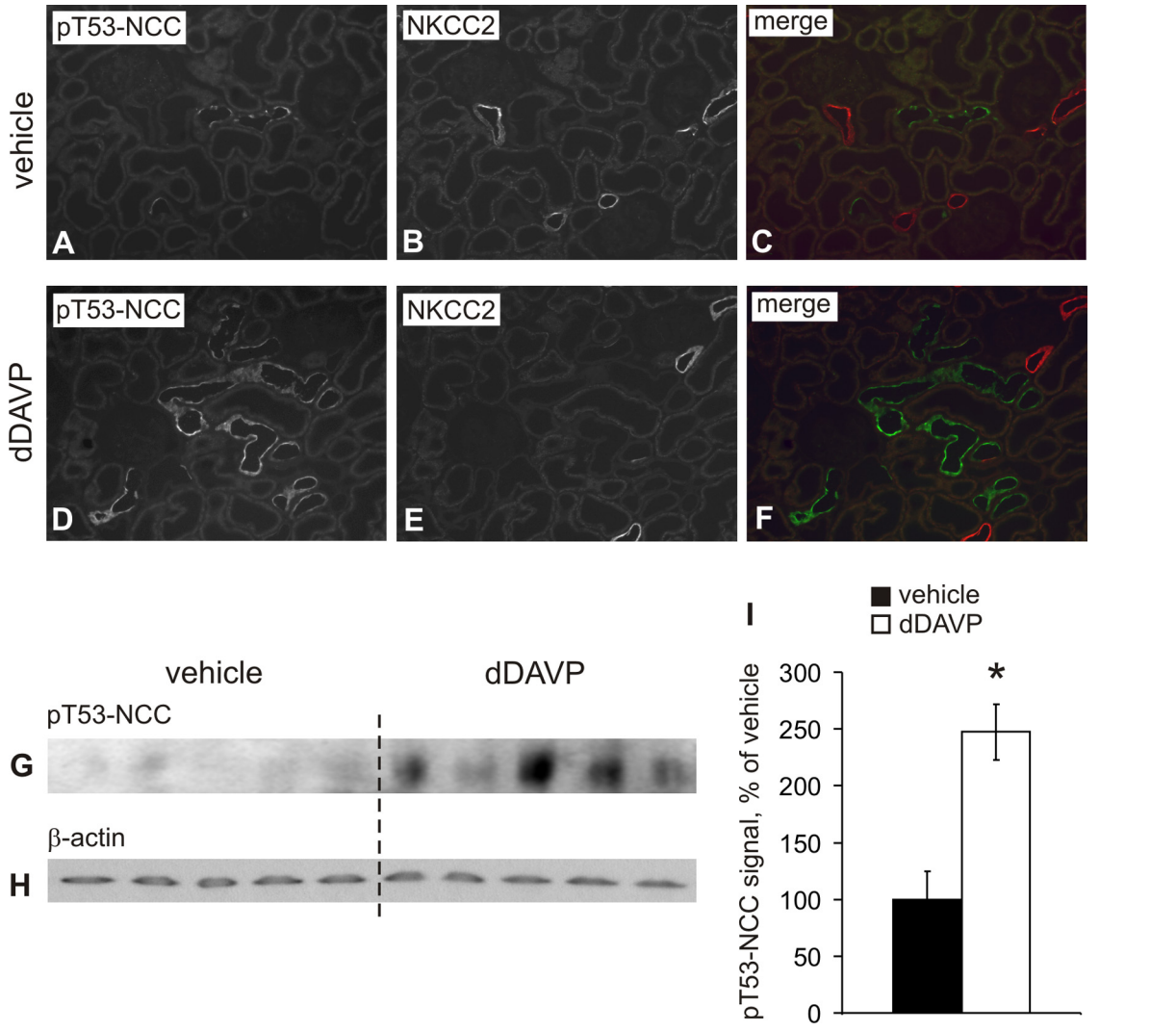

Fig. 2. Effects of dDAVP on NCC phosphorylation at Thr53. *A–F*: comparative image pairs from DI rats are presented after double immunostaining of pT53-NCC and Na^+-K^+-$2Cl^-$ cotransporter (NKCC2); in the color images, pT53-NCC (green) and NKCC2 (red) signals are merged. Original magnification ×400. *G* and *H*: Western blots from kidney cortical homogenates showing immunoreactive bands for pT53-NCC (*G*; ~160 kDa) and β-actin as loading control (*H*; ~42 kDa). *I*: densitometric evaluation of pT53-NCC-immunoreactive signals normalized for β-actin. Data are means ± SD from $n = 5$ rats/group; $^*P < 0.05$ for differences between vehicle- and dDAVP-treated group.

intracellular distribution of NCC was analyzed in DI rats receiving dDAVP (1 ng/g body wt for 30 min) or vehicle. The supraphysiological dose of dDAVP was selected for its established effects in previous work (13, 28). For comparison, a physiological range was tested as well (see below).

NCC immunoreactivity was diffuse in the apical cytoplasm of controls but clearly concentrated in the apical plasma membrane upon dDAVP administration (Fig. 1, *A* and *B*). Corresponding quantification of immunogold staining showed that the intracellular distribution of gold particles had shifted to the luminal plasma membrane of the dDAVP- vs. vehicle-treated groups (79 ± 12 vs. 56 ± 17% of total NCC immunoreactivity, respectively; $P < 0.01$) without concomitant change of total NCC immunoreactivity (Fig. 1, *C*, *D*, and *G*). NCC distribution was further evaluated by Western blot analysis of vesicle-enriched fractions from kidney cortex. Densitometric quantification of the respective signal intensities confirmed the results of the immunocytochemical analysis; administration of dDAVP produced a significant decrease in the vesicle-enriched fractions (−33 ± 9%, $P < 0.05$) (Fig. 1, *E*, *F*, and *H*). NCC total abundances in cortical homogenates were not different (see Fig. 3, *I*, *J*, and *L*). These findings demonstrate effective membrane translocation of the transporter upon short-term dDAVP administration in DI rats.

Effects of dDAVP on NCC phosphorylation. Visual evaluation of immunoreactive pT53-NCC signals revealed a substan-

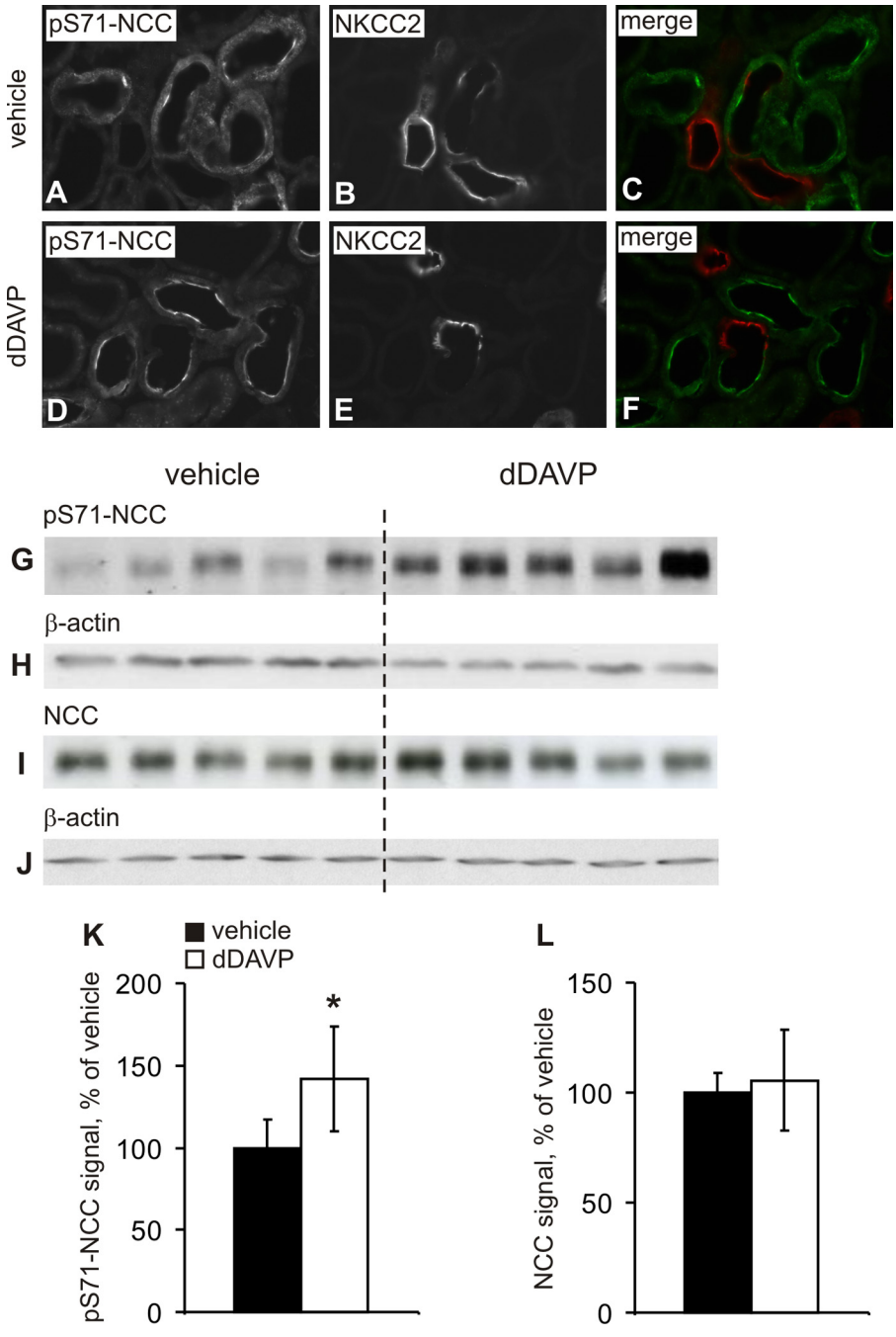

Fig. 3. Effects of dDAVP on NCC phosphorylation at Ser71. *A–F*: comparative image pairs from DI rats are presented after double immunostaining of pS71-NCC and NKCC2; in the color images, pS71-NCC (green) and NKCC2 (red) signals are merged. Original magnification ×400. *G–J*: Western blots from kidney cortical homogenates showing immunoreactive bands for pS71-NCC (*G*; ~160 kDa), NCC (*I*; ~160 kDa), and β-actin (*H* and *J*; ~42 kDa) as loading controls. *K* and *L*: densitometric evaluation of pS71-NCC- and NCC-immunoreactive signals normalized for β-actin. Data are means ± SD from $n = 5$ rats/group; $^*P < 0.05$ for differences between vehicle- and dDAVP-treated group.

tially higher proportion of positive DCT profiles in the dDAVP-treated rats than in controls (Fig. 2, *A* and *D*). Cross-reactivity of pT53-NCC antibody with NKCC2 was excluded by double-staining with anti-NKCC2 antibody (Fig. 2, *A–F*). Western blot evaluation of pT53-NCC signals obtained from postnuclear cortical fractions revealed significant increases in dDAVP-treated rats (+147%; Fig. 2, *G–I*). For a more comprehensive analysis of the changes in NCC phosphorylation, additional antibody directed against the alternative, specific phosphorylation site of NCC at Ser71 was studied; cross-reactivity of pS71-NCC antibody with NKCC2 was again excluded by double-staining using anti-NKCC2 antibody. pS71-NCC signal was markedly stronger after dDAVP (Fig. 3, *A–F*), and changes were confirmed by Western blot, revealing increases in pS71-NCC signal in the postnuclear fractions (+42 ± 31%, $P < 0.05$); by contrast, whole NCC levels were unchanged (Fig. 3, *G–L*).

To verify that the observed dDAVP-induced changes in NCC phosphorylation directly resulted from activation of V_2R in DCT, we performed dDAVP stimulation of renal tubules in suspension. Confocal evaluation of fluorescence intensity revealed significant increases of pS71-NCC signal in dDAVP- compared with vehicle-treated DCTs (+72 ± 22%, $P < 0.05$) (Fig. 4).

In the treated DI rats, increases in luminal pS71-NCC signal were confined to DCT1 (+184 ± 20%; $P < 0.05$; Fig. 5, *A–F* and *M*), whereas 11HSD2-positive DCT2 showed no major changes in pS71-NCC signal compared with the vehicle group (Fig. 5, *G–L* and *N*).

Together, these results demonstrate that stimulation of V_2R by short-term dDAVP application in DI rats induces rapid and strong phosphorylation of NCC.

Comparative application of physiological dose of dDAVP. Because the dose of dDAVP applied for the above experiments (1 ng/g body wt), albeit validated in previous studies, rather corresponds to a supraphysiological range of AVP (2), we comparatively administered the more physiological dose of 0.3 pg/g body wt in DI rats. As a result, the lower dose produced similar changes with respect to NCC phosphorylation, thus validating the above experiments (Supplemental Fig. 2, *A* and *B*).

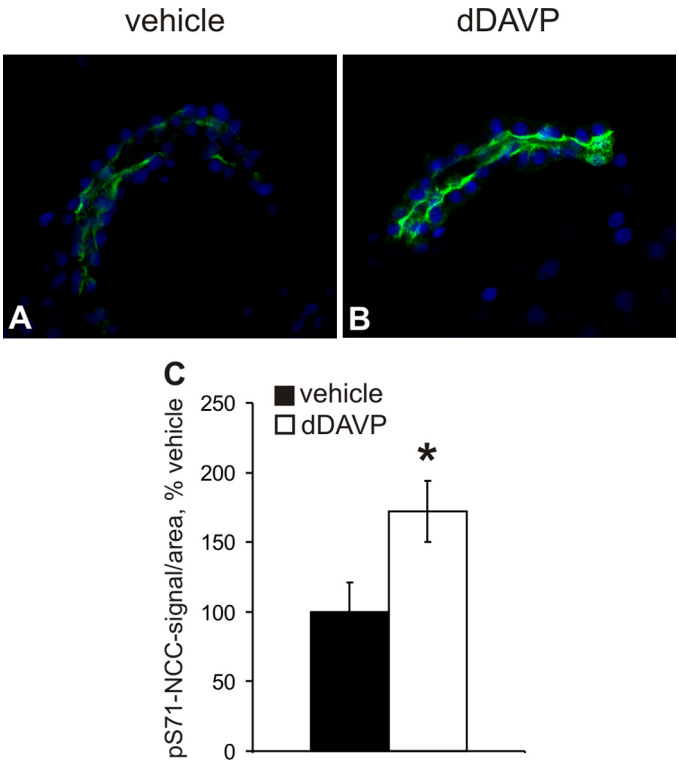

Fig. 4. Effects of dDAVP on NCC phosphorylation in suspensions of cortical renal tubules. *A* and *B*: representative confocal images of DCT profiles from tubular suspensions from kidneys of Wistar rats treated with vehicle or dDAVP (10^{-6} M; 30 min) and stained with pS71-NCC antibody. *C*: fluorimetric evaluation of luminal pS71-NCC signal intensity. Data are means ± SD from $n = 4$ rats/group; *$P < 0.05$ for differences between vehicle- and dDAVP-treated groups; original magnification ×400.

DISCUSSION

Vasopressin exerts both antidiuretic and antinatriuretic actions, which are primarily the result of its binding to V_2R in kidney. The capacity of AVP to increase Na^+ reabsorption in acute and chronic settings using tissues (8), isolated perfused tubules (15), and cell lines (44) has been appreciated for a long time. Although TAL and collecting ducts are established effector sites in this respect (2, 16), a role for DCT has not been clearly determined so far. The DCT mediates NaCl reabsorption of no more than 5–10% of the glomerular filtrate exclusively via the NCC, yet, it achieves an important part of the fine control of Na^+ excretion, which should be as high as that accomplished by the ENaC-expressing late distal segments (10). Modulation of NCC functions may therefore be quite effective. This is illustrated by mutations of the cotransporter causing salt wasting in Gitelman's syndrome with decreased NCC performance (18, 22), by its hyperactivity in pseudohypoaldosteronism type II (PHA II) caused by mutations of WNK isoforms (45, 46), and by the substantial clinical efficacy of thiazide diuretics to reduce blood pressure. Modulation of DCT's reabsorptive capacity by AVP has been inferred from earlier data reporting upregulation of NCC in association with the vasopressin-escape phenomenon (9) and by chronic, systemic application of dDAVP to DI rats (8), but specific information on local AVP signaling in DCT compared with TAL or collecting duct is still scarce.

In TAL, a number of key features of AVP signaling have been identified (6, 11). Short-term regulation of NKCC2 by AVP involves phosphorylation of NH_2-terminal threonine residues (12, 13, 28). SPAK and oxidative stress response kinase were found to interact with the phosphoacceptor site of NKCC isoforms (7, 27, 32, 34). Apical trafficking and surface expression of NKCC2 have further been established upon application of AVP (13, 25, 44), and regulatory domains of NKCC2 have been identified (4, 47).

Our present data provide clear evidence for a significant relation between V_2R signaling and activation of NCC in terms of luminal trafficking and rapid, pronounced phosphorylation in response to dDAVP. Application of dDAVP in supraphysiological and near-physiological doses (2, 13, 28) exerted similar effects on NCC phosphorylation, supporting the physiological relevance of the observed changes.

Thirty minutes of dDAVP application in DI rats produced a clear shift of a substantial proportion of immunoreactive NCC from the subapical vesicle compartment to the plasma mem-

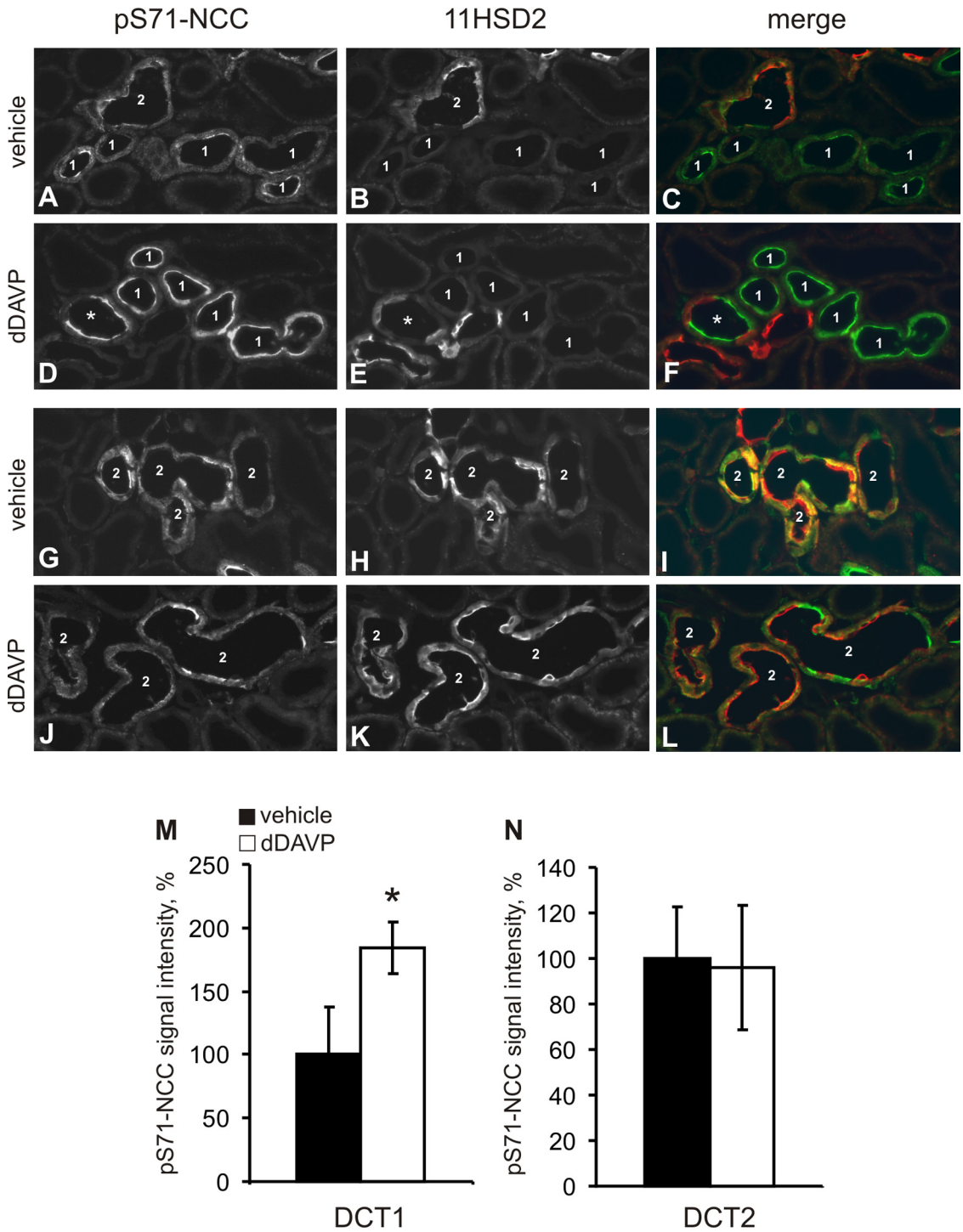

Fig. 5. Effects of dDAVP on NCC phosphorylation in DCT1 vs. DCT2. *A–L*: representative image pairs from DI rats are presented after double immunostaining with pS71-NCC and anti-11HSD2 antibodies. *A–F*: dDAVP treatment leads to marked increase of luminal pS71-NCC immunoreactivity in DCT1 segments (1) identified by the absence of 11HSD2; *early-to-late DCT (DCT1/DCT2) transition; 2, DCT2. *G–L*: in contrast, dDAVP induces no major changes of pS71-NCC immunoreactivity in DCT2 identified by concomitant 11HSD2 labeling. In the color images, pS71-NCC (green) and 11HSD2 (red) signals are merged. Original magnification ×400. *M* and *N*: fluorimetric evaluation of luminal pS71-NCC signal intensity in DCT1 and DCT2. Data are means ± SD from $n = 5$ rats/group; $^*P < 0.05$ for differences between vehicle- and dDAVP-treated groups.

brane without concomitant changes in total NCC abundance. The magnitude of the adluminal shift of NCC, as obtained by immunogold staining, fairly agreed with the densitometric differences resulting from Western blot evaluations, taking into account procedural differences between these approaches. The magnitude of these changes also agreed with previous data on endocrine stimulation of NCC (39).

So far, several lines of evidence have highlighted that trafficking of NCC per se is a major regulatory step in Na^+ transport activation. Mutations of NCC found in Gitelman's

syndrome caused reduced surface expression compatible with salt wasting in this disorder (18); genetic variants of WNK1 and WNK4 found in PHA II led to higher surface expression of NCC related with the increased Na^+ reabsorption in this defect (19, 46). In a mouse model for PHAII, in which mutant WNK4 D561A was knocked in, NCC was more concentrated in the apical membrane as well (5). Likewise, chronic salt loading and acute ANG II infusion or the induction of hypertension caused significant redistribution of NCC (20, 38, 39). Therefore, the luminal shift of NCC in response to dDAVP, as observed in this study, likely contributes to the activation of the transporter.

Another major finding of our study is the increased phosphorylation of NCC at NH_2-terminal phosphoacceptor sites after dDAVP treatment. In analogy to NKCC2, a cluster of threonine/serine residues in NCC was shown to be related with activation of the cotransporter (pT53, pT58, and pS71 in rat NCC) (30, 40). We have demonstrated increases in NCC phosphorylation with specific antibodies recognizing phospho-Thr53 or phospho-Ser71 of NCC (5, 40). The effects were predominantly confined to DCT1. As shown earlier for NKCC2 (12, 13, 28), vasopressin-induced NH_2-terminal phosphorylation of NCC in this study obviously also coincided with increased luminal trafficking, supporting a role for NCC's phosphoacceptor domain as an end point in AVP-induced signaling. Physiologically, hypotonic, low-Cl^- stress is an established, major stimulus to activate phosphorylation at this site in both NKCC2 and NCC, which accounts for increased Na^+ transport activity (30, 33, 35). In analogy, pronounced phosphorylation of NCC in DCT1 in response to dDAVP, as observed in our study, is likely associated with increased activity of the transporter, especially when the accompanying enhanced luminal abundance of NCC is considered.

It may be argued that AVP administered in DI rats may have triggered other endocrine stimuli such as components of the renin-angiotensin-aldosterone system that in turn may activate NCC as well (17, 39). However, stimulation of enzymatically isolated suspensions of renal cortical tubules with dDAVP, as performed in our study, also resulted in significant phosphorylation of NCC. This demonstrates that V_2R-mediated signaling of AVP can stimulate NCC in the absence of systemic endocrine components. It must further be considered that the effects of AVP were localized in 11HSD2-negative DCT1, which does not belong to the "aldosterone-sensitive distal nephron" as defined elsewhere (1, 21, 26).

Because AVP-induced, V_2R-mediated activation of NKCC2 in TAL and NCC in DCT at short term appears to be phenomenologically similar with respect to phosphorylation and apical trafficking of the transporters, one may speculate on the similarity of the signal transduction pathways involved in the two segments. In TAL, we and others have clearly shown that the V_2R-mediated activation of NKCC2 is triggered by cAMP and protein kinase A (PKA) (44). One may assume that this applies for the DCT as well, but compelling evidence for the role of cAMP/PKA is still scarce (14), probably because of the difficulty to obtain a suitable cell model for the DCT. With regard to the downstream signaling cascade, NKCC2 and NCC also appear to utilize similar pathways involving WNK and SPAK (5, 6, 24, 34). The interaction of SPAK with CCC and its WNK activators has been illustrated by the identification of an RFX[I/V] docking motif that is required for efficient phosphorylation of NCC (34, 41, 42, 43). Notably for NCC, the important role within its specific interaction with SPAK kinase and resulting increased phosphorylation was observed in WNK4 knockin mice (5). However, this occurred in an aldosterone-dependent manner and was probably confined to DCT2, which selectively expresses 11HSD2 conferring mineralocorticoid specificity to this subsegment (1, 21). Contrastingly, the present changes were occurring preferentially in DCT1. A heterogeneity in phosphokinase-dependent signaling may therefore exist among DCT subsegments, mediating either the effect of AVP in DCT1 or of aldosterone in DCT2. The particular role for WNK isoforms and SPAK herein remains to be studied.

In summary, our study extends the current knowledge on V_2R-mediated regulative effects of AVP in DCT. Our data are compatible with an AVP-induced activation of NCC that may effectively contribute to distal tubular NaCl conservation. Activation occurs chiefly in early DCT. Under pathological conditions, excessive action of AVP, which has been shown to affect blood pressure homeostasis (23), may thus aggravate salt-sensitive hypertensive conditions by its action on DCT1. We consider these findings relevant for antihypertensive treatment strategies.

GRANTS

This work was supported by the Deutsche Forschungsgemeinschaft (DFG FOR 667/2).

DISCLOSURES

No conflicts of interest are declared by the authors.

REFERENCES

1. **Bachmann S, Bostanjoglo M, Schmitt R, Ellison DH.** Sodium transport-related proteins in the mammalian distal nephron: distribution, ontogeny and functional aspects. *Anat Embryol* 200: 447–468, 1999.
2. **Bankir L.** Antidiuretic action of vasopressin: quantitative aspects and interaction between V1a and V2 receptor-mediated effects. *Cardiovasc Res* 51: 372–390, 2001.
3. **Carmosino M, Brooks HL, Cai Q, Davis LS, Opalenik S, Hao C, Breyer MD.** Axial heterogeneity of vasopressin receptor subtypes along the human and mouse collecting duct. *Am J Physiol Renal Physiol* 292: F351–F360, 2007.
4. **Carmosino M, Giménez I, Caplan M, Forbush B.** Exon loss accounts for differential sorting of Na-K-Cl cotransporters in polarized epithelial cells. *Mol Biol Cell* 19: 4341–4351, 2008.
5. **Chiga M, Rai T, Yang SS, Ohta A, Takizawa T, Sasaki S, Uchida S.** Dietary salt regulates the phosphorylation of OSR1/SPAK kinases and the sodium chloride cotransporter through aldosterone. *Kidney Int* 74: 1403–1409, 2008.
6. **Delpire E, Gagnon KB.** SPAK and OSR1: STE20 kinases involved in the regulation of ion homoeostasis and volume control in mammalian cells. *Biochem J* 409: 321–331, 2008.
7. **Dowd BF, Forbush B.** PASK (proline-alanine-rich STE20-related kinase), a regulatory kinase of the Na-K-Cl cotransporter (NKCC1). *J Biol Chem* 278: 27347–27353, 2003.
8. **Ecelbarger CA, Kim GH, Wade JB, Knepper MA.** Regulation of the abundance of renal sodium transporters and channels by vasopressin. *Exp Neurol* 171: 227–234, 2001.
9. **Ecelbarger CA, Knepper MA, Verbalis JG.** Increased abundance of distal sodium transporters in rat kidney during vasopressin escape. *J Am Soc Nephrol* 12: 207–217, 2001.
10. **Ellison DH, Velazquez H, Wright FS.** Thiazide-sensitive sodium chloride cotransport in early distal tubule. *Am J Physiol Renal Fluid Electrolyte Physiol* 253: F546–F554, 1987.
11. **Gamba G.** Molecular physiology and pathophysiology of electroneutral cation-chloride cotransporters. *Physiol Rev* 85: 423–493, 2005.

12. **Giménez I, Forbush B.** Regulatory phosphorylation sites in the NH2 terminus of the renal Na-K-Cl cotransporter (NKCC2). *Am J Physiol Renal Physiol* 289: F1341–F1345, 2005.
13. **Gimenez I, Forbush B.** Short-term stimulation of the renal Na-K-Cl cotransporter (NKCC2) by vasopressin involves phosphorylation and membrane translocation of the protein. *J Biol Chem* 278: 26946–16951, 2003.
14. **González-Núñez D, Morales-Ruiz M, Leivas A, Hebert SC, Poch E.** In vitro characterization of aldosterone and cAMP effects in mouse distal convoluted tubule cells. *Am J Physiol Renal Physiol* 286: F936–F944, 2004.
15. **Hebert SC, Andreoli TE.** Control of NaCl transport in the thick ascending limb. *Am J Physiol Renal Fluid Electrolyte Physiol* 246: F745–F756, 1984.
16. **Inoue T, Nonoguchi H, Tomita K.** Physiological effects of vasopressin and atrial natriuretic peptide in the collecting duct. *Cardiovasc Res* 51: 470–480, 2001.
17. **Kim GH, Masilamani S, Turner R, Mitchell C, Wade JB, Knepper MA.** The thiazide-sensitive Na-Cl cotransporter is an aldosterone-induced protein. *Proc Natl Acad Sci USA* 95: 14552–14557, 1998.
18. **Kunchaparty S, Palcso M, Berkman J, Velázquez H, Desir GV, Bernstein P, Reilly RF, Ellison DH.** Defective processing and expression of thiazide-sensitive Na-Cl cotransporter as a cause of Gitelman's syndrome. *Am J Physiol Renal Physiol* 277: F643–F649, 1999.
19. **Lalioti MD, Zhang J, Volkman HM, Kahle KT, Hoffmann KE, Toka HR, Nelson-Williams C, Ellison DH, Flavell R, Booth CJ, Lu Y, Geller DS, Lifton RP.** Wnk4 controls blood pressure and potassium homeostasis via regulation of mass and activity of the distal convoluted tubule. *Nat Genet* 38: 1124–1132, 2006.
20. **Lee DH, Riquier AD, Yang LE, Leong PK, Maunsbach AB, McDonough AA.** Acute hypertension provokes acute trafficking of distal tubule Na-Cl cotransporter (NCC) to subapical cytoplasmic vesicles. *Am J Physiol Renal Physiol* 296: F810–F818, 2009.
21. **Loffing J, Korbmacher C.** Regulated sodium transport in the renal connecting tubule (CNT) via the epithelial sodium channel (ENaC). *Pflugers Arch* 458: 111–135, 2009.
22. **Loffing J, Vallon V, Loffing-Cueni D, Aregger F, Richter K, Pietri L, Bloch-Faure M, Hoenderop JG, Shull GE, Meneton P, Kaissling B.** Altered renal distal tubule structure and renal Na^+ and Ca^{2+} handling in a mouse model for Gitelman's syndrome. *J Am Soc Nephrol* 15: 2276–2288, 2004.
23. **Luft FC.** Vasopressin, urine concentration, and hypertension: a new perspective on an old story. *Clin J Am Soc Nephrol* 2: 196–197, 2007.
24. **McCormick JA, Yang CL, Ellison DH.** WNK kinases and renal sodium transport in health and disease: an integrated view. *Hypertension* 51: 588–596, 2008.
25. **Meade P, Hoover RS, Plata C, Vázquez N, Bobadilla NA, Gamba G, Hebert SC.** cAMP-dependent activation of the renal-specific Na^+-K^+-$2Cl^-$ cotransporter is mediated by regulation of cotransporter trafficking. *Am J Physiol Renal Physiol* 284: F1145–F1154, 2003.
26. **Meneton P, Loffing J, Warnock DG.** Sodium and potassium handling by the aldosterone-sensitive distal nephron: the pivotal role of the distal and connecting tubule. *Am J Physiol Renal Physiol* 287: F593–F601, 2004.
27. **Moriguchi T, Urushiyama S, Hisamoto N, Iemura S, Uchida S, Natsume T, Matsumoto K, Shibuya H.** WNK1 regulates phosphorylation of cation-chloride-coupled cotransporters via the STE20-related kinases, SPAK and OSR1. *J Biol Chem* 280: 42685–42693, 2005.
28. **Mutig K, Paliege A, Kahl T, Jöns T, Müller-Esterl W, Bachmann S.** Vasopressin V_2 receptor expression along rat, mouse, and human renal epithelia with focus on TAL. *Am J Physiol Renal Physiol* 293: F1166–F1177, 2007.
29. **Nedvetsky PI, Tamma G, Beulshausen S, Valenti G, Rosenthal W, Klussmann E.** Regulation of aquaporin-2 trafficking. *Handb Exp Pharmacol* 190: 133–157, 2009.
30. **Pacheco-Alvarez D, Cristóbal PS, Meade P, Moreno E, Vazquez N, Muñoz E, Díaz A, Juárez ME, Giménez I, Gamba G.** The Na+:Cl- cotransporter is activated and phosphorylated at the amino-terminal domain upon intracellular chloride depletion. *J Biol Chem* 281: 28755–28763, 2006.
31. **Perucca J, Bichet DG, Bardoux P, Bouby N, Bankir L.** Sodium excretion in response to vasopressin and selective vasopressin receptor antagonists. *J Am Soc Nephrol* 19: 1721–1731, 2008.
32. **Piechotta K, Lu J, Delpire E.** Cation chloride cotransporters interact with the stress-related kinases Ste20-related proline-alanine-rich kinase (SPAK) and oxidative stress response 1 (OSR1). *J Biol Chem* 277: 50812–50819, 2002.
33. **Ponce-Coria J, San-Cristobal P, Kahle KT, Vazquez N, Pacheco-Alvarez D, de Los Heros P, Juárez P, Muñoz E, Michel G, Bobadilla NA, Gimenez I, Lifton RP, Hebert SC, Gamba G.** Regulation of NKCC2 by a chloride-sensing mechanism involving the WNK3 and SPAK kinases. *Proc Natl Acad Sci USA* 105: 8458–8463, 2008.
34. **Richardson C, Alessi DR.** The regulation of salt transport and blood pressure by the WNK-SPAK/OSR1 signalling pathway. *J Cell Sci* 121: 3293–3304, 2008.
35. **Richardson C, Rafiqi FH, Karlsson HK, Moleleki N, Vandewalle A, Campbell DG, Morrice NA, Alessi DR.** Activation of the thiazide-sensitive Na^+-Cl^- cotransporter by the WNK-regulated kinases SPAK and OSR1. *J Cell Sci* 121: 675–684, 2008.
36. **Rinehart J, Kahle KT, de Los Heros P, Vazquez N, Meade P, Wilson FH, Hebert SC, Gimenez I, Gamba G, Lifton RP.** WNK3 kinase is a positive regulator of NKCC2 and NCC, renal cation-Cl^- cotransporters required for normal blood pressure homeostasis. *Proc Natl Acad Sci USA* 102: 16777–16782, 2005.
37. **Sachs AN, Pisitkun T, Hoffert JD, Yu MJ, Knepper MA.** LC-MS/MS analysis of differential centrifugation fractions from native inner medullary collecting duct of rat. *Am J Physiol Renal Physiol* 295: F1799–F1806, 2008.
38. **Sandberg MB, Maunsbach AB, McDonough AA.** Redistribution of distal tubule Na^+-Cl^- cotransporter (NCC) in response to a high-salt diet. *Am J Physiol Renal Physiol* 291: F503–F508, 2006.
39. **Sandberg MB, Riquier AD, Pihakaski-Maunsbach K, McDonough AA, Maunsbach AB.** ANG II provokes acute trafficking of distal tubule Na^+-Cl^- cotransporter to apical membrane. *Am J Physiol Renal Physiol* 293: F662–F669, 2007.
40. **Vallon V, Schroth J, Lang F, Kuhl D, Uchida S.** Expression and phosphorylation of the Na-Cl-cotransporter NCC in vivo is regulated by dietary salt, potassium and SGK1. *Am J Physiol Renal Physiol* 297: F704–F712, 2009.
41. **Villa F, Goebel J, Rafiqi FH, Deak M, Thastrup J, Alessi DR, van Aalten DM.** Structural insights into the recognition of substrates and activators by the OSR1 kinase. *EMBO Rep* 8: 839–845, 2007.
42. **Vitari AC, Deak M, Morrice NA, Alessi DR.** The WNK1 and WNK4 protein kinases that are mutated in Gordon's hypertension syndrome phosphorylate and activate SPAK and OSR1 protein kinases. *Biochem J* 391: 17–24, 2005.
43. **Wang Y, O'Connell JR, McArdle PF, Wade JB, Dorff SE, Shah SJ, Shi X, Pan L, Rampersaud E, Shen H, Kim JD, Subramanya AR, Steinle NI, Parsa A, Ober CC, Welling PA, Chakravarti A, Weder AB, Cooper RS, Mitchell BD, Shuldiner AR, Chang YP.** From the Cover: Whole-genome association study identifies STK39 as a hypertension susceptibility gene. *Proc Natl Acad Sci USA* 106: 226–231, 2009.
44. **Welker P, Böhlick A, Mutig K, Salanova M, Kahl T, Schlüter H, Blottner D, Ponce-Coria J, Gamba G, Bachmann S.** Renal Na-K-Cl cotransporter activity and vasopressin-induced trafficking are lipid raft-dependent. *Am J Physiol Renal Physiol* 295: F559–F567, 2008.
45. **Wilson FH, Disse-Nicodème S, Choate KA, Ishikawa K, Nelson-Williams C, Desitter I, Gunel M, Milford DV, Lipkin GW, Achard JM, Feely MP, Dussol B, Berland Y, Unwin RJ, Mayan H, Simon DB, Farfel Z, Jeunemaitre X, Lifton RP.** Human hypertension caused by mutations in WNK kinases. *Science* 293: 1107–1112, 2001.
46. **Yang CL, Zhu X, Wang Z, Subramanya AR, Ellison DH.** Mechanisms of WNK1 and WNK4 interaction in the regulation of thiazide-sensitive NaCl cotransport. *J Clin Invest* 115: 1379–1387, 2005.
47. **Zaarour N, Demaretz S, Defontaine N, Mordasini D, Laghmani K.** A highly conserved motif at the C-terminus dictates ER exit and cell-surface expression of NKCC2. *J Biol Chem* 284: 21752–21764, 2009.

3.3 Activation of the bumetanide-sensitive Na+,K+,2Cl- cotransporter (NKCC2) is facilitated by Tamm-Horsfall protein in a chloride-sensitive manner.

Mutig K*, Kahl T*, Saritas T, Godes M, Persson P, Bates J, Raffi H, Rampoldi L, Uchida S, Hille C, Dosche C, Kumar S, Castañeda-Bueno M, Gamba G, Bachmann S.

* equal contribution

***J Biol Chem.* 2011 Aug 26;286(34):30200-10.**

In our previous work we have studied the V2R-mediated activation of NKCC2 and NCC (see 3.1 and 3.2). Both transporters responded to AVP with acute increases of their surface expression and phosphorylation. In the present study we suggested that Tamm-Horsfall protein (THP) is involved in these events in TAL. THP, also known as uromodulin, is abundantly produced in TAL cells. It reaches the luminal membrane, where it is co-localized with NKCC2, and is finally excreted into the urine by a proteolytic cleavage to serve as a defensive factor against urinary tract infects [51]. Like all other GPI-anchored proteins, intracellular THP is incorporated into specialized membrane microdomaines enriched in cholesterol and glycosphingolipids, known as lipid rafts. NKCC2 shares lipid raft localization with THP during its apical trafficking [52]. We have previously suggested a role for THP in the urinary concentrating mechanism since THP-deficient mice showed impaired urinary concentration ability [53]. To explain this, functional interactions between THP and NKCC2 has been investigated in the present study. We show here, that THP substantially facilitates baseline and AVP-induced phosphorylation of NKCC2 thus increasing its activity. We suggest that these effects depend on the co-distribution of THP and NKCC2 in apical lipid rafts since disruption of lipid rafts has been shown to substantially attenuate AVP-dependent activation of NKCC2 in our previous work [52]. THP may stabilize apical lipid rafts via its GPI-anchor and thus facilitate NKCC2 function [54,55].

THE JOURNAL OF BIOLOGICAL CHEMISTRY VOL. 286, NO. 34, pp. 30200–30210, August 26, 2011

Activation of the Bumetanide-sensitive Na^+,K^+,$2Cl^-$ Cotransporter (NKCC2) Is Facilitated by Tamm-Horsfall Protein in a Chloride-sensitive Manner*

Received for publication, January 19, 2011, and in revised form, June 7, 2011 Published, JBC Papers in Press, July 7, 2011, DOI 10.1074/jbc.M111.222968

Kerim Mutig[‡1], Thomas Kahl[‡1], Turgay Saritas[‡], Michael Godes[§], Pontus Persson[§], James Bates[¶], Hajamohideen Raffi[¶], Luca Rampoldi[‖], Shinichi Uchida[**], Carsten Hille[‡‡], Carsten Dosche[‡‡], Satish Kumar[¶], Maria Castañeda-Bueno[§§], Gerardo Gamba[§§2], and Sebastian Bachmann[‡3]

*From the Departments [‡]Anatomy and [§]Physiology, Charité-Universitätsmedizin Berlin, 10115 Berlin, Germany, the [¶]University of Oklahoma Health Sciences Center, Oklahoma City, Oklahoma 73104, the [‖]Dulbecco Telethon Institute, Molecular Genetics of Renal Disorders Unit Dibit, San Raffaele Scientific Institute, 20132 Milan, Italy, the **Department of Nephrology, Tokyo Medical and Dental University, Tokyo 113-8519, Japan, the [‡‡]Department of Physical Chemistry, University of Potsdam, 14476 Potsdam, Germany, and the [§§]Instituto de Investigaciones Biomédicas, Universidad Nacional Autónoma de México, Instituto Nacional de Ciencias Médicas y Nutrición Salvador Zubirán, and Instituto Nacional de Cardiología Ignacio Chávez, Mexico City, Distrito Federal 14000, Mexico*

Active transport of NaCl across thick ascending limb (TAL) epithelium is accomplished by Na^+,K^+,$2Cl^-$ cotransporter (NKCC2). The activity of NKCC2 is determined by vasopressin (AVP) or intracellular chloride concentration and includes its amino-terminal phosphorylation. Co-expressed Tamm-Horsfall protein (THP) has been proposed to interact with NKCC2. We hypothesized that THP modulates NKCC2 activity in TAL. THP-deficient mice ($THP^{-/-}$) showed an increased abundance of intracellular NKCC2 located in subapical vesicles (+47% compared with wild type (WT) mice), whereas base-line phosphorylation of NKCC2 was significantly decreased (−49% compared with WT mice), suggesting reduced activity of the transporter in the absence of THP. Cultured TAL cells with low endogenous THP levels and low base-line phosphorylation of NKCC2 displayed sharp increases in NKCC2 phosphorylation (+38%) along with a significant change of intracellular chloride concentration upon transfection with THP. In NKCC2-expressing frog oocytes, co-injection with THP cRNA significantly enhanced the activation of NKCC2 under low chloride hypotonic stress (+112% *versus* +235%). Short term (30 min) stimulation of the vasopressin V2 receptor pathway by V2 receptor agonist (deamino-*cis*-D-Arg vasopressin) resulted in enhanced NKCC2 phosphorylation in WT mice and cultured TAL cells transfected with THP, whereas in the absence of THP, NKCC2 phosphorylation upon deamino-*cis*-D-Arg vasopressin was blunted in both systems. Attenuated effects of furosemide along with functional and structural adaptation of the distal convoluted tubule in $THP^{-/-}$ mice supported the notion that NaCl reabsorption was impaired in TAL lacking THP. In summary, these results are compatible with a permissive role for THP in the modulation of NKCC2-dependent TAL salt reabsorptive function.

The bumetanide-sensitive, apical Na^+,K^+,$2Cl^-$ cotransporter (NKCC2[4] or BSC1; *SLC12A1*) belongs to the family of electroneutral cation-coupled chloride cotransporters and is expressed in the luminal membrane of the thick ascending limb of Henle's loop (TAL; Refs. 1 and 2) where it determines Na^+, K^+, and Cl^- reabsorption (3) and serves to maintain the cortico-medullary osmotic gradient. The fundamental role of NKCC2 in renal salt reabsorption has been firmly established (4–6) and is illustrated by severe salt loss in patients with mutated NKCC (4) as well as by fatal extracellular volume depletion in homozygous NKCC2 knock-out mice (7). Principal mechanisms of NKCC2 activation include modulation of its surface expression (8, 9) as well as phosphorylation of conserved amino-terminal threonines (2, 10) mediated by with no lysine (K) kinases (WNK) and oxidative stress-responsive kinase 1 or STE20/SPS1-related Pro/Ala-rich kinase (5, 11). Vasopressin (AVP) is particularly effective in stimulating NKCC2 via $G\alpha_s$-coupled V2 receptor (V2R; Ref. 10), adenylate cyclase-induced cAMP release, and PKA activation (2, 8, 12, 13). Basal activity of the transporter is dependent on intracellular chloride concentration (14). Mechanisms involved into the intracellular regulation of the transporter are a focus of current research.

NKCC2 is co-localized with Tamm-Horsfall protein (THP, also termed uromodulin), and both are unique products of TAL (15–18). The role of THP has remained obscure for many years, but recent studies have permitted a clearer distinction between

* This work was supported by the Deutsche Forschungsgemeinschaft (FOR 667) and Leducq Foundation and Consejo Nacional de Ciencia y Tecnologia Grant 59992 (to G. G.).

[1] Both authors contributed equally to this paper.

[2] To whom correspondence may be addressed: IIB-INNSZ-INCICH, Vasco de Quiroga 15, Colonia Seccion XVI, Tlalpan, C.P. 14000, Mexico D.F., Mexico. Tel.: 5255-55133868; Fax: 5255-56550382; E-mail: gamba@biomedicas.unam.mx.

[3] To whom correspondence may be addressed: Institut für Vegetative Anatomie, Charité-Universitätsmedizin Berlin, Campus Charité-Mitte, Philippstrasse 12, D-10115 Berlin, Germany. Tel.: 49-30-450-528-001; Fax: 49-30-450-528-922; E-mail: sbachm@charite.de.

[4] The abbreviations used are: NKCC2, Na^+,K^+,$2Cl^-$ cotransporter; V2R, V_2 rho protein receptor; THP, Tamm-Horsfall protein; NCC, NaCl cotransporter; DCT, distal convoluted tubule; dDAVP, deamino-*cis*-D-Arg vasopressin; TAL, thick ascending limb; rbTAL, rabbit TAL cells; HCTZ, hydrochlorothiazide; MQAE, 6-methoxy-quinolyl acetoethyl ester; AVP, vasopressin; WNK, with no lysine (k) kinase; FLIM, fluorescence lifetime imaging microscopy.

its intra- and extracellular functions. The former are related with the urinary concentrating mechanism and potentially interfere with transcellular electrolyte transport (15, 19), whereas the latter have been associated with anti-inflammatory roles of the glycoprotein in the urinary tract and renal interstitium (20–22). Insights into the functional relation between both products have been obtained from gene mutations in humans and from animal models. Mutations of NKCC2 lead to the antenatal variant of Bartter syndrome with severely compromised urinary concentrating ability and reduced expression of THP (4, 23). Mutations of THP are associated with disease (familial juvenile hyperuricemic nephropathy/autosomal dominant medullary cystic kidney disease type 2) characterized by impaired urinary concentration as well (24, 25). In analogy to medullary cystic kidney disease type 2/familial juvenile hyperuricemic nephropathy in humans, chemical induction of a missense mutation in the THP gene produced a mouse line with compromised urinary concentration (26). THP-deficient ($THP^{-/-}$) mice showed moderately impaired urinary concentrating ability; their expression of distal ion transporters and channels including the thiazide-sensitive NaCl cotransporter (NCC) of distal convoluted tubule (DCT) was enhanced, which suggested a compensatory adaptation for putatively insufficient NaCl reabsorption in TAL (15, 27, 28).

We postulate that THP indirectly affects NKCC2-mediated transport function of TAL. This study was designed to evaluate the effects of THP on the mechanisms of NKCC2 activation *in vivo*, in cell culture, and in the *Xenopus* oocyte system and to reveal the putative compensatory adaptation of DCT. Our results suggest a permissive role for THP/uromodulin in TAL reabsorptive function.

EXPERIMENTAL PROCEDURES

Animals, Tissues, Treatments—$THP^{-/-}$ mice and wild-type (WT; $^{+/+}$) controls (15, 20) were bred in the local animal facility and kept on standard diet and tap water. Genotypes of WT and $THP^{-/-}$ mice were confirmed by PCR technique (not shown here; Ref. 15). For morphology studies, adult mice were anesthetized, and the kidneys were perfused retrogradely through the abdominal aorta using 3% paraformaldehyde dissolved in PBS (29), removed, and prepared for cryostat sectioning, standard paraffin sectioning, or ultrastructural resin embedding. For Western blot, mice were killed by an overdose of Nembutal, and the kidneys removed and frozen. Short term vasopressin treatment was administered by intraperitoneal injection of the V2 receptor agonist desmopressin (deamino-*cis*-D-Arg vasopressin (dDAVP); 1 μg/kg of body weight for 30 min; Sigma) or vehicle in adult WT and $THP^{-/-}$ mice.

Cells—Cultured SV40-transformed rabbit TAL cells (rbTAL) obtained from rabbit kidney medulla were cultured as described previously (30). rbTAL cells were transiently transfected with human THP cloned into pcDNA3.1 or GFP-tagged THP (THP-GFP) in pcDNA3.1 vector (31) using FuGENE® HD transfection reagent (Roche Diagnostics) according to the manufacturer's manual. Empty pcDNA3.1 vector or GFP in pcDNA3.1 were applied for control transfections (31). Short term activation (30 min) of the V2R-signaling pathway was performed by combined administration of dDAVP (10^{-7} M) and forskolin (10^{-4} M). For Western blot evaluation cells were harvested, homogenized by sonication, and centrifuged at 1,000 × *g* for 10 min to obtain post-nuclear fractions. For immunohistochemical evaluation cells were fixed in 3% paraformaldehyde/PBS for 20 min.

Intracellular Chloride Recordings—For quantitative intracellular chloride ($[Cl^-]_i$) recordings, two-photon fluorescence lifetime imaging microscopy (FLIM) was performed with the Cl^--sensitive fluorescent dye MQAE (Sigma) as described (32). Briefly, GFP-THP-transfected, GFP-transfected, and non-transfected rbTAL cells were loaded with 10 mM MQAE for 20 min in hypotonic saline. Two-photon fluorescence lifetime imaging microscopy was performed using a MicroTime 200 microscope system (PicoQuant) equipped with a 400–680-nm emission filter and a C-fiber laser (λ_{ex} = 780 nm, 50 MHz, 90-fs pulse width; MenloSystems). Fluorescence was detected by a single-photon avalanche diode. Transfected cells were identified by two-photon-excited GFP fluorescence, and a bandpass filter (450/40 nm) was then added to reject the GFP-signal.

Assessment of the NKCC2 Function—NKCC2 activity was assessed by functional expression in *Xenopus laevis* oocytes as described (5, 14, 33). Oocytes injected with water, NKCC2 cRNA alone (14), THP cRNA alone (31), NKCC2 cRNA + THP cRNA, NKCC2 cRNA + WNK3 cRNA (14), or NKCC2 cRNA + WNK3 cRNA + THP cRNA (each 10 ng/oocyte) were exposed to a low chloride hypotonic stress to promote a decrease in the $[Cl^-]_i$. After injection, oocytes were maintained for 3 days in isotonic ND96 medium (96 mM NaCl, 2 mM KCl, 1.8 mM $CaCl_2$, 1.0 mM $MgCl_2$, and 5 mM HEPES/Tris; 210 mosmol/kg H_2O, pH 7.4). Before the uptake assay, oocytes were incubated overnight either in isotonic or low Cl^- hypotonic stress medium (79 mM sodium isothionate, 2 mM potassium gluconate, 1.8 mM calcium gluconate, 1.0 mM magnesium gluconate, 5 mM HEPES/Tris, 170 mosmol/kg H_2O, pH 7.4). The ensuing $^{86}Rb^+$ uptake experiment included a 30-min preincubation in the control or low Cl^- hypotonic stress medium followed by a 60-min uptake period in a Na^+-, K^+-, and Cl^--containing medium supplemented with 1 mM ouabain in the absence or presence of 0.1 mM bumetanide. At the end of the uptake period, oocytes were washed 5 times in ice-cold uptake solution without isotope, dissolved in 10% sodium dodecyl sulfate, and counted in a β-scintillation counter. Each experiment was performed in duplicate. Because *X. laevis* oocytes express an endogenous Na^+-K^+-$2Cl^-$ cotransporter (5, 8, 14, 33), the mean value observed in oocytes injected with water or THP alone was subtracted to the uptake observed in NKCC2- or NKCC2 + THP-injected oocytes from each experiment.

Furosemide Test—Thirteen- to fourteen-week-old WT and $THP^{-/-}$ mice received a single intraperitoneal injection of vehicle (0.9% saline) or furosemide (40 mg/kg body weight in saline; Sigma). Urine was then collected in metabolic cages for 4 h. Urinary sodium, potassium, chloride, and creatinine concentrations were determined.

Hydrochlorothiazide Test—Thirteen- to fourteen-week-old WT and $THP^{-/-}$ mice were anesthetized with a mixture of ketamine (80 mg/kg body weight) and xylazine (10 mg/kg body weight). After placing the animals on a thermostat table (37 °C), surgical implantation of a tracheal catheter (for sufficient res-

piratory function), an arterial catheter (into the right carotid artery for blood pressure control), and a urinary catheter (into the bladder for urine collection) was performed. To obtain sufficient volumes in the urine fractions, osmotic diuresis was induced by intraarterial infusion of 3.2% mannitol plus 3.2% glucose in water (2 ml/h). Urine fractions were collected every 15 min. After induction of osmotic diuresis, four consecutive urine fractions were collected (fractions 1–4). Vehicle or hydrochlorothiazide (HCTZ; 50 mg/kg body weight; Sigma) were then administered intraperitoneally, and the following six consecutive urine fractions were collected (fractions 5–10). Urinary sodium and potassium concentrations were determined. At the end of the experiments, animals were sacrificed, and plasma samples were obtained to determine electrolytes and osmolality.

Immunohistochemistry—The primary antibodies applied for immunohistochemical labeling of kidney sections and fixed rbTAL-cells were goat anti-THP (ICN Biomedicals), rabbit anti-phospho-NKCC2 (pNKCC2; directed against phosphorylated threonines 95 and 100; Ref. 10), rabbit NCC (provided by D.H. Ellison), and rabbit anti-phospho-NCC (Ser(P)-71-NCC; directed against phosphorylated serine 71; Ref. 34). Signals were generated using immunofluorescence or HRP-based detection as described (10, 29).

Ultrastructural Immunogold Labeling—Mouse kidney tissue was embedded in LR White resin science services, sectioned, and incubated according to established methodology (16) using anti-THP (provided by J. R. Hoyer, Philadelphia, PA), anti-NKCC2 (T4, Developmental Studies Hybridoma Bank; University of Iowa, IA), or anti-phospho-NKCC2 (10) primary antibodies and appropriate secondary antibodies coupled to nanogold particles. Ultrathin sections were viewed with a transmission electron microscope. Quantification of immunogold signal in medullary TAL profiles was performed on micrographs according to an established protocol (35). Gold particles were attributed to the apical cell membrane when located near (within 20 nm of distance) or within the bilayer; particles found below 20 nm of distance to the membrane up to a depth of 2 μm or until the nuclear envelope were assigned to cytoplasmic localization.

Morphometric Procedures—The fractional volume of DCT segments among strains was measured by light microscopy according to previously characterized methods (36, 37). Briefly, 5-μm-thick paraffin sections were stained for NCC whose localization is restricted to the DCT. Cortical areas extending between the renal capsule and the outer medullary boundary were evaluated. Sections were photographed, and a transparent grid with rectangular crossed lines was electronically superimposed on the micrographs; the distances between lines corresponded to 50 μm. The proportion of grid intersections over DCT segments was expressed as the fractional volume of DCT.

Western Blotting—Methods used were as described previously (29, 38). Briefly, kidneys were homogenized in buffer containing 250 mM sucrose, 10 mM triethanolamine, protease inhibitors (Complete; Roche Diagnostics), and phosphatase inhibitors (Phosphatase Inhibitor Mixture 1; Sigma), pH 7.5. The homogenates were subjected to sequential centrifugation steps to obtain post-nuclear fractions (1,000 $\times$ *g*, 15 min), low speed fractions containing large membrane fragments (17,000 $\times$ *g* for 1 h), and high speed fractions enriched in cytoplasmic vesicles (200,000 $\times$ *g* for 1 h). Thirty μg of protein/lane were run on 10% polyacrylamide minigels. After electrophoretic transfer, polyvinylidene fluoride membranes were incubated with specific primary antibodies against NKCC2, pNKCC2, Ser(P)-71-NCC, THP, flotillin-1 (BD Biosciences), or β-actin (Sigma) followed by HRP-conjugated secondary antibodies (Dako Cytomation; 1:3000), induction of chemiluminescence, exposure of x-ray films, and densitometric evaluation.

Statistical Analysis of Data—Experimental data were evaluated by Student's *t* test or the Mann-Whitney U test. $p < 0.05$ was accepted as significant. Values are given as the means $\pm$ S.D. or $\pm$ S.E. where appropriate. Data were analyzed using SPSS for Windows (Version 12.0; SPSS, Chicago, IL).

RESULTS

Steady State Evaluations in TAL and in Frog Oocytes

Cellular Distribution and Phosphorylation of NKCC2—Protein A gold immunocytochemistry was applied to compare the intracellular distribution of NKCC2 in medullary TAL between WT and THP$^{-/-}$ mice. Double-staining with gold particles of different size was performed to analyze topographical relations between NKCC2 and THP. NKCC2 was frequently co-localized with THP in the apical membrane and subapical vesicles at a resolution of less than 10 nm (Fig. 1*a*). Quantification of NKCC2 immunoreactivity in the apical membrane revealed no differences between WT and THP$^{-/-}$ mice, whereas in the subapical vesicle compartment, NKCC2 signal density was significantly higher in THP$^{-/-}$ compared with WT mice (+47%; $p < 0.05$). Accordingly, overall immunogold NKCC2 signal was significantly higher in THP$^{-/-}$ than in WT mice (+27%; $p < 0.05$; Fig. 1, *b–d*). Cellular distribution of NKCC2 was further evaluated by Western blot analysis from cell fractions obtained by either high speed or low speed differential fractionation of kidney homogenates. Densitometric quantification revealed an increase of NKCC2 signal in the vesicle-enriched high speed fractions of THP$^{-/-}$ compared with WT mice (+75%; $p < 0.05$; Fig. 2, *a* and *c*), whereas the low speed fractions were not different. Along with our previous data (15) these results indicate an accumulation of NKCC2 in the subapical vesicular compartment of THP$^{-/-}$ mice.

In contrast to the total NKCC2 levels, phospho-NKCC2 signals were lower in THP$^{-/-}$ compared with WT mice as revealed by Western blot quantification from post-nuclear kidney homogenates (-49%, $p < 0.05$; Fig. 2, *a* and *c*). This was confirmed by immunogold labeling of phospho-NKCC2 showing significantly decreased luminal signal in TAL of THP$^{-/-}$ kidneys (-46%, $p < 0.05$; Fig. 2, *b* and *c*). In cultured rbTAL cells, base-line THP expression was very low to absent. Transient transfection with THP resulted in an ~60% transfection rate (Fig. 3*a*). Phospho-NKCC2 signal in the transfected cells was significantly higher than in controls (+38%; $p < 0.05$; Fig. 3, *b* and *c*). These results suggest that THP facilitates base-line NKCC2 phosphorylation.

Intracellular Chloride Levels—The regulatory influence of intracellular chloride levels ($[Cl^-]_i$) on the phosphorylation and

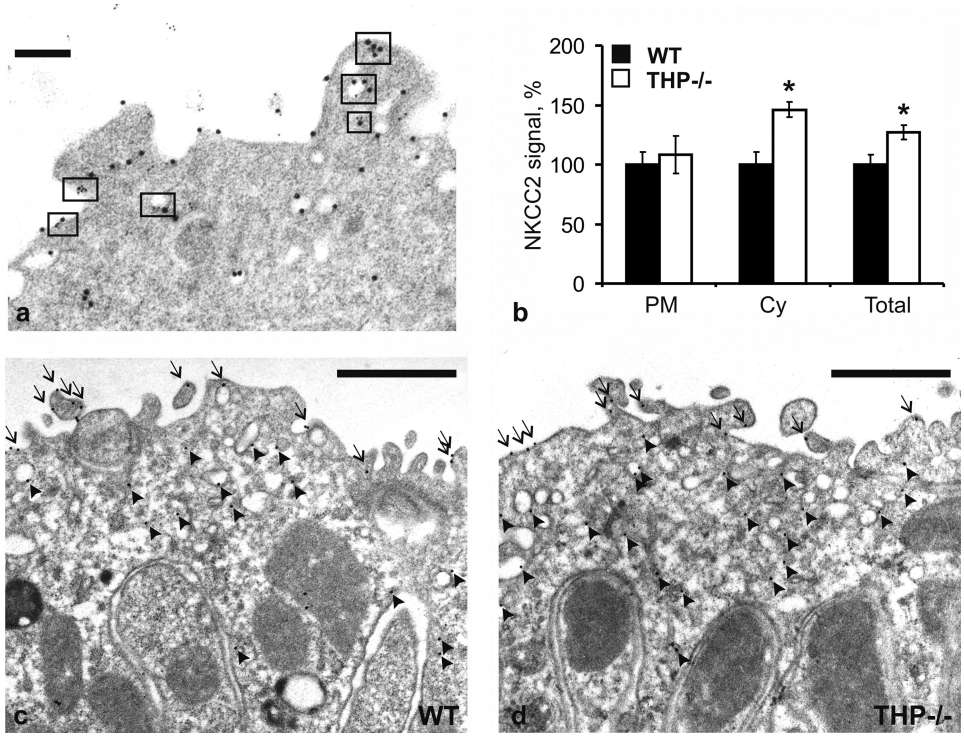

FIGURE 1. **Intracellular distribution of NKCC2 in WT and THP$^{-/-}$ mice (each $n = 3$) as evaluated with protein A-gold immunostaining of medullary thick ascending limbs.** *a*, double immunostaining for THP (5-nm gold particles) and NKCC2 (10-nm gold particles) demonstrates their co-distribution (*rectangular boxes*) within the apical membrane and subapical vesicles (*scale bar* = 0.1 μm). *b–d*, quantification of the NKCC2 signal (*b*) by counting the gold particles on representative micrographs from WT (*c*) and THP$^{-/-}$ mice (*d*) reveals no differences in luminal plasma membrane (*PM*, *arrows*) between strains but significant increases in cytoplasmic vesicles (*Cy*, *arrowheads*) in THP$^{-/-}$ compared with WT mice (*scale bars* = 1 μm). The total NKCC2 signal was accordingly increased in THP$^{-/-}$ mice. At least 10 profiles containing an average of five cells per profile were evaluated per individual. Data are the means ± S.D.; *, $p < 0.05$ for interstrain differences; WT was set at 100%.

activation of NKCC2 has been established (14). To address potential underlying mechanisms of the observed THP-dependent changes in NKCC2 phosphorylation, we evaluated $[Cl^-]_i$ in cultured rbTAL-cells using fluorescence-decay-time-based chloride detection with the Cl^--sensitive dye MQAE. For two-photon FLIM, cells were transfected with GFP-tagged THP and compared with native cells in separate preparations. Transfected cells were identified by two-photon-excited GFP-fluorescence, and a bandpass filter (450/40 nm) was then added to reject the GFP signal. A resting $[Cl^-]_i$ of ~32 mM was observed in the non-transfected cells. $[Cl^-]_i$ was significantly decreased in THP-GFP-transfected cells (−40.4%, $p < 0.01$). Transfection with GFP vector alone did not influence $[Cl^-]_i$ (Fig. 4, *a–d*).

NKCC2 Activation by Low Chloride Hypotonic Stress—Functional consequences of THP transfection upon NKCC2 activity were assessed using the heterologous expression system of *X. laevis* oocytes as this system has been shown to provide a robust and highly reproducible strategy for functional analysis of NKCC2 (3, 5, 8, 14). Oocytes were injected with water, NKCC2 cRNA alone, THP cRNA alone, NKCC2 cRNA + THP cRNA, NKCC2 cRNA + WNK3 cRNA, or NKCC2 cRNA + WNK3 cRNA + THP cRNA. Three days later NKCC2 activity was assessed under basal conditions and after exposing oocytes to a low chloride hypotonic stress, as previously described (14). THP facilitated low chloride hypotonic stress-induced activation of NKCC2 (+112% in the absence of THP *versus* +235% in the presence of THP; $p < 0.01$; Fig. 5*a*). Moreover, THP increased the sensitivity of NKCC2 to intracellular chloride depletion also in the presence of WNK3, a strong activator of NKCC2. In oocytes coinjected with NKCC2 and WNK3, low chloride hypotonic stress induced no further increase of NKCC2 activity, whereas the additional coinjection of THP produced a sharp increase (+286%; $p < 0.01$; Fig. 5*b*).

Effect of Furosemide

To further support our hypothesis of a permissive role of THP for NKCC2-mediated salt reabsorption in TAL, we have studied the effects of furosemide treatment during 4h in WT and THP$^{-/-}$ mice. This resulted in significantly more pronounced increases in sodium excretion in WT compared with THP$^{-/-}$ mice (+462% *versus* +375%; $p < 0.05$), and increases in potassium and chloride excretion were also numerically higher in WT mice. By contrast, the changes in urine flow were similar in both strains (Fig. 6, *a–d*). These results indicate that the effects of furosemide were attenuated in THP$^{-/-}$ mice, which is consistent with a partial decrease of NKCC2 function in the absence of THP.

Vasopressin-induced Effects in TAL

To test the hypothesis that THP facilitates the activation of NKCC2, short term stimulation of the V2R-signaling pathway using the V2R agonist, dDAVP (30 min), or a combination of dDAVP and forskolin (30 min) was performed in mice and in cultured rbTAL cells. In WT mice, dDAVP administration produced significant increases of phospho-NKCC2 in the post-nuclear kidney homogenates (+92%; $p < 0.05$), whereas no changes were found in THP$^{-/-}$ mice (Fig. 7, *a* and *c*). THP-transfected rbTAL-cells responded to dDAVP + forskolin by a significant increase in phospho-NKCC2 signal in post-nuclear

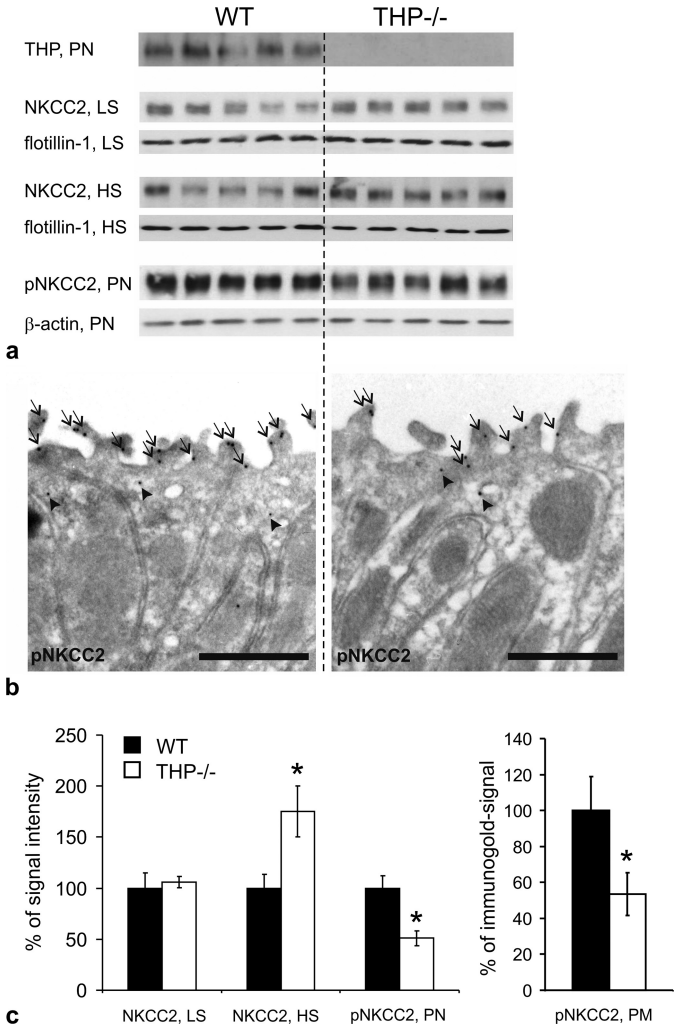

FIGURE 2. **Evaluation of total NKCC2- and phospho (*p*) NKCC2-immunoreactive signals in kidneys of WT and THP$^{-/-}$ mice (each *n* = 5).** *a*, shown are immunoblots of plasma membrane-enriched low speed fractions (*LS*), intracellular vesicle-enriched high speed fractions (*HS*), or post-nuclear fractions (*PN*) from kidneys of WT and THP$^{-/-}$ mice recognized by antibodies directed against THP (~100 kDa), NKCC2 (~160 kDa), and pNKCC2 (~160 kDa) paralleled by appropriate loading controls with antibodies against flotillin-1 (~50 kDa) as a membrane resident protein or β-actin (~40 kDa). *b*, shown is immunogold staining of WT and THP$^{-/-}$ ultrathin kidney sections (medullary thick ascending limbs) for pNKCC2 (6-nm gold particles; signal in luminal plasma membrane, *arrows*; signal in cytoplasmic vesicles, *arrowheads*; *scale bars* = 1 μm). *c*, shown is a densitometric evaluation of immunoreactive signals normalized for the respective loading controls and quantification of pNKCC2 signals in the apical plasma membrane (*PM*) by counting the gold particles on representative micrographs from WT and THP$^{-/-}$ mice (at least 10 profiles containing an average of 5 cells per profile were evaluated per individual). Data are the means ± S.D.; *, $p < 0.05$ for interstrain differences; WT is set at 100%.

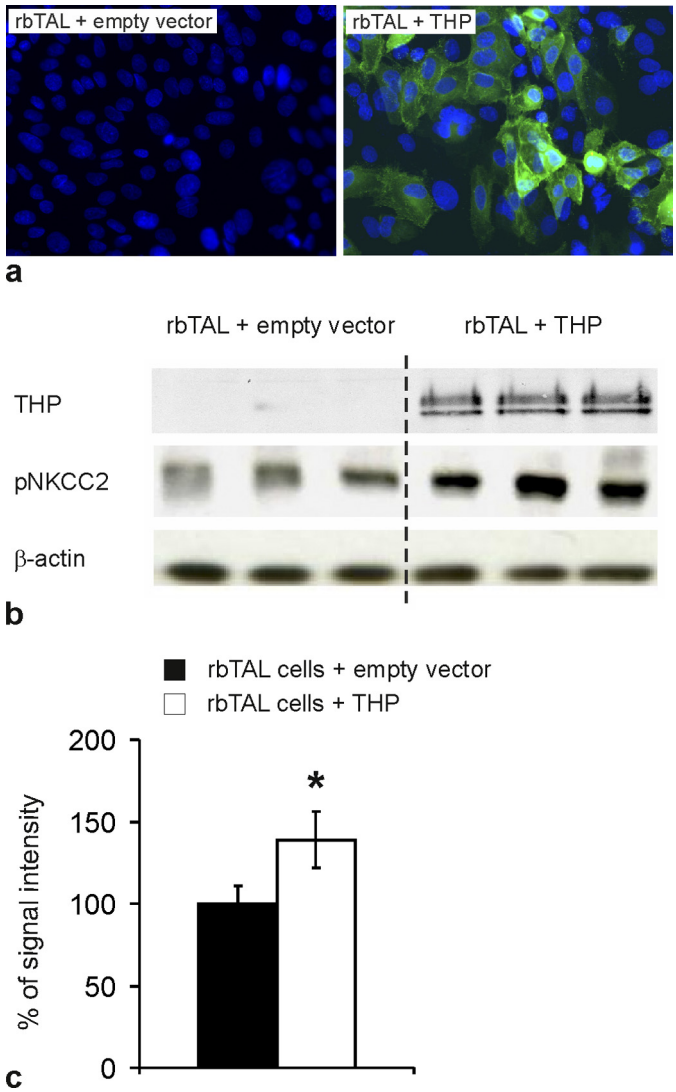

FIGURE 3. **Evaluation of NKCC2 phosphorylation in cultured rbTAL cells transiently transfected with empty vector or THP.** *a*, transfected cells are stained with anti-THP (*green* immunofluorescence), and nuclei are counterstained with DAPI (*blue*); the transient THP-transfection rate was ~60% (original magnification −400). *b*, post-nuclear fractions were detected by anti-THP and anti-pNKCC2 and anti-β-actin as the loading control (representative immunoblots are from three independent experiments). *c*, shown is a densitometric evaluation of pNKCC2 immunoreactive signals normalized for the loading control. Data are the means ± S.D.; *, $p < 0.05$ for differences between THP-transfected and control cells.

homogenates (+67%, $p < 0.05$), whereas cells transfected with control vector showed no change (Fig. 7, *b* and *c*). These data further confirm a role for THP in the activation of NKCC2 by phosphorylation.

Compensatory Changes in DCT

Evaluation of Fractional Volume of DCT and Phosphorylation of NCC—Any chronic deficit in TAL NaCl reabsorption is commonly reflected by compensatory increases of NaCl reabsorption, chiefly in the ensuing DCT segment. The immunoreactive signal intensity for NCC was generally enhanced in DCT of THP$^{-/-}$ compared with WT mice, consistent with previous Western blot data (15). The fractional cortical volume of DCT was compared between strains, revealing a significantly higher proportion of NCC-immunoreactive DCT segments in the cortex of THP$^{-/-}$ compared with WT mice (+40%; $p < 0.05$; Fig. 8, *a*, *b*, and *g*). Apical signal intensity of phospho-NCC was clearly enhanced in THP$^{-/-}$ compared with WT mice (Fig. 8, *c* and *d*). This difference was reflected by a 128% increase in phospho-NCC-signal of the plasma membrane-enriched fractions from THP$^{-/-}$ mice (Fig. 8, *e*, *f*, and *h*). Together, hypertrophy and/or elongation of the DCT along with enhanced phosphorylation of NCC thus corroborate our hypothesis of a compensatory adaptation of DCT in the absence of THP.

Osmotic Diuresis and HCTZ Test—Osmotic diuresis was induced in all mice to obtain sufficiently large urine volumes for

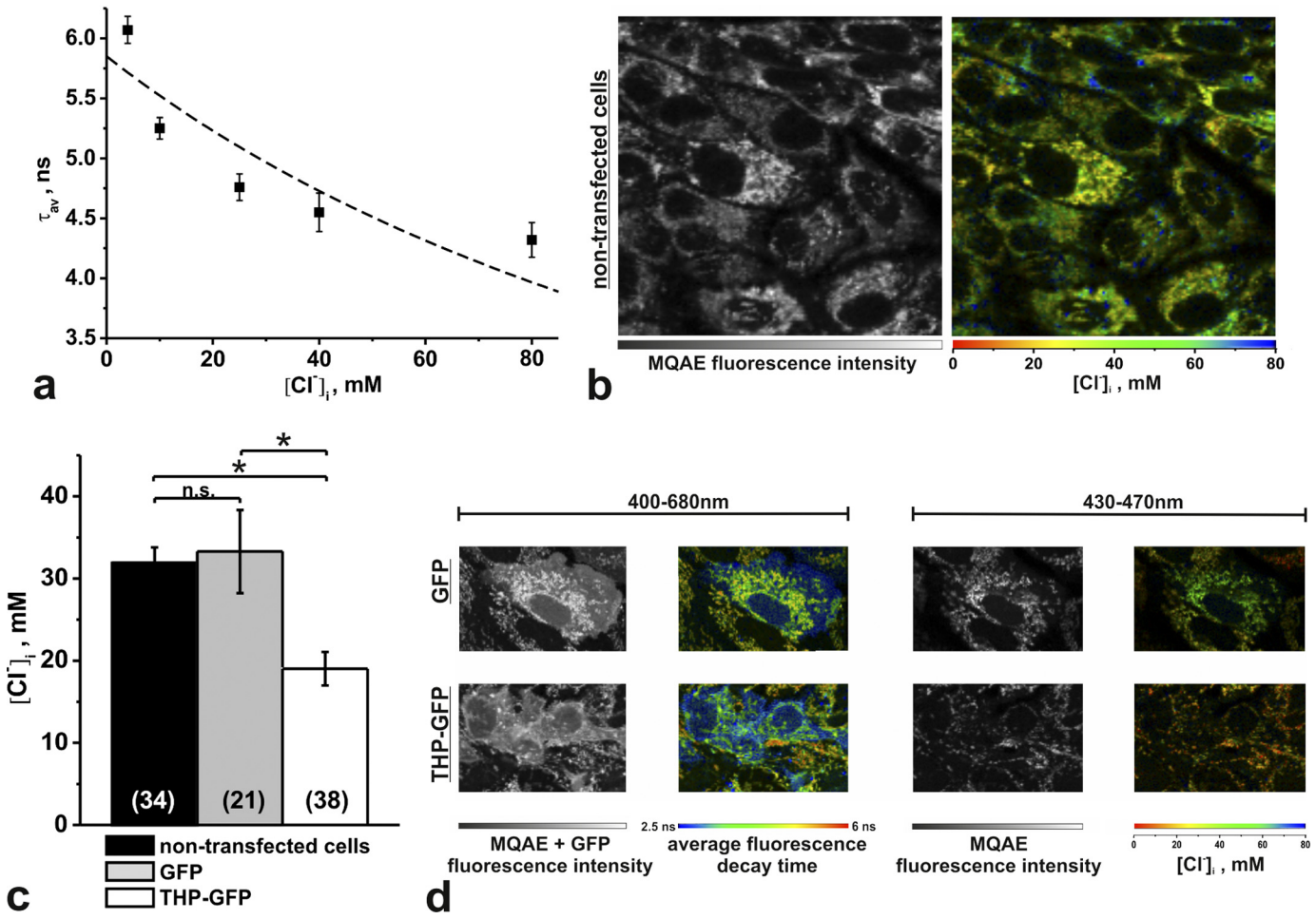

FIGURE 4. **$[Cl^-]_i$ recordings in rbTAL cells using two-photon FLIM and the Cl^--sensitive fluorescent dye MQAE.** *a*, *in situ* calibration using the ionophores tributyltin (40 μM) and nigericin (10 μM) demonstrate the dependence of the MQAE average fluorescence decay time (τ_{av}) on $[Cl^-]_i$. Data were fitted to the Stern-Volmer equation, $\tau_{av} = \tau_{av,0}/(1 + K_{SV}[Cl^-]_i)$, where $\tau_{av,0}$ and τ_{av} are the decay times in the absence and presence of chloride, respectively, and K_{SV} is the Stern-Volmer constant ($n = 4$–9 measurements, each corresponding to one FLIM image covering 10–20 cells). *b*, shown are MQAE fluorescence intensity and a corresponding FLIM image of non-transfected cells (τ_{av} is converted into $[Cl^-]_i$ and shown in false colors; scale 80 × 80 μm). *c*, shown is a statistical comparison (analysis of variance) of resting $[Cl^-]_i$ in non-transfected cells and cells transfected with GFP or THP-GFP (*n.s.*, not significant; *, $p < 0.01$; sample numbers are in *parentheses*). *d*, representative images of GFP- and THP-GFP-transfected cells are shown. Images recorded at 400–680 nm unravel both MQAE and GFP fluorescence and display an additional short fluorescence decay time of GFP (*blue*), which was used to identify and evaluate the transfected cells. Images recorded at 430–470 nm detect only the MQAE fluorescence and allow $[Cl^-]_i$ quantification (*scale*, 25 × 40 μm). Data are the means ± S.E.

urinalysis. Body weight, plasma osmolality, and plasma electrolytes were not different between strains after the administration of vehicle or HCTZ (Table 1). Urine flow was not different between strains during the osmotic diuresis phase as revealed by the four urine fractions that had been collected before treatment and after vehicle application. Administration of HCTZ in $THP^{-/-}$ mice significantly increased the mean urine volume per fraction (+37% in fraction 5 only, $p < 0.05$) without concomitant changes in urine osmolality as compared with the osmotic diuresis phase, whereas no significant changes were seen in WT mice. There were no interstrain differences with respect to mean fractional urine volumes and osmolalities during osmotic diuresis and after the administration of vehicle or HCTZ, respectively. Urinary sodium excretion was not different between strains during the osmotic diuresis phase and after vehicle application except for the last fraction (fraction 10). HCTZ significantly enhanced sodium excretion in both strains compared with vehicle. The initial natriuretic effect (first urine fraction collected after HCTZ injection *versus* the mean value of the 4 fractions from the osmotic diuresis phase) was significantly stronger in $THP^{-/-}$ than in WT mice (+88% in WT *versus* +188% in $THP^{-/-}$ mice, $p < 0.05$). The majority of the remaining fractions after HCTZ also showed higher sodium excretion in $THP^{-/-}$ compared with WT mice (Fig. 9*a*). The cumulative sodium excretion, calculated as the sum of the 6 urine fractions collected after HCTZ, was enhanced in both strains compared with vehicle, and the cumulative natriuretic effect of HCTZ was significantly stronger in $THP^{-/-}$ mice as compared with WT mice (+97%; $p < 0.01$; Fig. 9*b*). Urinary potassium excretion was not different between strains during the osmotic diuresis phase and after vehicle application, whereas the administration of HCTZ, in comparison to vehicle, significantly increased potassium excretion only in $THP^{-/-}$ mice (Fig. 10*a*). Cumulative potassium excretion was enhanced in $THP^{-/-}$ (+38%; $p < 0.05$) but not in WT mice after HCTZ administration, and interstrain differences were absent. To estimate potential compensatory transport adaptations in collecting ducts under HCTZ, the sodium/potassium ratio was

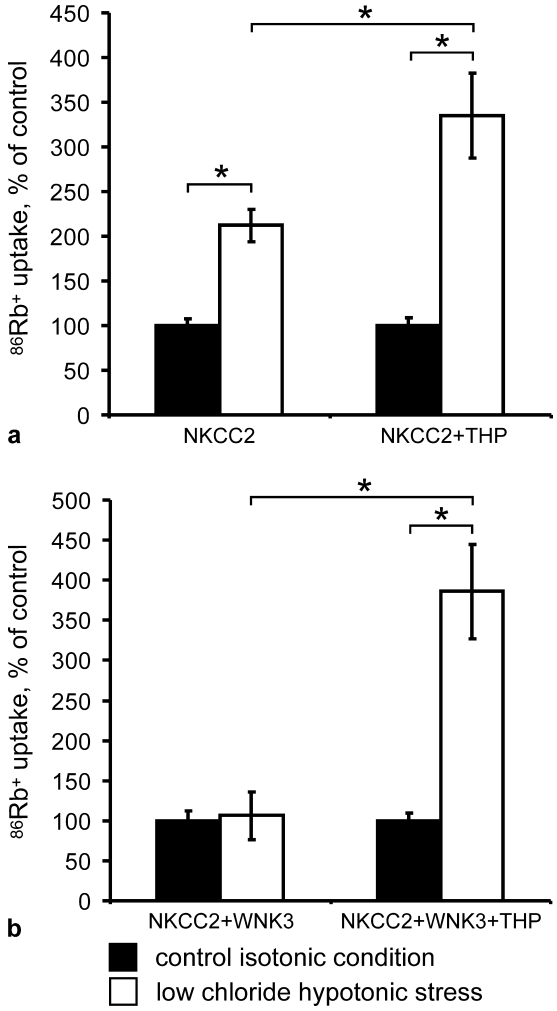

FIGURE 5. **THP facilitates activation of NKCC2 during low chloride hypotonic stress.** *a* and *b*, *Xenopus* oocytes were injected with water or the indicated cRNAs, and the bumetanide-sensitive $^{86}Rb^+$ uptake was measured as described under "Experimental Procedures." The uptake observed in control isotonic conditions (control) was set at 100%, and data recorded under low chloride hypotonic stress were normalized accordingly. Each panel shows the pooled results from two independent experiments with 10 oocytes per group each. Data are the means ± S.E.; *, $p < 0.01$ for differences between the indicated groups.

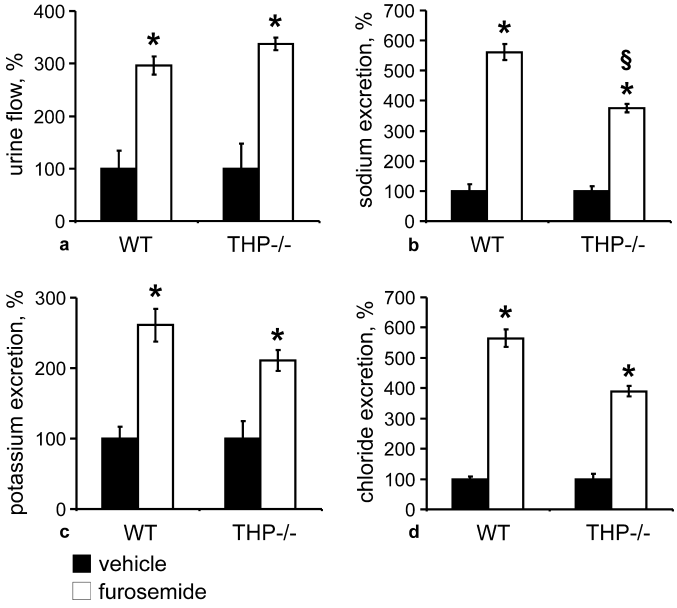

FIGURE 6. **Urinary flow and electrolyte excretion after application of vehicle or furosemide in WT and $THP^{-/-}$ mice (each $n = 10$).** *a–d*, urinary flow (*a*), sodium (*b*), potassium (*c*), and chloride excretion (*d*) obtained from WT and $THP^{-/-}$ mice treated with vehicle or furosemide for 4 h. *, $p < 0.05$ for intrastrain differences between vehicle and furosemide treatments; §, $p < 0.05$ for interstrain differences in the effects of furosemide. Note the significantly attenuated, furosemide-induced natriuresis in $THP^{-/-}$ compared with WT mice (*b*). Data are the means ± S.D. normalized to body weight (*a*) or creatinine excretion (*b–d*). The vehicle group was set at 100%.

calculated. Remarkably, administration of HCTZ induced by far stronger increases in the sodium/potassium ratio in $THP^{-/-}$ compared with WT mice (Fig. 10*b*). This suggests different compensatory capacities of the collecting duct between strains under HCTZ, likely due to persistent activation of the epithelial sodium channel in $THP^{-/-}$ mice (15).

DISCUSSION

Our previous findings on the role of THP had suggested a functionally relevant interaction between THP and transcellular ion transport in TAL (15). $THP^{-/-}$ mice displayed an impaired urinary concentrating ability under water deprivation. The abundances of distal tubular ion transporters or channels such as NCC and epithelial sodium channel were increased at steady state, although blood and urine electrolytes were not altered, suggesting compensatory adjustments by the renal tubule. The present results substantiate the functional relation between NKCC2 and THP; 1) phosphorylation of NKCC2 is modulated by THP likely in a chloride-sensitive manner, 2) activation of NKCC2 via intracellular chloride depletion is increased by cotransfection with THP, 3) effects of furosemide are blunted in $THP^{-/-}$ mice, and 4) DCT displays compensatory adaptation in $THP^{-/-}$ mice, likely reflecting impaired transport within the preceding TAL segment.

Our hypothesis of the role of THP affecting NKCC2-mediated TAL transport function has received substantial support by the present data. Two major criteria suitable to mirror the activity of NKCC2, *i.e.* its abundance at the luminal cell membrane and its phosphorylation state (2, 10), have been applied. While confirming the previously reported increase of total NKCC2 abundance in $THP^{-/-}$ mice (15), the present results have further revealed a disproportionate accumulation of NKCC2 in the subapical vesicle-enriched compartment of the TAL epithelium in $THP^{-/-}$ mice. The luminal abundance of NKCC2 was, however, not different between WT and $THP^{-/-}$ mice so that luminal trafficking of the transporter was probably not impaired. Instead, the subapical accumulation of the transporter in $THP^{-/-}$ mice may reflect an altered turnover, possibly via impaired degradation of NKCC2 in the absence of THP. However, because several other relevant distal transport proteins were enhanced as well (15), an increased intracellular abundance of NKCC2 may also reflect a broader need for compensation of the knock-out. The lack of THP further coincided with decreased steady state levels of phospho-NKCC2 *in vivo* as well as in cell culture, likely reflecting diminished activity of the cotransporter under this condition (2, 5, 11, 14). Along the same line, the present data on a blunted activation of NKCC2 upon stimulation of the V2R-signaling pathway as well as the

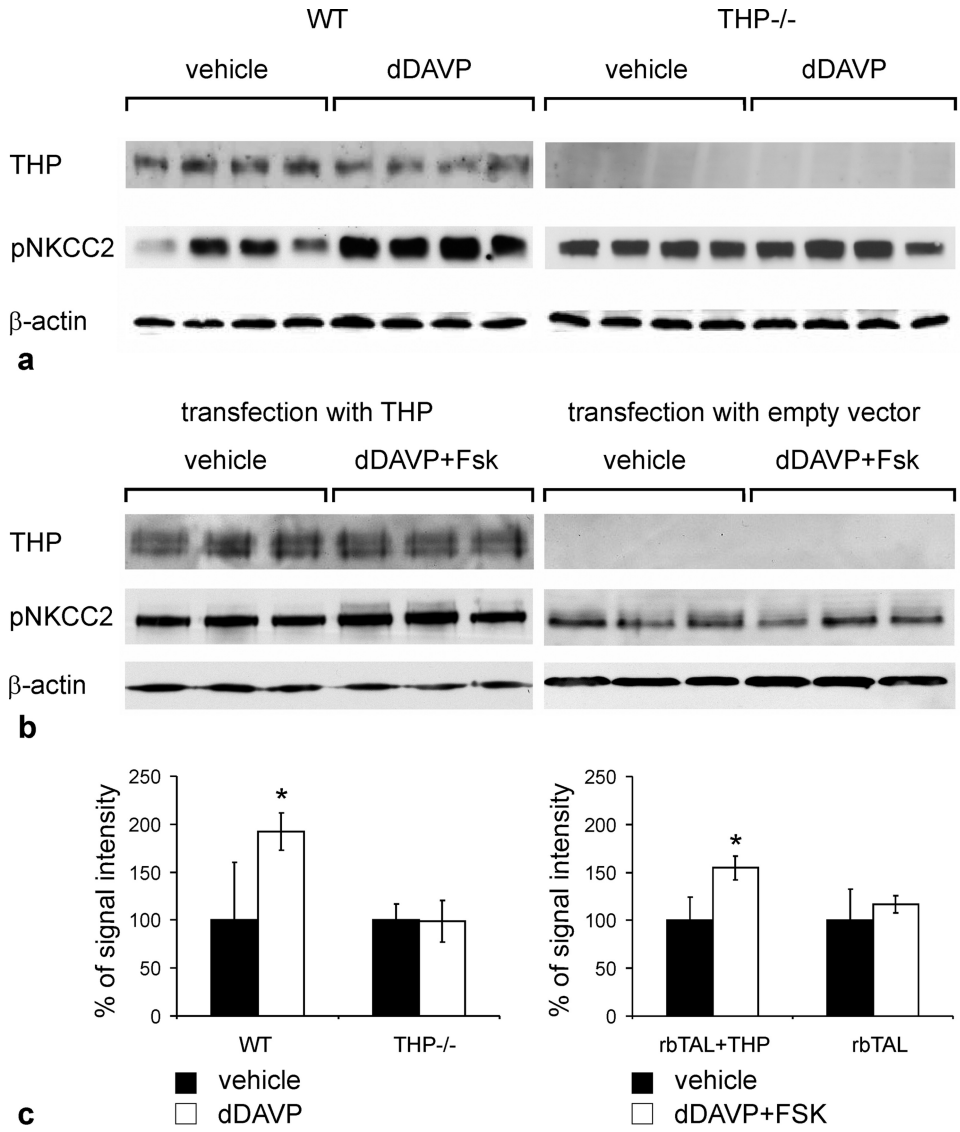

FIGURE 7. **Activation of NKCC2 by short term stimulation of V2 receptor signaling pathway in the presence or absence of THP.** *a* and *b*, immunoblots of post-nuclear fractions from WT and THP$^{-/-}$ mice (each $n = 8$; *a*) or rbTAL-cells transfected with THP or empty vector (*b*) show THP and pNKCC2 and β-actin as the loading control. *c*, shown is a densitometric evaluation of pNKCC2 signals normalized to β-actin. Data are the means ± S.D.; *, $p < 0.05$ for differences between vehicle treatment and stimulation (dDAVP for mice and dDAVP + forskolin (*Fsk*) for rbTAL-cells).

weakened response of THP$^{-/-}$ to furosemide also corroborate an altered NKCC2 function in THP$^{-/-}$ mice.

The mechanism of interaction between THP and NKCC2 is not clear. THP is an abundantly synthesized protein equipped with a glycosylphosphatidylinositol anchor (19). Glycosylphosphatidylinositol-anchored proteins have functions in trafficking of membrane proteins (39) and are ubiquitous components of lipid rafts, in which they may cluster to provide sorting signals for intracellular membrane compartments (30, 39). We have demonstrated close subcellular co-localization of THP and NKCC2, a raft protein itself as well, which suggests that the two proteins may share lipid raft localization (19, 30, 40). Our previous data indicated that activation of NKCC2 is dependent on its presence in lipid rafts (30). Glycosylphosphatidylinositol-anchored THP could, therefore, affect the function of rafts to provide scaffolding platforms that may promote interactions of relevant phosphokinases with NKCC2 (5, 11, 39). These possible interactions may thus serve to explain the failure of NKCC2 to be activated adequately in the absence of THP.

Our results from cultured rbTAL cells have unexpectedly revealed a marked reduction in $[Cl^-]_i$ upon transfection with THP. This may, however, reflect functional activation of NKCC2 nevertheless, since in the setting of an enhanced NaCl transport in medullary TAL induced by cAMP administration, the basolateral membrane conductance, equivalent to the chloride conductance in TAL, was primarily increased in conjunction with decreased transepithelial resistance, which eventually led to reduced $[Cl^-]_i$ levels (41). Along the same line, studies in the *Xenopus* oocyte system have identified the crucial role of a chloride-sensing mechanism in the context of activation of NKCC2 and related NCC by means of phosphorylation. For both transporters, $[Cl^-]_i$ depletion led to an augmented bumetanide/thiazide-sensitive Na^+ uptake; the changes in $[Cl^-]_i$ involved the interaction of distinct WNK isoforms and SPS1-

related Pro/Ala-rich kinase/oxidative stress-responsive kinase 1 kinases to phosphorylate NKCC2 or NCC (14, 33). These observations also imply that in the presence of THP, our finding of low $[Cl^-]_i$ levels at steady state may mirror enhanced transepithelial transport of NaCl triggered by higher NKCC2 phosphorylation as compared with the situation in control rbTAL cells lacking THP. Recently, the apical potassium channel ROMK of TAL was shown to reveal enhanced ROMK current amplitudes measured in *Xenopus* oocytes when co-expressed with THP (42). Therefore, the correction of an insufficient apical K-conductance in THP deficiency by substituting THP may as well help to explain our observations on decreased $[Cl^-]_i$ concentration. In humans, malfunction of this major apical K^+ channel is associated with major reabsorptive defects in TAL causing type II Bartter syndrome (4, 43), which is compatible with reduced basolateral Cl^- conductance.

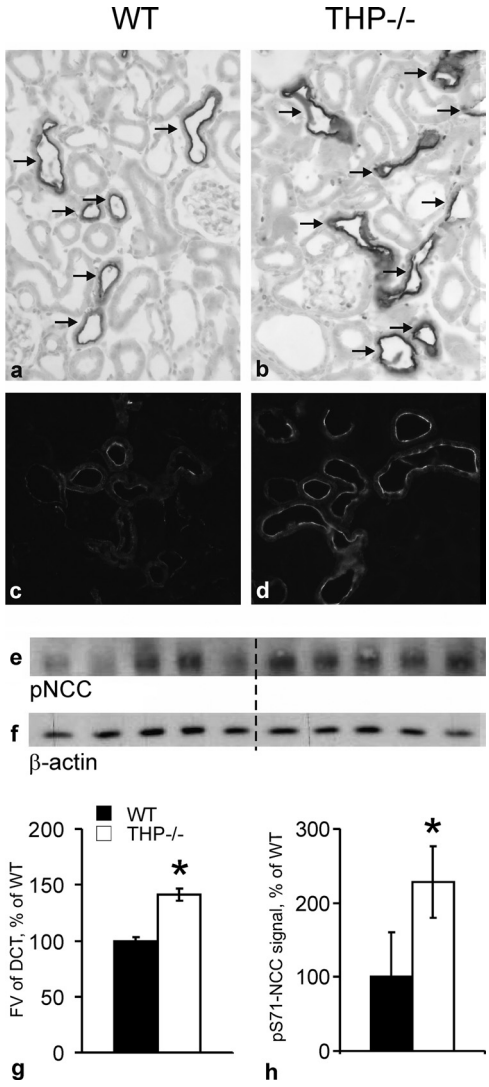

FIGURE 8. **Evaluation of fractional volumes of DCT and phosphorylation of the NCC in kidneys from WT and THP$^{-/-}$ mice (each $n = 4$ and $n = 5$, respectively) at steady state.** *a* and *b*, representative images show a larger proportion of DCT labeled with antibody against NCC in THP$^{-/-}$ than in WT mice (immunoperoxidase staining); *arrows* point to DCT. *c* and *d*, shown is enhanced phosphorylation of NCC in THP$^{-/-}$ mice compared with WT mice by immunostaining against phospho-NCC. *e*, shown are post-nuclear fractions from WT and THP$^{-/-}$ mice detected by Western blot and anti-phospho-NCC antibody (~160 kDa). *f*, shown are loading controls with antibody against β-actin. *g*, shown is morphometric quantification of the fractional volume (*FV*) of DCT. *h*, shown is a densitometric evaluation of phospho-NCC (Ser(P)-71 (*pS71-NCC*)) immunoreactive signals normalized for the loading control. Data are the means ± S.D.; *, $p < 0.05$ for interstrain differences. Original magnification in *a–d*, ×400.

More direct evidence for the facilitating effects of THP on NKCC2-mediated transport is provided by our present *Xenopus* oocyte study. THP enhanced the level of NKCC2 activation by the low chloride hypotonic stress maneuver both in the presence and in the absence of WNK3. Of note, we previously showed that activation of NKCC2 and related NCC by low chloride hypotonic stress is associated with phosphorylation of NKCC2 at the same amino-terminal threonines that become phosphorylated by vasopressin (14, 33).

In aggregate, these considerations point to an insufficient function of NKCC2 and lower sensitivity of the cotransporter to changes in intracellular chloride concentration in the absence of THP. THP appears to facilitate base-line and AVP-induced phosphorylation of NKCC2 by involving a chloride-sensing mechanism. We, therefore, assume that in THP$^{-/-}$ mice, a functional insufficiency of transepithelial NaCl transport occurs along TAL with the exception of the macula densa, which is free of THP by nature (16).

To corroborate our hypothesis we have analyzed the DCT of THP$^{-/-}$ mice for potential compensatory activity, balancing the insufficiency of the preceding TAL. The high effectivity of DCT in this respect has been established and functional as well as structural features of the adaptive response have been demonstrated (27, 28, 36, 37, 44).

At steady state, the measured increases in cortical fractional volume of DCT provides clear evidence for the hypertrophy or elongation of this segment in THP$^{-/-}$ mice. The parallel rise in NCC immunoreactivity in THP$^{-/-}$ agrees with previously reported increases in NCC biosynthesis (15). Because NCC, like NKCC2, is activated by phosphorylation (29, 34, 45), the observed increases in phospho-NCC abundance clearly point to a functional activation of this transporter in THP$^{-/-}$ mice. The present functional data on disproportionally enhanced loss of urinary sodium in THP$^{-/-}$ mice in response to HCTZ further confirms the compensatory role of DCT in THP$^{-/-}$ mice. The significantly higher sodium-to-potassium ratio in THP$^{-/-}$

TABLE 1
Body weight, plasma osmolality, and plasma electrolytes

	Vehicle, WT ($n = 6$)	Vehicle, THP$^{-/-}$ ($n = 9$)	HCTZ, WT ($n = 6$)	HCTZ, THP$^{-/-}$ ($n = 14$)
Body weight, g	29.6 ± 1.2	30.8 ± 3.2	32.5 ± 1.3	32.6 ± 0.7
Plasma osmolality, mosmol/liter	321.0 ± 5.6	317.4 ± 18.5	326.8 ± 7.0	314.1 ± 5.5
Plasma sodium, mmol/liter[a]	118.7 ± 2.5	118.0 ± 12.3	125.0 ± 5.6	121.5 ± 2.7
Plasma potassium, mmol/liter	6.1 ± 0.2	6.38 ± 1.7	4.8 ± 0.4	5.4 ± 0.3

[a] Plasma sodium levels were low probably due to the extensive dilution occurring during prolonged osmotic diuresis. All values are the mean values ± S.E.

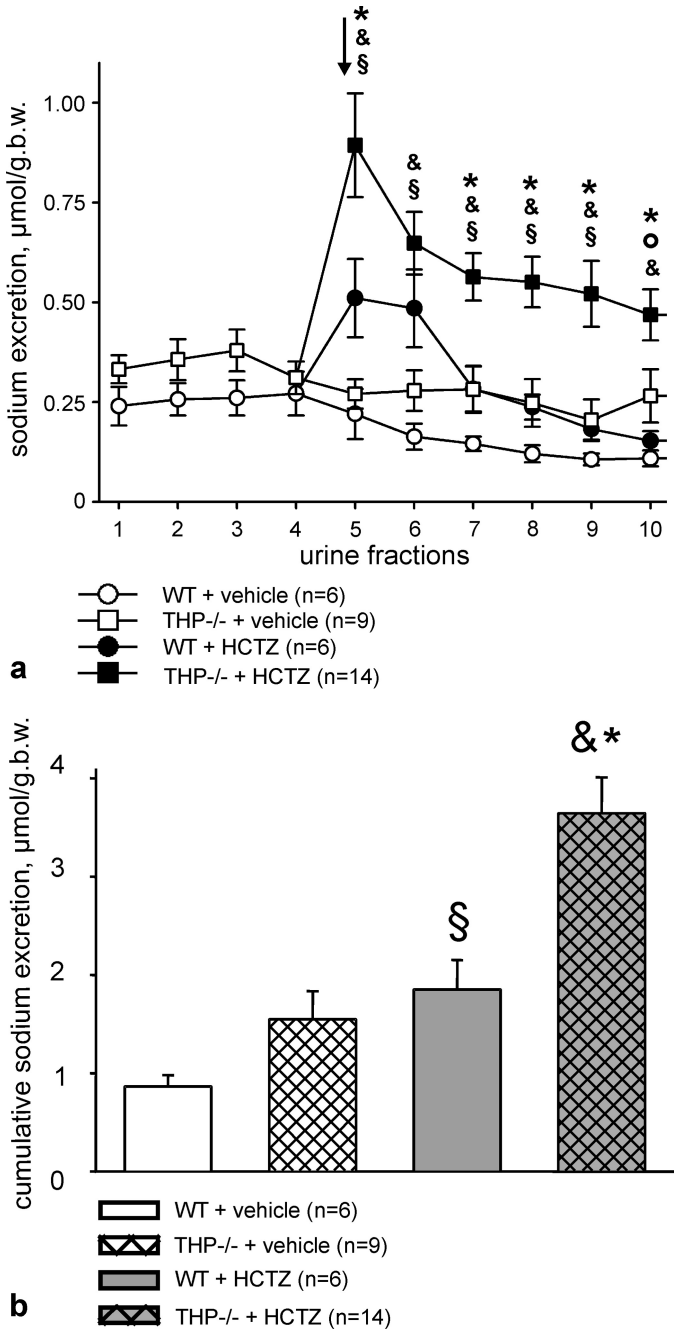

FIGURE 9. **Urinary sodium excretion under osmotic diuresis alone and after additional application of HCTZ or vehicle in WT and THP$^{-/-}$ mice.** *a*, urinary sodium excretion shows the mean values of urine fractions obtained during osmotic diuresis phase (urine fractions *1–4*; WT mice (n = 12), and THP$^{-/-}$ mice (n = 23) and after additional HCTZ or vehicle application (*fractions 5–10* after division of the groups; numbers of individuals are indicated in the diagrams). The *arrow* points to the first urine fraction collected after HCTZ or vehicle treatment. Each fraction was collected within 15 min. *b.w.*, body weight. *b*, shown is cumulative sodium excretion after HCTZ or vehicle application (sum of *fractions 5–10* in *a*). §, $p < 0.05$ for differences between HCTZ- and vehicle-treated WT mice; &, $p < 0.05$ for differences between HCTZ- and vehicle-treated THP$^{-/-}$ mice; °, $p < 0.05$ for differences between vehicle-treated WT and THP$^{-/-}$ mice; *, $p < 0.05$ for differences between HCTZ-treated WT and THP$^{-/-}$ mice. All data are given as the means ± S.E.

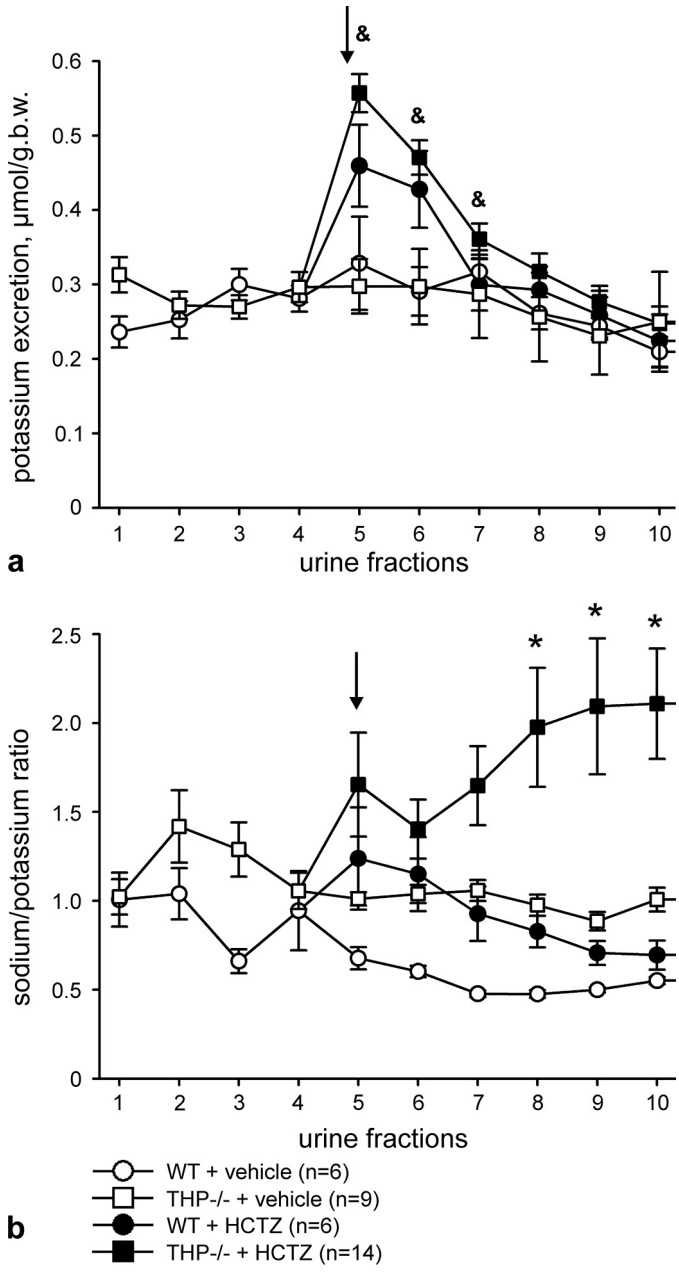

FIGURE 10. **Urinary potassium excretion and sodium/potassium ratio under osmotic diuresis alone and after additional application of HCTZ or vehicle in WT and THP$^{-/-}$ mice.** *a*, urinary potassium excretion shows the mean values of fractions obtained during the osmotic diuresis phase (urine fractions *1–4*; WT mice (n = 12) and THP$^{-/-}$ mice (n = 23)) and after additional HCTZ or vehicle application (*fractions 5–10* after division of the groups; numbers of individuals are indicated in the diagrams). The *arrow* points to the first urine fraction collected after HCTZ or vehicle treatment. Each fraction was collected within 15 min. *b*, in analogy, sodium/potassium ratios are shown as the means of the respective fractions. &, $p < 0.05$ for differences between HCTZ- and vehicle-treated THP$^{-/-}$ mice; *, $p < 0.05$ for differences between HCTZ treated WT and THP$^{-/-}$ mice. For the sodium/potassium ratio, only the differences between HCTZ-treated WT and THP$^{-/-}$ mice are calculated. All data are given as the means ± S.E.

than in WT mice suggests a different compensatory capacity of the collecting duct under HCTZ, likely due to persistent activation of the epithelial sodium channel in THP$^{-/-}$ mice. These results confirm the compensatory role of DCT in THP$^{-/-}$ mice and provide additional evidence for a decreased NaCl transport capacity of their TAL segments. Compared with the drastically impaired renal function in the NKCC2 knock-out mouse (7), however, it may reasonably be assumed that THP-deficient TAL still retains significant residual NKCC2 activity.

Our model presents some major inequities when compared with human defects in THP causing familial juvenile hyperuricemic nephropathy or medullary cystic kidney disease type 2 (24, 25) and a mouse model expressing mutated THP (26). In these studies, markedly compromised urinary concentrating ability associated with THP gene mutations has been proposed to result from the toxic effects of intracellularly accumulated, misfolded protein (24–26, 46). In contrast, $THP^{-/-}$ mice presented normal TAL morphology along with moderately decreased urinary concentrating ability (15).

Collectively, our study suggests that THP is functionally related with NKCC2-mediated NaCl reabsorption in TAL. Two hypotheses were confirmed; 1) activation of NKCC2 is facilitated by THP in a chloride sensitive manner, and 2) in $THP^{-/-}$ mice, structural and functional changes of the DCT indicate compensatory adaption of this segment, presumably in response to an impaired NaCl reabsorption in the preceding, THP-deficient TAL. Our results, therefore, provide convincing support for a role of THP in the functioning of the renal concentrating mechanism. Data may further explain urinary concentration defects in patients with THP/uromodulin mutations.

Acknowledgments—We thank Dr. D. H. Ellison (Portland, Oregon) for providing antibody to NCC, Drs. E. Seeliger and B. Flemming (Berlin) and M. Bleich (Kiel) for discussion of the physiological data, and K. Riskowsky, F. Grams, E. Schindler, M. Gutsmann, C. Riquelme, and N. Vazquez for expert technical assistance.

REFERENCES

1. Obermüller, N., Kunchaparty, S., Ellison, D. H., and Bachmann, S. (1996) *J. Clin. Invest.* **98,** 635–640
2. Giménez, I., and Forbush, B. (2003) *J. Biol. Chem.* **278,** 26946–26951
3. Gamba, G. (2005) *Physiol. Rev.* **85,** 423–493
4. Reinalter, S. C., Jeck, N., Peters, M., and Seyberth, H. W. (2004) *Acta Physiol. Scand.* **181,** 513–521
5. Rinehart, J., Kahle, K. T., de Los Heros, P., Vazquez, N., Meade, P., Wilson, F. H., Hebert, S. C., Gimenez, I., Gamba, G., and Lifton, R. P. (2005) *Proc. Natl. Acad. Sci. U.S.A.* **102,** 16777–16782
6. Schnermann, J. (1998) *Am. J. Physiol.* **274,** R263–R279
7. Takahashi, N., Chernavvsky, D. R., Gomez, R. A., Igarashi, P., Gitelman, H. J., and Smithies, O. (2000) *Proc. Natl. Acad. Sci. U.S.A.* **97,** 5434–5439
8. Meade, P., Hoover, R. S., Plata, C., Vázquez, N., Bobadilla, N. A., Gamba, G., and Hebert, S. C. (2003) *Am. J. Physiol. Renal Physiol.* **284,** F1145–F1154
9. Ortiz, P. A. (2006) *Am. J. Physiol. Renal Physiol.* **290,** F608–F616
10. Mutig, K., Paliege, A., Kahl, T., Jöns, T., Müller-Esterl, W., and Bachmann, S. (2007) *Am. J. Physiol. Renal Physiol.* **293,** F1166–F1177
11. Delpire, E., and Gagnon, K. B. (2008) *Biochem. J.* **409,** 321–331
12. Amlal, H., Legoff, C., Vernimmen, C., Paillard, M., and Bichara, M. (1996) *Am. J. Physiol.* **271,** C455–C463
13. Hebert, S. C., Culpepper, R. M., and Andreoli, T. E. (1981) *Am. J. Physiol.* **241,** F412–F431
14. Ponce-Coria, J., San-Cristobal, P., Kahle, K. T., Vazquez, N., Pacheco-Alvarez, D., de Los Heros, P., Juárez, P., Muñoz, E., Michel, G., Bobadilla, N. A., Gimenez, I., Lifton, R. P., Hebert, S. C., and Gamba, G. (2008) *Proc. Natl. Acad. Sci. U.S.A.* **105,** 8458–8463
15. Bachmann, S., Mutig, K., Bates, J., Welker, P., Geist, B., Gross, V., Luft, F. C., Alenina, N., Bader, M., Thiele, B. J., Prasadan, K., Raffi, H. S., and Kumar, S. (2005) *Am. J. Physiol. Renal Physiol.* **288,** F559–F567
16. Bachmann, S., Koeppen-Hagemann, I., and Kriz, W. (1985) *Histochemistry* **83,** 531–538
17. Bachmann, S., Bostanjoglo, M., Schmitt, R., and Ellison, D. H. (1999) *Anat. Embryol.* **200,** 447–468
18. Nielsen, S., Maunsbach, A. B., Ecelbarger, C. A., and Knepper, M. A. (1998) *Am. J. Physiol.* **275,** F885–F893
19. Malagolini, N., Cavallone, D., and Serafini-Cessi, F. (1997) *Kidney Int.* **52,** 1340–1350
20. Bates, J. M., Raffi, H. M., Prasadan, K., Mascarenhas, R., Laszik, Z., Maeda, N., Hultgren, S. J., and Kumar, S. (2004) *Kidney Int.* **65,** 791–797
21. Mo, L., Zhu, X. H., Huang, H. Y., Shapiro, E., Hasty, D. L., and Wu, X. R. (2004) *Am. J. Physiol. Renal Physiol.* **286,** F795–F802
22. Säemann, M. D., Weichhart, T., Zeyda, M., Staffler, G., Schunn, M., Stuhlmeier, K. M., Sobanov, Y., Stulnig, T. M., Akira, S., von Gabain, A., von Ahsen, U., Hörl, W. H., and Zlabinger, G. J. (2005) *J. Clin. Invest.* **115,** 468–475
23. Schröter, J., Timmermans, G., Seyberth, H. W., Greven, J., and Bachmann, S. (1993) *Kidney Int.* **44,** 401–410
24. Dahan, K., Devuyst, O., Smaers, M., Vertommen, D., Loute, G., Poux, J. M., Viron, B., Jacquot, C., Gagnadoux, M. F., Chauveau, D., Büchler, M., Cochat, P., Cosyns, J. P., Mougenot, B., Rider, M. H., Antignac, C., Verellen-Dumoulin, C., and Pirson, Y. (2003) *J. Am. Soc. Nephrol.* **14,** 2883–2893
25. Hart, T. C., Gorry, M. C., Hart, P. S., Woodard, A. S., Shihabi, Z., Sandhu, J., Shirts, B., Xu, L., Zhu, H., Barmada, M. M., and Bleyer, A. J. (2002) *J. Med. Genet.* **39,** 882–892
26. Kemter, E., Rathkolb, B., Rozman, J., Hans, W., Schrewe, A., Landbrecht, C., Klaften, M., Ivandic, B., Fuchs, H., Gailus-Durner, V., Klingenspor, M., de Angelis, M. H., Wolf, E., Wanke, R., and Aigner, B. (2009) *Am. J. Physiol. Renal Physiol.* **297,** F1391–F1398
27. Abdallah, J. G., Schrier, R. W., Edelstein, C., Jennings, S. D., Wyse, B., and Ellison, D. H. (2001) *J. Am. Soc. Nephrol.* **12,** 1335–1341
28. Wagner, C. A., Loffing-Cueni, D., Yan, Q., Schulz, N., Fakitsas, P., Carrel, M., Wang, T., Verrey, F., Geibel, J. P., Giebisch, G., Hebert, S. C., and Loffing, J. (2008) *Am. J. Physiol. Renal Physiol.* **294,** F1373–F1380
29. Mutig, K., Saritas, T., Uchida, S., Kahl, T., Borowski, T., Paliege, A., Böhlick, A., Bleich, M., Shan, Q., and Bachmann, S. (2010) *Am. J. Physiol. Renal Physiol.* **298,** F502–F509
30. Welker, P., Böhlick, A., Mutig, K., Salanova, M., Kahl, T., Schlüter, H., Blottner, D., Ponce-Coria, J., Gamba, G., and Bachmann, S. (2008) *Am. J. Physiol. Renal Physiol.* **295,** F789–F802
31. Schaeffer, C., Santambrogio, S., Perucca, S., Casari, G., and Rampoldi, L. (2009) *Mol. Biol. Cell* **20,** 589–599
32. Hille, C., Lahn, M., Löhmannsröben, H. G., and Dosche, C. (2009) *Photochem. Photobiol. Sci.* **8,** 319–327
33. Pacheco-Alvarez, D., Cristóbal, P. S., Meade, P., Moreno, E., Vazquez, N., Muñoz, E., Díaz, A., Juárez, M. E., Giménez, I., and Gamba, G. (2006) *J. Biol. Chem.* **281,** 28755–28763
34. Chiga, M., Rai, T., Yang, S. S., Ohta, A., Takizawa, T., Sasaki, S., and Uchida, S. (2008) *Kidney Int.* **74,** 1403–1409
35. Sandberg, M. B., Riquier, A. D., Pihakaski-Maunsbach, K., McDonough, A. A., and Maunsbach, A. B. (2007) *Am. J. Physiol. Renal Physiol.* **293,** F662–F669
36. Ellison, D. H., Velázquez, H., and Wright, F. S. (1989) *J. Clin. Invest.* **83,** 113–126
37. Kaissling, B., Bachmann, S., and Kriz, W. (1985) *Am. J. Physiol.* **248,** F374–F381
38. Sachs, A. N., Pisitkun, T., Hoffert, J. D., Yu, M. J., and Knepper, M. A. (2008) *Am. J. Physiol. Renal Physiol.* **295,** F1799–F1806
39. Paladino, S., Lebreton, S., Tivodar, S., Campana, V., Tempre, R., and Zurzolo, C. (2008) *J. Cell Sci.* **121,** 4001–4007
40. Wilson, B. S., Steinberg, S. L., Liederman, K., Pfeiffer, J. R., Surviladze, Z., Zhang, J., Samelson, L. E., Yang, L. H., Kotula, P. G., and Oliver, J. M. (2004) *Mol. Biol. Cell* **15,** 2580–2592
41. Schlatter, E., and Greger, R. (1985) *Pflügers Arch.* **405,** 367–376
42. Renigunta, A., Renigunta, V., Saritas, T., Decher, N., Mutig, K., and Waldegger, S. (2011) *J. Biol. Chem.* **286,** 2224–2235
43. Welling, P. A., and Ho, K. (2009) *Am. J. Physiol. Renal Physiol.* **297,** F849–F463
44. Na, K. Y., Oh, Y. K., Han, J. S., Joo, K. W., Lee, J. S., Earm, J. H., Knepper, M. A., and Kim, G. H. (2003) *Am. J. Physiol. Renal Physiol.* **284,** F133–F143
45. Richardson, C., Rafiqi, F. H., Karlsson, H. K., Moleleki, N., Vandewalle, A., Campbell, D. G., Morrice, N. A., and Alessi, D. R. (2008) *J. Cell Sci.* **121,** 675–684
46. Choi, S. W., Ryu, O. H., Choi, S. J., Song, I. S., Bleyer, A. J., and Hart, T. C. (2005) *J. Am. Soc. Nephrol.* **16,** 3006–3014

3.4 A SPAK isoform switch modulates renal salt transport and blood pressure.

***McCormick JA*, Mutig K*, Nelson JH*,* Saritas T, Hoorn EJ, Yang CL, Rogers S, Curry J, Delpire E, Bachmann S, Ellison DH.**

* equal contribution

***Cell Metab.* 2011 Sep 7;14(3):352-64.**

Phosphorylation of NKCC2 and NCC at their conserved N-terminal threonine and serine residues critically defines their transport activity [33]. Previous work indicated that phosphorylation of these transporters is provided by two homologous kinases, SPAK and OSR1 [35]. In the present collaborative study we have taken advantage of SPAK-deficient mice and focused on the role of SPAK in regulation of NKCC2 and NCC *in vivo*. We have shown here that renal SPAK gene gives rise to two structurally and functionally different splice variants, the catalytically-active full-length SPAK variant (FL-SPAK) and the truncated, kidney-specific splice variant totally lacking the catalytic domain and kinase activity (KS-SPAK). Analysis of their renal distribution revealed that the FL-SPAK predominates in the DCT, where it plays crucial role in phosphorylation of NCC, whereas the KS-SPAK variant is chiefly expressed in the TAL, where it acts as an endogenous inhibitors of NKCC2 phosphorylation via competing with the FL-SPAK or OSR1 kinases for the binding with the transporter. This study provides new mechanistic insights into the regulation of the key distal salt transporters, NKCC2 and NCC, by the two divergent SPAK variants.

Cell Metabolism
Article

A SPAK Isoform Switch Modulates Renal Salt Transport and Blood Pressure

James A. McCormick,[1,5,*] Kerim Mutig,[2,5] Joshua H. Nelson,[1,5] Turgay Saritas,[2] Ewout J. Hoorn,[1] Chao-Ling Yang,[1] Shaunessy Rogers,[1] Joshua Curry,[1] Eric Delpire,[3] Sebastian Bachmann,[2] and David H. Ellison[1,4]
[1]Division of Nephrology and Hypertension, Oregon Health and Science University, Portland, OR 97239-3098, USA
[2]Institut für Vegetative Anatomie, Charité-Universitätsmedizin Berlin, Campus Charité-Mitte, 10115 Berlin, Germany
[3]Vanderbilt University, Nashville, TN 37240, USA
[4]VA Medical Center, Portland, OR 97239, USA
[5]These authors contributed equally to this work
*Correspondence: mccormij@ohsu.edu
DOI 10.1016/j.cmet.2011.07.009

SUMMARY

The renal thick ascending limb (TAL) and distal convoluted tubule (DCT) play central roles in salt homeostasis and blood pressure regulation. An emerging model suggests that bumetanide- and thiazide-sensitive NaCl transporters (NKCC2 and NCC) along these segments are phosphorylated and activated by WNK kinases, via SPAK and OSR1. Here, we show that a kidney-specific SPAK isoform, which lacks the kinase domain, inhibits phosphorylation of NCC and NKCC2 by full-length SPAK in vitro. Kidney-specific SPAK is highly expressed along the TAL, whereas full-length SPAK is more highly expressed along the DCT. As predicted from the differential expression, SPAK knockout in animals has divergent effects along TAL and DCT, with increased phosphorylated NKCC2 along TAL and decreased phosphorylated NCC along DCT. In mice, extracellular fluid volume depletion shifts SPAK isoform abundance to favor NaCl retention along both segments, indicating that a SPAK isoform switch modulates sodium avidity along the distal nephron.

INTRODUCTION

Arterial pressure and extracellular fluid (ECF) volume are determined largely by renal NaCl excretory capacity. A key signaling pathway that modulates NaCl reabsorption and K^+ secretion involves WNK kinases interacting with SPAK and OSR1. These kinases act along the distal nephron to modulate the bumetanide-sensitive Na-K-2Cl cotransporter (NKCC2) and the thiazide-sensitive NaCl cotransporter (NCC). The STE20 (sterile 20)-like kinases SPAK (STE20- and SPS1-related proline/alanine-rich kinase) and OSR1 (oxidative stress response kinase-1, abbreviated *OXSR1* in GenBank) contribute to ion homeostasis and cell volume control (Delpire and Gagnon, 2008). In mammalian cells, SPAK phosphorylates and activates the cation chloride cotransporters, NKCC1, NKCC2, and NCC, under hyperosmotic or hypotonic low-Cl^- conditions (Richardson et al., 2011); members of the WNK family act upstream of SPAK, phosphorylating it within the T-loop of the catalytic domain and within a C-terminal noncatalytic region (Vitari et al., 2005). WNK kinase effects on SPAK activity may contribute to human hypertension, as mutations in genes encoding WNK 1 and 4 cause the human disease familial hyperkalemic hypertension (FHHt, also known as pseudohypoaldosteronism II, or Gordon Syndrome) (Wilson et al., 2001), a disease associated with increased NCC activity (Mayan et al., 2002).

These data have led to a linear model of WNK/SPAK-OSR1/NKCC2-NCC signaling in which WNKs phosphorylate and activate SPAK-OSR1, which phosphorylates and activates NCC and NKCC2 (Richardson and Alessi, 2008). This suggests that SPAK-OSR1 inhibition should suppress the activity of both NCC and NKCC2 (Richardson et al., 2011). Yet recent data from animal models are not entirely consistent with this view. Alessi and colleagues (Rafiqi et al., 2010) generated mice that express a SPAK mutant that cannot be activated. The animals exhibited reductions in phosphorylated (activated) NCC and NKCC2 and were substantially hypotensive. In contrast, Yang and colleagues reported that, in SPAK knockout animals, there was less phosphorylated NCC, but more phosphorylated NKCC2 in kidney; the salt-wasting phenotype in these mice was also milder. Thus, deletion of SPAK and inactivation of SPAK have similar effects on NCC, but divergent effects on NKCC2; this discrepancy was pointed out recently in an editorial (Rodan and Huang, 2010). Here, we show that renal SPAK comprises several structurally and functionally dissimilar isoforms, at least one of which is inhibitory rather than stimulatory. These isoforms are differentially expressed along the TAL and DCT and are regulated according to ECF volume. The data provide an explanation for the discrepant results described above; suggest a reason that two very similar kinases, OSR1 and SPAK, are present in the same kidney epithelial cells; and unravel a mechanism for NaCl and blood pressure homeostasis.

RESULTS

Renal SPAK Products Include Antagonistic Isoforms

Typically, SPAK is believed to be a full-length kinase (Delpire and Gagnon, 2008), but additional forms have been described (Piechotta et al., 2003). Full-length SPAK is expressed prominently in brain and most other tissues (Rafiqi et al., 2010); on immunoblots from kidney, however, nearly all SPAK runs as

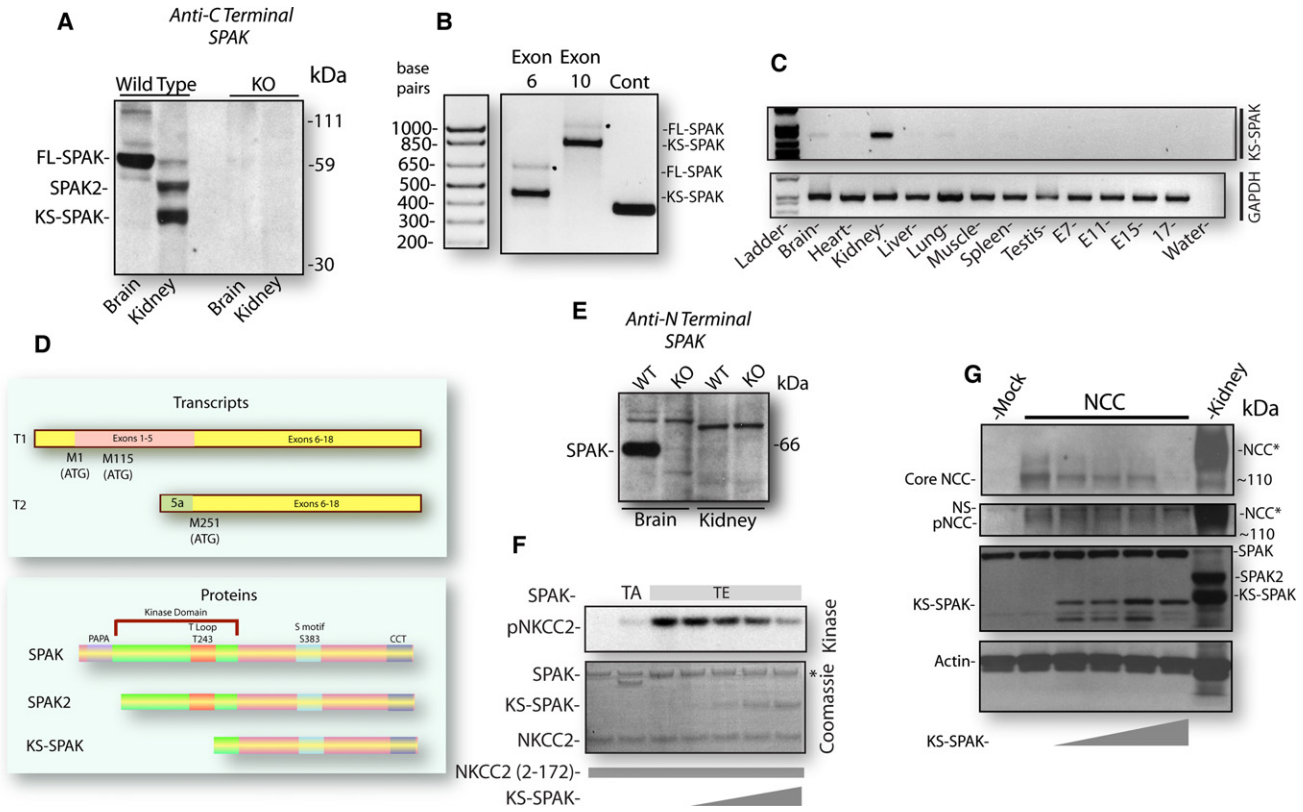

Figure 1. Characterization of SPAK Isoforms

(A) Immunoblot of mouse kidney and brain, probed with an anti-SPAK antibody recognizing a carboxyl-terminal domain. Brain SPAK runs predominantly near 59 kDa, whereas kidney SPAK runs primarily as two smaller bands, labeled SPAK2 and KS-SPAK. Tissue from SPAK knockout (KO) animals (see Figure 3) is shown as a control.

(B) 5′ RACE, using primers directed to exon 6 and 10. Note faint bands running as expected for full-length SPAK and dark bands running representing KS-SPAK. A positive control (Cont) is also shown.

(C) RT-PCR on a multitissue panel (E, whole embryo), using forward primer to exon 5a and reverse primer to exon 10, shows that KS-SPAK expression is almost exclusively restricted to kidney. GAPDH serves as a positive control and water as a negative control.

(D) Top panel shows transcripts showing the alternative translation initiation sites (top) and the alternative transcript showing exon 5a and the third ATG (bottom). Bottom panel shows protein products derived from these transcripts, including the PAPA box, and the kinase domain, with T243 within the T loop, the S motif, and the CCT domain.

(E) Immunoblot of brain and kidney probed with an anti-N-SPAK antibody. Tissue from SPAK KO mice (see Figure 3) is included as a control. Note the faint band in WT kidney. Other bands are nonspecific, as indicated by their presence in the KO animals.

(F) In vitro kinase assay; NKCC2 was incubated with low-activity SPAK (T243A) or constitutively active SPAK (T243E). Effects of increasing KS-SPAK (triangle) on SPAK-dependent NKCC2 phosphorylation (pNKCC2) are shown. Coomassie (lower panel) shows protein products, with * indicating that a contaminant (appearing even in the first lane, when SPAK was not added) runs at the same apparent size as SPAK. Note that inactive SPAK T243A (TA) migrates at a different size compared with constitutively active SPAK T243E (TE).

(G) Kinase activity in HEK cells transfected with NCC. Increasing KS-SPAK (triangle) decreases total and phosphorylated NCC. Phosphorylated NCC from cells is the diffuse band (pNCC, not the nonspecific band, NS). Note that KS-SPAK runs as a doublet, suggesting posttranslational modification. Kidney tissue is shown at the right, with fully glycosylated, mature NCC marked with *.

smaller products (Rafiqi et al., 2010). Furthermore, SPAK precipitated from kidney is largely devoid of kinase activity (Rafiqi et al., 2010). Here (Figure 1A), we confirmed that SPAK in brain runs as expected for the full-length product (~60 kDa), whereas kidney SPAK runs primarily as faster-migrating bands. Piechotta and colleagues (Piechotta et al., 2003) showed that SPAK can be generated from two translation initiation sites, one 115 base pairs downstream from the full-length SPAK START codon. This smaller product lacks the entire PAPA box and was predicted to be kinase defective (Piechotta et al., 2003); we term it SPAK2. Immunoblots from kidney and other tissues show a band of a size near to that predicted for the second translation initiation site (Figure 1A) (Rafiqi et al., 2010). In addition, however, a smaller band appears prominently in kidney (Figure 1A); this band has not been observed in other tissues (Figure 1A) (Rafiqi et al., 2010).

Our observation of at least three SPAK products on renal immunoblots suggested the existence of either yet another alternative translation START or a splice variant. To address this possibility, we performed 5′ and 3′ RACE, using total RNA from mouse kidney. The major product identified in kidney corresponded to a transcript that differs from that predicted for the full-length SPAK, which was a minor amplified product (Figure 1B). The smaller transcript was isolated using primers

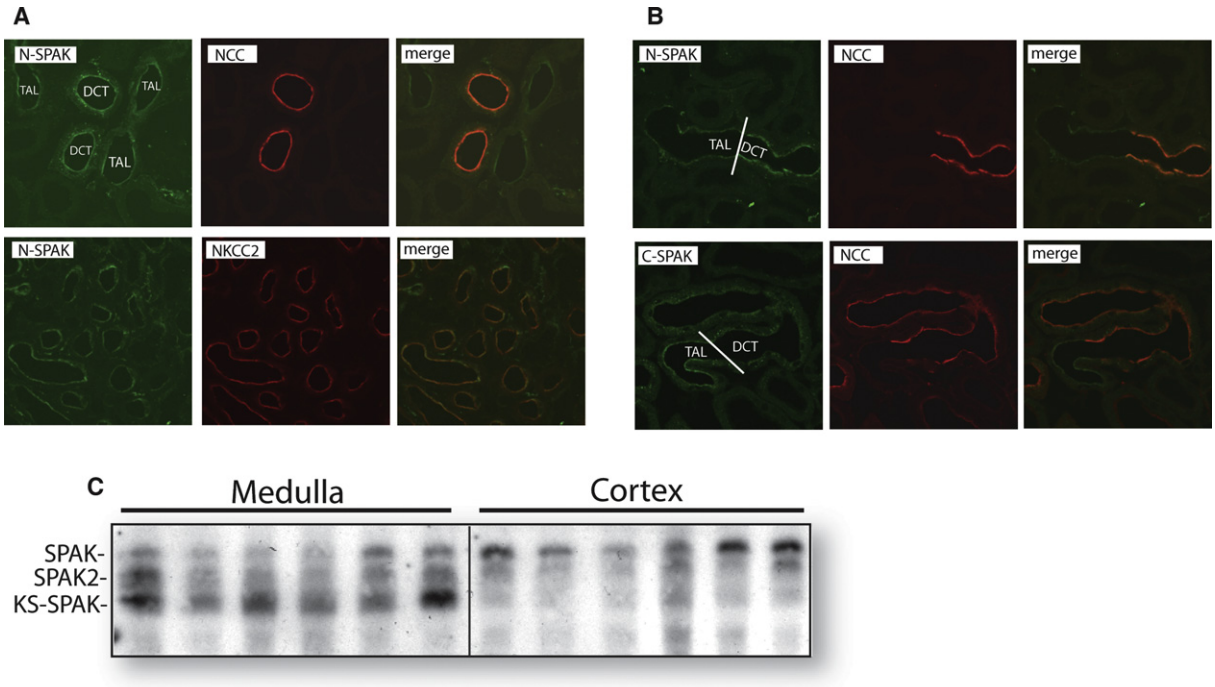

Figure 2. Sites of SPAK Expression in Kidney

(A) SPAK (here detected with an anti-N-SPAK antibody) is expressed along both the TAL and the DCT, as indicated by colocalization with NCC and anti-NKCC2.

(B) Sites of expression of full-length SPAK (detected with anti-N-SPAK) and total SPAK (detected with anti-C-SPAK). Transitional segments containing both TAL and DCT are shown, as determined using anti-NCC and anti-NKCC2 antibodies. Note that full-length SPAK expression is higher along DCT than TAL, whereas total SPAK expression is higher along TAL than DCT.

(C) Total SPAK immunoblot of medullary and cortical tissue. Note that most cortical SPAK is the full-length isoform (SPAK), whereas KS-SPAK and SPAK2 are more highly expressed in medulla.

targeting both exons 6 and 10 and contained a distinct first exon (exon 5a, see Figure S1 for sequence), located within intron 5–6, about 17 kb upstream of exon 6, in the genomic sequence. The same transcript has been identified previously as an expressed sequence tag (EST) in mouse mammary tumor (NCBI accessions BL110429.1 and AQ988594.1), but based on western blotting data (Rafiqi et al., 2010), its expression pattern appears largely restricted to kidney. To confirm this, we performed RT-PCR using primers specific for the novel transcript-specific exon 5a and the shared exon 10. As shown in Figure 1C, the transcript was not detected at substantial levels in other tissues; thus, we have termed it kidney-specific SPAK (KS-SPAK) (GenBank accession JN368425). Seven out-of-frame START codons are present in exons 5a and 6 prior to the first in-frame START (equivalent to M251 in full-length SPAK), so the proposed protein does not contain any novel amino acid sequence, but is rather a truncation of full-length SPAK (Figure 1D).

Both KS-SPAK and SPAK2 are predicted to lack the N terminus (Figure 1D), which is present in the full-length protein. To confirm the identity of these products, we used antibodies directed against the SPAK N terminus. Figure 1E confirms that full-length SPAK, but not SPAK2 or KS-SPAK, is recognized by the antibody directed toward an amino-terminal epitope. Full-length SPAK is prominent in the brain (and other tissues, data not shown); in kidney, however, its abundance is substantially lower. Thus, much of renal SPAK lacks an amino terminus. When apparent molecular weights were examined at higher resolution (Figure S2), the three renal SPAK forms ran somewhat larger than their predicted sizes. Furthermore, when expressed in HEK293 cells by transfection, the three SPAK isoforms ran close to, but not precisely at, the sizes observed in kidney. These data suggest that SPAK isoforms undergo significant posttranslational modification in vivo.

KS-SPAK retains its conserved C-terminal (CCT) domain, which has been shown to bind to NKCC2, to participate in phosphorylation and activation (Richardson et al., 2011). Furthermore, synthetic kinase-dead SPAK mutants exhibit dominant-negative effects on wild-type (WT) SPAK (Dowd and Forbush, 2003). Thus, we tested whether KS-SPAK might inhibit SPAK activity; in vitro, KS-SPAK inhibited phosphorylation of both NKCC2 and NCC by SPAK, rendered constitutively active (T243E), in a dose-dependent manner (Figures 1F and S3). To confirm the relevance of this observation in mammalian tissue, we used HEK293 cells, which express SPAK primarily as the kinase-active full-length form (see Figure 1G). The cells were transfected with both NCC and KS-SPAK. Cotransfection with KS-SPAK led not only to a dose-dependent decrease in phosphorylated NCC, but also to a substantial decrease in total NCC abundance. (Figure 1G).

SPAK Isoforms Are Differentially Expressed along TAL and DCT

Figure 2A shows that SPAK is expressed along both the DCT and the TAL, where it colocalizes with both NCC and NKCC2;

expression was not detected in other segments. To determine whether the full-length SPAK is expressed equally along TAL and DCT, additional immunofluorescence compared transitional nephron segments, using both anti-N-SPAK and anti-C-SPAK antibodies. Figure 2B shows that full-length SPAK is modestly expressed along the TAL, but is more apparent along the DCT. In contrast, total SPAK (comprising both full-length and truncated forms and detected using the anti-C-SPAK antibody) appears to be much more abundant along the TAL than the DCT. Immunofluorescence is not quantitative, so we examined immunoblots of kidney cortex and medulla. We reasoned that medulla contains only TAL, whereas cortex contains both DCT and TAL. Figure 2C shows striking differences in SPAK isoform expression; in cortex, SPAK is predominantly full length, whereas in medulla, most SPAK is SPAK2 and KS-SPAK. Together, these data suggest that SPAK along the DCT should stimulate NCC transport, as the full-length, kinase-active form predominates. In contrast, SPAK along the TAL should be inhibitory, as the predominant forms lacking the kinase domain can inhibit SPAK activity.

SPAK Knockout Mice Display Salt-Sensitive Hypotension and Electrolyte Imbalance

To test the hypothesis that SPAK forms exert opposite effects on cation chloride cotransporter activity along the TAL and DCT, we used SPAK knockout mice (Delpire and Gagnon, 2008; Geng et al., 2010). Due to the strategy used to generate them, SPAK$^{+/-}$ mice (referred to hereafter as heterozygotes, or HETs) cannot be distinguished from SPAK$^{-/-}$ mice (referred to hereafter as knockouts, or KOs) by PCR. Thus, we used all offspring obtained from HET intercrosses and performed phenotypic identification after completion of experimental maneuvers. The genotypes of WT, HET, and KO mice were verified using PCR, western blotting, and immunofluorescence (Figures 3A and 3B).

To determine the role of SPAK in blood pressure regulation, systolic blood pressure was measured by volume pressure-recording tail plethysmography (Feng et al., 2008). When consuming a control NaCl diet (0.49% NaCl), blood pressures of the three groups did not differ (Figure 3C). Dietary NaCl restriction (0.01% NaCl) for 7 days, however, reduced systolic pressure significantly in SPAK KO mice (−9.4 ± 2.1 mm Hg), but not in WT and HET mice (Figure 3C).

To characterize electrolyte and renin-angiotensin-aldosterone system (RAAS) status, whole blood from WT, HET, and KO mice maintained on a standard diet was collected and immediately analyzed using an iSTAT blood chemistry analyzer (Table S1). Compared with WT mice, KO mice did not display any significant differences in whole blood electrolyte levels. In KO mice, however, there was a trend toward hypokalemia (WT, 4.6 mmol/l versus KO, 4.2 mmol/l) and hypomagnesemia (WT, 0.96 mmol/l versus KO, 0.88 mmol/l). As expected, plasma renin activity (PRA) was higher in KO than in WT mice, but aldosterone levels were not (see Discussion). Finally, SPAK KO mice were hypocalciuric, as shown by a significantly lower urinary calcium: creatinine ratio than WT mice (WT, 0.52 ± 0.09 mg/mg versus KO, 0.20 ± 0.04, $p < 0.05$) (see also Table S1). HETs were also significantly hypocalciuric (0.29 ± 0.06, $p < 0.05$) compared with WT mice.

Mice were next subjected to manipulation of dietary electrolytes to aid identification of differences that were not apparent on a standard diet. Severe restriction of dietary K^+ resulted in dramatic reductions in whole blood K^+ in both WT and KO mice (data not shown), so a more modest restriction was performed (from 0.8% K^+ to 0.08% K^+). On this diet, whole blood K^+ was significantly lower in KO mice compared with WT mice (Figure 3D). Hypocalciuria owing to NCC deletion or inhibition has been proposed to result primarily from depletion of the ECF volume (Nijenhuis et al., 2005). To determine whether dietary NaCl loading could overcome the hypocalciuric effects of SPAK deletion, mice were salt loaded. In SPAK KO mice, urinary calcium/creatinine remained lower, compared with WT mice, even though urinary salt excretion rose to high levels, confirming that the ECF volume was expanded; HETs displayed an intermediate response (Figure 3E). PRA was significantly higher in KO mice on both normal and low-NaCl diet (Figure 3F). SPAK KO mice displayed a normal stimulation of aldosterone secretion in response to sodium restriction, but did not display a reduction in response to salt loading (Figure 3G).

SPAK Deletion Stimulates NKCC2, but Inhibits NCC

To determine whether SPAK KO mice display abnormalities in NKCC2 or NCC expression and activity, we performed immunoblot analysis of protein lysates from WT, HET, and SPAK KO mice. On a standard NaCl diet, total NKCC2 expression did not differ between WT and SPAK KO mice (Figures 4A and 4B), but phosphorylated NKCC2 was increased substantially in the SPAK KO animals (Figures 4A and 4B). These data were confirmed by immunohistochemistry, which showed a marked increase in phosphorylated NKCC2 abundance in SPAK KO animals (Figure 4C).

In contrast, total NCC expression in SPAK KO mice was dramatically reduced (by 90% versus WT mice) on a standard NaCl diet (Figures 4D and 4E). To assess NCC activation status, we examined phosphorylation at T53 (and, in some studies, S71); the reduction in total NCC expression was matched by a similar decrease in phosphorylated NCC (Figures 4D and 4E). While HETs displayed a reduction in total NCC, phosphorylated NCC was essentially normal, indicating a compensatory effect in HETs (Figures 4D and 4E). Even after dietary salt restriction (0.01% NaCl), the abundance of phosphorylated NCC remained substantially reduced in SPAK KO animals (Figures 4D and 4E).

Yang and colleagues (Yang et al., 2010) reported that SPAK KO mice exhibit substantial reductions in natriuretic response to thiazides, with a preserved response to loop diuretics. To confirm those results and test whether changes in NKCC2 and NCC abundance and phosphorylation have functional consequences, the acute urinary Na^+ excretion in response to furosemide or hydrochlorothiazide (HCTZ) injection was determined. At baseline, urinary Na^+ excretion during 3 hr was similar in WT, HET, and SPAK KO mice (Table S1). Compared with WT animals, the natriuretic response to furosemide was increased in the SPAK KO animals, whereas the HCTZ response was reduced (Figure 4F); thus, the ratio of furosemide/HCTZ-induced natriuresis was significantly higher in the SPAK KO animals compared with WT animals ($p < 0.05$), consistent with the changes in phosphorylated NKCC2 and NCC.

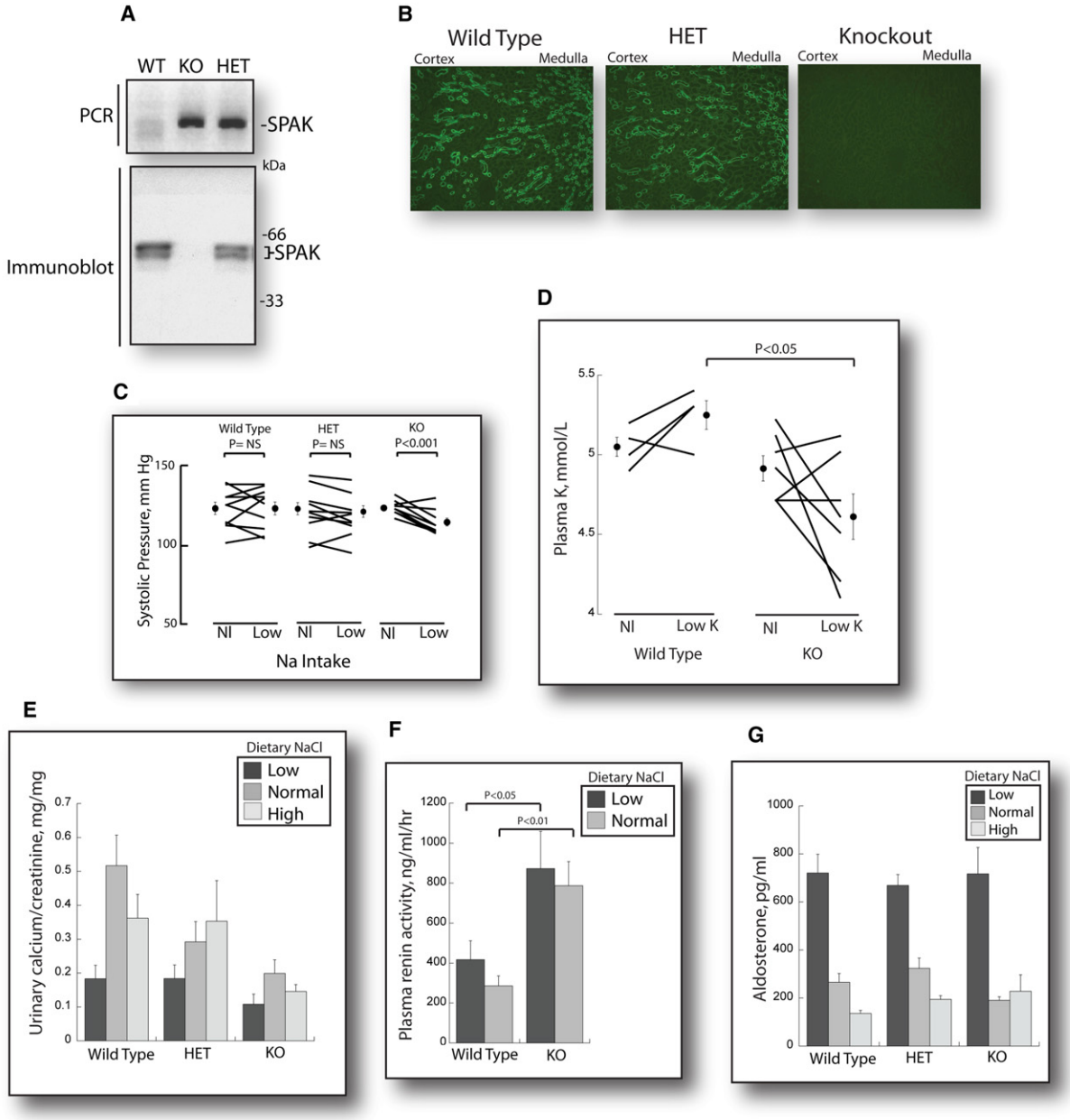

Figure 3. Targeted Disruption of SPAK and SPAK Isoforms

(A) PCR and immunoblot analysis to identify WT, HET, and KO mice. In this low-penetrated blot, full-length SPAK is not evident.

(B) Immunofluorescent analysis of kidney sections revealed expression of SPAK in WT and HET mice and confirmed ablation of SPAK in SPAK KO mice.

(C) Systolic blood pressure on normal- (Nl) NaCl intake diet (0.49% NaCl) and after 10 days on a low-NaCl intake diet (0.01% NaCl). Data are plotted as lines for individual mice on each diet; the mean systolic pressures ± SEM are shown as closed circles. Systolic pressure was reduced in SPAK KO mice (Mann-Whitney test) after NaCl restriction.

(D) On a normal- (Nl) K^+ intake diet (0.8% K^+), whole blood K^+ did not significantly differ between WT and KO mice. Whole blood K^+ was significantly lower in SPAK KO mice on a K^+-restricted diet than in WT mice (Mann-Whitney test). Values here are slightly higher than in Table S1, as the blood was obtained here by saphenous puncture rather than cardiac puncture. Data are plotted as above.

(E) Effects of dietary NaCl intake on urinary calcium excretion, expressed as the ratio of calcium to creatinine. Data are mean ratio ± SEM, n = 8–14.

(F) Plasma renin activity (PRA) in SPAK KO mice on both low- and normal-NaCl-intake diets. Data are mean ± SEM, n = 4–6.

(G) Effects of SPAK KO and of dietary NaCl on aldosterone. Data are mean ± SEM n = 8–10 on normal-NaCl intake, 5–7 on high NaCl intake, and 5 WT, 6 KO, and 13 HETs on low-NaCl intake.

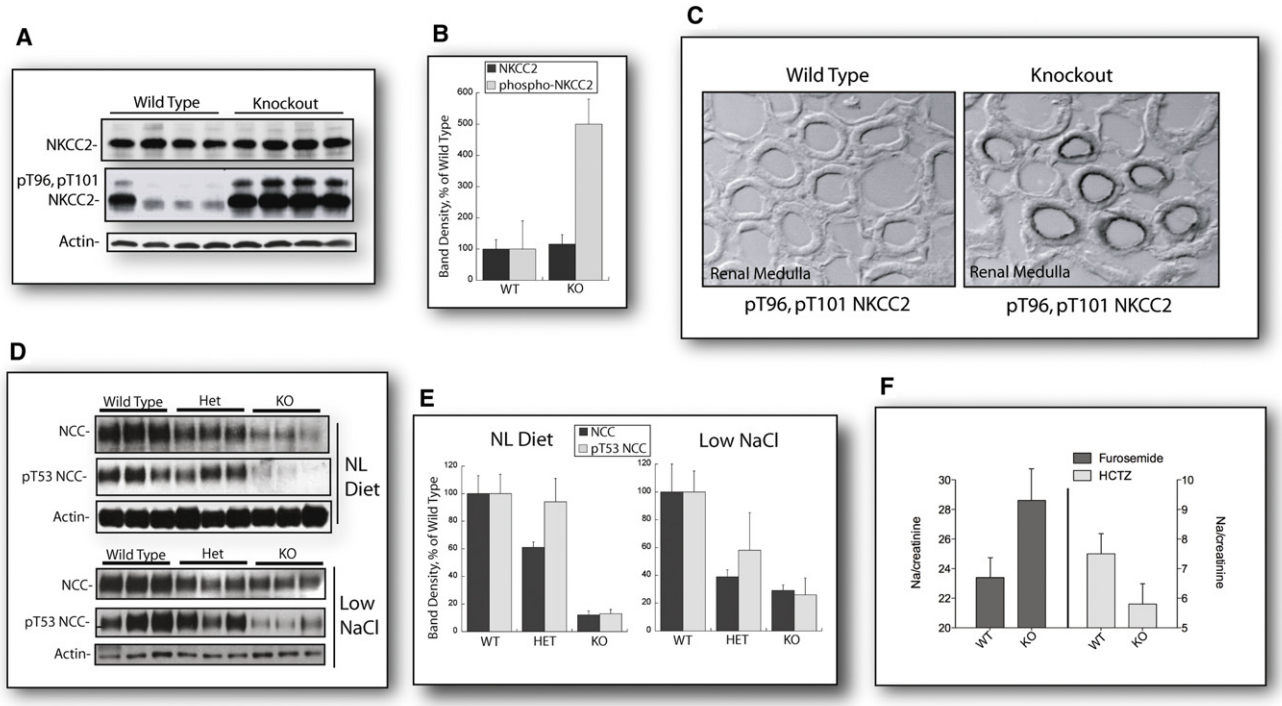

Figure 4. SPAK Deletion Increases Phosphorylated NKCC2 and Decreases Phosphorylated NCC

(A) Western blotting of kidney protein lysates revealed no change in total expression of NKCC2, but increased expression of phospho-NKCC2 (pT96, pT101) in SPAK KO mice.

(B) Densitometry revealed that SPAK KO mice display a 4-fold increase in phospho-NKCC2 levels (±SEM, n = 4, $p < 0.001$, Mann-Whitney test).

(C) This was also apparent on immunofluorescent analysis of kidney.

(D) Total and p-NCC (pT53) expression is reduced in NCC KO mice on normal and low-salt diet.

(E) Total and p-NCC (±SEM) were reduced by 90% relative to β-actin (n = 3, $p < 0.05$ versus WT, Mann-Whitney test). Similar results were seen in salt-deprived animals.

(F) Natriuretic effects (±SEM) of furosemide tended to be greater, and of hydrochlorothiazide (HCTZ) less, in KO compared to WT mice. The differential response between groups was significant. (n = 6 and 5 in WT and KO, $p < 0.05$, Mann-Whitney test.)

SPAK Deletion Reduces DCT Mass, but Does Not Shift NCC from the Apical Membrane

To determine whether SPAK KO reduced NCC at the apical membranes preferentially, kidney sections were examined by immunofluorescence and by immunogold electron microscopy. The results confirmed that SPAK KO reduced total NCC abundance, as well as the abundance of NCC phosphorylated at T53 and S71 (Figures 5A and 5B). Despite the reduction, both total and phosphorylated NCC remained predominantly at the apical membrane; SPAK KO did not lead to an intracellular shift (Figure 5C). Apical expression is clearly a requirement for NCC to transport NaCl into the cell; these data suggest that NCC trafficking to and residence in the plasma membrane is not affected substantially by SPAK phosphorylation, a finding consistent with in vitro data (Glover et al., 2009). Even in the SPAK KO animals, phosphorylated NCC was restricted to the apical membrane and did not appear in intracellular vesicles (Figure 5D).

Low-power immunohistochemistry suggested that the number of DCT profiles is reduced in SPAK KO mice (Figure 5E). Quantitative analysis confirmed that the fractional DCT volume (determined as the fraction of tubules that express NCC) is approximately 50% lower in SPAK KO mice compared to WT (Figure 5F). Thus, a substantial portion of the reduction in total and phosphorylated NCC reflects underdevelopment of the DCT.

OSR1 Expression Is Maintained in SPAK KO Animals

The observation that deletion of SPAK increases NKCC2 phosphorylation suggests that SPAK (presumably KS-SPAK) along the TAL is inhibiting a kinase at baseline, yet the kinase cannot be SPAK alone, as NKCC2 phosphorylation is increased even though all SPAK is absent. OSR1 and SPAK share the ability to phosphorylate cation chloride cotransporters, and both proteins are expressed in kidney (Rafiqi et al., 2010). To confirm that OSR1 expression patterns mirror those of SPAK, we examined OSR1 abundance in WT and SPAK KO animals by immunofluorescence. The results confirm that OSR1 is expressed along the TAL (Figure 6A) and DCT (Figure 6B) in a distribution resembling that of SPAK. OSR1 expression was not affected substantially by SPAK deletion (Figure 6C); it remained predominantly near the apical membrane, close to NCC and NKCC2 (Figures 6A and 6B). Of note, in DCT profiles of SPAK KO mice, OSR1 did exhibit a more punctate distribution than it did in WT animals. We also confirmed (Figure 6C) the observation of Yang and colleagues (Yang et al., 2010) that the abundance of phosphorylated OSR1 is increased by SPAK KO (approximately

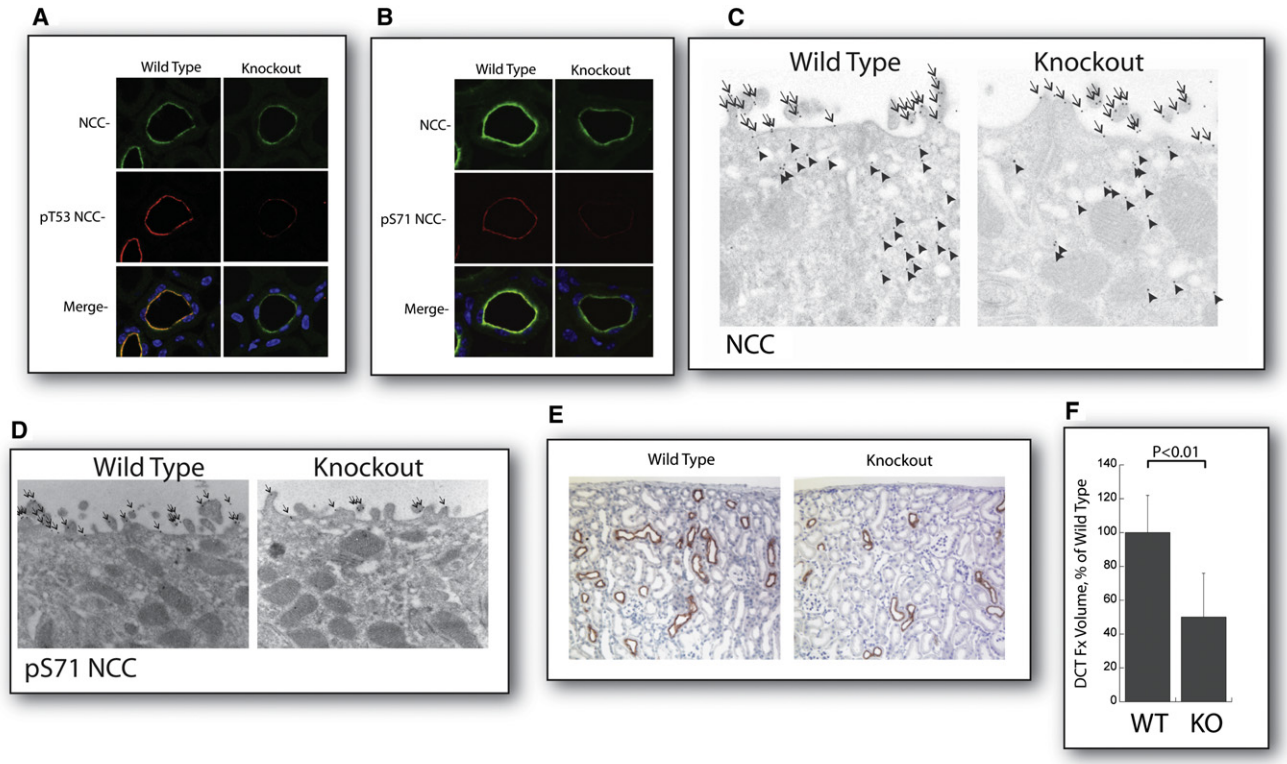

Figure 5. Apical Membrane Localization of NCC Is Unchanged in SPAK KO Mice, but Fractional Volume of the DCT Is Reduced

(A and B) Immunofluorescence on kidney sections using antibodies against total NCC (A and B), pT53 NCC (A), and pS71 NCC (B) revealed that total and p-NCC apical membrane distribution is not altered in SPAK KO mice, despite a 90% reduction in total and p-NCC expression levels.

(C and D) Immunogold electron microscopy against total and p-NCC revealed that the relative abundance of total NCC (C) and pS71 (D) in the apical membrane versus inside of cells was not altered by SPAK KO. Note that while total NCC is detected at both apical and subapical regions, pS71 NCC is expressed only on the apical surface. Arrows indicate apical localization, and arrowheads indicate subapical localization.

(E) Low-power images of kidney sections stained for NCC expression (brown staining) by immunohistochemistry suggest fewer DCT segments.

(F) Quantification of the fractional volume of the DCT (DCT Fx volume) confirmed a 54% reduction in DCT in SPAK KO mice (mean ± SEM, n = 4).

2× that of WT, p = 0.01). Together, these results suggest that an important function of KS-SPAK along the TAL is to inhibit OSR1. In support of this model, we found that KS-SPAK is capable of inhibiting the ability of OSR1 to phosphorylate NKCC2 in vitro (Figure 6D).

Extracellular Volume Depletion Generates a SPAK Isoform Switch

We next tested the hypothesis that dietary NaCl intake alters the relative abundance of SPAK products. Figure 7A shows that dietary NaCl restriction reduced the abundance of KS-SPAK (the inhibitory form) while increasing the abundance of longer (presumably stimulatory) forms. Further, the activated SPAK isoforms shifted to a higher apparent molecular weight, an effect described previously (Anselmo et al., 2006). It should also be noted that additional, undefined forms of SPAK appeared following dietary NaCl restriction. These results suggested that mild depletion of the ECF volume, as induced by dietary restriction, was sufficient to effect this change. We confirmed this hypothesis by comparing NCC KO animals with their WT controls. Figure 7B shows that NCC KO animals exhibit a similar SPAK isoform shift compared with their WT controls (quantified in Figure S4). The animals also exhibit an increase in total and phosphorylated NKCCs (Figure S5). In contrast, the pattern and abundance of OSR1 do not appear to be affected by NCC KO (Figure 7C).

DISCUSSION

SPAK, OSR1, and the WNK kinases interact in the distal nephron to regulate NCC and NKCC2 activity, modulating salt and potassium balance and arterial pressure. While it is now clear that WNK kinases can phosphorylate and activate both SPAK and OSR1 and that SPAK and OSR1 can activate and phosphorylate NCC and NKCC2 (Richardson and Alessi, 2008), there is less information about how these kinases interact to regulate salt transport in animals. Here, we identified interactions between previously unrecognized SPAK isoforms that modulate NCC and NKCC2 in vivo. We determined that a KS-SPAK isoform exerts inhibitory rather than stimulatory effects on NaCl transport both in vitro and in vivo. Further, we show that loss of this isoform accounts for the anomalous effects of SPAK KO on NKCC2 activity. Finally, we showed that SPAK isoform abundance is subject to substantial regulatory modulation; together, these proteins form a WNK/SPAK-OSR1 signaling complex in the distal nephron.

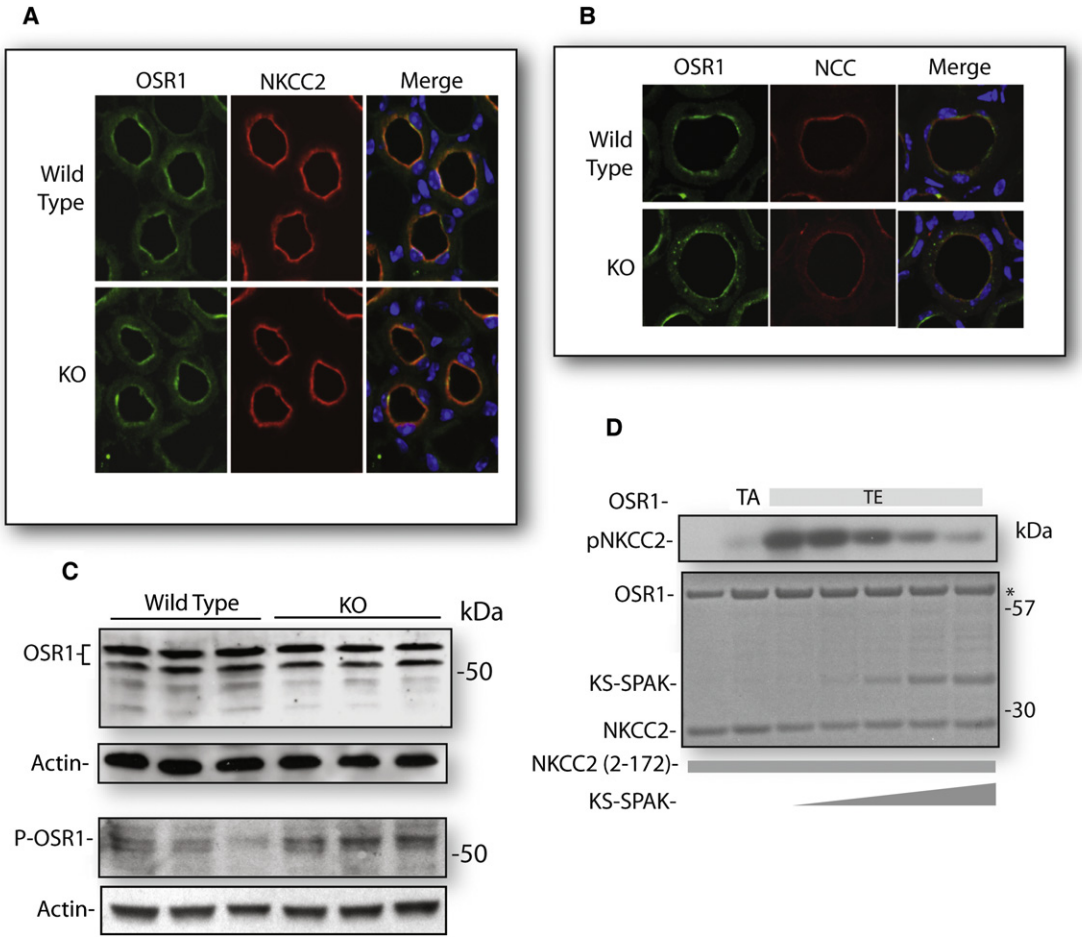

Figure 6. Distribution and Expression of OSR1 in SPAK KO Mice

(A) OSR1, expressed along the TAL with NKCC2, is not affected by SPAK KO.

(B) OSR1 also expressed along the DCT with NCC; in SPAK KO mice, OSR1 expression appeared more punctuate than in WT mice.

(C) Immunoblot analysis of total expression of OSR1 revealed no substantial difference between WT and SPAK KO mice. Bottom panel shows, however, that phosphorylated OSR1 was increased by SPAK KO (216% in SPAK KO, n = 3, p = 0.01).

(D) In vitro kinase assay; NKCC2 was incubated with low-activity OSR1 (T185A) or constitutively active OSR1 (T185E). Effects of increasing KS-SPAK (triangle) on OSR1-dependent NKCC2 phosphorylation (pNKCC2) are shown. Coomassie (below) shows protein products, with * representing a contaminant in the protein prep that was present even when OSR1 was not included (first lane). Note that when OSR1 is included, the band becomes darker and runs as a subtle doublet.

In vitro, SPAK can activate both NKCC2 and NCC by phosphorylating residues along their amino-terminal cytoplasmic domains; SPAK and OSR1, in turn, can be activated by several WNK kinases (Richardson and Alessi, 2008). Based upon these properties and the documented expression of SPAK along the TAL and DCT, it would be predicted that SPAK deletion should impair NaCl reabsorption along both nephron segments, generating a phenotype combining features of both Bartter and Gitelman syndromes. Two mouse models have been consistent with this view (Table S2). First, $SPAK^{T243A/T243A}$ knockin mice, which express a SPAK protein devoid of kinase activity, have lower arterial pressure and less phosphorylated NKCC2 and NCC than WT mice (Rafiqi et al., 2010). Second, mice deficient in SORLA (sorting-protein-related receptor with A-type repeats), which is expressed along the TAL and DCT, display a phenotype with features of mild type I Bartter Syndrome (in which NKCC2 has been disrupted), including excessive urinary K^+ and Ca^{2+} excretion (Reiche et al., 2010). In SORLA KO mice, levels of total SPAK were unchanged, but SPAK shifted away from NKCC2 to a more subapical region with reductions in phosphorylated NKCC2.

In contrast, the results of Yang and colleagues (Yang et al., 2010) and the current results both show that SPAK KO increases the phosphorylation (and activity) of one transporter (NKCC2) while reducing the phosphorylation of the other (NCC). We considered several explanations to account for these differences. First, ECF volume depletion, owing to NCC inactivity, might have stimulated NKCC2 phosphorylation secondarily, independent of SPAK. Yet ECF volume depletion per se does not seem to be the dominant cause, as $SPAK^{T243A/T243A}$ mice, which exhibit the same or even greater ECF fluid volume depletion, display less, not more, phosphorylated NKCC2 (Rafiqi et al., 2010; Rodan and Huang, 2010). A second possibility was that SPAK deletion might somehow have led to compensatory

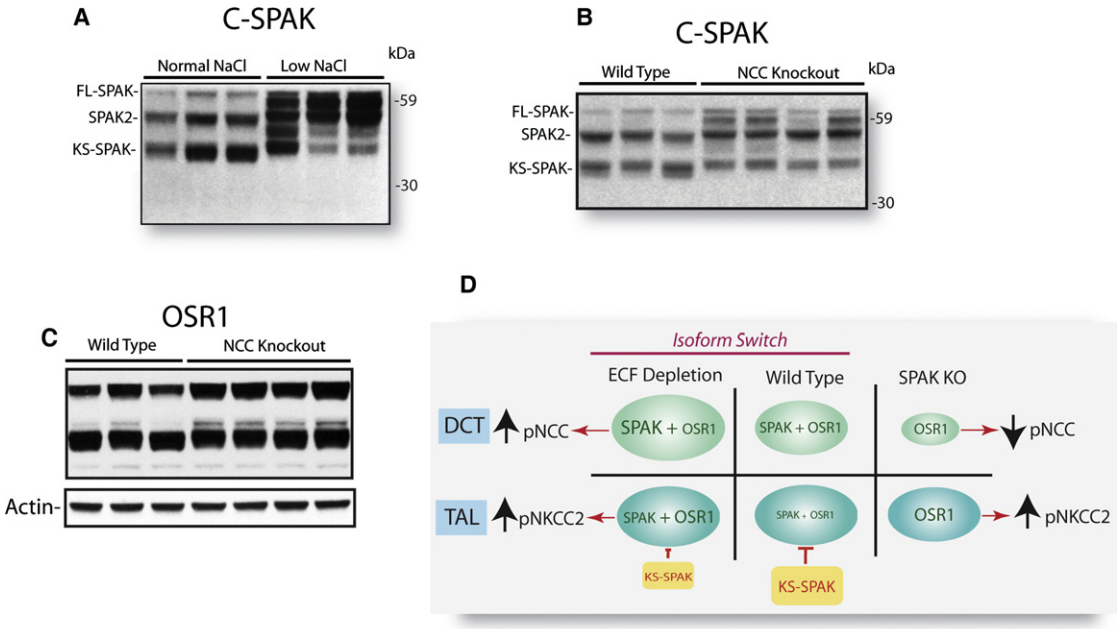

Figure 7. SPAK Isoform Shift

(A) C-SPAK immunoblot comparing WT mice on a normal and restricted-NaCl diet. Note the increase in KS-SPAK and SPAK2, the decline in KS-SPAK abundance, and the appearance of additional products.

(B) C-SPAK immunoblot comparing WT mice on a normal diet with NCC KO mice on a normal diet. Qualitatively similar changes as in (A) were observed.

(C) OSR1 immunoblot comparing WT mice and NCC KO mice, showing no changes comparable to those for SPAK.

(D) Model of SPAK and OSR1 actions along the distal nephron. Model is simplified by assuming that all SPAK in DCT is full length whereas most SPAK in TAL is truncated. Active kinases are labeled in green, while the inactive KS-SPAK is labeled in red. KS-SPAK in TAL inhibits SPAK and OSR1 in WT animals. SPAK KO leads to the changes in transport activity observed by removing active SPAK from DCT (decreasing NCC activity), but alleviating KS-SPAK inhibition of OSR in TAL (increasing NKCC2 activity). The model also shows how the SPAK isoform switch, induced by ECF depletion, stimulates transport along TAL and DCT by reducing the abundance of KS-SPAK in TAL, but increasing the abundance of active kinases in both segments. This model does not show phosphorylation of the kinases, but this is clearly an essential element of activation.

increases in OSR1 abundance along TAL. Figure 6 provides evidence that OSR1 abundance is not increased by SPAK deletion, a finding similar to that of Rafiqi and colleagues in $SPAK^{T243A/T243A}$ mice (Rafiqi et al., 2010). Thus, there is little evidence that SPAK deletion or inactivation itself increases the abundance of OSR1. A third possibility is that SPAK expressed by TAL cells acts to suppress rather than stimulate transport; we suggest that this inhibitory activity is mediated by KS-SPAK, as this isoform appears to be most abundant along this segment. Comparison of the current results with those derived from the $SPAK^{T243A/T243A}$ mice provides support for such a model (see Figure 7D). When SPAK kinase activity is disrupted but SPAK abundance is maintained (as in $SPAK^{T243A/T243A}$ mice), the balance between kinase-inactive SPAK and kinase-active SPAK reduces the abundance of phosphorylated NKCC2 (Rafiqi et al., 2010); when SPAK is deleted entirely, however, the inhibitory protein (KS-SPAK) is absent, and the abundance of phosphorylated NKCC2 rises (Yang et al., 2010). Deletion of KS-SPAK along the TAL increases OSR1 phosphorylation in vivo. We suggest that this occurs because KS-SPAK normally acts along the TAL to inhibit OSR1 phosphorylation (see Figure 6D).

This model (Figure 7D) also accounts for the effect of SPAK KO along the DCT, where decreased rather than increased NCC activity is observed. Along DCT, most SPAK appears to be kinase active (Figure 2); deleting it reduces NCC phosphorylation. As noted (Figure 7), ECF volume depletion shifts SPAK isoforms away from short products (such as KS-SPAK) and toward full-length products, favoring SPAK-mediated phosphorylation (Figure 7D); whether this shift occurs uniformly along the TAL and DCT remains to be established. Possible mediators of the switch include angiotensin II and arginine vasopressin (Mutig et al., 2010; van der Lubbe et al., 2011; Welker et al., 2008), but not aldosterone, as SPAK KO animals exhibit reduced plasma aldosterone levels. The reduced aldosterone levels may reflect SPAK-mediated regulation of aldosterone secretion, as adrenal glands express SPAK abundantly (Delpire and Gagnon, 2008).

This renal-specific expression of a kinase-deficient truncated product is strikingly reminiscent of the renal-specific expression of KS-WNK1, a kinase-defective WNK1 isoform, along the distal nephron that modulates NCC activity both in vitro (Subramanya et al., 2006) and in vivo (Hadchouel et al., 2010; Liu et al., 2009). This protein inhibits the kinase activity of WNK1 (Lazrak et al., 2006; Subramanya et al., 2006; Wade et al., 2006), acting as a molecular switch in the distal nephron. One interesting difference between KS-WNK1 and KS-SPAK is that the former appears to be modulated primarily by dietary KCl intake (Lazrak et al., 2006; Wade et al., 2006), whereas the latter is modulated strongly by ECF volume (Figure 7); although effects of KCl intake on KS-SPAK have yet to be tested directly, this raises the

possibility that interactions between WNK kinases and SPAK/OSR1 are instrumental in balancing NaCl and K excretion.

These data also illuminate mechanisms by which the WNK/SPAK/OSR1 signaling complex modulates NCC activity. To transport NaCl, NCC must be inserted into the apical membrane and also be phosphorylated (activated). In vitro, NCC trafficking can be dissociated from NCC phosphorylation (Glover et al., 2009), but the relationship between the two processes in vivo has remained obscure. There is strong evidence that NCC is inserted into and removed from the apical membrane in response to physiological need (Lee et al., 2009; Sandberg et al., 2006, 2007); as noted, there is also evidence that NCC phosphorylation can be regulated under many of the same circumstances. In the case of SPAK deletion, NCC remains predominantly apical, even though phosphorylation is largely abrogated by SPAK deletion; this result is reminiscent of the effects of SORLA KO on NKCC2; SORLA KO leads to a redistribution of SPAK away from the plasma membrane, but NKCC2 remains strictly apical. Thus, NCC activation likely reflects two distinct processes: trafficking to the apical membrane and activation by phosphorylation, perhaps within the apical membrane.

As reported previously, SPAK KO mice recapitulate many features that occur when NCC is disrupted genetically, either in mice or Gitelman patients. These features include hypokalemia, hypomagnesemia, and hypocalciuria (Schultheis et al., 1998; Simon et al., 1996). Hypokalemia is a cardinal feature of Gitelman syndrome; although the tendency for SPAK KO mice to be hypokalemic did not reach significance at baseline, moderate dietary potassium depletion led to greater hypokalemia in SPAK KO animals than in WT mice. Similarly, dietary K^+ depletion was required for NCC KO mice to develop hypokalemia (Morris et al., 2006; Schultheis et al., 1998). The trend to hypomagnesemia observed in the SPAK KO animals is likely the result of a deficiency in Trpm6, owing to atrophy or underdevelopment of the DCT, its predominant site of expression (Nijenhuis et al., 2005); it is also consistent with the observation that profound magnesium wasting does not typically occur when humans are treated with thiazide diuretics. Thiazides have not been reported to lead to distal atrophy when administered to humans (Ellison and Loffing, 2009). The observation that dietary NaCl loading did not normalize calcium excretion in SPAK KO animals supports the suggestion of Belge and colleagues (Belge et al., 2007) that both distal and proximal effects contribute to thiazide-induced hypocalciuria. Notably, the increased abundance of p-NKCC2 observed in the SPAK KO animals is mimicked by an increase in p-NKCC2 in NCC KO animals. Thus, in both cases (and, we presume, in patients with Gitelman syndrome), the tendency toward salt wasting is attenuated by activation of NKCC2 along the TAL.

Although the focus of the present work was not OSR1, the results do provide insight into the role of OSR1. OSR1 is expressed along both DCT and TAL, and differential OSR1 isoform expression was not detected. We have suggested that SPAK deletion activates NKCC2 by activating OSR1. Yet OSR1 is also expressed by DCT, whereas SPAK KO has the opposite effect. We suggest that the opposite effects reflect differing ratios of KS-SPAK to SPAK or OSR1 along TAL and DCT (also perhaps between medullary and cortical TAL segments). It is noteworthy, however, that SPAK deletion leads to the redistribution of OSR1 only along the DCT to a punctate, intracellular compartment. The functional consequences of this shift and of OSR1 in general have not been addressed directly because targeted disruption of OSR1 is embryonic lethal (Delpire and Gagnon, 2008), as is knockin of an inactivating T loop mutation (Rafiqi et al., 2010). Kidney-specific disruption of OSR1 will provide valuable insight into its role in ion homeostasis and blood pressure regulation.

In conclusion, the present data provide insight into the increasingly complex WNK-SPAK/OSR1-NCC/NKCC2 signaling complex in the kidney. They show that SPAK exerts substantial effects not only on NCC along the DCT, but also on NKCC2 along the TAL. They define an isoform switch, which should work to maintain homeostasis during ECF volume challenge by stimulating NaCl reabsorption along both segments by different mechanisms. The results also resolve a conundrum with respect to the divergent effects of SPAK KO and SPAK inactivation (Rodan and Huang, 2010). Finally, they provide support for the view that WNK signaling via SPAK/OSR1 to NCC/NKCC2 is neither unidirectional nor always stimulatory, but is instead highly recursive and tightly modulated, permitting mammals to tolerate diets that vary widely in K^+ and NaCl.

EXPERIMENTAL PROCEDURES

Animals

Animal studies were approved by the OHSU Institutional Animal Care and Usage Committee (Protocol A858). Generation of SPAK KO mice has been reported (Delpire and Gagnon, 2008). Briefly, the *SPAK* gene was disrupted by duplicating exon 6 and inserting tyrosinase, neomycin resistance, and 5′ hprt genes between the two exons. Animals carrying the mutant allele were identified by PCR genotyping of tail DNA, and final determination of genotype was performed by western blotting of kidney protein lysates following sacrifice.

PCR Genotyping

Crude genomic DNA extracts were prepared from tail snips by heating at 95°C for 45 min in NaOH (pH 12.0), followed by neutralization with Tris-HCl (pH 5.0). To distinguish mice carrying at least one modified *SPAK* allele from WT mice, 4 μl of extract was used directly in PCR reactions as described (Delpire and Gagnon, 2008).

Antibodies

The polyclonal NCC (Bostanjoglo et al., 1998), anti-NKCC2 (Schmitt et al., 2003), phospho-NKCC2 (Reiche et al., 2010), C-SPAK (Piechotta et al., 2002), p-T243SPAK/pT185OSR1 (purchased from Division of Signal Transduction Therapy, University of Dundee) (Rafiqi et al., 2010), pS71-NCC (Yang et al., 2007), and OSR1 (Zagórska et al., 2007) antibodies have all been published. The N-SPAK antibody was generated by ligating cDNA corresponding to amino acids 2–74 of mouse SPAK downstream of the GST open reading frame in the pGEX4 vector. The resulting fusion protein was injected into rabbits to produce polyclonal antibodies, and the antibody was purified by incubation with a GST fusion protein column at 4°C for 48 hr. After several washes, the antibody was eluted using 3 ml 100 mM Na-citrate (pH 2.5) and neutralized with 1.5 ml 1 M Tris-HCl (pH 8.5) and then dialyzed against 4 l of 1× PBS using a Spectra/Por 12,000–14,000 molecular weight cut-off (Spectrum Labs, Rancho Dominguez, CA). The affinity-purified antibody was then concentrated to a volume of 0.5–1 ml using a 15 ml 30,000 MWCO Amicon Ultra Centrifugal Filter device (Millipore, Danvers, MA). Finally, a small amount of BSA (1:400 dilution of 20 mg/ml) was added prior to freezing of aliquots at −20°C. This antibody recognized a band of the expected size in lysates from HEK293 cells (data not shown) and, importantly, on lysates from WT but not KO animals (see Figure 1D), indicating its high specificity for the N terminus of SPAK.

Western Blot Analyses

Kidneys were removed, snap frozen in liquid nitrogen, and homogenized in chilled homogenization buffer containing protease and phosphatase inhibitors (50 mM Tris-HCl [pH 7.4], 1 mM EDTA, 1 mM EGTA, 0.3 M sucrose, 1 mM PMSF, 8.5 mM leupeptin, 1 mM orthovanadate, 50 mM Na fluoride, 1 mg/ml aprotinin, 1 mM dithiothreitol) on ice using a Potter Homogenizer. The homogenate was centrifuged at 4000× *g* for 15 min at 4°C, and the supernatant was separated on 3%–8% NuPage Tris acetate gel at 20 mA. Following transfer to PVDF membrane, equal loading was confirmed by staining the membrane with Ponceau red. Membranes were cut to allow parallel blotting with anti-β-actin to allow normalization. The blot was blocked with Blotto-T (5% nonfat dried milk in PBS-T) and incubated with the primary antibody for 1 hr, then washed and incubated with secondary antibody (HRP-coupled, diluted 1:4000, Zymed) and detected using the Western Lightning kit (Perkin Elmer). Densitometry using ImageJ software (NIH), normalized to β-actin, was performed to compare relative protein concentrations.

5′ RACE PCR and RT-PCR

5′ RACE PCR was performed using the SMARTer RACE cDNA Amplification Kit (Clontech) according to the manufacturer's protocol. Primers were: SPAKRACE6R, 5′ CCGTGTAACATCACCCCCTGTGGCTAAG; SPAKRACE10R, 5′CCTTCTTGGCTCTTTGGGCTATGTCTGGGG. PCR products were A-tailed and cloned in pGEM-T Easy (Promega), and minipreps were sequenced. To determine tissue expression of exon 5a-containing transcripts, RT-PCR was performed using primers against exon 5a (see Figure S1) and SPAKRACE10R with multitissue panel I (Clontech, Palo Alto, CA) as template. For brain, which is not part of cDNA panel I, total RNA from mouse brain was isolated and used in PCR following reverse transcription.

In Vitro Kinase Assay

GST fusion proteins were made by subcloning mouse-derived fragments into pGex6P-1, followed by induction of protein expression in BL21 cells (Novagen); the GST moiety was cleaved using PreScission Protease (GE Healthcare). In vitro kinase assays were performed by combining in a 30 μl reaction 1 μg of NCC N2-142 or NKCC2 N2-172 and 0.5 μg of a constitutively active mutant of SPAK (T243E) or OSR1 (T185E) with 0.4, 1.2, 2.4, or 4.8 μg KS-SPAK in kinase assay buffer (10 mM HEPES [pH 8.0], 10 mM $MgCl_2$, 2 mM benzamidine, 2 mM DTT) with 0.15 mM cold ATP and 10 μCi ATP γ-^{32}P. Reactions were incubated at 30°C for 45 min, then stopped by adding SDS-PAGE sample buffer and boiling for 5 min at 100°C. Samples were then resolved on 4%–12% Bis-tris polyacrylamide gels, Coomassie stained, dried, and exposed to autoradiographic film.

NCC Phosphorylation in HEK293 Cells

All plasmids were generated by cloning cDNAs into pMO-myc, which uses the SV40 promoter to drive expression in mammalian cells. HEK293 cells were plated at a density of 1.75×10^5 cells/well in 12-well plates. The next day, cells were transfected with 0.25 μg mouse NCC and increasing amounts of mouse KS-SPAK (0, 1, 1.5, 2.5, or 5 μg) using calcium phosphate precipitation. Medium was changed 24 hr later, and cells were harvested in lysis buffer 48 hr posttransfection for western blotting.

Blood Pressure Measurement

Blood pressures were measured using CODA-6 tail cuff blood pressure monitoring system (Kent Scientific). The mice were trained prior to the studies by restraint with 25 cycles of cuff inflation/deflation on 5 consecutive days. On subsequent days, measurements were made after 5 min of restraint with no external manipulation or stimulation. Ten acclimation cycles, followed by fifteen measurement cycles, were performed. Blood pressure measurements were done for 5 consecutive days on alternating channels of the CODA-6. When dietary changes were made, 14 days were allowed to pass before measurements were made. During this time, the blood pressures were measured 5 days a week to keep mice acclimated to the procedure, but the data were discarded.

Diuretic Response

Diuretic responses were determined using a method previously reported. Mice maintained on 0.49% NaCl control diet had their bladders emptied via manual massage. Mice were then placed in metabolic cages, and urine was then collected under water-saturated light mineral oil for 3 hr. Furosemide or HCTZ (dissolved in 1.7% ethanolamine) was injected intraperitoneally at 25 mg/kg, and a further 3 hr urine collection was performed. Urinary sodium and creatinine levels were then assayed as described below.

Analysis of Blood Electrolytes

Whole blood was collected via lateral saphenous vein sampling or terminal cardiac puncture (under anesthesia) and placed into heparinized Eppendorf tubes. One hundred microliters of whole blood was then immediately added to a Chem8 cartridge, or 65 μl was added to E3 cartridge and analyzed using i-STAT analyzer (Abbot Point of Care, Inc.). Plasma magnesium was measured by a colorimetric assay (Pointe Scientific).

Plasma Aldosterone and Renin Activity

Plasma aldosterone levels were measured by ELISA (IBL-America). PRA was measured as the amount of angiotensin I generated after incubation with excess angiotensinogen (MP Biomedicals). Two microliters of plasma were incubated with excess porcine angiotensinogen (4 μM) in a 10 μl reaction containing sodium acetate (50 mM, pH 6.5), AEBSF (2.5 mM), 8-hydroxyquinoline (1 mM), and EDTA (5 mM) for 15 min at 37°C. The assay was linear for at least 30 min. The reaction was stopped by boiling for 5 min and diluted 1:50, and angiotensin I was measured by ELISA (Phoenix Pharmaceuticals).

Analysis of Urine

For calcium determination, spot urine samples were collected by placing mice in a clean metabolic cage until the mice spontaneously voided. Urinary calcium was measured by o-Cresolphthalein Complexone method (Pointe Scientific), according to the manufacturer's protocol, except that samples were diluted 1:2. Urinary creatinine was measured by modified Jaffe method (Pointe Scientific) on samples diluted 1:10. Urinary calcium:creatinine ratios were calculated from this data. Urinary sodium in samples obtained in the diuretic response study was measured by flame photometry.

Dietary Manipulation

Custom research diets with varying NaCl levels (0.01%, 0.49%, and 8% NaCl) and potassium-deficient diet (Harlan Teklad) were used. Mice aged 3–4 months were placed on control diet (0.49% NaCl, 0.8% K^+) or NaCl-deficient diet and subjected to blood pressure, urinary, and plasma electrolyte analysis. The diet was then changed to the other diet, and blood pressure, urinary, and plasma electrolyte analysis was performed after 7–14 days, followed by harvesting of kidneys. Mice were placed on high-NaCl diet for 2 weeks, and spot urine was collected, followed by cardiac puncture with electrolyte analysis and harvesting of kidneys.

Immunofluorescence

Mice were anesthetized and kidneys perfusion-fixed by retrograde abdominal aortic perfusion of 3% paraformaldehyde in PBS (pH 7.4). After cryoprotection with 30% sucrose and freezing, 5 μm sections were cut, washed in 1× PBS ×3, incubated in 1× PBS with 0.5%Triton X for 30 min, washed in PBS, and blocked in 5% milk in PBS for 1 hr. Primary antibody (1:500) in 5% milk in 1× PBS was added for 1 hr, followed by a wash in PBS. Sections were incubated for 1 hr with 1:500 FITC-conjugated secondary antibody (Zymed) in block, then washed.

Morphometric Procedures

The fractional volume of DCT segments among strains was measured by light microscopy according to previously characterized methods (Ellison et al., 1989). Briefly, 5 μm-thick paraffin sections were stained for NCC to identify DCT. Cortical areas extending between the renal capsule and the outer medullary boundary were evaluated. Sections were photographed and printed at a final magnification of ×100. At least five prints per animal were evaluated.

Statistical Analyses

Data were analyzed using SPSS (Version 17.0, Chicago, IL). All values are expressed as means ± standard error of the mean. If a Kolmogorov-Smirnov test indicated that data were normally distributed, data were analyzed using analysis of variance (ANOVA) and, if significant, a least-significant-difference post

hoc test. Alternatively, data were analyzed using a Kruskal-Wallis (nonparametric) test or a Mann-Whitney U test, as indicated in the figure legends.

SUPPLEMENTAL INFORMATION

Supplemental Information includes five figures and two tables and can be found with this article online at doi:10.1016/j.cmet.2011.07.009.

ACKNOWLEDGMENTS

This work was supported by grants from the NIH (K01 DK076617 to J.A.M. and DK51496 to D.H.E.), the Department of Veterans Affairs (Merit Review to D.H.E.), and the American Heart Association (to D.H.E.). E.J.H. is supported by an Erasmus MC Fellowship and by the Dutch Kidney Foundation (KJPB 08.004). J.H.N was supported by NIDDK 1T32 DK067864. Prior support from the American Society of Nephrology to D.H.E. is also acknowledged. We also acknowledge Nicole Desmarais for technical assistance.

Received: February 25, 2011
Revised: June 9, 2011
Accepted: July 29, 2011
Published: September 6, 2011

REFERENCES

Anselmo, A.N., Earnest, S., Chen, W., Juang, Y.C., Kim, S.C., Zhao, Y., and Cobb, M.H. (2006). WNK1 and OSR1 regulate the Na+, K+, 2Cl- cotransporter in HeLa cells. Proc. Natl. Acad. Sci. USA *103*, 10883–10888.

Belge, H., Gailly, P., Schwaller, B., Loffing, J., Debaix, H., Riveira-Munoz, E., Beauwens, R., Devogelaer, J.P., Hoenderop, J.G., Bindels, R.J., and Devuyst, O. (2007). Renal expression of parvalbumin is critical for NaCl handling and response to diuretics. Proc. Natl. Acad. Sci. USA *104*, 14849–14854.

Bostanjoglo, M., Reeves, W.B., Reilly, R.F., Velázquez, H., Robertson, N., Litwack, G., Morsing, P., Dørup, J., Bachmann, S., and Ellison, D.H. (1998). 11Beta-hydroxysteroid dehydrogenase, mineralocorticoid receptor, and thiazide-sensitive Na-Cl cotransporter expression by distal tubules. J. Am. Soc. Nephrol. *9*, 1347–1358.

Delpire, E., and Gagnon, K.B. (2008). SPAK and OSR1: STE20 kinases involved in the regulation of ion homoeostasis and volume control in mammalian cells. Biochem. J. *409*, 321–331.

Dowd, B.F., and Forbush, B. (2003). PASK (proline-alanine-rich STE20-related kinase), a regulatory kinase of the Na-K-Cl cotransporter (NKCC1). J. Biol. Chem. *278*, 27347–27353.

Ellison, D.H., and Loffing, J. (2009). Thiazide effects and adverse effects: insights from molecular genetics. Hypertension *54*, 196–202.

Ellison, D.H., Velázquez, H., and Wright, F.S. (1989). Adaptation of the distal convoluted tubule of the rat. Structural and functional effects of dietary salt intake and chronic diuretic infusion. J. Clin. Invest. *83*, 113–126.

Feng, M., Whitesall, S., Zhang, Y., Beibel, M., D'Alecy, L., and DiPetrillo, K. (2008). Validation of volume-pressure recording tail-cuff blood pressure measurements. Am. J. Hypertens. *21*, 1288–1291.

Geng, Y., Byun, N., and Delpire, E. (2010). Behavioral analysis of Ste20 kinase SPAK knockout mice. Behav. Brain Res. *208*, 377–382.

Glover, M., Zuber, A.M., and O'Shaughnessy, K.M. (2009). Renal and brain isoforms of WNK3 have opposite effects on NCCT expression. J. Am. Soc. Nephrol. *20*, 1314–1322.

Hadchouel, J., Soukaseum, C., Büsst, C., Zhou, X.O., Baudrie, V., Zürrer, T., Cambillau, M., Elghozi, J.L., Lifton, R.P., Loffing, J., and Jeunemaitre, X. (2010). Decreased ENaC expression compensates the increased NCC activity following inactivation of the kidney-specific isoform of WNK1 and prevents hypertension. Proc. Natl. Acad. Sci. USA *107*, 18109–18114.

Lazrak, A., Liu, Z., and Huang, C.L. (2006). Antagonistic regulation of ROMK by long and kidney-specific WNK1 isoforms. Proc. Natl. Acad. Sci. USA *103*, 1615–1620.

Lee, D.H., Riquier, A.D., Yang, L.E., Leong, P.K., Maunsbach, A.B., and McDonough, A.A. (2009). Acute hypertension provokes acute trafficking of distal tubule Na-Cl cotransporter (NCC) to subapical cytoplasmic vesicles. Am. J. Physiol. Renal Physiol. *296*, F810–F818.

Liu, Z., Wang, H.R., and Huang, C.L. (2009). Regulation of ROMK channel and K+ homeostasis by kidney-specific WNK1 kinase. J. Biol. Chem. *284*, 12198–12206.

Mayan, H., Vered, I., Mouallem, M., Tzadok-Witkon, M., Pauzner, R., and Farfel, Z. (2002). Pseudohypoaldosteronism type II: marked sensitivity to thiazides, hypercalciuria, normomagnesemia, and low bone mineral density. J. Clin. Endocrinol. Metab. *87*, 3248–3254.

Morris, R.G., Hoorn, E.J., and Knepper, M.A. (2006). Hypokalemia in a mouse model of Gitelman's syndrome. Am. J. Physiol. Renal Physiol. *290*, F1416–F1420.

Mutig, K., Saritas, T., Uchida, S., Kahl, T., Borowski, T., Paliege, A., Böhlick, A., Bleich, M., Shan, Q., and Bachmann, S. (2010). Short-term stimulation of the thiazide-sensitive Na+-Cl- cotransporter by vasopressin involves phosphorylation and membrane translocation. Am. J. Physiol. Renal Physiol. *298*, F502–F509.

Nijenhuis, T., Vallon, V., van der Kemp, A.W., Loffing, J., Hoenderop, J.G., and Bindels, R.J. (2005). Enhanced passive Ca2+ reabsorption and reduced Mg2+ channel abundance explains thiazide-induced hypocalciuria and hypomagnesemia. J. Clin. Invest. *115*, 1651–1658.

Piechotta, K., Lu, J., and Delpire, E. (2002). Cation chloride cotransporters interact with the stress-related kinases Ste20-related proline-alanine-rich kinase (SPAK) and oxidative stress response 1 (OSR1). J. Biol. Chem. *277*, 50812–50819.

Piechotta, K., Garbarini, N., England, R., and Delpire, E. (2003). Characterization of the interaction of the stress kinase SPAK with the Na+-K+-2Cl- cotransporter in the nervous system: evidence for a scaffolding role of the kinase. J. Biol. Chem. *278*, 52848–52856.

Rafiqi, F.H., Zuber, A.M., Glover, M., Richardson, C., Fleming, S., Jovanović, S., Jovanović, A., O'Shaughnessy, K.M., and Alessi, D.R. (2010). Role of the WNK-activated SPAK kinase in regulating blood pressure. EMBO Mol. Med. *2*, 63–75.

Reiche, J., Theilig, F., Rafiqi, F.H., Carlo, A.S., Militz, D., Mutig, K., Todiras, M., Christensen, E.I., Ellison, D.H., Bader, M., et al. (2010). SORLA/SORL1 functionally interacts with SPAK to control renal activation of Na(+)-K(+)-Cl(-) cotransporter 2. Mol. Cell. Biol. *30*, 3027–3037.

Richardson, C., and Alessi, D.R. (2008). The regulation of salt transport and blood pressure by the WNK-SPAK/OSR1 signalling pathway. J. Cell Sci. *121*, 3293–3304.

Richardson, C., Sakamoto, K., de los Heros, P., Deak, M., Campbell, D.G., Prescott, A.R., and Alessi, D.R. (2011). Regulation of the NKCC2 ion cotransporter by SPAK-OSR1-dependent and -independent pathways. J. Cell Sci. *124*, 789–800.

Rodan, A.R., and Huang, C.L. (2010). An emerging role for SPAK in NCC, NKCC, and blood pressure regulation. J. Am. Soc. Nephrol. *21*, 1812–1814.

Sandberg, M.B., Maunsbach, A.B., and McDonough, A.A. (2006). Redistribution of distal tubule Na+-Cl- cotransporter (NCC) in response to a high-salt diet. Am. J. Physiol. Renal Physiol. *291*, F503–F508.

Sandberg, M.B., Riquier, A.D., Pihakaski-Maunsbach, K., McDonough, A.A., and Maunsbach, A.B. (2007). ANG II provokes acute trafficking of distal tubule Na+-Cl(-) cotransporter to apical membrane. Am. J. Physiol. Renal Physiol. *293*, F662–F669.

Schmitt, R., Klussmann, E., Kahl, T., Ellison, D.H., and Bachmann, S. (2003). Renal expression of sodium transporters and aquaporin-2 in hypothyroid rats. Am. J. Physiol. Renal Physiol. *284*, F1097–F1104.

Schultheis, P.J., Lorenz, J.N., Meneton, P., Nieman, M.L., Riddle, T.M., Flagella, M., Duffy, J.J., Doetschman, T., Miller, M.L., and Shull, G.E. (1998). Phenotype resembling Gitelman's syndrome in mice lacking the apical Na+-Cl- cotransporter of the distal convoluted tubule. J. Biol. Chem. *273*, 29150–29155.

Simon, D.B., Nelson-Williams, C., Bia, M.J., Ellison, D., Karet, F.E., Molina, A.M., Vaara, I., Iwata, F., Cushner, H.M., Koolen, M., et al. (1996). Gitelman's variant of Bartter's syndrome, inherited hypokalaemic alkalosis, is caused by mutations in the thiazide-sensitive Na-Cl cotransporter. Nat. Genet. *12*, 24–30.

Subramanya, A.R., Yang, C.L., Zhu, X., and Ellison, D.H. (2006). Dominant-negative regulation of WNK1 by its kidney-specific kinase-defective isoform. Am. J. Physiol. Renal Physiol. *290*, F619–F624.

van der Lubbe, N., Lim, C.H., Fenton, R.A., Meima, M.E., Jan Danser, A.H., Zietse, R., and Hoorn, E.J. (2011). Angiotensin II induces phosphorylation of the thiazide-sensitive sodium chloride cotransporter independent of aldosterone. Kidney Int. *79*, 66–76.

Vitari, A.C., Deak, M., Morrice, N.A., and Alessi, D.R. (2005). The WNK1 and WNK4 protein kinases that are mutated in Gordon's hypertension syndrome phosphorylate and activate SPAK and OSR1 protein kinases. Biochem. J. *391*, 17–24.

Wade, J.B., Fang, L., Liu, J., Li, D., Yang, C.L., Subramanya, A.R., Maouyo, D., Mason, A., Ellison, D.H., and Welling, P.A. (2006). WNK1 kinase isoform switch regulates renal potassium excretion. Proc. Natl. Acad. Sci. USA *103*, 8558–8563.

Welker, P., Böhlick, A., Mutig, K., Salanova, M., Kahl, T., Schlüter, H., Blottner, D., Ponce-Coria, J., Gamba, G., and Bachmann, S. (2008). Renal Na+-K+-Cl- cotransporter activity and vasopressin-induced trafficking are lipid raft-dependent. Am. J. Physiol. Renal Physiol. *295*, F789–F802.

Wilson, F.H., Disse-Nicodème, S., Choate, K.A., Ishikawa, K., Nelson-Williams, C., Desitter, I., Gunel, M., Milford, D.V., Lipkin, G.W., Achard, J.M., et al. (2001). Human hypertension caused by mutations in WNK kinases. Science *293*, 1107–1112.

Yang, S.S., Morimoto, T., Rai, T., Chiga, M., Sohara, E., Ohno, M., Uchida, K., Lin, S.H., Moriguchi, T., Shibuya, H., et al. (2007). Molecular pathogenesis of pseudohypoaldosteronism type II: generation and analysis of a Wnk4(D561A/+) knockin mouse model. Cell Metab. *5*, 331–344.

Yang, S.S., Lo, Y.F., Wu, C.C., Lin, S.W., Yeh, C.J., Chu, P., Sytwu, H.K., Uchida, S., Sasaki, S., and Lin, S.H. (2010). SPAK-knockout mice manifest Gitelman syndrome and impaired vasoconstriction. J. Am. Soc. Nephrol. *21*, 1868–1877.

Zagórska, A., Pozo-Guisado, E., Boudeau, J., Vitari, A.C., Rafiqi, F.H., Thastrup, J., Deak, M., Campbell, D.G., Morrice, N.A., Prescott, A.R., and Alessi, D.R. (2007). Regulation of activity and localization of the WNK1 protein kinase by hyperosmotic stress. J. Cell Biol. *176*, 89–100.

Supplemental Information
Cell Metabolism, *Volume 14*

A SPAK Isoform Switch Modulates Renal Salt Transport and Blood Pressure

James A. McCormick, Kerim Mutig, Joshua H. Nelson, Turgay Saritas, Ewout J. Hoorn, Chao-Ling Yang, Shaunessy Rogers, Joshua Curry, Eric Delpire, Sebastian Bachmann, and David H. Ellison

Inventory of Supplemental Information

Figure or Table	Relates to	Subject
Figure S1	Figure 1B	Exon 5a sequence
Figure S2	Figures 1B and 1E	High resolution SPAK blot
Figure S3	Figure 1F	KS-SPAK inhibits SPAK phosphorylation of NCC
Figure S4	Figure 7B	SPAK isoform switch in NCC knockout animals
Figure S5	Figure 7B	Increased phosphorylation of NKCC2 in NCC knockout animals
Table S1	Figure 3D	Blood and urine measurements
Table S2	Text	Models of SPAK disruption in vivo

Figure S1. Exon 5A Sequence

**5'AGTCACAGCAGGTTCCTCGATGAGAGAGAGCGGACTAGCAGCTGCTTGAAAT
CCCCAGGCCAGCGTTCACCGACTCCGCGGCTTTGGATGAGTTACCGAGCTGAG
CCTCTTTAGGACTCATTTCCTTTAGAGGAGATTAAAGAAAATACTGCCTTTTACT
ATTGCTGGCACACAGTAGGTACACTATAGCCACCAACTCAAGCTGTTGCTATGG
TTACTAGTGTTACCGTCATTCCTAACTTTACTGCAGCCAGCAGGACCACACTTG
CACTGCCTGGAGGTTATGTGTACCTCAGATTTGTCTTACAAGAGCTTCAACCAT
GAAAGCCTTTCTGAGTCACAAAAAAAG**ATTTTGGAGTAAGCGCATTCTTAG3'

Sequence of exon 5A is shown in bold. The location of the forward primer used in 3' RACE PCR and RT-PCR (Figure 1C) is underlined; exon 6 is shaded. The 5' end of exon 5A was identified in 3 independent 5' RACE clones.

Figure S2. HEK Cell and Kidney Immunoblot

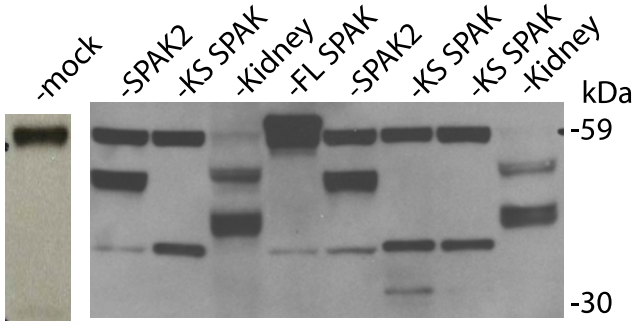

Blot using anti-C SPAK antibody shows three bands recognized in kidney. The other lanes are lysates from HEK293 cells. The lane at the left was mock transfected and shows only SPAK, near 59 kDa that appears to be expressed endogenously. Note that transfection of myc-SPAK (FL-SPAK) generates a larger product, just above the endogenous protein. The bands in the lanes with transfected SPAK2 and KS-SPAK run near 50 and 38 kDa, in contrast to the native kidney SPAK2 and KS-SPAK at 57 and 43 kDa, respectively. In both cases the kidney bands are more diffuse, suggesting post-translational processing.

Figure S3. NCC Kinase Assay

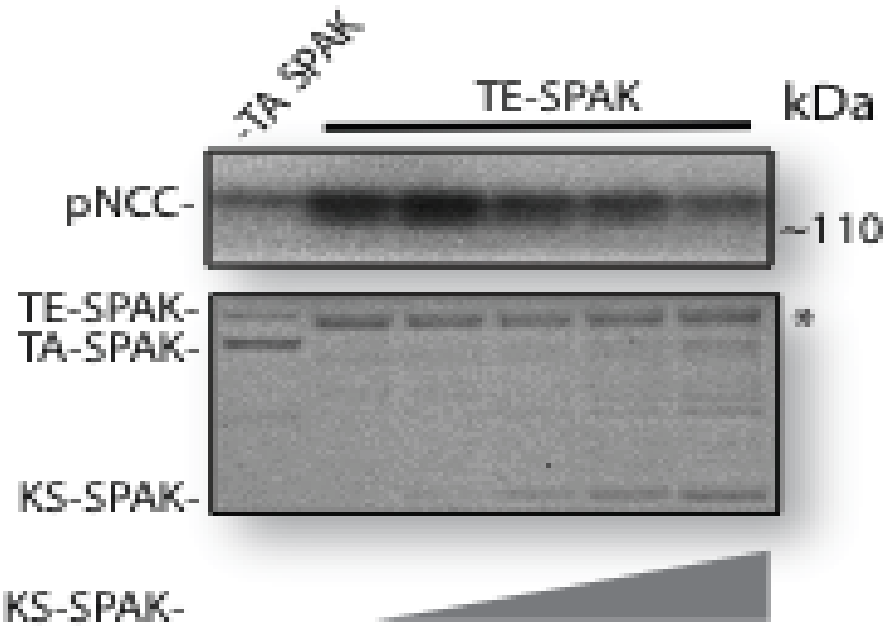

Kinase assay using the N terminus of NCC as substrate. KS-SPAK inhibits SPAK phosphorylation of NCC. The definitions of TA SPAK and TE SPAK are as in Figure 1. The asterisk shows the same contaminant band as in other kinase assays. All lanes contained NCC.

Figure S4. Effect of NCC KO on the Ratio of SPAK/KS-SPAK

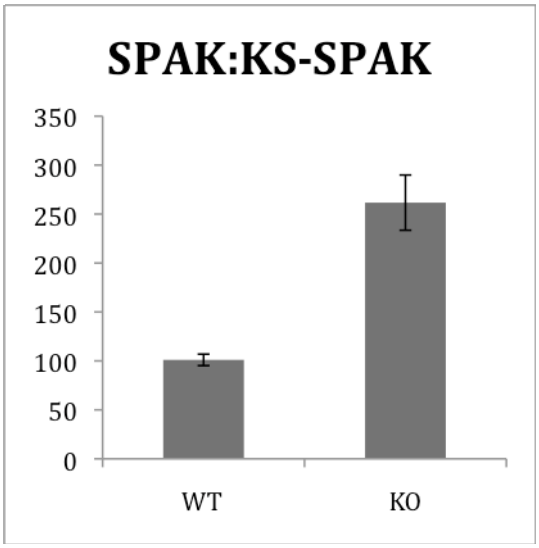

Quantification of the ratio of SPAK:KS-SPAK in wild-type and NCC knockout animals. The data are expressed as mean ± S.E.M. The scale is arbitrary units.

Figure S5. Comparison of Phosphorylated NKCC2 in Wild-Type and NCC KO Animals

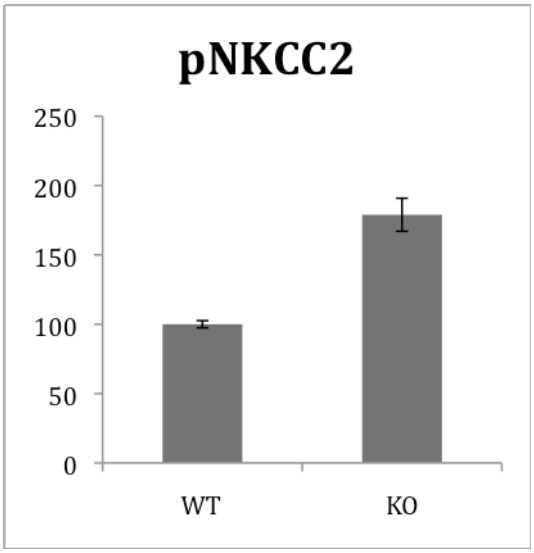

Quantification (arbitrary units) of the abundance of pNKCC2 from wild-type animals and NCC knockouts, showing a significant ($P<0.05$ by Mann Whitney test) increase in phosphorylated NKCC2 in the KO animals. Data are expressed as mean ± S.E.M.

Table S1. Blood and Urinary Electrolytes and the Renin Angiotensin System

	Wild-type	HETs	KO
Blood[a]			
Sodium, mmol/L	148.0 ± 0.7 (n = 16)	147.1 ± 0.6 (n = 24)	146.7 ± 0.5 (n = 15)
Chloride, mmol/L	110.7 ± 1.3 (n = 11)	107.8 ± 1.0 (n = 17)	109.5 ± 1.1 (n = 12)
Potassium, mmol/L	4.6 ± 0.1 (n = 16)	4.2 ± 0.1 (n = 22)	4.2 ± 0.2 (n = 8)
Ionized calcium, mmol/L	1.14 ± 0.04 (n = 10)	1.21 ± 0.02 (n = 15)	**1.11 ± 0.02**[b] (n = 11)
Magnesium, mmol/L	0.96 ± 0.05 (n = 8)	1.00 ± 0.04 (n = 10)	0.88 ± 0.05 (n = 9)
Bicarbonate, mmol/L	21.1 ± 0.6 (n = 11)	20.8 ± 0.7 (n = 17)	21.8 ± 0.6 (n = 12)
Glucose, mmol/L	11.9 ± 0.5 (n = 11)	**13.6 ± 0.6**[c] (n = 17)	11.5 ± 0.5 (n = 12)
Renin angiotensin system			
Plasma renin activity, ng/ml/h	286 ± 50 (n = 4)	Not determined.	**788 ± 121**[d] (n = 5)
Plasma aldosterone, pg/mL	265 ± 35 (n = 8)	324 ± 43 (n = 10)	**190 ± 15**[b] (n = 9)
Urine			
Calcium:creatinine (mg/mg)	0.52 ± 0.09 (n = 14)	**0.29 ± 0.06**[d] (n = 13)	**0.20 ± 0.04**[d] (n =14)
Sodium:creatinine (mmol/mmol)	31 ± 5 (n = 12)	34 ± 5 (n = 15)	35 ± 5 (n = 12)

[a] All parameters measured in whole blood obtained, except for magnesium (measured in plasma). Conversions from mmol/L to mg/dL, for magnesium x2.4, for glucose x18; to convert urine calcium: creatinine to mmol/mmol, x2.82.

[b] $p < 0.05$ compared to SPAK HET

[c] $p < 0.05$ compared to both wild-type and SPAK KO

[d] $p < 0.05$ compared to wild-type

All values are ± SEM.

Table S2. Comparison of SPAK Mouse Models

	SPAK$^{T243A/T243A}$ (Rafiqi et al., 2010)	**SORLA KO** (Reiche et al., 2010)	**SPAK KO**
SPAK	Non-activatable mutant	↔, pSPAK ↑ (96%)*, Altered distribution	Complete knockout
NCC	↓ (30%)	↑ (25%)	↓ (90%)
pNCC	↓ (61-86%)	↑ (40-220%)	↓ (90%)
NKCC2	↓ (16-37%)	↔	↔
pNKCC2	↓ (82%)	↓ (75%)	↑ (400%)
OSR1	↔	Not tested	↔
pOSR1	↔	Not tested	Not tested
Phenotype	Gitelman-like	Bartter-like	Gitelman-like

See text for details.

3.5 SPAK differentially mediates vasopressin effects on sodium cotransporters.

Saritas T, Borschewski A, McCormick JA, Paliege A, Dathe C, Uchida S, Terker A, Himmerkus N, Bleich M, Demaretz S, Laghmani K, Delpire E, Ellison DH, Bachmann S, Mutig K.

***J Am Soc Nephrol.* 2013 Feb;24(3):407-18.**

Our previous work has shown that AVP is particularly effective in activating of NKCC2 and NCC by inducing their phosphorylation (see 3.1 and 3.2). We have also characterized the role of the SPAK kinase in phosphorylation of the distal transporters *in vivo* (see 3.4). Based on this information we have now focused on the role of SPAK and its homologue OSR1 in the AVP signaling along the distal nephron. This study was designed to evaluate acute and chronic effects of AVP on the two kinases and their substrates, NKCC2 and NCC, in SPAK-deficient mice and AVP-deficient rats. The results of the study clearly establish SPAK as the AVP-responsive kinase and show how SPAK mediates the effects of the hormone on NKCC2 and NCC. The cellular effects of AVP observed in this study included rapid activation of SPAK, as was evident from the increased phosphorylation of the kinase within its catalytic and regulatory domains and substantial phosphorylation of renal SPAK substrates, NKCC2 and NCC. Moreover, AVP facilitated interaction of NKCC2 with the catalytically-active FL-SPAK isoform and attenuated the binding of the truncated, inhibitory SPAK variants to the transporter suggesting that the respective binding affinities of the SPAK isoforms may be regulated by the hormone. In contrast, the homologous OSR1 kinase appeared to provide some baseline transporter's phosphorylation rather than to mediate their activation in response to AVP. The results of this study illuminate the kinase pathways involved in the action of AVP and provide further information on divergent roles of the homologous SPAK and OSR1 kinases along the distal nephron.

SPAK Differentially Mediates Vasopressin Effects on Sodium Cotransporters

Turgay Saritas,* Aljona Borschewski,* James A. McCormick,† Alexander Paliege,* Christin Dathe,* Shinichi Uchida,‡ Andrew Terker,† Nina Himmerkus,§ Markus Bleich,§ Sylvie Demaretz,‖ Kamel Laghmani,‖ Eric Delpire,¶ David H. Ellison,† Sebastian Bachmann,* and Kerim Mutig*

*Department of Anatomy, Charité Universitätsmedizin, Berlin, Germany; †Division of Nephrology and Hypertension, Oregon Health & Science University, Portland, Oregon; ‡Department of Nephrology, Medical and Dental University, Tokyo, Japan; §Institute of Physiology, Christian-Albrechts-University, Kiel, Germany; ‖INSERM, UMRS872, Paris, France; and ¶Department of Anesthesiology, Vanderbilt University, Nashville, Tennessee

ABSTRACT

Activation of the Na^+-K^+-$2Cl^-$-cotransporter (NKCC2) and the Na^+-Cl^--cotransporter (NCC) by vasopressin includes their phosphorylation at defined, conserved N-terminal threonine and serine residues, but the kinase pathways that mediate this action of vasopressin are not well understood. Two homologous Ste20-like kinases, SPS-related proline/alanine-rich kinase (SPAK) and oxidative stress responsive kinase (OSR1), can phosphorylate the cotransporters directly. In this process, a full-length SPAK variant and OSR1 interact with a truncated SPAK variant, which has inhibitory effects. Here, we tested whether SPAK is an essential component of the vasopressin stimulatory pathway. We administered desmopressin, a V2 receptor–specific agonist, to wild-type mice, SPAK-deficient mice, and vasopressin-deficient rats. Desmopressin induced regulatory changes in SPAK variants, but not in OSR1 to the same degree, and activated NKCC2 and NCC. Furthermore, desmopressin modulated both the full-length and truncated SPAK variants to interact with and phosphorylate NKCC2, whereas only full-length SPAK promoted the activation of NCC. In summary, these results suggest that SPAK mediates the effect of vasopressin on sodium reabsorption along the distal nephron.

J Am Soc Nephrol 24: 407–418, 2013. doi: 10.1681/ASN.2012040404

The furosemide-sensitive Na^+-K^+-$2Cl^-$-cotransporter (NKCC2) of the thick ascending limb (TAL) and the thiazide-sensitive Na^+-Cl^--cotransporter (NCC) of the distal convoluted tubule (DCT) are key regulators of renal salt handling and therefore participate importantly in BP and extracellular fluid volume homeostasis.[1] Loss-of-function mutants in the *SLC12A1*/ A3 genes encoding NKCC2 and NCC cause salt-losing hypotension and hypokalemic alkalosis in Bartter's and Gitelman's syndromes,[2,3] whereas their overactivity may contribute to essential hypertension.[4,5] Recently, attention has been focused on the two closely related STE20-like kinases, SPS-related proline/alanine-rich kinase (SPAK) and oxidative stress responsive kinase 1 (OSR1), which can phosphorylate NKCC2 and NCC at their N-terminal conserved threonine or serine residues (T96, T101, and T114 of mouse NKCC2 and T53, T58, and S71 of mouse NCC) and thereby activate the transporters.[6–8] Despite the high homology between SPAK and OSR1 and their overlapping renal expression patterns, distinct roles along the nephron have been suggested based on data from SPAK-deficient and kidney-specific OSR1-deficient mice: deletion of SPAK

Received April 23, 2012. Accepted November 20, 2012.

Published online ahead of print. Publication date available at www.jasn.org.

Correspondence: Dr. Kerim Mutig or Dr. Sebastian Bachmann, Department of Anatomie, Charité–Universitätsmedizin Berlin, Philippstraße 12, 10115 Berlin, Germany. Email: kerim.mutig@charite.de or sbachm@charite.de

primarily impairs the function of NCC, whereas deletion of OSR1 negatively affects NKCC2.[9–11] The complex functional properties of a WNK-SPAK/OSR1-N(K)CC interaction cascade are currently being defined.[12] Recently, arginine vasopressin (AVP), signaling *via* the V2 receptor (V2R), has been identified as an efficient activator of both cotransporters, affecting their luminal trafficking and phosphorylation.[13–18] Because plasma AVP levels may vary not only with the sleep-wake cycle or long-term physiologic challenges, but also with pulsatile changes over the short term, distinct, time-dependent responses may occur.[19] SPAK and OSR1 are well placed to regulate distal NaCl reabsorption in response to AVP. Here we tested the role of SPAK in AVP-induced activation of NKCC2 and NCC, acutely and during long-term treatment. The results suggest that SPAK is an essential kinase that modulates distal nephron function in response to AVP stimulation.

RESULTS

Steady State Distribution of SPAK and OSR1 in Wild-Type and SPAK−/− Mice

We first characterized the abundance and distribution of SPAK and OSR1 in wild-type (WT) and SPAK−/− mice, extending previous work.[9] To characterize SPAK, we first used an anti-C-terminal SPAK (C-SPAK) antibody that recognized both the full-length and the inhibitory forms.[9] Immunohistochemistry with anti-C-SPAK antibody revealed strong apical signal in the TAL, whereas in the DCT, a particulate cytoplasmic signal was dominant, along with weaker subapical staining in WT (Figure 1, A, B, E, and F); the signal was absent in SPAK−/− kidneys (Figure 1, C, D, G, and H). Anti-OSR1 antibody signal was apically strong in TAL but weak in DCT of WT (Figure 1, I and J), whereas in SPAK−/−, the inverse distribution, with diminished TAL but enhanced cytoplasmic and apical DCT signals, was evident (Figure 1, K and L). These patterns, suggesting compensatory redistribution of OSR1 in SPAK deficiency, are schematized in Figure 1M.

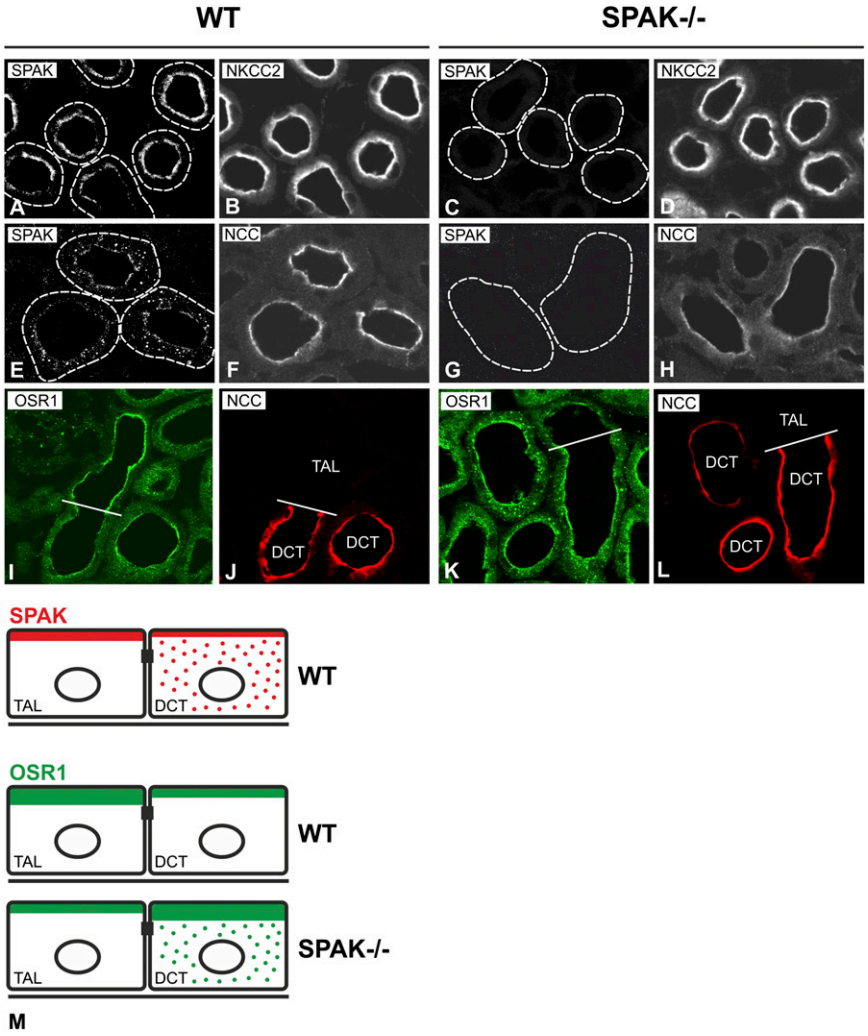

Figure 1. SPAK deficiency is associated with compensatory adaptation of OSR1. (A–L) SPAK and OSR1 immunostaining in TAL and DCT and double-staining with segment-specific antibodies to NKCC2 for TAL or NCC for DCT. (A–H) In WT kidneys, SPAK signal in TAL is concentrated apically (A and B). (E and F) DCT shows also cytoplasmic SPAK signal. (C, D, G, and H) Note the complete absence of SPAK signal in TAL and DCT in SPAK-deficient (SPAK−/−) kidney. (I–L) OSR1 signal is concentrated apically in TAL and DCT of WT kidneys, whereas DCT shows additional cytoplasmic signal in SPAK−/− kidneys. Note that OSR1 signal is stronger in TAL than in DCT in WT, whereas SPAK −/− shows the inverse. Bars show TAL/DCT transitions. (M) The distribution patterns of SPAK and OSR1 are schematized. Original magnification, ×400.

Steady State Phosphorylation of SPAK and OSR1 in WT and SPAK−/− Mice

Next, we studied the phosphorylation of SPAK and OSR1 within their catalytic domains (T243 in SPAK and T185 in OSR1) as an indicator of their activity.[6] The antibodies directed against phosphorylated forms of SPAK and OSR1 cannot distinguish between the two, because the phosphorylation sites are similar. Staining with anti-phospho-(p) T243-SPAK/pT185-OSR1 antibody was absent in medullary TAL (mTAL) and weak in cortical TAL (cTAL) of both genotypes, whereas in DCT, moderate apical signal in WT, but weaker staining in SPAK−/− mice was observed (Figure 2, A, C, E, G, I, K, M, O, and Q). Phosphorylation of the kinases within their regulatory domains (S383 for SPAK and S325 for OSR1) may facilitate their activity as well,[20] so that staining with

anti-pS383-SPAK/pS325-OSR1 antibody was also performed; moderate apical TAL and apical plus cytoplasmic signal in DCT were obtained in WT (Figure 3, A, E, I, M, and Q), whereas in SPAK−/−, TAL and DCT were nearly negative (Figure 3, C, G, K, O, Q). These data are in agreement with earlier data showing that baseline phosphorylation of renal SPAK and OSR1 is low.[21] They also indicate that SPAK deficiency does not elicit compensatory increase of OSR1 phosphorylation.

Steady State Abundance and Phosphorylation of NKCC2 and NCC upon SPAK Disruption

As reported previously,[9] SPAK deficiency caused opposing baseline phosphorylation patterns of the cotransporters with NKCC2 showing enhanced pT96/pT101 signal without a difference in NKCC2 abundance, whereas NCC revealed substantially decreased pT58/pS71 signal along with decreased NCC abundance (Supplemental Figure 1).

Effects of Short-Term Desmopressin on SPAK and OSR1 Phosphorylation in WT and SPAK−/− Mice

To test whether AVP-V2R activates SPAK and/or OSR1 acutely, desmopressin (dDAVP) or vehicle were administered intraperitoneally to WT and SPAK−/− mice. Baseline endogenous AVP was slightly lower in SPAK−/− compared with WT mice (0.7 versus 1.5 ng/ml), which led us to use an established supraphysiologic dDAVP dose (1 μg/kg body weight) in order to reach saturation of AVP signaling in both genotypes.[13,15] Phosphorylation of SPAK and/or OSR1 within their catalytic domains was studied with anti-pT243-SPAK/pT185-OSR1 antibody. Because immunoblotting produced unclear results, confocal evaluation was preferred. dDAVP increased pT243-SPAK/pT185-OSR1 signals in mTAL and DCT of both WT (15-fold for mTAL and 3-fold for DCT) and SPAK−/− mice (8-fold for mTAL and 2-fold for DCT), whereas significant changes were not detected in cTAL in either genotype (Figure 2). Phosphorylation of the regulatory domain was assessed with anti-pS383-SPAK/pS325-OSR1 antibody. Here, dDAVP increased the signal in mTAL and DCT of WT kidneys (1.5- and 2-fold, respectively), whereas no significant changes were recorded in SPAK−/− kidneys (Figure 3). Corresponding immunoblots showed increased signals in WT but not in SPAK−/− kidneys (Figure 4). The abundances of SPAK and OSR1 were unaffected by dDAVP (data not shown). Short-term dDAVP administration thus stimulated phosphorylation of the kinases differentially with a focus on pSPAK in mTAL and DCT.

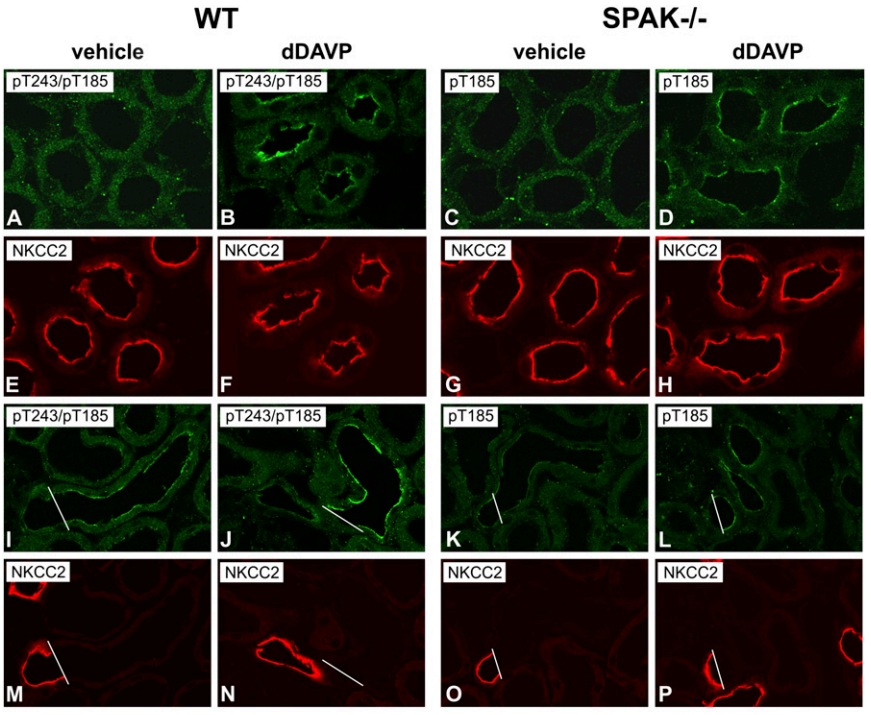

Q

	WT		SPAK-/-	
	vehicle	dDAVP	vehicle	dDAVP
mTAL	3.3 ± 1.3	44.4 ± 9.9*	3.6 ± 1.8	25.7 ± 12.5*
cTAL	14.0 ± 7.4	23.0 ± 10.7	7.4 ± 8.2	8.3 ± 4.7
DCT	31.9 ± 17.4	107.6 ± 25.1*	25.8 ± 7.1	59.7 ± 9.3*

Figure 2. Short-term dDAVP induces differential phosphorylation of SPAK and OSR catalytic domains; confocal microscopy. (A–P) Immunolabeling of pT243-SPAK/pT185-OSR1 (pT243/pT185) and double-staining for NKCC2 in renal medulla (A–H) and cortex (I–P) of vehicle- and dDAVP-treated (30 minutes) WT and SPAK−/− kidneys. Bars indicate TAL/DCT transitions. (Q) Signal intensities (units) obtained after confocal evaluation of pT243-SPAK/pT185-OSR1 signals in medullary (mTAL) and cortical segments (cTAL, DCT) using ZEN software. Data are the mean ± SD. *$P<0.05$ for intrastrain differences (vehicle versus dDAVP). Note the more pronounced response to dDAVP in WT compared with SPAK−/− mice.

Effects of Short-Term dDAVP on NKCC2 and NCC in WT and SPAK−/− Mice

Next, we studied the effects of dDAVP on surface expression and phosphorylation of NKCC2 and NCC. Short-term dDAVP increased the NKCC2 surface expression in both WT and SPAK−/− mice (+21% in WT and +26% SPAK−/− mice; Figure 5, A, B, E, F, and I), whereas dDAVP had no effect on NCC surface expression in either genotype (Figure 5, C, D, G, H, and J). Immunoblots of NKCC2 phosphorylation at T96/T101 revealed that dDAVP increased

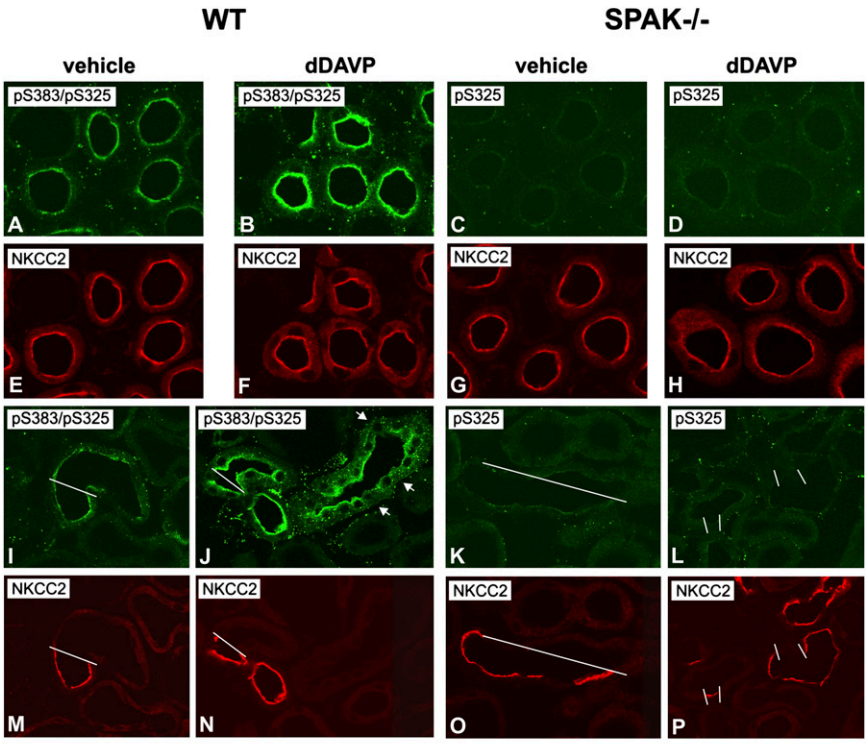

Q

	WT		SPAK-/-	
	vehicle	dDAVP	vehicle	dDAVP
mTAL	93.4 ± 13.9	149.4 ± 14.0*	6.5 ± 5.4	6.6 ± 2.3
cTAL	89.2 ± 29.3	105.9 ± 35.1	11.5 ± 3.7	9.0 ± 5.7
DCT	56.3 ± 15.2	100.0 ± 22.5*	11.0 ± 5.3	7.5 ± 1.0

Figure 3. Short-term dDAVP induces phosphorylation of the regulatory domain of SPAK but not of OSR1; confocal microscopy. (A–P) Immunolabeling of pS383-SPAK/pS325-OSR1 (pS383/pS325) and double-staining for NKCC2 in renal medulla (A–H) and cortex (I–P) of vehicle- and dDAVP-treated (30 minutes) WT and SPAK−/− kidneys. Bars indicate TAL/DCT transitions. Note that dDAVP induces increases in both early and late DCT as identified by the absence or presence of intercalated cells (arrows). (Q) Signal intensities (units) obtained after confocal evaluation of pS383-SPAK/pS325-OSR1 signals in mTAL, cTAL, and DCT. Data are the mean ± SD. *$P<0.05$ for intrastrain differences (vehicle versus dDAVP). Note nearly absent pS325-OSR1 signal in SPAK−/− kidneys.

the abundance of pNKCC2 in WT (+55%) and more so in SPAK −/− mice (+187%). The abundance of total NKCC2 protein was concomitantly augmented in WT, but unaffected in SPAK−/− mice (Figure 6). dDAVP increased NCC phosphorylation substantially in WT (+164% for pS71-NCC and +50% for pT58-NCC), but less so in SPAK−/− mice (+53% for pS71-NCC [$P<0.05$] and n.s. for pT58-NCC; Figure 6). These results were confirmed and extended by confocal analysis of DCT profiles including the use of an additional anti-pT53-NCC antibody (Supplemental Figure 2). SPAK deficiency thus had no effect on dDAVP-induced trafficking of NKCC2, facilitated its phosphorylation, and attenuated NCC phosphorylation.

Effects of Short-Term dDAVP on Interactions of SPAK and OSR1 with NKCC2 and NCC

The truncated KS-SPAK isoform may limit the kinase activities of FL-SPAK or OSR1 in a dominant-negative fashion (9). Here we used Brattleboro rats with central diabetes insipidus (DI)[13,15] to test whether dDAVP alters the association of activating or inhibitory SPAK and OSR1 isoforms with NKCC2 and NCC using co-immunoprecipitation assays. Presence of KS-SPAK in the rat kidney was confirmed at the RNA and protein levels (Supplemental Figure 3). At baseline, NKCC2 was chiefly bound to KS-SPAK, whereas NCC was predominantly associated with FL-SPAK. OSR1 isoforms interacted prominently with NKCC2, but less so with NCC (Figure 7, A and B). Short-term dDAVP significantly reduced binding of KS-SPAK (−30%) and increased binding of FL-SPAK to NKCC2 (+62%), whereas SPAK2 and OSR1 isoforms were not affected (Figure 7, A and C). In contrast, binding of SPAK and OSR1 isoforms to NCC was not affected by dDAVP (Figure 7, B and D). dDAVP thus specifically modulated the interaction of NKCC2 with activating and inhibiting SPAK forms.

Effects of Long-Term dDAVP on Renal Function in WT and SPAK−/− Mice

We next evaluated whether SPAK is involved in the response of the distal nephron to long-term dDAVP treatment (3 days *via* osmotic minipumps). Physiologic effects, compared with vehicle, were more marked in WT (urine volume reduced to 25%, fraction excretion of sodium [FENa] to 23%, potassium [FEK] to 26%, and chloride [FECl] to 47%) than in SPAK−/− mice (urine volume reduced to 38%, FENa to 57%; Figure 8). NKCC2 phosphorylation was raised in WT (+87%) but not in SPAK−/−, which conversely showed an increase in NKCC2 abundance (+96%; Figure 9A). NCC abundance was raised in WT (+45%) and more so in SPAK−/− mice (+201%), and NCC phosphorylation was stimulated as well in WT (+393% for pT58-NCC and +519% for pS71-NCC) and in SPAK−/− (+475% for pT58-NCC and +355% for pS71-NCC; Figure 9A). However, due to different baseline levels among strains, values were normalized for WT vehicle levels (Figure 9). Thus, NKCC2, pNKCC2, and NCC abundances had reached similar levels in either genotype, whereas

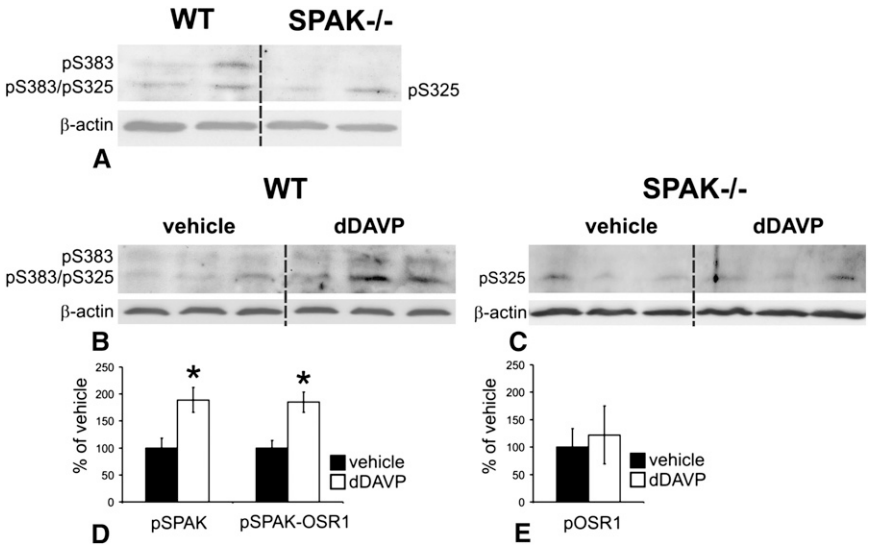

Figure 4. Short-term dDAVP induces phosphorylation of the regulatory domain of SPAK but not of OSR1; immunoblotting. (A–C) Representative immunoblots from WT and SPAK−/− kidneys at steady state (A) and after 30 minutes of vehicle or dDAVP treatment (B and C) show two pS383-SPAK/pS325-OSR1 (pS383/pS325)–immunoreactive bands between 50 and 75 kD in WT, whereas only the smaller product is clearly detectable in SPAK−/−. The larger product probably corresponds to pSPAK and the smaller, at least in part, to pOSR1. β-actin signals serve as the respective loading controls. (D and E) Densitometric evaluation of the immunoreactive signals normalized to loading controls shows increased signals in WT (+89% for the larger and +85% for the smaller products) but not in SPAK−/− kidneys upon dDAVP. Data are the mean ± SD. *$P<0.05$ for intrastrain differences.

dDAVP-induced NCC phosphorylation was selectively attenuated upon SPAK disruption over the long term.

Effects of Long-Term dDAVP on Relative SPAK and OSR Isoform Abundances

We next studied whether dDAVP alters the relative abundance of SPAK and OSR1 products. Administration of dDAVP for 3 days significantly increased the abundances of FL-SPAK (+62%) and SPAK2 (+67%) in WT, whereas OSR1 isoforms were unaffected in either strain (Figure 10). These data were verified in DI rats receiving long-term dDAVP administration as well; resulting changes were similar to those obtained in WT mice (Supplemental Figure 4). These results suggest a prominent role for SPAK products in distal nephron adaptation at long term.

DISCUSSION

Our results add to a growing body of work documenting substantial effects of AVP on cation chloride transporters along the nephron. Here, we show that the serine/threonine kinases SPAK and OSR1 participate in that signaling mechanism. Although expressed largely by the same distal nephron segments, SPAK and OSR1 affect TAL and DCT differentially. This was illustrated earlier by the phenotype of SPAK−/− mice, which display a Gitelman-like syndrome pointing to DCT malfunction[9,10]; in contrast, deletion of OSR1 in the kidney caused Bartter-like syndrome, indicating TAL insufficiency.[11] In SPAK−/−, we resolved a confusing phenotype of upregulated pNKCC2 in TAL and downregulated pNCC in DCT, by identifying novel SPAK isoforms with opposing actions. Whereas truncated KS-SPAK inhibited FL-SPAK- and OSR1-dependent phosphorylation of NKCC2 in TAL, FL-SPAK was critically involved in the phosphorylation of NCC in DCT.[9]

This study further elucidates the role of SPAK in the distal nephron and the potential of homologous OSR1 to replace its function. In spite of the known effect of OSR1 on NKCC2 function,[11] SPAK disruption did not trigger any compensatory increase of its homolog in TAL. This may be related with a diminished demand for an NKCC2-activating kinase in the absence of an inhibitory one (KS-SPAK) or with parallel actions of alternative kinase pathways such as protein kinase A or AMP-activated protein kinase.[8,18] In the DCT, however, the higher total OSR1 abundance may be compensatory. Because NCC abundance and phosphorylation were markedly below control levels in the SPAK-deficient mice, however, increased OSR1 is not capable of fully compensating for SPAK deficiency. The phosphorylation status of the catalytic and regulatory domains of SPAK/OSR revealed no compensatory increase of OSR1 phosphorylation in the absence of SPAK either; rather, decreased signals for the two OSR1 phosphoacceptor sites were detected in TAL and DCT. It therefore appears that SPAK is essential for NCC function, which agrees with the physiologic deficits of this model.[9,10]

Renal compensatory reactions are commonly triggered by endocrine stimuli.[16] Surprisingly, plasma AVP and aldosterone levels were diminished in SPAK−/− mice in spite of extracellular volume depletion and a stimulated renin status.[9,10] Because substantial expression of SPAK has been shown in hypothalamic brain regions and in adrenal glomerulosa cells,[22–24] SPAK deletion at those sites may interfere with AVP as well as aldosterone release. AVP release itself can also affect aldosterone secretion, which may further contribute to the endocrine phenotype in SPAK−/−.[25,26] In DI rats lacking AVP, reduced aldosterone levels have been observed in spite of a stimulated renin-angiotensin system as well, with the known consequences of decreased N(K)CC abundance and activity.[26,27] Manifestations of SPAK deficiency such as reduced baseline phosphorylation of OSR1 and NCC may therefore be partially related with the diminished AVP and aldosterone levels.

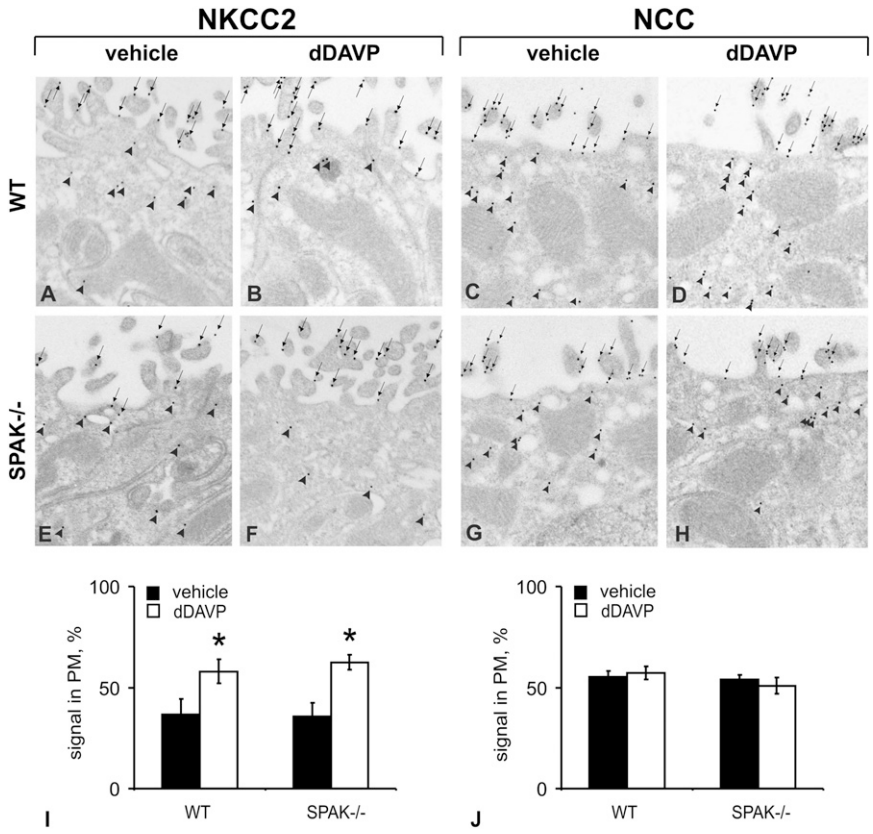

Figure 5. Short-term dDAVP stimulates luminal trafficking of NKCC2 in WT and SPAK−/− but has no effect on NCC in either genotype. (A–F) Immunogold staining of NKCC2 in cortical TAL (A, B, E, and F) and NCC in DCT (C, D, G, and H) from WT and SPAK−/− mice after vehicle or dDAVP treatment (30 minutes). Transporters are distributed in the luminal plasma membrane (PM, arrows) and in cytoplasmic vesicles (arrowheads); a change is visualized for NKCC2 but not NCC (I and J). Numerical evaluations of PM NKCC2 signals (I) and NCC signals (J) per total of signals. Data are the mean ± SD. *$P<0.05$ for intrastrain differences.

Rapid activation of WNK1 and the SPAK/OSR1 kinases upon hypertonic or hypotonic low-chloride conditions has been reported.[28,29] Here, short-term dDAVP-V2R stimulation rapidly increased the abundance of phosphorylated SPAK/OSR1 within their homologous catalytic domain. This was detected chiefly in mTAL and DCT by the recognition of a common epitope (pT243-SPAK/pT185-OSR1).[4] dDAVP treatment also led to moderate increase in the abundance of phosphorylated OSR1, in the SPAK−/− animals, in which the SPAK deletion rendered the antibody specific to OSR1. The heterogenous response to AVP along the distal tubule was likely related with the distinct localization of upstream V2R signaling components such as the WNK isoforms.[30] The regulatory domain (pS383-SPAK/pS325-OSR1) was activated only in WT mice, which underlines the functional heterogeneity between the kinases. Indeed, previous site-directed mutagenesis has shown that phosphorylation of SPAK at S383 facilitates its activity by abolishing an autoinhibitory action of the regulatory domain,[20] whereas no such effects were described for OSR1.[4]

In WT, as expected from prior reports,[13–17] dDAVP rapidly increased the abundance of pNKCC2 and pNCC. Interestingly, the ability of dDAVP to increase pNKCC2 abundance was not only preserved in the SPAK−/− animals, but was enhanced. Although NKCC2 phosphorylation in SPAK−/− mice may be affected predominantly by OSR1, the modest OSR1 activation under these circumstances suggests that other kinases may be involved. By contrast, the weak response of NCC to desmopressin in SPAK−/− indicates that SPAK plays a dominant role in signaling AVP to NCC in the DCT.

Acute activation of the SPAK/OSR1-substrates, NKCC2 and NCC, occurs *via* their apical trafficking and, independently of this translocation, by their phosphorylation at the luminal membrane.[13–17] Deletion of SPAK did not affect dDAVP-induced luminal trafficking of NKCC2. Apart from the thus far unrecognized effect of OSR1, other pathways involved in NKCC2 trafficking, such as cAMP/protein kinase A signaling, may be more relevant herein.[18] Surface expression of NCC was not altered by dDAVP in either mouse strain. This is in contrast to our previous report of dDAVP-induced NCC trafficking in DI rats.[15] This difference, however, may have resulted from differences in experimental model; in the former study, we used DI rats, which lack any AVP at baseline. Here, WT mice, with basal AVP, were utilized.

Because KS-SPAK may limit the activities of FL-SPAK and OSR1 in a dominant-negative fashion, the interactions of SPAK/OSR1 isoforms with NKCC2 and NCC were studied in DI rats supplemented with dDAVP. In agreement with previous data on the segmental distribution of SPAK and OSR1 isoforms,[9–11] the present co-immunoprecipitation experiments revealed prominent binding of KS-SPAK to NKCC2 and of FL-SPAK to NCC, whereas OSR1 strongly co-immunoprecipitated with NKCC2 but less so with NCC at baseline. Short-term dDAVP substantially modulated SPAK isoforms in their interaction with NKCC2, providing *in vivo* evidence that indeed, activating as well as inhibiting kinase isoforms may compete for the RFXV/I motif.[9] We believe that the AVP-induced, quantitative switch between FL- and KS-SPAK isoforms bound to NKCC2 facilitates the activation of the transporter. Binding of SPAK isoforms to NCC was unaffected. Individual adjustments of FL- and KS-SPAK therefore occur selectively in TAL as previously suggested.[31] Conversely, the absence of a response of OSR1 isoforms to dDAVP corroborated existing data on the heterogeneity between SPAK and OSR1.[4,20] Our

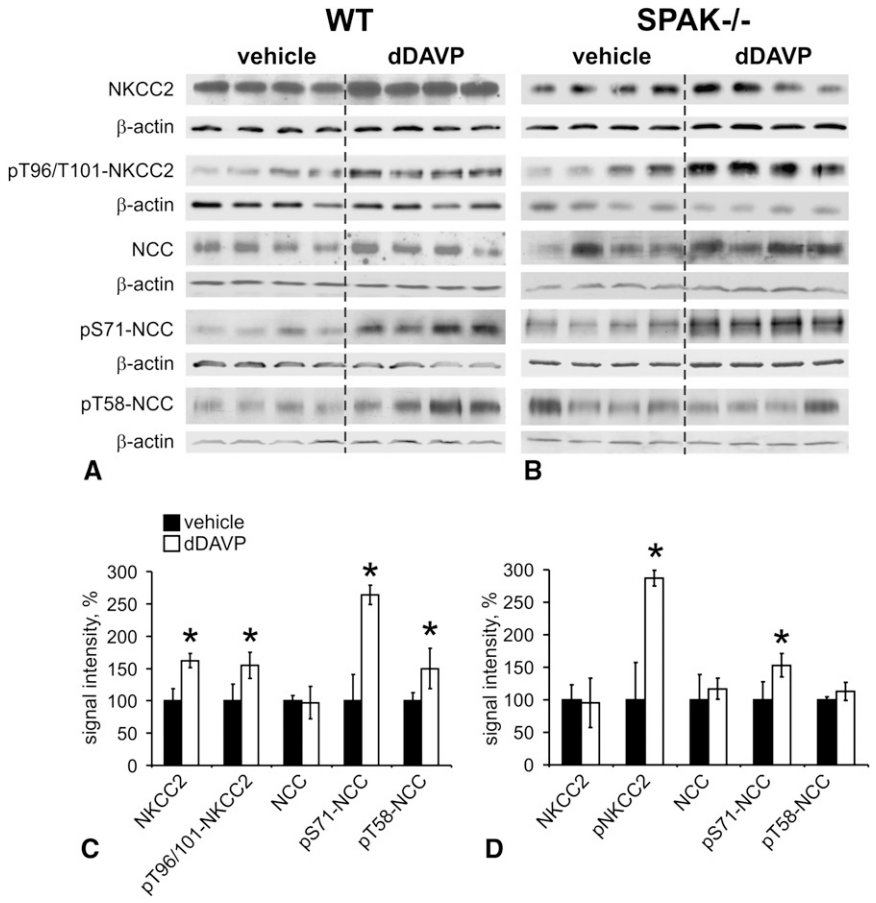

Figure 6. SPAK disruption facilitates short-term dDAVP-induced NKCC2 phosphorylation but attenuates NCC phosphorylation. Taking into account the dramatic differences in steady state phosphorylation of NKCC2 and NCC between genotypes, immunoblots from WT and SPAK−/− kidney extracts are run in parallel and the detection conditions are adapted to obtain a linear range for adequate signal generation. (A and B) Representative immunoblots from WT (A) and SPAK−/− kidneys (B) after 30 minutes of vehicle or dDAVP treatment showing NKCC2, pT96/pT101-NKCC2, NCC, pS71-NCC, and pT58-NCC immunoreactive bands (all approximately 160 kD). β-actin signals serve as the respective loading controls (approximately 40 kD). (C and D) Densitometric evaluation of immunoreactive signals normalized for the loading controls. Data are the mean ± SD. *$P<0.05$ for intrastrain differences.

data thus show for the first time that interactions between SPAK isoforms and their substrates can be selectively modulated in TAL and that this can be triggered by AVP.

Long-term dDAVP decreased water and electrolyte excretion in WT and SPAK−/− mice consistent with earlier data.[32] The effects of dDAVP were less pronounced in SPAK−/− mice. This difference is likely to result from the reduction in NCC abundance and phosphorylation in these animals, at baseline.[9] The weaker NCC phosphorylation in SPAK−/− mice upon dDAVP supported this interpretation. It can be argued that a substitution with dDAVP for only 3 days may not have been sufficient to restore the established hypotrophy of DCT in SPAK−/− mice[9]; however, NCC abundance had reached WT levels upon dDAVP. An attenuation of NCC phosphorylation upon SPAK disruption must therefore be noticed. On the other hand, the effects of long-term dDAVP on NCC reveal a previously unrecognized, SPAK-independent, stimulation of NCC phosphorylation. This suggests that the increased NCC phosphorylation during chronic treatment may be an indirect response to physiologic changes, because acute dDAVP has little effect in SPAK−/− animals (see above). Given the compensatory redistribution of OSR1 in SPAK-deficient DCT and its ability to respond to AVP, we believe that OSR1 may partly mediate activation of NCC in the absence of SPAK.

The changes in kinase abundances upon long-term AVP substitution in mice and rats further confirm a clear dominance of SPAK over OSR1 in the respective nephron adaptations to AVP, which include a rise in abundance and activity of both cotransporters.[27] Selective changes of SPAK but not OSR1 abundance have likewise been reported after long-term angiotensin II administration.[33] Although V2R-mediated effects of AVP along TAL and DCT are well established,[13–17] we cannot rule out potential interference of dDAVP with the renin-angiotensin system in our setting.[25,26] Further studies are required to dissect between the direct and indirect effects of AVP in the distal nephron.

In summary, our results show an essential role for SPAK in acute AVP signaling to NCC in the DCT. Interestingly, however, compensatory processes occur during chronic V2R stimulation, which can permit AVP to stimulate NCC in a SPAK-independent manner. In contrast to the effects along DCT, SPAK deletion, which increases basal NKCC2 phosphorylation along the TAL, leads to an enhanced acute dDAVP effect on NKCC2. As shown diagrammatically in Figure 11, the dominant inhibitory KS-SPAK and the stimulatory FL-SPAK variants were modulated differentially in response to AVP to selectively bind to and control the activation of NKCC2, whereas the phosphorylation of NCC was chiefly governed by FL-SPAK. By contrast, OSR1 appeared to exert predominantly baseline functions, mainly in TAL, where its activity may be highly dependent on KS-SPAK abundance. Our data thus identify SPAK as a crucial kinase that differentially regulates Na^+ reabsorption in the renal cortex and medulla under the endocrine control of AVP.

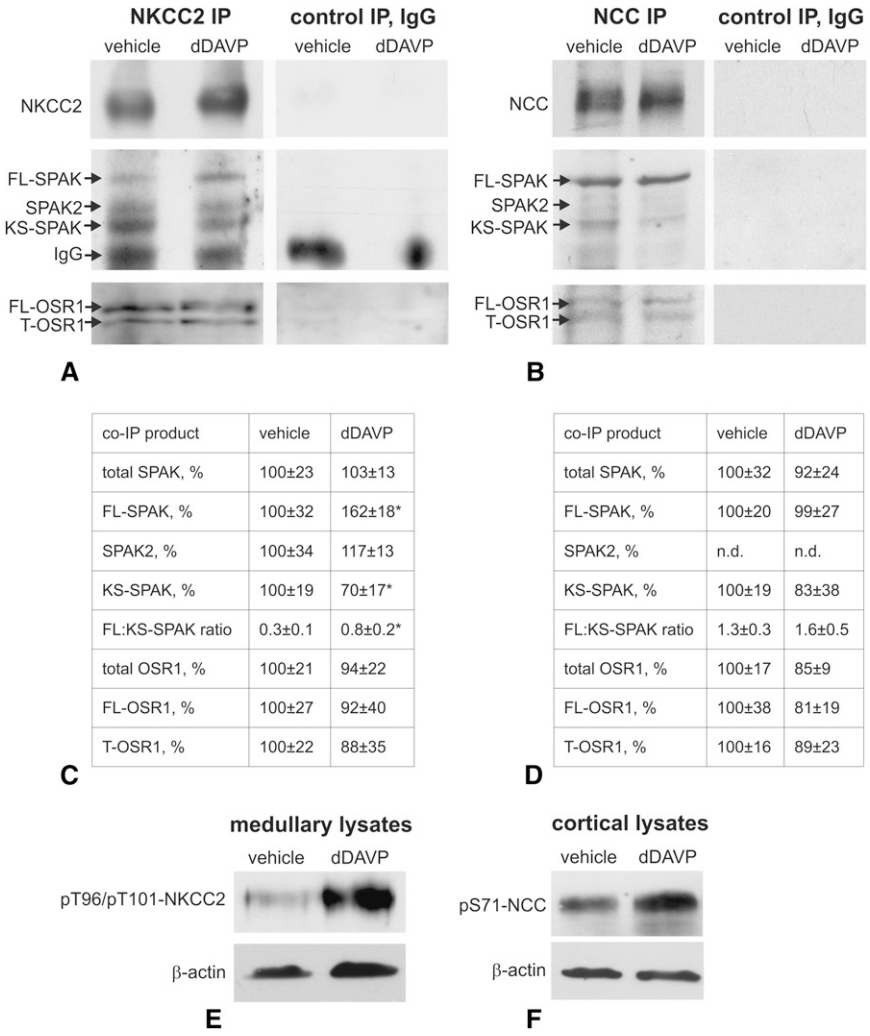

Figure 7. Short-term dDAVP selectively modulates interactions of SPAK variants with NKCC2 but has no effects on OSR1. (A and B) Representative immunoblots of precipitates obtained after immunoprecipitation of NKCC2 from medullary (A) or NCC from cortical kidney homogenates (B) of DI rats treated with vehicle or dDAVP (30 minutes). NKCC2-, NCC-, C-SPAK- (full-length SPAK, translationally truncated SPAK2, and kidney-specific truncated splice SPAK variant), and OSR1-immunoreactive bands (full-length and truncated OSR1 forms) are depicted. IgG bands are recognized owing to the identical host species for antibodies to NKCC2 and SPAK. Control immunoprecipitation with IgG is performed to exclude nonspecific binding of co-immunoprecipitates. (C and D) Results of densitometric quantification of single SPAK- and OSR1 isoforms normalized to NKCC2- (C) or NCC signals (D) and evaluation of FL-SPAK/KS-SPAK ratios. Data are the mean ± SD. *$P<0.05$ for intrastrain differences. (E and F) Effects of dDAVP stimulation were verified by parallel increases of pNKCC2 or pNCC signals in kidney extracts obtained before immunoprecipitation. IP, immunoprecipitation; FL, full-length; KS, kidney specific; T, truncated; n.d., not detectable, indicates no significant signal.

CONCISE METHODS

Animals, Tissues, and Treatments

Adult (aged 10–12 weeks) male WT and SPAK−/− mice[9] and Brattleboro rats with central DI rats (aged 10–12 weeks) were kept on standard diet and tap water. For evaluation of short-term AVP effects, mice and DI rats were divided into groups (n=8 for mice [4 mice for morphologic- and 4 mice for biochemical evaluation] and n=5 for rats [biochemical analysis only]) receiving dDAVP (1 μg/kg body weight) or vehicle (saline) for 30 minutes by intraperitoneal injection. A supraphysiologic dose was chosen in order to reach saturation of AVP signaling, because SPAK−/− had lower baseline AVP levels than WT mice (0.7 versus 1.5 ng/ml; $P<0.05$). Plasma AVP levels were determined using ELISA (Phoenix Pharmaceuticals, Burlingame, CA); to this end, blood was collected from the vena cava concomitantly with organ removal. For the long-term study of AVP, WT- and SPAK−/− mice and DI rats were divided into groups receiving 5 ng/h dDAVP or saline as vehicle (n=3 in each group of mice and n=6 in each group of rats) for 3 days *via* osmotic minipumps (Alzet). Rats received normal food and tap water *ad libitum*. Mice received a water-enriched food in order to keep endogenous AVP levels low; food was prepared as described.[34] Mice received this food (21 g/animal) for 3 days before implantation of the minipumps and during treatment. After minipump implantation, mice were individually placed in metabolic cages and urine was collected during the last 24 hours of the experiment. Plasma and urine sodium, potassium, chloride, and creatinine concentrations were determined and the FE of electrolytes calculated. For morphologic evaluation, mice were anesthetized and perfusion-fixed retrogradely *via* the aorta using 3% paraformaldehyde.[13,15] For biochemical analysis, mice and rats were sacrificed and the kidneys removed. All experiments were approved by the Berlin Senate (permission G0285/10) and Oregon Health & Science University Institutional Animal Care and Usage Committee (Protocol A858).

Immunohistochemistry

Antibodies against NKCC2,[13] NCC,[15] pNCC (pT53, pT58, and pS71 of mouse NCC),[10,11,15] SPAK (C-terminal antibody; Cell Signaling), OSR1 (University of Dundee),[4] and phosphorylated SPAK-OSR1 (pT243-SPAK/pT185-OSR1; antibody recognizes pT243 of mouse SPAK and pT185 of mouse OSR1 [T-loop; University of Dundee] and pS383-SPAK/pS325-OSR1; antibody recognizes pS383 of mouse SPAK and pS325 of mouse OSR1 [S-motif; University of Dundee])[4] were applied as primary antibodies. For detection of phosphorylated kinases and

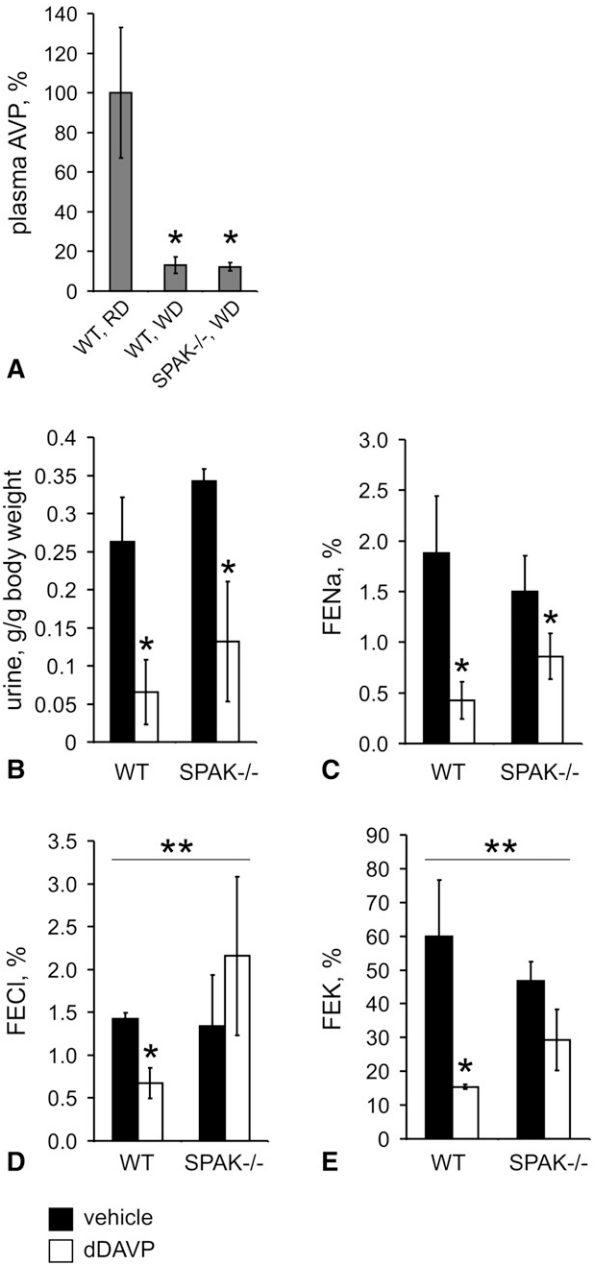

Figure 8. SPAK disruption attenuates dDAVP-induced water and electrolyte retention at long term. (A) Water-enriched diet (food mixed with a water-containing agar) during 3 days before dDAVP or vehicle administration strongly decreases endogenous plasma AVP levels in both genotypes compared with normal AVP levels in WT mice on a regular diet. (B–E) Urine volume and FENa, FECl, and FEK are shown. The two-tailed *t* test is utilized to analyze the intrastrain differences between vehicle and dDAVP treatments (*$P<0.05$), whereas the differences in strength of dDAVP effects between WT and SPAK−/− mice are evaluated by two-way ANOVA (**$P<0.05$). Data are the mean ± SD. WD, water-enriched diet; RD, regular diet.

transporters, the antibodies were preabsorbed with corresponding non-phosphorylated peptides in 10-fold excess before the application on kidney sections. Cryostat sections from mouse and rat kidneys were incubated with blocking medium (30 minutes), followed by primary antibody diluted in blocking medium (1 hour). For multiple staining, antibodies were sequentially applied, separated by washing step. Fluorescent Cy2-, Cy3-, or Cy5-conjugated antibodies (DIANOVA) or horseradish peroxidase–conjugated antibodies (Santa Cruz Biotechnology) were applied for detection. Sections were evaluated in a Leica DMRB or a Zeiss confocal microscope (LSM 5 Exciter). For confocal evaluation of pSPAK/OSR1 and pNCC signal intensities, kidney sections were double-stained for NKCC2 or NCC to identify TAL and DCT, respectively. At least 20 similar tubular profiles were evaluated per individual animal. Intensities of the confocal fluorescent signals were scored across each profile using ZEN2008 software (Zeiss), and mean values within 2 μm distance at the apical side of each tubule were obtained. Background fluorescence levels were determined over cell nuclei and subtracted from the signal.

Ultrastructural Analyses

For immunogold evaluation of NKCC2 and NCC, perfusion-fixed kidneys were embedded in LR White resin. Ultrathin sections were incubated with primary antibodies to NKCC2 or NCC.[13,15] Signal was detected with 10-nm nanogold-coupled secondary antibodies (Amersham) and visualized using transmission electron microscopy. Quantification of immunogold signals in TAL and DCT profiles was performed on micrographs according to an established protocol.[35] Gold particles were attributed to the apical cell membrane when located near (within 20 nm of distance) or within the bilayer; particles found below 20 nm of distance to the membrane up to a depth of 2 μm or until the nuclear envelope were assigned to cytoplasmic localization. At least 10 profiles and 4–5 cells per profile were evaluated per individual animal.

Immunoblotting and Co-Immunoprecipitation

For immunoblotting, kidneys were homogenized in buffer containing 250 mM sucrose, 10 mM triethanolamine, protease inhibitors (Complete; Roche Diagnostics), and phosphatase inhibitors (Phosphatase Inhibitor Cocktail 1; Sigma) (pH 7.5) and nuclei removed by centrifugation (1000×*g* for 15 minutes). Supernatants (postnuclear homogenates) were separated in 10% polyacrylamide minigels, electrophoretically transferred to polyvinylidene fluoride membranes, and detected using primary antibodies against NKCC2, pT96/T101-NKCC2, NCC, pT58-NCC, pS71-NCC, SPAK, pSPAK-OSR1,[4,9,10,13,15] β-actin (Sigma), or glyceraldehyde-3-phosphate dehydrogenase (Santa Cruz Biotechnology), horseradish peroxidase–conjugated secondary antibodies, and chemiluminescence exposure of x-ray films. Films were evaluated densitometrically. Immunoprecipitation of NKCC2 from rat medullary kidney homogenates or NCC from rat cortical homogenates was performed overnight at 4°C in TBS/0.5% Tween using anti-NKCC2 (Millipore) or anti-NCC[15] antibodies covalently bound to Dynabeads M-270 Epoxy (Invitrogen). The detergent concentration was established by testing a concentration range from 0.1% to 2% Tween. The co-immunoprecipitated products were detected by immunoblotting as described above. The specificity of the co-immunoprecipitation experiments was confirmed by IgG controls.

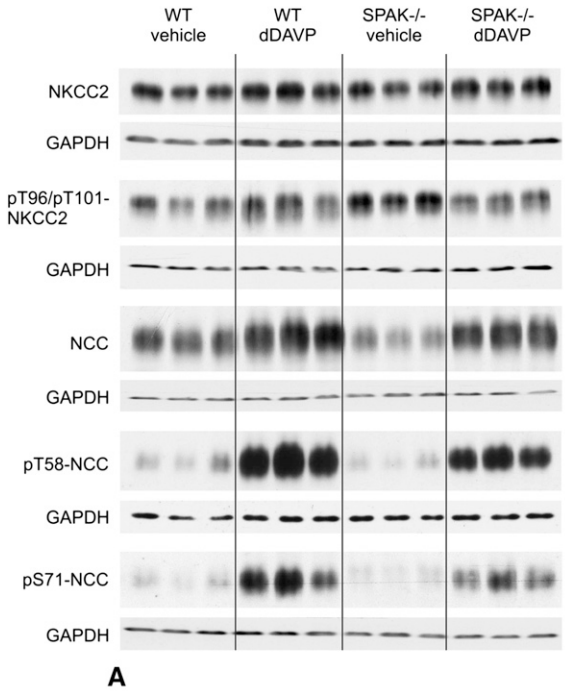

	WT (%)		SPAK-/- (%)	
	vehicle	dDAVP	vehicle	dDAVP
NKCC2	100±35	120±8	63±23	103±10*
pNKCC2	100±22	187±18*	228±23§	171±9
pNKCC2:NKCC2	100±56	138±23	341±110§	123±8$
NCC	100±12	145±15*	48±17§	146±25*
pT58-NCC	100±40	493±18*	42±14§	244±19*$
pT58-NCC:NCC	100±49	333±22*	90±43	171±60$
pS71-NCC	100±32	619±21*	116±35	530±34*
pS71-NCC:NCC	100±39	431±33*	249±44	369±42

B

Figure 9. SPAK disruption selectively attenuates activation of NCC upon long-term dDAVP. (A) Representative immunoblots from WT and SPAK−/− kidneys after 3 days of vehicle or dDAVP treatment showing NKCC2, pT96/pT101-NKCC2, NCC, pS71-NCC, and pT58-NCC immunoreactive bands (all approximately 160 kD). GAPDH signals serve as the respective loading controls (approximately 40 kD). (B) Densitometric evaluation of immunoreactive signals normalized to loading controls and calculation of pNCC/NCC ratios. Values obtained in WT after vehicle application are set at 100%. Data are the mean ± SD. *$P<0.05$ for intrastrain differences (vehicle versus dDAVP); §$P<0.05$ for baseline interstrain differences (WT versus SPAK−/− upon vehicle); $$P<0.05$ for different responses to dDAVP in WT versus SPAK−/− genotypes as analyzed by two-way ANOVA. GAPDH, glyceraldehyde-3-phosphate dehydrogenase.

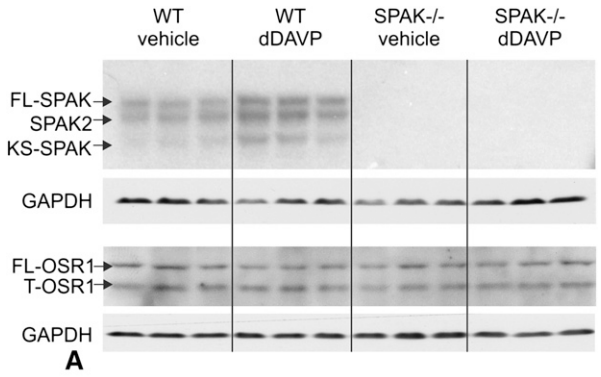

product	vehicle	dDAVP	vehicle	dDAVP
total SPAK	100±18	169±20*	n.d.	n.d.
FL-SPAK	100±12	162±11*	n.d.	n.d.
SPAK2	100±21	167±17*	n.d.	n.d.
KS-SPAK	100±49	275±39	n.d.	n.d.
FL:KS-SPAK	3.5±1.9	2.0±0.7	n.d	n.d
total OSR1	100±17	102±7	91±13	101±16
FL-OSR1	100±38	97±34	84±30	95±20
T-OSR1	100±5	90±9	74±18	93±4

B

Figure 10. Long-term dDAVP increases abundances of SPAK but not OSR1 variants. (A) Representative immunoblots showing SPAK and OSR1 immunoreactive bands in kidneys from WT and SPAK−/− mice after 3 days of vehicle or dDAVP treatment. GAPDH bands below the corresponding immunoblots serve as loading controls. (B) Densitometric evaluation of single immunoreactive bands normalized to loading controls. Values obtained in WT after vehicle application set as 100%. Data are the mean ± SD. *$P<0.05$ for intrastrain differences (vehicle versus dDAVP). GAPDH, glyceraldehyde-3-phosphate dehydrogenase; n.d., not detectable, indicates no significant signal.

Cloning of Rat KS-SPAK

For identification of the alternatively spliced KS.-SPAK in rat kidney cDNA primers were designed based on alignment of rat intron 5 with mouse exon 5A sequence and two primer pares were selected from regions of aligned sequence with low homology to mouse exon 5A to reduce the possibility of amplifying mouse cDNA (forward primer 5′ CATGTGTATGCCAGATTCATCTCGAAAGAG 3′ [putative exon 5A] + reverse primer 5′ GGGCTATGTCTGGTGTTCGTGTCAGCA 3′ [exon 10], predicted PCR product size 510 bp and forward primer 5′ CCCAGGCTTTGTGGCTTTGGGTAAC 3′ [putative exon 5A] + reverse primer 5′ CAGGGGCCATCCAACATGGGG 3′ [exon 6], predicted PCR product size 363 bp). RT-PCR was performed using total RNA extracted from whole rat kidney and PCR products were cloned into pGEMT-easy vector and verified by sequencing.

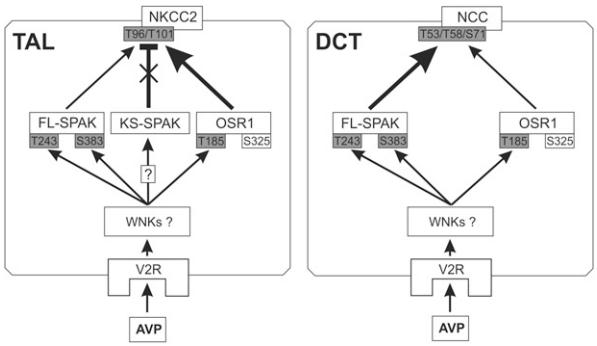

Figure 11. Proposed model of AVP-WNK-SPAK/OSR1-NKCC2/NCC signaling in the distal nephron. Arrows indicate the downstream effects of V2R activation, and the T bar indicates inhibition. The thickness of the arrows indicates the significance of the respective kinases and their actions in AVP-induced phosphorylation of NKCC2 or NCC. Boxes shaded in gray indicate phosphoacceptor sites activated by AVP signaling. In TAL, AVP attenuates the inhibitory action of KS-SPAK (cross) and facilitates the actions of FL-SPAK and OSR1. In DCT, expression of KS-SPAK is nearly absent and FL-SPAK plays the dominant role in AVP signaling. It is presently unclear which WNK isoforms mediate AVP signaling upstream of SPAK/OSR1.

Statistical Analyses

Results were evaluated using routine parametric statistics. Groups were compared by means of the *t* test or, if the data violated a normal distribution, the nonparametric Mann–Whitney test. The two-way ANOVA with Bonferroni correction was utilized to analyze the differences in effect of dDAVP between WT and SPAK−/− genotypes. A probability level of $P<0.05$ was accepted as significant. All results are expressed as the mean ± SD.

ACKNOWLEDGMENTS

The authors thank Kerstin Riskowski, Petra Schrade, John Horn, Shaunessy Rogers, and Joshua Nelson for assistance and advice.

This work was supported by Deutsche Forschungsgemeinschaft (FOR667).

DISCLOSURES

None.

REFERENCES

1. Gamba G: Molecular physiology and pathophysiology of electroneutral cation-chloride cotransporters. *Physiol Rev* 85: 423–493, 2005
2. Simon DB, Karet FE, Hamdan JM, DiPietro A, Sanjad SA, Lifton RP: Bartter's syndrome, hypokalaemic alkalosis with hypercalciuria, is caused by mutations in the Na-K-2Cl cotransporter NKCC2. *Nat Genet* 13: 183–188, 1996
3. Simon DB, Nelson-Williams C, Bia MJ, Ellison D, Karet FE, Molina AM, Vaara I, Iwata F, Cushner HM, Koolen M, Gainza FJ, Gitleman HJ, Lifton RP: Gitelman's variant of Bartter's syndrome, inherited hypokalaemic alkalosis, is caused by mutations in the thiazide-sensitive Na-Cl cotransporter. *Nat Genet* 12: 24–30, 1996
4. Vitari AC, Deak M, Morrice NA, Alessi DR: The WNK1 and WNK4 protein kinases that are mutated in Gordon's hypertension syndrome phosphorylate and activate SPAK and OSR1 protein kinases. *Biochem J* 391: 17–24, 2005
5. Uchida S: Pathophysiological roles of WNK kinases in the kidney. *Pflugers Arch* 460: 695–702, 2010
6. Richardson C, Alessi DR: The regulation of salt transport and blood pressure by the WNK-SPAK/OSR1 signalling pathway. *J Cell Sci* 121: 3293–3304, 2008
7. Piechotta K, Lu J, Delpire E: Cation chloride cotransporters interact with the stress-related kinases Ste20-related proline-alanine-rich kinase (SPAK) and oxidative stress response 1 (OSR1). *J Biol Chem* 277: 50812–50819, 2002
8. Richardson C, Sakamoto K, de los Heros P, Deak M, Campbell DG, Prescott AR, Alessi DR: Regulation of the NKCC2 ion cotransporter by SPAK-OSR1-dependent and -independent pathways. *J Cell Sci* 124: 789–800, 2011
9. McCormick JA, Mutig K, Nelson JH, Saritas T, Hoorn EJ, Yang CL, Rogers S, Curry J, Delpire E, Bachmann S, Ellison DH: A SPAK isoform switch modulates renal salt transport and blood pressure. *Cell Metab* 14: 352–364, 2011
10. Yang SS, Lo YF, Wu CC, Lin SW, Yeh CJ, Chu P, Sytwu HK, Uchida S, Sasaki S, Lin SH: SPAK-knockout mice manifest Gitelman syndrome and impaired vasoconstriction. *J Am Soc Nephrol* 21: 1868–1877, 2010
11. Lin SH, Yu IS, Jiang ST, Lin SW, Chu P, Chen A, Sytwu HK, Sohara E, Uchida S, Sasaki S, Yang SS: Impaired phosphorylation of Na(+)-K(+)-2Cl(-) cotransporter by oxidative stress-responsive kinase-1 deficiency manifests hypotension and Bartter-like syndrome. *Proc Natl Acad Sci U S A* 108: 17538–17543, 2011
12. McCormick JA, Ellison DH: The WNKs: Atypical protein kinases with pleiotropic actions. *Physiol Rev* 91: 177–219, 2011 [Review]
13. Mutig K, Paliege A, Kahl T, Jöns T, Müller-Esterl W, Bachmann S: Vasopressin V2 receptor expression along rat, mouse, and human renal epithelia with focus on TAL. *Am J Physiol Renal Physiol* 293: F1166–F1177, 2007
14. Giménez I, Forbush B: Short-term stimulation of the renal Na-K-Cl cotransporter (NKCC2) by vasopressin involves phosphorylation and membrane translocation of the protein. *J Biol Chem* 278: 26946–26951, 2003
15. Mutig K, Saritas T, Uchida S, Kahl T, Borowski T, Paliege A, Böhlick A, Bleich M, Shan Q, Bachmann S: Short-term stimulation of the thiazide-sensitive Na+-Cl- cotransporter by vasopressin involves phosphorylation and membrane translocation. *Am J Physiol Renal Physiol* 298: F502–F509, 2010
16. Pedersen NB, Hofmeister MV, Rosenbaek LL, Nielsen J, Fenton RA: Vasopressin induces phosphorylation of the thiazide-sensitive sodium chloride cotransporter in the distal convoluted tubule. *Kidney Int* 78: 160–169, 2010
17. Welker P, Böhlick A, Mutig K, Salanova M, Kahl T, Schlüter H, Blottner D, Ponce-Coria J, Gamba G, Bachmann S: Renal Na+-K+-Cl- cotransporter activity and vasopressin-induced trafficking are lipid raft-dependent. *Am J Physiol Renal Physiol* 295: F789–F802, 2008
18. Ares GR, Caceres PS, Ortiz PA: Molecular regulation of NKCC2 in the thick ascending limb. *Am J Physiol Renal Physiol* 301: F1143–F1159, 2011
19. van Vonderen IK, Wolfswinkel J, Oosterlaken-Dijksterhuis MA, Rijnberk A, Kooistra HS: Pulsatile secretion pattern of vasopressin under basal conditions, after water deprivation, and during osmotic stimulation in dogs. *Domest Anim Endocrinol* 27: 1–12, 2004
20. Gagnon KB, Delpire E: On the substrate recognition and negative regulation of SPAK, a kinase modulating Na+-K+-2Cl- cotransport activity. *Am J Physiol Cell Physiol* 299: C614–C620, 2010

21. Rafiqi FH, Zuber AM, Glover M, Richardson C, Fleming S, Jovanović S, Jovanović A, O'Shaughnessy KM, Alessi DR: Role of the WNK-activated SPAK kinase in regulating blood pressure. *EMBO Mol Med* 2: 63–75, 2010
22. Piechotta K, Garbarini N, England R, Delpire E: Characterization of the interaction of the stress kinase SPAK with the Na+-K+-2Cl- cotransporter in the nervous system: Evidence for a scaffolding role of the kinase. *J Biol Chem* 278: 52848–52856, 2003
23. Nugent BM, Valenzuela CV, Simons TJ, McCarthy MM: Kinases SPAK and OSR1 are upregulated by estradiol and activate NKCC1 in the developing hypothalamus. *J Neurosci* 32: 593–598, 2012
24. Ushiro H, Tsutsumi T, Suzuki K, Kayahara T, Nakano K: Molecular cloning and characterization of a novel Ste20-related protein kinase enriched in neurons and transporting epithelia. *Arch Biochem Biophys* 355: 233–240, 1998
25. Mazzocchi G, Malendowicz LK, Rocco S, Musajo F, Nussdorfer GG: Arginine-vasopressin release mediates the aldosterone secretagogue effect of neurotensin in rats. *Neuropeptides* 24: 105–108, 1993
26. Möhring J, Kohrs G, Möhring B, Petri M, Homsy E, Haack D: Effects of prolonged vasopressin treatment in Brattleboro rats with diabetes insipidus. *Am J Physiol* 234: F106–F111, 1978
27. Ecelbarger CA, Kim GH, Wade JB, Knepper MA: Regulation of the abundance of renal sodium transporters and channels by vasopressin. *Exp Neurol* 171: 227–234, 2001
28. Zagórska A, Pozo-Guisado E, Boudeau J, Vitari AC, Rafiqi FH, Thastrup J, Deak M, Campbell DG, Morrice NA, Prescott AR, Alessi DR: Regulation of activity and localization of the WNK1 protein kinase by hyperosmotic stress. *J Cell Biol* 176: 89–100, 2007
29. Richardson C, Rafiqi FH, Karlsson HK, Moleleki N, Vandewalle A, Campbell DG, Morrice NA, Alessi DR: Activation of the thiazide-sensitive Na+-Cl- cotransporter by the WNK-regulated kinases SPAK and OSR1. *J Cell Sci* 121: 675–684, 2008
30. Ohno M, Uchida K, Ohashi T, Nitta K, Ohta A, Chiga M, Sasaki S, Uchida S: Immunolocalization of WNK4 in mouse kidney. *Histochem Cell Biol* 136: 25–35, 2011
31. Reiche J, Theilig F, Rafiqi FH, Carlo AS, Militz D, Mutig K, Todiras M, Christensen EI, Ellison DH, Bader M, Nykjaer A, Bachmann S, Alessi D, Willnow TE: SORLA/SORL1 functionally interacts with SPAK to control renal activation of Na(+)-K(+)-Cl(-) cotransporter 2. *Mol Cell Biol* 30: 3027–3037, 2010
32. Perucca J, Bichet DG, Bardoux P, Bouby N, Bankir L: Sodium excretion in response to vasopressin and selective vasopressin receptor antagonists. *J Am Soc Nephrol* 19: 1721–1731, 2008
33. van der Lubbe N, Lim CH, Fenton RA, Meima ME, Jan Danser AH, Zietse R, Hoorn EJ: Angiotensin II induces phosphorylation of the thiazide-sensitive sodium chloride cotransporter independent of aldosterone. *Kidney Int* 79: 66–76, 2011
34. Bouby N, Bachmann S, Bichet D, Bankir L: Effect of water intake on the progression of chronic renal failure in the 5/6 nephrectomized rat. *Am J Physiol* 258: F973–F979, 1990
35. Sandberg MB, Riquier AD, Pihakaski-Maunsbach K, McDonough AA, Maunsbach AB: ANG II provokes acute trafficking of distal tubule Na +-Cl(-) cotransporter to apical membrane. *Am J Physiol Renal Physiol* 293: F662–F669, 2007

This article contains supplemental material online at http://jasn.asnjournals.org/lookup/suppl/doi:10.1681/ASN.2012040404/-/DCSupplemental.

Supplemental Figure 1

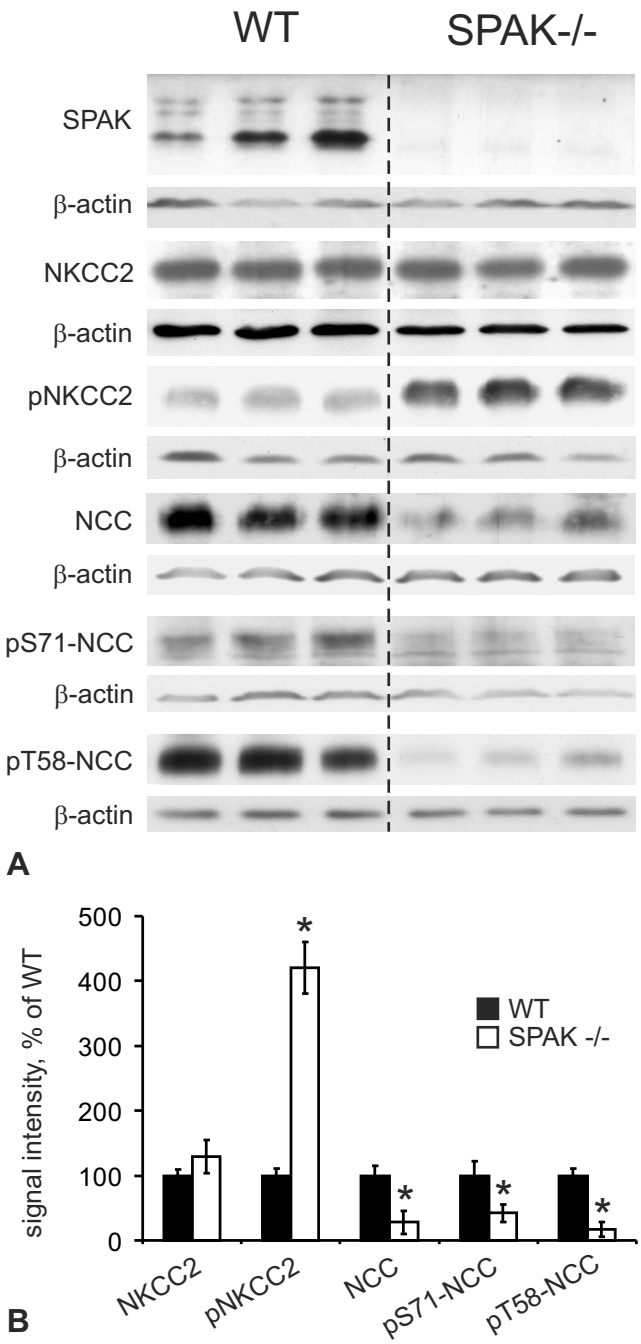

Supplemental Figure 2

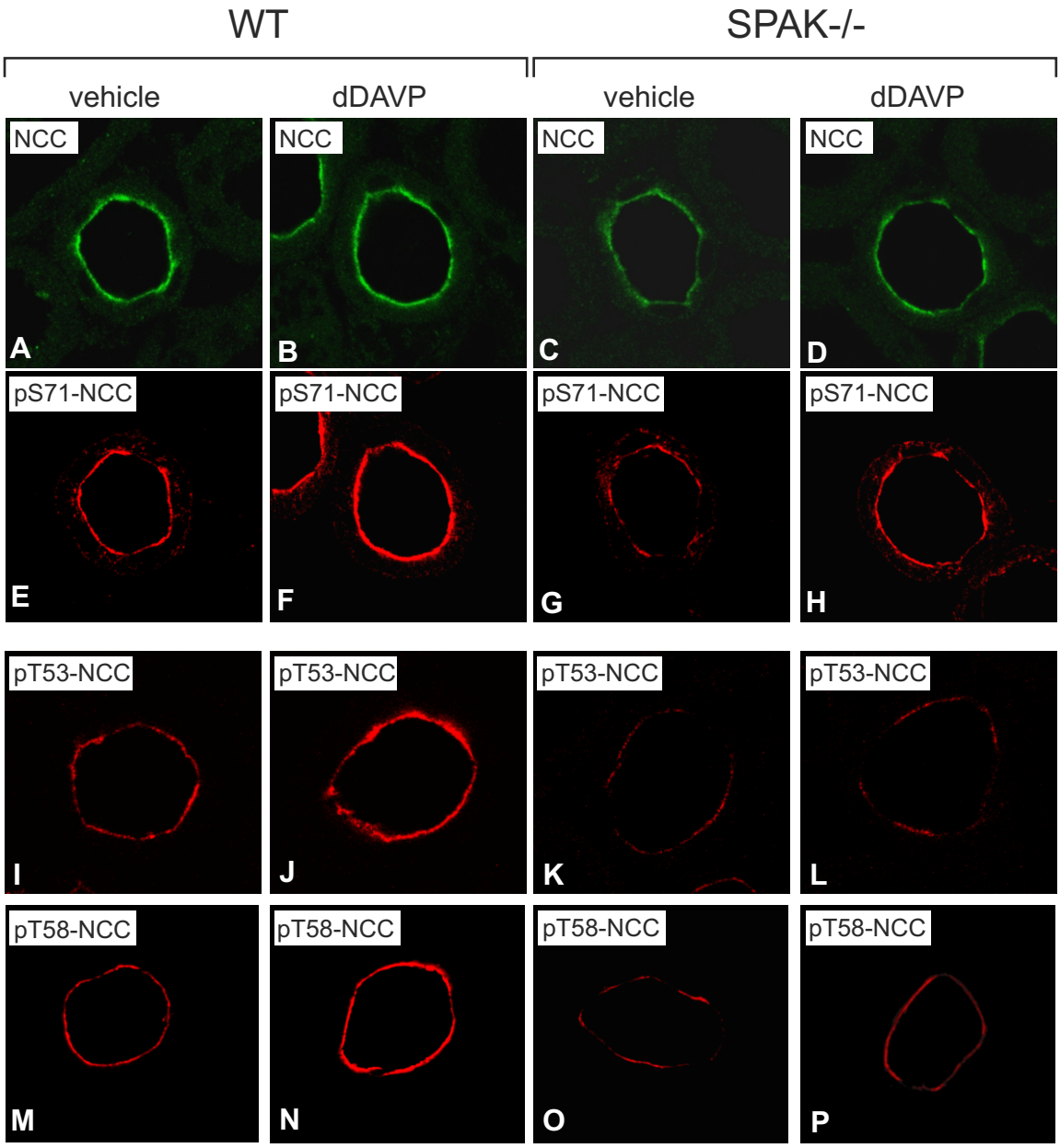

	WT		SPAK-/-	
	vehicle	dDAVP	vehicle	dDAVP
NCC	100±25	111±35	61±7§	62±5
pS71-NCC	100±24	147±6*	65±11§	60±11
pT53-NCC	100±45	263±35*	47±17§	37±13
pT58-NCC	100±32	498±163*	86±36	145±52

Q

Supplemental Figure 3

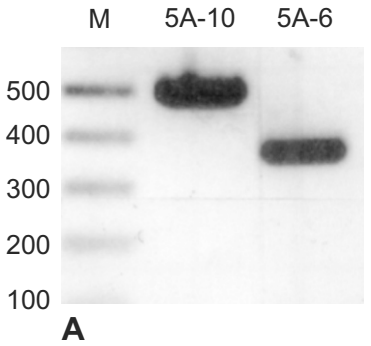

A

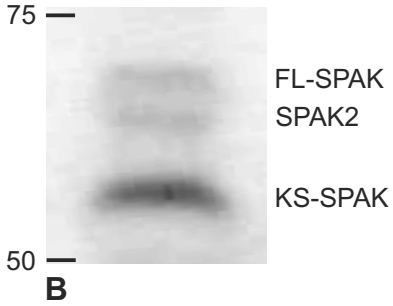

B

AGTCCAGTCACAAGCAGTCTCCTCGGTGAGTGCAG
ACTATCAGCTGGTTGAAACCCCCAGGCTTTGTGGCT
TTGGGTAA**C**TTACCAAAGGACTCATTTCCTTTAGCA
AAGAGTAAAGAAAATATTGCCTTTTACCATTGCTGG
CACACAGTAGGTACACTATATAGCCATCAACGAACG
GTGTTGCTATGGTTACTAGTGTTACCCTCCTCCCTA
ACGTTACTGCAGCCAGCAGGACCACACTTGCGCTG
CCTGGAGGTCATGTGTATGCCAGATTCATCTCGAAA
GAGATTCAGCTCTGAGAGACTGTGAGTTACAAAAAG

C

Supplemental Figure 4

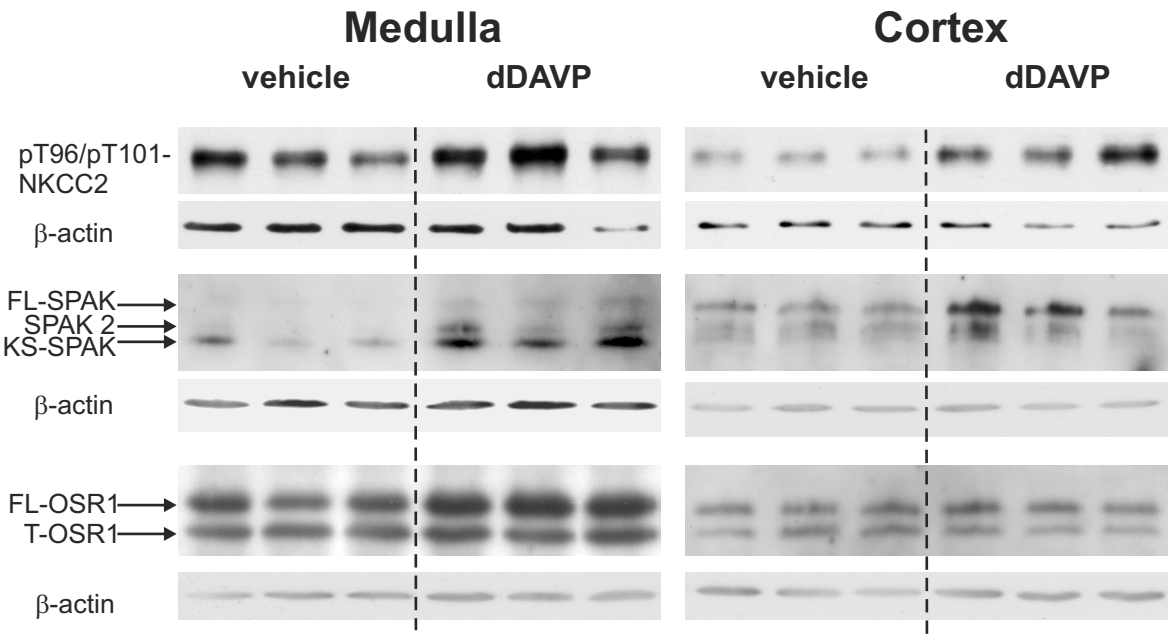

A **B**

product	vehicle, %	dDAVP, %
pT96/pT101-NKCC2	100±31	248±47*
total SPAK	100±38	255±17*
FL-SPAK	100±5	225±11*
SPAK2	100±6	214±63
KS-SPAK	100±15	227±9*
total OSR1	100±4	120±5*
FL-OSR1	100±8	122±7*
T-OSR1	100±6	117±9*

C

product	vehicle, %	dDAVP, %
pT58-NCC	100±19	482±38*
total SPAK	100±25	150±17
FL-SPAK	100±14	195±22*
SPAK2	100±21	106±28
KS-SPAK	100±32	98±35
total OSR1	100±42	89±37
FL-OSR1	100±41	98±36
T-OSR1	100±42	88±29

D

Supplemental Figure 1

Steady state abundance and phosphorylation of NKCC2 and NCC in WT and SPAK-/- mice. (A) Representative immunoblots from WT and SPAK-/- kidney homogenates detected with antibodies to SPAK (three bands between 50 and 75 kDa), NKCC2, pT96/pT101-NKCC2, NCC, pS71-NCC, and pT58-NCC (bands at approximately 160 kDa throughout). Loading was controlled by concomitant detection of β-actin (approximately 40 kDa) as shown below the corresponding immunoblots. (B) Densitometric evaluation of the blots normalized to loading controls. Data are the means ± SD, * $p<0.05$.

Supplemental Figure 2

Acute effects of dDAVP on the abundance and phosphorylation of NCC, confocal evaluation. (A-H) Representative images of DCT profiles from WT and SPAK-/- kidney sections double-stained with anti-NCC and anti-pS71-NCC antibodies after 30 min vehicle or dDAVP treatment. (E-P) Parallel confocal images of DCT profiles labeled with anti-pT53-NCC and anti-pT58-NCC antibodies (concomitant labeling of NCC was performed; not shown). (Q) Evaluation of the confocal signals by intensity. Values obtained in WT after vehicle application set at 100%. Data are the means ± SD; * $p<0.05$ for intrastrain differences (vehicle vs. dDAVP); § $p<0.05$ for interstrain differences (WT vs. SPAK-/- upon vehicle).

Supplemental Figure 3

Verification of KS-SPAK expression and abundance in rat kidney. (A) RT-PCR from total rat kidney RNA using forward primer in the alternative exon 5 (5A) of KS-SPAK and reverse primers in exon 10 (5A-10) or exon 6 (5A-6) produced products of predicted sizes (M = DNA ladder). (B) Immunoblotting from rat kidney homogenates using C-SPAK antibody produced the characteristic three bands corresponding to FL-SPAK, SPAK2, and KS-SPAK. Note high abundance of KS-SPAK. (C) Sequencing of both KS-SPAK PCR products (A) confirmed the expression of this splice variant in rat kidney. Clones contained rat exon 5A fused to rat exon 6. Shaded text indicates location of the forward primer within rat exon 5A; the underlined sequence is homologous to mouse exon 5A.

Supplemental Figure 4

Long term effects of dDAVP on SPAK-OSR1 in Brattleboro rats with diabetes insipidus. (A, B) Representative immunoblots showing SPAK and OSR1 immunoreactive bands in renal medulla containing TAL but not DCT (A) and cortex containing DCT (B) from DI rats after 3 days of vehicle or dDAVP treatment. The effect of dDAVP was confirmed by substantially increased NKCC2- or NCC phosphorylation. β-actin bands below the corresponding immunoblots served as loading controls. (C, D) Densitometric evaluation of single immunoreactive bands from medulla (C) and cortex (D) normalized to loading controls. Note strong signal increases of SPAK isoforms in both renal medulla and cortex compared to modest increases of OSR1 variants in renal medulla only. Data are the means ± SD, * $p<0.05$.

4 Discussion

4.1 Vasopressin V2 receptor expression along rat, mouse, and human renal epithelia with focus on TAL.

AVP is vital for the urinary concentrating mechanism which is reflected by severe failure of the urinary concentration in patients with the central or nephrogenic diabetes insipidus caused by the absence of the circulating AVP or inactivating mutations of the V2R, respectively [4,56]. Although several previous studies addressed the distribution of V2R in the kidney, their results obtained for the distal nephron remained largely inconclusive [11,13,14]. Furthermore, the majority of the previous studies have been performed in the rat kidney, whereas the information on V2R distribution in the mouse- or human kidney was scarce [11,13,14]. The present study was, therefore, designed to provide solid data on V2R distribution along rat, mouse, and human nephron, both at the mRNA- and protein levels using *in situ* hybridization and immunohistochemistry. The results of the study have demonstrated substantial V2R mRNA expression in TAL, DCT, and the principal cells of CNT/CD in all analyzed species thus corroborating and extending previous work. Since earlier studies were not consistent with respect to the expression of V2R in TAL [11,13,14], acute effects of the V2R agonist desmopressin (dDAVP) were evaluated in AVP-deficient Brattleboro rats and cultured TAL cells. Rapid dDAVP-induced activation of NKCC2 observed in both settings provided strong functional support for our localization data.

In view of the fact, that several transgenic mouse strains have been generated to study the AVP/V2R axis in mice, the exact knowledge on the V2R distribution in the mouse kidney is absolutely necessary for the understanding of their phenotypes [39,57,58]. Thus, the substantial V2R expression along the mouse distal nephron helps to explain the decreased abundance and phosphorylation of NKCC2 and NCC in mice deficient for adenylyl cyclase VI mediating the effects of V2R activation [39]. Another major highlight of the present study is the localization of the V2R to the human TAL and DCT. Since V2R antagonists have become available for use in patients, the knowledge on V2R distribution along the human nephron is also of clinical relevance [59].

The major drawback of the present study was the insufficient subcellular resolution of the V2R distribution along the nephron. Although the subcellular localization of the receptor was addressed in several previous studies, all these attempts failed or provided insufficient information due to the lack of robust anti-V2R antibodies [13,14,60]. The available data were controversial and reported both basolateral and luminal presence of the receptor [14,60].

To resolve this issue, I have recently generated a new anti-V2R antibody. Using this antibody I have localized the receptor to the basolateral membrane of TAL, DCT, and principal cells of CNT and CD (Figures 2-4; manuscript in preparation). Thus, our unpublished data suggest that the V2R chiefly resides in the basolateral membrane where it can readily respond to changes in

plasma AVP levels.

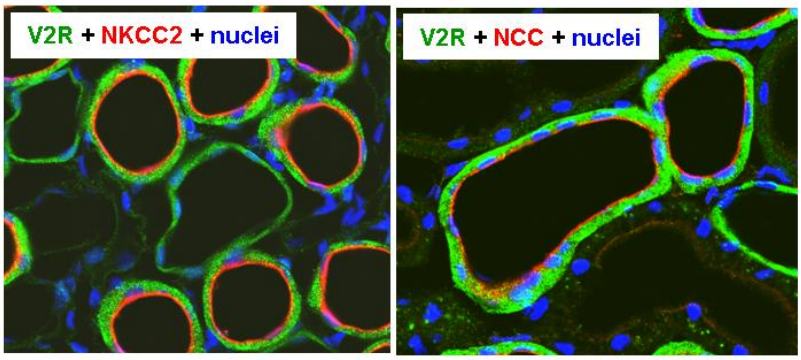

Figure 2. Application of self-made anti-V2R antibody revealed the basolateral distribution of the receptor (green signal) in the NKCC2-positive TAL and NCC-positive DCT (red signals). Nuclei are counterstained with DAPI (blue).

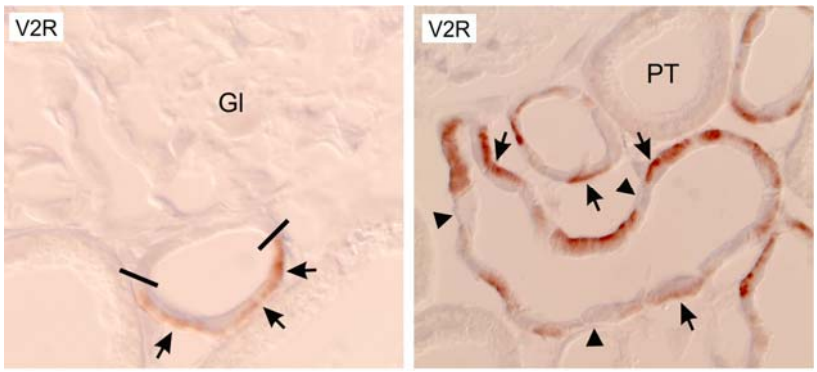

Figure 3. Basolateral localization of V2R in TAL (left image, arrows) and principal cells of CD (right image, arrows) as revealed by our anti-V2R antibody. Note that macula densa cells (flanked by bars) of TAL and in tercalated cells of CD (arrowheads) are V2R-negative.

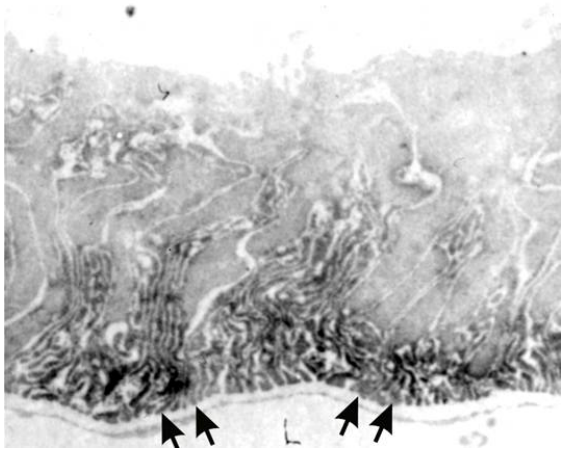

Figure 4. High re solution analysis of the subcellular V2R distribution using pre-embedding labeling of the receptor for electr on microscopy. Arrows point to the V2R signal in the folding of the basolateral membrane of TAL cells. No significant luminal immunoreactivity was detected.

To provide further functional information on the role of AVP-V2R signaling I have collaborate d with Prof. Michael Bader (MDC Berlin) to generate a transgenic rat model with suppressed V2R activity in the TAL. To this end we used the Tamm-Horsfall protein promoter to drive an overexpression of a dominant-negative V2R mut ant selectively in the TAL of transgenic rat s. Evaluation of the tran sgenic rats revealed imp aired urinary concentration an d decreased abundance and phosphorylation of NKCC2 indicating that V2R activity in TAL is critical for the NKCC2 function (Figure 5; manuscript in preparation).

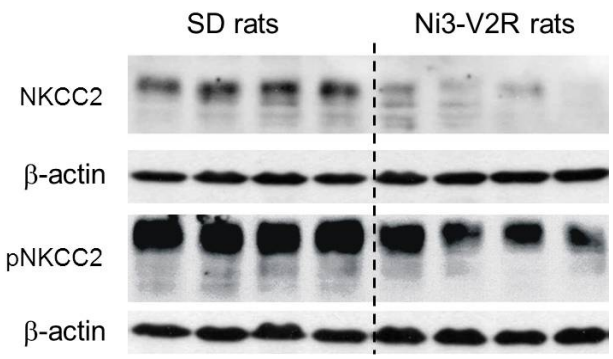

Figure 5. Representative immunoblots showing decreased abundance and phosphorylation (p) of NKCC2 in rat s transgenic for the dominant-negative V2 R mutant (Ni3-V2R), as co mpared to the control SD rats. The dominant-negative properties of the Ni3-V2R have been established in previous work [58,61].

In summary, the prese nt study cle arly showed that the V2R expression is not r estricted to principal cells of CNT and CD but is substantially present throughout the dist al nephron. These conclusions were further supporte d by our yet unpublish ed data (Figures 1-4). The present localization study was the prerequisite for our late r functional studies on characterization of the AVP action along the TAL and DCT.

4.2 Short-term stimulation of the thiazide-sensitive Na+-Cl- cotransporter by vasopressin involves phosphorylation and membrane translocation.

NCC plays an important role in the renal sodium and potassium handling [50]. On one hand, reabsorption of up to 10 % of the filtered NaCl i n DCT via NCC substantially contributes to the fine tuning of the renal salt excretion in healthy individuals [29]. On the other hand, activity of NCC defines the sodium lo ad in the downstream CD and is, thus, rate limiting f or sodium reabsorption via the epithelial sod ium channel (ENaC) and the pot assium secretion via th e Kir1.1 potassium channel (rat outer medullary channel; R OMK) [50]. Late portion of DCT, CNT, and CD constitute the a ldosterone-sensitive nephron [62]. Consequently, aldosterone has been shown to activate both NCC and ENaC [2,50]. AngII is another potent endocrine stimu lus of NCC and ENaC activity [2,50,63]. Although often viewed independently of each other , RAAS and AVP indeed act synergistically to adjust salt and water reabsorption to the needs of the body [4,23,25]. In this context, AVP not only promote s the reabsorption of w ater but also af fects the renal sa lt handling either directly via activation of the V2R or indirectly via modu lating the RAAS [4]. It is, therefore, important to dissect b etween the direct and ind irect effects of AVP along the dist al nephron. It was known, that AVP stimulates ENaC function activation via activation of V2R in the CD [22]. Moreover, AVP-induced ENaC activation has been linked to sodium retention and volume expansion in cert ain hypertensive conditions [22]. In the present study we elucidate the role of AVP in the regulation of NCC and for the first time demonst rate direct effects of the hormone in the DCT. We show that AVP, acting via V2R, facilitates the activating N-terminal phosphorylation of the transporter and increases its surface expression. From the physiologic point of view, AVP-

induced stimulation of NaCl reabsorption in water-impermeable DCT may serve to potentiate the urinary concentrating. Likewise, activation of NCC may serve to limit the sodium load in the downstream CD and, thus, help to balance the renal potassium excretion during the prolonged AVP-induced antidiuresis [64,65]. From a clinical point of view, effects of AVP on the distal salt transporters may contribute to the regulation of the arterial pressure in health and disease [23]. Considering the role of NCC in the pathogenesis of certain hypertensive disorders [66], the effects of AVP on NCC described in the present study may also have clinical implications.

4.3 Activation of the bumetanide-sensitive Na+,K+,2Cl- cotransporter (NKCC2) is facilitated by Tamm-Horsfall protein in a chloride-sensitive manner.

Although regulation of the renal salt transporters by AVP has been intensively studied during the last decade, the underlying molecular mechanisms, beyond the cAMP/PKA cascade, have received only minor attention so far [19,67]. In our previous work we have shown that association of NKCC2 with lipid rafts facilitates its AVP-induced apical trafficking and activation [52]. Lipid rafts are specialized membrane microdomains enriched in cholesterol, glycosphingolipids, and proteins which serve to compartmentalize cellular processes such as trafficking or signaling events [54]. The co-expressed proteins may thus affect function of NKCC2 through lipid-rafts-mediated interactions. One of these potential interaction partners is the Tamm-Horsfall protein (THP; also known as uromodulin) which is abundantly expressed in TAL and co-localized with NKCC2 within the apical lipid rafts [53].

THP is a GPI-anchored glycoprotein with a large extracellular moiety which undergoes proteolytic cleavage and is abundantly excreted with the urine [51]. Urinary THP binds with high affinity to the S- and P-fimbriae of *Escherichia coli* and inhibits the fimbriae-mediated penetration of bacteria in the urothelial layer, thus serving as a defense factor against urinary infects [51]. THP is also believed to protect from urinary stones due to its ability to bind calcium [51]. Mutations of THP cause uromodulin-associated kidney disease, also known as medullary cystic kidney disease type 2 or familiar juvenile kidney nephropathy. The disease phenotype is characterized by impaired urinary concentration and development of medullary cysts, and has been attributed to impaired trafficking and intracellular accumulation of THP followed by apoptosis of TAL cells [51].

Our previous work suggested that apart from its well characterized extracellular functions, THP is also implicated in the NaCl reabsorption in TAL cells [53]. This hypothesis was based on several lines of evidence suggesting a permissive role of THP in the transport function of the TAL. An early study of our group described dramatic reduction of THP expression in patients with the antenatal form of Bartter syndrome [68]. Since this type of Bartter syndrome is caused by mutations in the NKCC2 gene impairing the activity of the transporter, the concomitant reduction

of THP expression suggested functional links between THP and NKCC2. Furthermore, our analysis of THP-deficient mice revealed impaired urinary concentration and also suggested an interference of THP with the function of NKCC2 [53]. The present study demonstrates that THP indeed facilitates both baseline and AVP-induced NKCC2 activity by promoting its phosphorylation. These results suggested that THP may be implicated in volume regulation by modulating the transcellular NaCl reabsorption in the TAL. In this context, association between THP gene variants and salt-sensitive hypertension have been demonstrated in a recent study involving large cohorts of hypertensive patients [69]. In that study, increased expression of THP has been shown to cause hypertension in mice and to contribute to development of hypertension in human patients via stimulation of NKCC2 [69]. Although molecular mechanisms mediating effects of THP on NKCC2 have not been fully characterized, available data points to activation of SPAK/OSR1 kinases in the presence of THP, which may eventually result in increased NKCC2 phosphorylation and activity [69]. Alternatively, THP may stabilize NKCC2 in the apical lipid rafts and thus promote its interaction with the activating kinases [52]. Taken together, physiologic and clinical relevance of the functional interaction between THP and NKCC2 established in the present study has been clearly demonstrated, whereas the underlying molecular mechanisms still need further clarification.

4.4 A SPAK isoform switch modulates renal salt transport and blood pressure.

N-terminal phosphorylation of CCC transporters critically defines their transport capacity [33]. Recent work has identified WNK, SPAK, and OSR1 kinases as the key components of the molecular pathway responsible for the phosphorylation of CCCs, including their kidney-specific members, NKCC2 and NCC [33–35]. Early studies *in vitro*, in oocytes, and in cultured cells led to generation of a linear model of the WNK-SPAK/OSR1-CCC signaling suggesting that the homologous SPAK and OSR1 kinases provide phosphorylation of the transporters and are themselves phosphorylated and activated by the upstream WNK kinases [35]. More recently, a mouse strain carrying catalytically inactive SPAK mutant ($SPAK^{243A/243A}$) has been shown to display decreased phosphorylation of NKCC2 and NCC, salt loss, and hypotension suggesting a prominent role of the kinase in the regulation of blood pressure [70]. In the present study, we have evaluated the role of SPAK in regulation of NKCC2 and NCC *in vivo* using SPAK-deficient mice. Surprisingly, the deletion of the kinase produced opposite effects on phosphorylation of NKCC2 (strong increase) and NCC (marked reduction), indicating divergent roles of the kinase in TAL vs. DCT. To explain this fact, we have hypothesized that renal SPAK gene might give rise to functionally different SPAK variants. Indeed, our analysis of renal SPAK transcripts has identified a truncated, kidney-specific SPAK splice variant completely lacking the catalytic domain and kinase activity which we termed KS (kidney-specific)-SPAK. We have further shown that KS-SPAK is chiefly expressed in the TAL, where it acts as a dominant negative kinase

variant by competing with the full-length SPAK or OSR1 for the interaction with NKCC2, whereas the kinase-active full-length SPAK predominates in the DCT. These different distribution patterns of activating and inhibitory SPAK variants along the distal nephron provide a simple and conclusive explanation for the divergent effects of SPAK deletion in TAL vs. DCT. In SPAK-knockout mice, deletion of the inhibitory KS-SPAK in TAL has obviously facilitated the phosphorylation of NKCC2 by the OSR1 kinase, whereas deletion of the full-length SPAK in DCT attenuated the NCC phosphorylation.

Parallel to our study, an alternative SPAK-deficient mouse strain has been generated and characterized by Yang SS and colleagues [71]. The phenotypes of both available SPAK-deficient models are similar and present with moderate hypotension and electrolyte imbalance resembling Gitelman's syndrome. In addition, the study of Yang SS et al. describes vascular effects of SPAK-deficiency such as reduced arterial contractility in response to adrenergic stimulation [71]. When extrapolated to human species, these results suggest that inhibition of SPAK might improve salt handling and peripheral arterial resistance in hypertensive patients. Thus, pharmacologic targeting of the kinase has a therapeutic potential for the management of high blood pressure.

4.5 SPAK differentially mediates vasopressin effects on sodium cotransporters.

In our previous studies, AVP has been shown to activate NKCC2 and NCC by rapid increase of their phosphorylation (see 3.1 and 3.2). Previous work on elucidation of molecular mechanisms governing the function of the distal transporters has identified the homologous SPAK and OSR1 kinases as key elements in the regulation of NKCC2 and NCC phosphorylation [35,70]. Although highly homologous and largely co-expressed along the distal nephron, the two kinases showed selective effects on NKCC2 and NCC, as was evident from the analysis of SPAK-deficient and kidney-specific OSR1-deficient mice. While SPAK kinase was critical for intact phosphorylation and activity of NCC, OSR1 kinase appeared to differ from SPAK by providing baseline phosphorylation of NKCC2 rather than of NCC [71,72]. The present study aimed at further dissecting between the functions of the two homologous kinases during the AVP action along the distal nephron. Effects of extrinsic stimulation of the AVP-V2R axis on the SPAK/OSR1-NKCC2/NCC cascade have been studied in acute and chronic settings using SPAK-deficient mice and AVP-deficient rats. The results of the study strongly suggested implication of SPAK variants in the AVP signaling both in TAL and DCT. Increased phosphorylation of SPAK at its catalytic domain in response to AVP indicated its increased kinase activity upon stimulation. Moreover, the kinase-active SPAK isoform exhibited more prominent interaction with NKCC2 after application of a V2R agonist, whereas binding of the inhibitory KS-SPAK variant to NKCC2 was attenuated in this setting. In contrast, the homologous OSR1 kinase was less involved in

the AVP signaling.

Interestingly, in a further collaborative study we have shown that SPAK also mediates effects of aldosterone on NCC [49]. In summary, our results suggest that SPAK plays major role in mediating the effects of relevant endocrine stimuli, such as AVP or RAAS, on the distal transporters. Considering the essential role of the distal salt handling in the regulation of the extracellular volume and arterial pressure, these data have clinical implications. From the physiologic point of view, the present study extends information on molecular pathways mediating the effects of AVP in TAL and DCT.

5 Conclusions (Zusammenfassung)

The furosemide-sensitive NKCC2 and the thiazide-sensitive NCC are the key salt transporters of the distal nephron. Their essential role in the maintenance of the extracellular volume and blood pressure is reflected by the broad clinical use of the respective diuretica in patients with arterial hypertension or edema. For this reason, regulation of these transporters has been one of the major topics of recent and current research [29,33]. The studies presented above elucidate molecular mechanisms of AVP signaling in the distal nephron and show how AVP activates NKCC2 and NCC. AVP plays crucial role in the control of the body water and electrolyte balance [4]. Insufficient levels of circulating AVP or inability of the kidney to respond to the hormone lead to severe failure of the urine concentrating mechanism [4]. Although urinary concentration is a complex process requiring synergistic work of the renal electrolyte-, urate-, and water transport systems, AVP has often been simplistically viewed as a water-sparing hormone due to its prominent and well characterized facilitating effects on the AQP2-mediated water reabsorption in CD [4]. However, the role of the hormone in the renal salt handling and volume regulation has been increasingly recognized in the last years [1,4,29]. The studies included in this habilitation thesis address the molecular mechanisms mediating the effects of AVP along the distal nephron. The first study addressed the renal distribution of the V2 vasopressin receptor (see 3.1). Rat, mouse, and human kidney specimens were analyzed with special focus on the distal nephron. The results of the study robustly demonstrated the expression of the V2R along the entire distal nephron in all evaluated species. On one hand, this localization data resolved the previous controversy on the presence of the receptor in TAL and DCT [11,13,14]. On the other hand, this study provided the necessary morphologic basis for our later work, which was focused on functional and molecular aspects of the AVP-induced activation of NKCC2 and NCC. Since phosphorylation of conserved N-terminal threonine- and serine residues has been shown to critically affect the activity of the CCC transporters, including NKCC2 and NCC [35], we have next evaluated the effects of AVP on the NKCC2 and NCC phosphorylation (see 3.1 and 3.2). Results of these studies revealed rapid and strong phosphorylation of both transporters in

response to extrinsic administration of a V2R agonist. The direct V2R-mediated activation of NCC was demonstrated for the first time and was the major advance of that work. We speculate that the AVP-induced stimulation of NaCl reabsorption in DCT may have an impact on the sodium and potassium balance during the antidiuresis. From a clinical point of view, implications of AVP in volume regulation via the activation of the distal transporters have been discussed [23]. The next study has dealt with further characterization of the molecular pathways involved in the AVP signaling along the TAL and the role of THP herein (see 3.3). We identified THP as a factor that facilitates the phosphorylation and activation of NKCC2 in response to AVP (see 3.3). The mechanisms of functional interference between THP and NKCC2 may depend on their co-distribution in the apical lipid rafts, although further details should be addressed in the future work [52]. Interestingly, the role of THP for NKCC2 activity has received supportive clinical evidence in a recent study involving analysis of hypertensive patients [69]. In view of the growing evidence linking CCC activity with their phosphorylation we have next addressed the kinase pathways acting to phosphorylate NKCC2 and NCC *in vivo* (see 3.4 and 3.5). Results of these studies have substantially contributed to understanding of complex interactions between the activating and inhibitory SPAK variants and OSR1 kinase at baseline and during action of AVP. SPAK was identified as an important element of AVP signaling in the DCT. The genetic deletion of the kinase resulted in decreased baseline function of NCC and attenuated AVP-induced activation of the transporter. Considering the substantial involvement of NCC in the pathogenesis of several hypertensive conditions such as pseudohypoaldosteronism type II (PHAII) or salt-sensitive hypertension [32], pharmacologic targeting of the kinase may have therapeutic potential for treatment of such volume disorders.

In summary, the studies presented in this habilitation thesis have dealt with the V2R-mediated AVP signaling along the distal nephron of TAL and DCT. The results support the concept of a V2R-dependent activation of salt transporters along the entire distal nephron, complementing the water-sparing effects of AVP in the principal cells of CNT and CD. From a physiological perspective, the V2R-mediated stimulation of salt reabsorption may be seen as part of an integrative renal response to AVP to achieve efficient urinary concentration. In addition, salt-sparing effects of AVP may play role in the pathogenesis of certain hypertensive conditions [23]. Characterization of the kinase pathways linking AVP to the distal transporter functions was a major achievement of this work. The prominent role of SPAK in short- and long term adaptations of the distal nephron under the control of AVP has been established. In the future, pharmacological targeting of the kinase therefore bears therapeutic potentials for a better management of volume disorders in a clinical context.

6. References (Literatur)

1. Ares, G. R., Caceres, P. S. & Ortiz, P. A. Molecular regulation of NKCC2 in the thick ascending limb. *Am. J. Physiol. Renal Physiol.* **301,** F1143–1159 (2011).
2. Castañeda-Bueno, M. & Gamba, G. Mechanisms of sodium-chloride cotransporter modulation by angiotensin II. *Curr. Opin. Nephrol. Hypertens.* **21,** 516–522 (2012).
3. Fenton, R. A. & Knepper, M. A. Mouse models and the urinary concentrating mechanism in the new millennium. *Physiol. Rev.* **87,** 1083–1112 (2007).
4. Bankir, L. Antidiuretic action of vasopressin: quantitative aspects and interaction between V1a and V2 receptor-mediated effects. *Cardiovasc. Res.* **51,** 372–390 (2001).
5. Grazzini, E. *et al.* Vasopressin regulates adrenal functions by acting through different vasopressin receptor subtypes. *Adv. Exp. Med. Biol.* **449,** 325–334 (1998).
6. Mazzocchi, G., Malendowicz, L. K., Rocco, S., Musajo, F. & Nussdorfer, G. G. Arginine-vasopressin release mediates the aldosterone secretagogue effect of neurotensin in rats. *Neuropeptides* **24,** 105–108 (1993).
7. Möhring, J. *et al.* Effects of prolonged vasopressin treatment in Brattleboro rats with diabetes insipidus. *Am. J. Physiol.* **234,** F106–111 (1978).
8. Lolait, S. J. *et al.* Cloning and characterization of a vasopressin V2 receptor and possible link to nephrogenic diabetes insipidus. *Nature* **357,** 336–339 (1992).
9. Morel, A., O'Carroll, A. M., Brownstein, M. J. & Lolait, S. J. Molecular cloning and expression of a rat V1a arginine vasopressin receptor. *Nature* **356,** 523–526 (1992).
10. Thibonnier, M., Berti-Mattera, L. N., Dulin, N., Conarty, D. M. & Mattera, R. Signal transduction pathways of the human V1-vascular, V2-renal, V3-pituitary vasopressin and oxytocin receptors. *Prog. Brain Res.* **119,** 147–161 (1998).
11. Ostrowski, N. L., Young, W. S., 3rd, Knepper, M. A. & Lolait, S. J. Expression of vasopressin V1a and V2 receptor messenger ribonucleic acid in the liver and kidney of embryonic, developing, and adult rats. *Endocrinology* **133,** 1849–1859 (1993).
12. Wesche, D., Deen, P. M. T. & Knoers, N. V. A. M. Congenital nephrogenic diabetes insipidus: the current state of affairs. *Pediatr. Nephrol. Berl. Ger.* **27,** 2183–2204 (2012).
13. Fenton, R. A., Brønd, L., Nielsen, S. & Praetorius, J. Cellular and subcellular distribution of the type-2 vasopressin receptor in the kidney. *Am. J. Physiol. Renal Physiol.* **293,** F748–760 (2007).
14. Sarmiento, J. M. *et al.* Differential distribution of the vasopressin V receptor along the rat nephron during renal ontogeny and maturation. *Kidney Int.* **68,** 487–496 (2005).
15. Moeller, H. B. & Fenton, R. A. Cell biology of vasopressin-regulated aquaporin-2 trafficking. *Pflüg. Arch. Eur. J. Physiol.* **464,** 133–144 (2012).
16. Sands, J. M. & Layton, H. E. The physiology of urinary concentration: an update. *Semin. Nephrol.* **29,** 178–195 (2009).
17. Hebert, S. C. & Andreoli, T. E. Control of NaCl transport in the thick ascending limb. *Am. J. Physiol.* **246,** F745–756 (1984).
18. Knepper, M. A., Kim, G. H., Fernández-Llama, P. & Ecelbarger, C. A. Regulation of thick ascending limb transport by vasopressin. *J. Am. Soc. Nephrol. JASN* **10,** 628–634 (1999).
19. Giménez, I. & Forbush, B. Short-term stimulation of the renal Na-K-Cl cotransporter (NKCC2) by vasopressin involves phosphorylation and membrane translocation of the protein. *J. Biol. Chem.* **278,** 26946–26951 (2003).
20. Ecelbarger, C. A. *et al.* Regulation of potassium channel Kir 1.1 (ROMK) abundance in the thick ascending limb of Henle's loop. *J. Am. Soc. Nephrol. JASN* **12,** 10–18 (2001).
21. Aoyagi, T., Koshimizu, T. & Tanoue, A. Vasopressin regulation of blood pressure and volume: findings from V1a receptor-deficient mice. *Kidney Int.* **76,** 1035–1039 (2009).

22. Bankir, L., Bichet, D. G. & Bouby, N. Vasopressin V2 receptors, ENaC, and sodium reabsorption: a risk factor for hypertension? *Am. J. Physiol. Renal Physiol.* **299,** F917–928 (2010).
23. Luft, F. C. Vasopressin, urine concentration, and hypertension: a new perspective on an old story. *Clin. J. Am. Soc. Nephrol. CJASN* **2,** 196–197 (2007).
24. Fujiwara, Y., Tanoue, A., Tsujimoto, G. & Koshimizu, T.-A. The roles of V1a vasopressin receptors in blood pressure homeostasis: a review of studies on V1a receptor knockout mice. *Clin. Exp. Nephrol.* **16,** 30–34 (2012).
25. Aoyagi, T. *et al.* Vasopressin regulates the renin-angiotensin-aldosterone system via V1a receptors in macula densa cells. *Am. J. Physiol. Renal Physiol.* **295,** F100–107 (2008).
26. Mironova, E., Bugaj, V., Roos, K. P., Kohan, D. E. & Stockand, J. D. Aldosterone-independent regulation of the epithelial Na+ channel (ENaC) by vasopressin in adrenalectomized mice. *Proc. Natl. Acad. Sci. U. S. A.* **109,** 10095–10100 (2012).
27. Stockand, J. D. Vasopressin regulation of renal sodium excretion. *Kidney Int.* **78,** 849–856 (2010).
28. Ecelbarger, C. A., Kim, G. H., Wade, J. B. & Knepper, M. A. Regulation of the abundance of renal sodium transporters and channels by vasopressin. *Exp. Neurol.* **171,** 227–234 (2001).
29. Gamba, G. Molecular physiology and pathophysiology of electroneutral cation-chloride cotransporters. *Physiol. Rev.* **85,** 423–493 (2005).
30. Hoorn, E. J., Nelson, J. H., McCormick, J. A. & Ellison, D. H. The WNK kinase network regulating sodium, potassium, and blood pressure. *J. Am. Soc. Nephrol. JASN* **22,** 605–614 (2011).
31. Simon, D. B. & Lifton, R. P. The molecular basis of inherited hypokalemic alkalosis: Bartter's and Gitelman's syndromes. *Am. J. Physiol.* **271,** F961–966 (1996).
32. Uchida, S. Pathophysiological roles of WNK kinases in the kidney. *Pflüg. Arch. Eur. J. Physiol.* **460,** 695–702 (2010).
33. Gamba, G. Regulation of the renal Na+-Cl- cotransporter by phosphorylation and ubiquitylation. *Am. J. Physiol. Renal Physiol.* **303,** F1573–1583 (2012).
34. Richardson, C. *et al.* Regulation of the NKCC2 ion cotransporter by SPAK-OSR1-dependent and -independent pathways. *J. Cell Sci.* **124,** 789–800 (2011).
35. Richardson, C. & Alessi, D. R. The regulation of salt transport and blood pressure by the WNK-SPAK/OSR1 signalling pathway. *J. Cell Sci.* **121,** 3293–3304 (2008).
36. Subramanya, A. R., Yang, C.-L., Zhu, X. & Ellison, D. H. Dominant-negative regulation of WNK1 by its kidney-specific kinase-defective isoform. *Am. J. Physiol. Renal Physiol.* **290,** F619–624 (2006).
37. Susa, K. *et al.* WNK-OSR1/SPAK-NCC signal cascade has circadian rhythm dependent on aldosterone. *Biochem. Biophys. Res. Commun.* **427,** 743–747 (2012).
38. Gunaratne, R. *et al.* Quantitative phosphoproteomic analysis reveals cAMP/vasopressin-dependent signaling pathways in native renal thick ascending limb cells. *Proc. Natl. Acad. Sci. U. S. A.* **107,** 15653–15658 (2010).
39. Rieg, T. *et al.* Adenylyl cyclase 6 enhances NKCC2 expression and mediates vasopressin-induced phosphorylation of NKCC2 and NCC. *Am. J. Pathol.* **182,** 96–106 (2013).
40. Caceres, P. S., Ares, G. R. & Ortiz, P. A. cAMP stimulates apical exocytosis of the renal Na(+)-K(+)-2Cl(-) cotransporter NKCC2 in the thick ascending limb: role of protein kinase A. *J. Biol. Chem.* **284,** 24965–24971 (2009).
41. Imbert, M., Chabardès, D., Montegut, M., Clique, A. & Morel, F. Vasopressin dependent adenylate cyclase in single segments of rabbit kidney tubule. *Pflüg. Arch. Eur. J. Physiol.* **357,** 173–186 (1975).
42. Chabardès, D. *et al.* Adenylate cyclase responsiveness to hormones in various portions of the human nephron. *J. Clin. Invest.* **65,** 439–448 (1980).
43. Duong Van Huyen, J. P., Bens, M., Teulon, J. & Vandewalle, A. Vasopressin-stimulated chloride transport in transimmortalized mouse cell lines derived from the distal convoluted

tubule and cortical and inner medullary collecting ducts. *Nephrol. Dial. Transplant. Off. Publ. Eur. Dial. Transpl. Assoc. - Eur. Ren. Assoc.* **16,** 238–245 (2001).
44. Dai, L. J., Bapty, B., Ritchie, G. & Quamme, G. A. Glucagon and arginine vasopressin stimulate Mg2+ uptake in mouse distal convoluted tubule cells. *Am. J. Physiol.* **274,** F328–335 (1998).
45. Nguyen, M. T. X., Lee, D. H., Delpire, E. & McDonough, A. A. Differential regulation of Na+ transporters along nephron during ANG II-dependent hypertension: distal stimulation counteracted by proximal inhibition. *Am. J. Physiol. Renal Physiol.* **305,** F510–519 (2013).
46. Sandberg, M. B., Riquier, A. D. M., Pihakaski-Maunsbach, K., McDonough, A. A. & Maunsbach, A. B. ANG II provokes acute trafficking of distal tubule Na+-Cl(-) cotransporter to apical membrane. *Am. J. Physiol. Renal Physiol.* **293,** F662–669 (2007).
47. Bostanjoglo, M. *et al.* 11Beta-hydroxysteroid dehydrogenase, mineralocorticoid receptor, and thiazide-sensitive Na-Cl cotransporter expression by distal tubules. *J. Am. Soc. Nephrol. JASN* **9,** 1347–1358 (1998).
48. Ko, B. *et al.* Aldosterone acutely stimulates NCC activity via a SPAK-mediated pathway. *Am. J. Physiol. Renal Physiol.* **305,** F645–652 (2013).
49. Van der Lubbe, N. *et al.* Aldosterone does not require angiotensin II to activate NCC through a WNK4-SPAK-dependent pathway. *Pflüg. Arch. Eur. J. Physiol.* **463,** 853–863 (2012).
50. Moes, A. D., van der Lubbe, N., Zietse, R., Loffing, J. & Hoorn, E. J. The sodium chloride cotransporter SLC12A3: new roles in sodium, potassium, and blood pressure regulation. *Pflugers Arch.* (2013). doi:10.1007/s00424-013-1407-9
51. Serafini-Cessi, F., Malagolini, N. & Cavallone, D. Tamm-Horsfall glycoprotein: biology and clinical relevance. *Am. J. Kidney Dis. Off. J. Natl. Kidney Found.* **42,** 658–676 (2003).
52. Welker, P. *et al.* Renal Na+-K+-Cl- cotransporter activity and vasopressin-induced trafficking are lipid raft-dependent. *Am. J. Physiol. Renal Physiol.* **295,** F789–802 (2008).
53. Bachmann, S. *et al.* Renal effects of Tamm-Horsfall protein (uromodulin) deficiency in mice. *Am. J. Physiol. Renal Physiol.* **288,** F559–567 (2005).
54. Simons, K. & Sampaio, J. L. Membrane organization and lipid rafts. *Cold Spring Harb. Perspect. Biol.* **3,** a004697 (2011).
55. Sangiorgio, V., Pitto, M., Palestini, P. & Masserini, M. GPI-anchored proteins and lipid rafts. *Ital. J. Biochem.* **53,** 98–111 (2004).
56. Bichet, D. G. V2R mutations and nephrogenic diabetes insipidus. *Prog. Mol. Biol. Transl. Sci.* **89,** 15–29 (2009).
57. Li, J. H. *et al.* A selective EP4 PGE2 receptor agonist alleviates disease in a new mouse model of X-linked nephrogenic diabetes insipidus. *J. Clin. Invest.* **119,** 3115–3126 (2009).
58. Yun, J. *et al.* Generation and phenotype of mice harboring a nonsense mutation in the V2 vasopressin receptor gene. *J. Clin. Invest.* **106,** 1361–1371 (2000).
59. Izumi, Y., Miura, K. & Iwao, H. Therapeutic potential of vasopressin-receptor antagonists in heart failure. *J. Pharmacol. Sci.* **124,** 1–6 (2014).
60. Nonoguchi, H. *et al.* Immunohistochemical localization of V2 vasopressin receptor along the nephron and functional role of luminal V2 receptor in terminal inner medullary collecting ducts. *J. Clin. Invest.* **96,** 1768–1778 (1995).
61. Zhu, X. & Wess, J. Truncated V2 vasopressin receptors as negative regulators of wild-type V2 receptor function. *Biochemistry (Mosc.)* **37,** 15773–15784 (1998).
62. Subramanya, A. R., Yang, C.-L., McCormick, J. A. & Ellison, D. H. WNK kinases regulate sodium chloride and potassium transport by the aldosterone-sensitive distal nephron. *Kidney Int.* **70,** 630–634 (2006).
63. Mamenko, M. *et al.* Chronic angiotensin II infusion drives extensive aldosterone-independent epithelial Na+ channel activation. *Hypertension* **62,** 1111–1122 (2013).
64. Field, M. J. & Giebisch, G. J. Hormonal control of renal potassium excretion. *Kidney Int.* **27,** 379–387 (1985).
65. Field, M. J., Stanton, B. A. & Giebisch, G. H. Influence of ADH on renal potassium

handling: a micropuncture and microperfusion study. *Kidney Int.* **25,** 502–511 (1984).
66. Glover, M., Zuber, A. M. & O'Shaughnessy, K. M. Hypertension, dietary salt intake, and the role of the thiazide-sensitive sodium chloride transporter NCCT. *Cardiovasc. Ther.* **29,** 68–76 (2011).
67. Giménez, I. Molecular mechanisms and regulation of furosemide-sensitive Na-K-Cl cotransporters. *Curr. Opin. Nephrol. Hypertens.* **15,** 517–523 (2006).
68. Schröter, J., Timmermans, G., Seyberth, H. W., Greven, J. & Bachmann, S. Marked reduction of Tamm-Horsfall protein synthesis in hyperprostaglandin E-syndrome. *Kidney Int.* **44,** 401–410 (1993).
69. Trudu, M. *et al.* Common noncoding UMOD gene variants induce salt-sensitive hypertension and kidney damage by increasing uromodulin expression. *Nat. Med.* **19,** 1655–1660 (2013).
70. Rafiqi, F. H. *et al.* Role of the WNK-activated SPAK kinase in regulating blood pressure. *EMBO Mol. Med.* **2,** 63–75 (2010).
71. Yang, S.-S. *et al.* SPAK-knockout mice manifest Gitelman syndrome and impaired vasoconstriction. *J. Am. Soc. Nephrol. JASN* **21,** 1868–1877 (2010).
72. Lin, S.-H. *et al.* Impaired phosphorylation of Na(+)-K(+)-2Cl(-) cotransporter by oxidative stress-responsive kinase-1 deficiency manifests hypotension and Bartter-like syndrome. *Proc. Natl. Acad. Sci. U. S. A.* **108,** 17538–17543 (2011).

Danksagung

Mein herzlicher Dank gilt an erster S telle Herrn Professor Dr. Sebastian Bachmann für seine fördernde Unt erstützung meiner wi ssenschaftlichen Arbeit sowie für die kontinuierliche Beratung und kritische Durchsicht der Manuskripte.

Darüber hinaus gilt mein besonderer Dank meinen Arbeitskollegen Anette Drobbe, Aljona Borschewski, Christin Dathe, Thomas Kahl und Alexander Paliege für die hervorragende wissenschaftliche Zusammenarbeit und das motivierende Arbeitsklima, sowie den TA-Kräften Kerstin Riskowski, Frauke Serowka, Petra Schrade und Petr a Landmann für die exz ellente technische Assistenz bei der Fertigstellung einiger der i n dieser Schrift vorgestellten Untersuchungen.

Nicht zuletzt gebührt mein herzlichster D ank meiner Frau Tatyana Mutig und meiner Mutter Rimma Mutig für ihre liebevolle und ve rständnisvolle Unterstützung im Laufe des Vorhabens.

Erklärung

§ 4 Abs. 3 (k) der HabOMed der Charité

Hiermit erkläre ich, dass

- weder früher noch gleichzeitig ein Habilitationsverfahren durchgeführt oder angemeldet wurde,
- die vorgelegte Habilitationsschrift ohne fremde Hilfe verfasst, die beschriebenen Ergebnisse selbst gewonnen sowie die verwendeten Hilfsmittel, die Zusammenarbeit mit anderen Wissenschaftlern/ Wissenschaftlerinnen und mit technischen Hilfskräften sowie die verwendete Literatur vollständig in der Habilitationsschrift angegeben wurden,
- mir die geltende Habilitationsordnung bekannt ist.

…… ……..

Datum Unterschrift